PB88-136528

UILU-ENG-87-2009

CIVIL ENGINEERING STUDIES
STRUCTURAL RESEARCH SERIES NO. 538

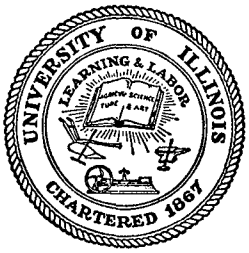

ISSN: 0069-4274

EVALUATION OF STRUCTURAL RESPONSE AND DAMAGE RESULTING FROM EARTHQUAKE GROUND MOTION

By
STEVEN L. McCABE
University of Kansas
WILLIAM J. HALL
University of Illinois at Urbana-Champaign

A Technical Report of
Research Supported by the
NATIONAL SCIENCE FOUNDATION
Under Grant Nos. PFR 80-02582, CEE 82-03973
and DFR 84-19191

UNIVERSITY OF ILLINOIS
AT URBANA-CHAMPAIGN
URBANA, ILLINOIS
SEPTEMBER 1987

50272-101

REPORT DOCUMENTATION PAGE	1. REPORT NO. UILU-ENG-87-2009	2.	3. Recipient's Accession No. PB88-136528
4. Title and Subtitle: EVALUATION OF STRUCTURAL RESPONSE AND DAMAGE RESULTING FROM EARTHQUAKE GROUND MOTION			5. Report Date: September 1987 6.
7. Author(s): S. L. McCabe and W. J. Hall			8. Performing Organization Rept. No. SRS 538
9. Performing Organization Name and Address: University of Illinois at Urbana-Champaign Department of Civil Engineering 208 N. Romine Street Urbana, IL 61801			10. Project/Task/Work Unit No. 11. Contract(C) or Grant(G) No. (G) PFR 80-02582 (G) CEE 82-03973 (G) DFR 84-19191
12. Sponsoring Organization Name and Address			13. Type of Report & Period Covered 14.

15. Supplementary Notes

16. Abstract (Limit: 200 words)

The initial studies reported involve investigation of simple elastoplastic structures when subjected to various pulse-types of ground excitation, including actual earthquake ground motions. Among the results documented are structural deformation response, input and hysteretic energies, and numbers of yield excursions. Also included are the results of a limited Fast Fourier Transform study and the observations arising from an experimental investigation of a simple structure.

The second set of studies reported involve the development of two comprehensive seismic damage evaluation criteria. One criterion converts the dissipated hysteretic energy into an equivalent number of identical hysteretic cycles employing three different cycle definitions. The second damage criterion accounts for the accumulation of structural damage caused by random inelastic cyclic response through hysteretic plastic ductility and damage index parameters founded on low-cycle fatigue concepts. Comparison against existing experimental data show the criteria depict damage well. Three applications of the damage criteria are presented, and possible applications to current design philosophy are presented.

17. Document Analysis a. Descriptors

Seismic, Earthquake Resistant Design, Inelastic Systems, Seismic Damage Evaluation, Dynamic Response Ductility, Hysteretic Energy, Low-cycle Fatigue

b. Identifiers/Open-Ended Terms

c. COSATI Field/Group

18. Availability Statement	19. Security Class (This Report)	21. No. of Pages
Release Unlimited	UNCLASSIFIED	294
	20. Security Class (This Page) UNCLASSIFIED	22. Price A13 $5.95

EVALUATION OF STRUCTURAL RESPONSE AND DAMAGE RESULTING FROM EARTHQUAKE GROUND MOTION

by

STEVEN L. McCABE

and

WILLIAM J. HALL

A Report on a Research Project Sponsored by the

NATIONAL SCIENCE FOUNDATION

Research Grant Nos. PFR 80-02582, CEE 82-03973 and DFR 84-19191

UNIVERSITY OF ILLINOIS

URBANA, ILLINOIS

SEPTEMBER 1987

ACKNOWLEDGMENT

This dissertation was prepared by Steven L. McCabe and submitted to the Graduate College of the University of Illinois at Urbana-Champaign in partial fulfillment of the requirements for the degree of Doctor of Philosophy in Civil Engineering. The dissertation was completed under the supervision of Professor William J. Hall.

The investigation was a part of a research program sponsored by the National Science Foundation under Grants PFR 80-02582, Earthquake Engineering Design Investigation, CEE 82-03973, Design Studies in Earthquake Engineering, and DFR 84-19191, Studies Towards New Seismic Design Approaches. Any findings, conclusions or recommendations expressed in this dissertation are those of the authors and do not necessarily reflect the views of the National Science Foundation.

The numerical results were obtained using the CDC Cyber 174/175 computers of the Computer Science Office at the University of Illinois, the Harris 1000 machine of the Department of Civil Engineering of the University of Illinois, and the Harris 1000 computer of the Academic Computer Service at the University of Kansas. The authors gratefully acknowledge the support and assistance provided by these facilities.

The authors wish to thank Professors A. J. Hendron, D. A. W. Pecknold, A. R. Robinson, and M. A. Sozen for their constructive comments throughout the study. Also we wish to acknowledge with thanks the contributions, advice and support provided by Professor S. T. Rolfe of the University of Kansas, Lawrence, Kansas.

ABSTRACT

EVALUATION OF STRUCTURAL RESPONSE AND DAMAGE RESULTING FROM EARTHQUAKE GROUND MOTION

Steven Lee McCabe, Ph.D.
Department of Civil Engineering
University of Illinois at Urbana-Champaign, 1987
Professor William J. Hall, Advisor

The design of structures to limit or preclude strong response and damage from earthquake ground motion is a complex problem and is the subject of this thesis. The factors leading to strong response are not well understood and clearly involve more than peak acceleration and yield level. Present methods for evaluation of damage are approximate, generally focusing on the maximum ductility. This study was undertaken to identify the parameters responsible for strong response and to develop comprehensive new approaches for evaluating damage in simple structures.

The initial studies reported herein involve the response of various single-degree-of-freedom (SDOF) elastoplastic structures to pulse-type ground excitation and to actual earthquake ground motion; among the results documented are structural deformation response, input and hysteretic energies and number of yield excursions. Also included are the results of a limited Fast Fourier Transform study and experimental investigation of a SDOF structure subjected to pulse-type excitation.

The second set of studies reported involves development of two comprehensive seismic damage criteria. One criterion converts the dissipated hysteretic energy into an equivalent number of identical hysteretic cycles employing three different cycle definitions. The second damage criterion accounts for the accumulation of structural

damage caused by random inelastic cyclic response through hysteretic plastic ductility and Damage Index parameters founded on low-cycle fatigue concepts. These damage criteria are evaluated against experimental data and found to depict damage well.

Three applications of these damage criteria are presented, namely (a) evaluation of the dissipated hysteretic energy using equivalent cycle and fatigue damage concepts, (b) use of the fatigue damage criterion to construct inelastic response spectra, and (c) use of the fatigue damage criterion as the basis for a proposed drift criterion to limit the damage caused by cyclic response.

The study concludes with observations regarding the contribution of the various ground motion and structural parameters to strong response, performance of the proposed damage criteria, and the impact of this investigation on current design philosophy.

TABLE OF CONTENTS

Page

LIST OF TABLES

LIST OF FIGURES

LIST OF SYMBOLS

The symbols and notations employed in this dissertation are defined where they are used in the text. A list of the important symbols is provided as follows:

a = plastic hinge length

A_a = Effective Peak Acceleration Coefficient

A_v = Effective Peak Velocity Coefficient

b = strength exponent

c = distance to extreme bending fibers of beam cross section

c = Ductility Coefficient

C = structural damping

C = Structural Period Factor

C_d = Deflection Amplification Factor

C_s = Shear Coefficient

D = damage level

DI = Damage Index

E = Modules of Elasticity

f = shape factor

f_n = structural natural frequency

g = acceleration of gravity

h = overall cross section height

HYSN = dissipated hysteretic energy from negative phase of structural resistance

HYSP = dissipated hysteretic energy from positive phase of structural resistance

HYST = total dissipated hysteretic energy corresponding to a completely damaged simple structure

I = moment of inertia

σ = bending stress

σ_f' = fatigue strength coefficient

σ_y = bending stress for yielding of extreme fibers of member cross section

σ_Y = bending stress for yielding of entire member cross section

Σ = summation

θ = angle of plastic hinge rotation

CHAPTER 1

INTRODUCTION

1.1 Research Objectives

The development of seismic design procedures for buildings has benefited from the strong program of earthquake engineering research in recent years. Improved knowledge about the nature of possible earthquake ground motions and better understanding of the behavior of structures and structural elements from which they are constructed has led to improved design provisions and building codes. An example of the latter are the modern building design provisions incorporated into the Applied Technology Council Report ATC-3 (3) and the subsequent National Earthquake Hazards Reduction Program (NEHRP) Provisions (14). However, in spite of these improvements, as strong earthquakes occur throughout the world, deficiencies are still observed in construction practice, structural design details, and conceptual design philosophy. This latter observation is particularly true in strong earthquakes when significant nonlinear behavior occurs in building systems and is aggravated when this nonlinear behavior occurs repeatedly over several cycles of response.

This research is part of a National Science Foundation investigation entitled "Studies Towards New Seismic Design Approaches." Among the objectives of this study are two topics related to specific aspects of structural response to earthquakes, namely (a) the examination of input ground motion to identify the parameters responsible for strong response and (b) the development and explanation of new approaches for structural damage assessment. Improved

definition of the latter topic is badly needed as a part of future improvements in building codes and standards, and for post-earthquake damage assessment; no satisfactory approaches currently exist.

Accordingly, this research investigation was undertaken to obtain a better understanding of the generation of response and damage in simple structures. The contributions of this research are significant in that the interaction of structural and ground motion parameters in causing strong response has been studied and documented herein, confirming some previously known results and identifying new factors to consider in design. Moreover, new damage criteria are developed which provide a greatly improved ability to accurately describe damage in structures. The underlying goal of this research was to produce results that would be useful in design; therefore, this thesis concludes with some specific design applications of this research.

1.2 Scope of Research Undertaken

This dissertation centers on the findings from two interrelated studies that have been conducted to meet the foregoing objectives. The first study focused on defining the ground motion and structural parameters that combine to produce strong response; this goal was accomplished through detailed study of response to simple pulse-type excitation and to actual earthquake ground motion. This general topic has been addressed partially by other investigators. However, the present investigation isolated and studied the effects of these parameters from a design perspective, in a limited yet more systematic manner than previously had been the case.

The insight gained from the initial phase of this investigation then was applied to the important question of how best to describe and evaluate structural damage that may result from strong response. As a result, two new damage measures were developed to quantify the damage sustained during earthquake response. These measures are based on hysteretic energy and cyclic deformation considerations together with low-cycle fatigue theory adapted to this problem. These damage criteria provide a means to convert hysteretic energy into a quantitative, realistic measure of cyclic response as well as a method to modify conventional ductility concepts for the additional, and significant, damage that accumulates when plastic deformations occur over repeated cycles of response. Comparison with laboratory results suggest that these measures more accurately predict the damage caused by cyclic deformations than is possible with present ductility methods. Moreover, the usefulness of these damage measures in design situations is demonstrated through specific application of these criteria to the evaluation of hysteretic energy, to the construction of inelastic response spectra and to the development of new building drift limits.

The research contributions of this study, as summarized above, concern the basic single-degree-of-freedom (SDOF) system defined in Fig. 1.1. It can be observed from this figure that for a base excited simple system, clearly defining the input ground motion is an important part of the design process. At present, design methods frequently employ the peak ground acceleration as the sole description of the earthquake loading, ignoring the nonmaximum accelerations as well as the cyclic nature of the acceleration application. The problem is further complicated when the peak ground acceleration occurs in the

form of high frequency spikes or pulses of unusual configuration. Accordingly, the first phase of this investigation focused on the evaluation of ground motion involving simple acceleration pulses and spikes as well as actual earthquake records to study the parameters that are significant in causing response. The results of this work are reported in Chapter 2.

The evaluation of structural response to earthquake ground motion is another important part of the design process. The response can be depicted in terms of peak response, as reflected in response spectra, or in terms of an entire response time history. Regardless of the analysis procedure employed, once the response has been determined an evaluation must be made to compare the actual behavior with that allowed or desired. Traditionally, this evaluation has utilized the ductility factor, defined as the ratio of maximum displacement to yield displacement as shown in Fig. 1.2, as the basic criterion by which the strength of the response is judged. The ductility concept, proposed by Newmark (47), has been used extensively but is limited in application especially for repetitive type response.

The advantage of the ductility factor is that it can be readily applied in design to provide both a measure of the maximum deformation to be expected as well as an indication of the damage associated with the response. The problem is that the maximum ductility is an inadequate damage measure; it only addresses the maximum deformation and ignores all of the other factors of the response that may influence the damage level. Improvements in evaluation of damage require more complete information about the response. Recent research by Zahrah and Hall (72) has produced a more complete description of the response and

damage through calculation of the structural energy balance during response thereby providing a basis for the further advances reported herein. As will be developed later in this dissertation, the nonmaximum cycles of deformation, together with the hysteretic energy, play an important role in the generation of damage and must be included in any damage evaluation.

Therefore, the present investigation focused on the development of comprehensive means to quantify the damage sustained, and the reserve margins present, in a simple structure subjected to an earthquake. It is important to be able to quantify such factors if significant advances in design procedures are to be developed in the near future. Thus, a damage criterion was proposed employing low-cycle fatigue theory adapted to the earthquake response problem to account for the additional damage caused by the load reversals during the response. The advantage of this approach is that the damage assessment involves the entire response history of the structure, not one isolated peak value. Furthermore, damage is based on conventional ductility concepts that have been improved to account for the additional structural damage caused by cyclic deformations. A second damage criterion was proposed based on the number of equivalent hysteretic cycles of structural response. Structural deformation response is erratic and not easily assessed. When plotted on a resistance-deformation diagram, the response appears as hysteretic cycles of various sizes. A quantitative damage measure can be developed if this actual response is transformed into a number of identical, complete hysteretic cycles required to dissipate the actual amount of hysteretic energy. The development of these damage criteria is presented in Chapter 3.

The equivalent hysteretic cycle damage criterion and the Damage Index are evaluated in Chapter 4. This evaluation is a detailed comparison of the predicted damage levels from the proposed criteria with the experimental results of cyclic tests of structural members. The evaluation studies show the damage criteria to be accurate descriptors of the test results.

As a result of the foregoing studies, an improved understanding of the role of the various features of the ground motion and of the structure in generating damage has been developed. The results of this thesis point the way toward new building code procedures that address the entire response and are not based solely on the peak ground acceleration or maximum structural deformation. The procedures developed in this study provide the designer with the means to accurately assess the damage arising from the deformation pattern, yet in a way suitable for design application. Thus, an opportunity to improve existing design and building code provisions is clearly present through application of the concepts developed herein. The implications regarding building code philosophy are demonstrated in Chapter 5 where specific design applications of this research are presented. A brief overview of this study and its impact on design is contained in Chapter 6.

Four appendices contain supplementary material that supports the information presented in this dissertation. The results from tests of a small SDOF structure to pulse-type ground acceleration are reported in Appendix A. The detailed results of damped and undamped structural response to actual earthquake acceleration time histories are summarized in Appendix B. The results of structural response

calculations using filtered ground motions to explore the frequency coupling between earthquake and structure are presented in Appendix C. The derivations of strain-displacement and strain-ductility relationships employed in Chapter 3 are contained in Appendix D.

1.3 Previous Research and Review of Present Analysis Practice

Three basic methods have been developed to estimate the effects of earthquake excitation on structures. The most comprehensive technique available is response time history analysis usually employed only when detailed information is needed. Another way to estimate response is by employing pseudostatic methods, as typically found in building codes (3,14,68), that are based on simple representations of the earthquake ground motion and structural response. A third widely used technique is the response spectrum method, which is a plot of the maximum response of a family of SDOF oscillators to a particular earthquake excitation (51,52). Because the spectrum is based on the maximum response to the particular ground motion in question, the spectrum can provide more accurate estimates of response than pseudostatic methods. However, the response spectrum concerns only the single maximum response value and does not provide the complete information about the behavior that is contained in a response time history.

Response spectra can be constructed for elastic and inelastic response. Inelastic spectra traditionally have been based on maximum ductility considerations wherein the yield displacement is adjusted and the response computed until the actual maximum ductility matches the specified value for each structural frequency. An advantage of the inelastic spectrum is that smaller design loads result, and thus

smaller members can be used, if some degree of nonlinear behavior is permitted.

One drawback to the spectrum concept is the calculations required to construct an elastic or inelastic response spectrum. Housner (23,26), Veletsos and Newmark (69), Newmark and Hall (49) and Newmark, Blume and Kapur (48) developed procedures to construct smoothed elastic design spectra from basic structural and ground motion parameters without detailed calculation. This concept was extended to nonlinear response with the modified design spectrum based on an elastic design spectrum modified by a ductility-based factor to estimate the effects of inelastic behavior. An example of a modified design spectrum is that developed by Newmark and Hall (49,50).

These analysis procedures are limited because they employ the maximum ductility value as both the measure of the response and as the primary measure of damage and, secondly, because they evaluate the earthquake hazard based generally on the peak ground acceleration. Concentrating on the single value of maximum ductility alone produces incomplete damage estimates because the nonmaximum response is ignored; for example a structure reaching a ductility value once or many times would be considered to be equally damaged. Moreover, use of the ductility factor as a means of constructing modified spectra must be limited to only small values of maximum ductility because the accuracy of this approach decreases with larger specified ductilities, as observed by Mahin and Bertero (41).

The structural response is influenced by more factors than the peak ground acceleration; factors such as changes in frequency content, pulse shape, acceleration amplitude, impulse area and overall duration

of motion can substantially affect the structural response. Furthermore, the peak ground acceleration, which is used as the anchor point for design spectra, has been shown in several studies to be a poor indicator of damage potential (2,4,35,54). In summary, the present analysis procedures are not able to predict the damage resulting from response to an earthquake because these methods are founded on peak input and peak response parameters. The nonmaximum values of ground excitation and structural response are generally ignored, yet it is these parts of the excitation and response that are responsible for generating structural deformations and damage, as will be developed later herein.

The limitations of the present techniques have motivated researchers to propose other methods to predict and evaluate structural response. Several researchers have proposed improved response spectra methods to predict the response to earthquake ground motions. Among these studies are those by Shibata and Sozen (65), Riddell and Newmark (63), Nau and Hall (45), and Perez and Brady (55). The common factor in these studies was the use of the ductility factor as the basis of spectra scaling as well as the primary damage measure.

Several studies focused on the energy dissipated by hysteretic behavior such as those by Housner (24,25), Berg and Thomsaides (10), Blume (13), Jennings (31), Zahrah and Hall (72), Kennedy (35), and Kennedy and Short (36). Other researchers have recognized the need to address the accumulation of damage from cyclic deformations caused by earthquake response and have applied low-cycle fatigue theory to this process. Examples of these studies are those by Suidan and Eubanks (66), Kasiraj and Yao (34), and Lashka-Irvani (40). These

investigations produced methods too complex for design purposes, however, they do illustrate the potential for using fatigue theory to assess the structural damage from earthquakes.

It is for these reasons that the current studies were undertaken, namely to determine the parameters of the ground motion and of the structure that are responsible for strong response, and to propose improved methods to evaluate the damage caused by the response. The present methods are based on examination of only the maximum values of the input acceleration or the response deformation. The results of this particular study indicate that there are other factors involved that strongly influence the response and damage caused by earthquake excitation. These factors are identified and new measures proposed to evaluate damage more thoroughly than has formerly been possible. Such advancements in practice are necessary if improved rational design approaches are to be developed and implemented in the future.

CHAPTER 2

STRUCTURAL RESPONSE TO GROUND MOTION EXCITATION

2.1 Introduction

This chapter contains a brief examination of specific types of input ground motion and their effect on structural response. It is recognized that a great deal of such information already exists in the literature on this topic. However, for the purposes of this dissertation, wherein structural damage mechanisms are under study, it is important to examine strong ground motion input and its effects in special cases centering around limited nonlinear behavior. Such studies are important from several standpoints, not the least of which is that the development of comprehensive and consistent damage estimation procedures will lead in the future to more rational building code provisions, as well as methods for evaluating remaining margins of safety.

In order to accomplish the foregoing objective, the chapter begins with some introductory remarks on analysis procedures and follows with two major sections that summarize the input and response studies. The first section concerns simple regular triangular base-type excitation of single-degree-of-freedom (SDOF) systems and the examination of the influence of certain selected key parameters on response. The second portion of the chapter follows the same line of development for earthquake-based excitation studies. As a part of this study a great deal of computation was carried out and the material presented was

selected as being the most pertinent to the subsequent developments in this thesis.

Some additional comments on the matter of strong shaking are in order to place this portion of the study in perspective. It has been observed in earthquakes, as well as in various forms of military related shock-type studies, that high-frequency spikes of acceleration have little effect upon the response of simple systems, which is not particularly surprising in light of the fact that the impulses are quite small (30,70). On the other hand, when one examines the existing literature, there is not a well-organized systematic development of the patterns of behavior that would be expected for pulses of various types including those with high amplitude and high frequency. For this reason an attempt was made to develop a somewhat more concise picture than currently exists of the role of various ground motion excitations in terms of their effect upon the response of simple systems. Such studies were carried out for simple types of pulses as well as earthquake excitation; in turn these studies were helpful in providing a basis for development of damage criteria, one of the major contributions of this thesis.

2.2 Structural Response Evaluation Methods

2.2.1 Structural Response Calculations

The ground acceleration, $\ddot{Y}(t)$, causes the basic SDOF structure (Fig. 1.1) to respond as described by the equation of motion,

$$M\ddot{U}(t) + C\dot{U}(t) + R(U(t)) = - M\ddot{Y}(t), \qquad (2.1)$$

where U(t) is the structural displacement with respect to the ground, M is the structural mass, and C is the velocity-dependent energy dissipation capacity modeled as damping. Dots above the variable indicate differentiation with respect to time.

The structural resistance, R(U(t)), is based on an elastoplastic resistance model, as shown in Fig. 1.2. For elastic displacements, the resistance is a linear function of the stiffness, K, and displacement; for inelastic deformation, the resistance is equal to the yield value. Previous research has shown that the elastoplastic resistance model normally is an adequate representation of resistance for nondegrading structures as compared to other more complex models (45,51,72). This behavior also was confirmed by experimental results presented in Appendix A.

The closed form of the Newmark Beta Method (7) was employed to solve the equation of motion numerically using a value of 1/6 for β, corresponding to a linear variation in ground acceleration (27,46). A time step size of one-twentieth of the structural period (T) was used except when yielding or unloading was detected. In this situation, the resistance model corners were more precisely located by redoing the calculations using a T/80 time step. Once the particular corner was located again, the time step was reset to T/20.

2.2.2 Structural Energy Expressions

Computation of the structural energy balance can provide additional insight into the response process. The energy can be calculated by integrating the forces in each term of Eq. (2.1) through the distance, dU, moved in each time step. However, integration through time is more convenient than through distance, so a change in

integration variable was accomplished by noting that dU is equal to $\dot{U}dt$. This change results in the energy expression,

$$\int_o^t M\ddot{U}(t)\,\dot{U}(t)\,dt + \int_o^t C\dot{U}(t)\,\dot{U}(t)\,dt + \int_o^t KU(t)\,\dot{U}(t)\,dt = -\int_o^t M\ddot{Y}(t)\,\dot{U}(t)\,dt. \tag{2.2}$$

For a β value of 1/6, the following expressions were obtained by Zahrah and Hall (72) for the amount of energy imparted to the structure between t and t + Δt, with the incremental contributions as listed below,

Incremental Kinetic Energy,

$$\Delta E_{KE} = M[\dot{U}_t\Delta\dot{U} + (\Delta\dot{U}^2/2)], \tag{2.3}$$

Incremental Damping Energy,

$$\Delta E_{DE} = C([\dot{U}_t^2 + \dot{U}_t\Delta\dot{U} + (\Delta\dot{U}^2/2)]\Delta t - 1/6\,[\dot{U}_t\Delta\ddot{U} + 1/2\,\Delta\dot{U}\Delta\ddot{U}]\Delta t^2 + 1/120\,[\Delta\ddot{U}^2\Delta t^3]), \tag{2.4}$$

Incremental Strain Energy (Linear Response),

$$\Delta E_{SE} = K\Delta U(U + \Delta U/2), \tag{2.5}$$

Incremental Hysteretic Energy (Yielding Response),

$$\Delta E_{HYS} = (R_{yield})\,\Delta U, \tag{2.6}$$

Incremental Input Energy,

$$\Delta E_{INPUT} = \Delta E_{KE} + \Delta E_{DE} + \Delta E_{SE} + \Delta E_{HYS}. \tag{2.7}$$

The total energy value is computed by summing the incremental energies over the total time of the record. The results of the energy calculations can be presented as energy time history plots, or as energy spectra where the maximum energy values are plotted as functions of the structural frequency.

2.2.3 Fourier Transform Analysis

It was believed the information about the frequency components that comprise the earthquake ground motion would be of value in interpreting the factors affecting the structural response to various types of ground motion input. For this reason, a limited study was undertaken using the Fast Fourier Transform (FFT) technique (53) to determine the frequency composition of the ground motion excitation.

In addition to examining the overall earthquake excitation by the FFT technique, segments of the acceleration time history were examined through use of the Hamming Window Function to ascertain the change in frequency composition with time as the window was stepped through the excitation (20). Clearly, a rectangular window could have been employed, but the abrupt transition at each end of the window can distort the FFT results; this distortion can be reduced by tapering each end of the window in the same manner as one commonly does with a filter function. This tapering was produced through application of the Hamming Function.

2.3 Structural Response to Pulse-Type Ground Acceleration

The response of various SDOF structures to pulse-type ground acceleration is presented in this section. The pulses include single pulses, multiple pulses, and limited cases of repeated pulses with a

high amplitude spike interposed. As one would expect, these studies show that several key factors influence the structural response in addition to the peak ground acceleration, namely such factors as the synchronization of the frequency of the ground acceleration pulse to the natural frequency of the structure, the pulse configuration including the impulse contained therein, duration of the motion, damping, and yield resistance of the structural system. The specific role of these items will be described briefly in the material that follows. Additional observations pertaining to input and hysteretic energy as well as yielding cycles that serve to provide a foundation for the subsequent damage observations that are developed herein, also are presented.

The trends in response to a simple, triangular pulse of one cycle are presented in Fig. 2.1. The input energy versus pulse duration relationship presented in Fig. 2.1a shows that the maximum input energy for each pulse duration occurs in a structure with a period equal to the pulse duration. A 2 hz structure exhibits the maximum input energy when subjected to a 0.5 second pulse; a 5 hz structure has the maximum input energy when a 0.2 second pulse duration is employed. Also indicated in this figure is the increase in input energy values for all structures as the pulse duration, and hence the impulse, increases.

The same trends are evident in Fig. 2.1b. Of particular note is that for the single pulse, a minimum pulse duration is required before the response is strong enough to cause yielding and hysteretic energy dissipation. In fact, the lower frequency structures do not experience cyclic yielding and thus produce no hysteretic energy even with pulse durations of one second.

In Fig. 2.2a and b similar trends are shown for the case where a single pulse has more positive area than negative area. The frequency tuning effects are still present, but the response energies are suppressed as contrasted to the first case. Careful study will show that the suppression is related to the amount of impulse involved, which is less in the latter case.

The effects of damping on response are illustrated in Table 2.1. As would be expected, for the structures having the three frequencies shown, the displacement decreases as the damping increases. Also, the role of tuning or synchronization of the input pulse with the structural frequency is clearly shown, wherein the peak value of input energy and the maximum hysteretic energy occur for a 2 hz structure with a pulse duration of 0.5 second. For the other lower and higher structural frequencies, the response to this pulse is reduced.

In the case of repetition of the basic pulse, some of the trends are illustrated in Figs. 2.3, 2.4, and 2.5. It will be observed from Fig. 2.3, that the maximum relative displacements for durations of one, two, or five seconds are the same. This result was identified some years ago in connection with the estimation of the maximum deformation response for modified spectra to account for inelastic action. It is not known that such a graphic representation of this phenomenon has been reported previously. On the other hand, the energies are a function of duration as shown in Figs. 2.4 and 2.5. The increases in the input energy, as well as the hysteretic energy, is significant when the duration is increased from one to two, and then to five seconds, and also is a function of the frequency as shown therein.

The next demonstration of the effect of base excitation on response is presented in Fig. 2.6 where there is shown a series of repeated small amplitude simple pulses with one large amplitude spike in the center of the train of pulses. In Fig. 2.6b it will be noted that the yield resistance is reached just before the time at which the large spike occurs because the excitation is in resonance with the structure. Significant yielding takes place during the spike time with the resistance continuing at the yield level. As shown in Fig. 2.6c, a strong step in the energy curve also occurs at the time of the large pulse, further illustrating the effect of the strength of the response. Next a 2 hz structure is subjected to the same 5 hz excitation and the response (Fig. 2.6d and 2.6e) is smaller than for the 5 hz structure until the time of the large pulse. At that point there is sustained response, but not yielding; the energy input is reduced as well, as shown in Fig. 2.6e. Similarly for a stiff structure of 10 hz subjected to the same excitation one finds the results presented in Fig. 2.6f and 2.6g. As a result of the mistuning of the structure and the spike, the response is relatively low, as was observed for the 2 hz structure. Again, one sees the major influence of the excitation as it approaches the frequency of the structure.

The structural deformation was computed as a function of the resistance for various structures responding to a repeated triangular pulse of 0.5g maximum amplitude and 0.5 hz frequency. The plot of yield resistance versus deformation for a 0.5 hz undamped structure shown in Fig. 2.7a reveals that the deflection occurring at the first unloading is nearly constant for all of the resistance values. Moreover, systems with lower yield resistances were prone to slightly

larger unloading displacements. When these displacements are converted to ductilities and plotted on a logarithmic scale versus the yield resistance, the plot presented in Fig. 2.7b results. It can be observed from this result that the displacement at the first reversal can be directly predicted from the yield resistance value alone. These two figures provide partial verification of the assumptions by Veletsos and Newmark (69) that deflections are conserved.

As the number of reversals or unloadings is increased from one to five, the situation becomes more complex. The results shown in Fig. 2.7c indicate the changes in maximum displacement for each of the first five unloadings during the response as a function of the structural yield resistance level for a 0.5 hz undamped structure. For the lower values of structural resistance, the ground motion excitation continued to push the maximum displacement of the structure in one direction resulting in large maximum displacements that were additive from one cycle to the next. For structural resistances in the middle regions, above 20 pounds for this example, the maximum structural deformations over each response cycle began to oscillate causing considerable shifting in the values of maximum structural displacement at the unloading positions. As the resistance value approaches the value required for elastic response, the maximum deformations for each loading cycle were similar. From this figure it can be observed that, as discussed above, at the first unloading position the value of maximum displacement is essentially identical for all of the yield resistance values. Another observation can be made regarding the dotted line in this figure which shows the trends in the overall maximum excursions observed for the positive displacements from the

first five reversals. If the excitation were continued, some shake down of these maximum values would have been observed and a steady-state condition ultimately would have been reached. For the lower yield resistances, the excitation would have continued to increase significantly.

In summary, the foregoing observations serve to place in perspective the trends and limits in structural response caused by simple excitation and measured by deformation, resistance and energy.

2.4 Structural Response to Earthquake Ground Motion

The previous investigation into response to simple pulse excitation provided a basis for the study of structural response to actual earthquake excitation. Seven earthquake records were employed to observe the trends in response caused by these different earthquake ground motions. The results of response to three earthquakes, El Centro, Pacoima Dam and Melendy Ranch, were selected as being representative of the trends of response that occur with earthquake excitation. These earthquakes were selected from the standpoint of El Centro being sustained strong shaking, Melendy Ranch representing an earthquake with a short burst of energy and Pacoima Dam representing strong pulse-type excitation as well as a record with large acceleration amplitudes in the middle of the earthquake record. Information about the seven earthquake records employed in this study is presented in Table 2.2. It will be noted in this table that overall durations on the order of one-half of the total record duration were used and this period of time in all cases covered the principal strong

motion excitation. Detailed response results are presented in Appendix B for these seven records.

The trends in the response will be described in the following discussion with the significant parameters identified in light of the observations made earlier about simple pulses. All the results presented here are for a 2 hz simple structural system with damping of zero and five percent. In Fig. 2.8a is shown the ground acceleration and velocity for the El Centro record as taken from the California Institute of Technology's studies (28). The relative displacement and velocity for a 2 hz undamped structure are shown in Fig. 2.8b and c, and it will be observed that the principal responses occur at or near the times when the major excitations occur in the ground motion. This is further demonstrated in Fig. 2.8d, wherein the yield level is seen to be reached and sustained in those regions where the strong excitation takes place; similarly, the steps in the energy curve in Fig. 2.8e occur in those same regions.

Figure 2.8f contains a plot of the so-called "power" which is the slope of the energy curve as well as plots of the differential displacement and the equilibrium displacement. The differential displacement is a measure of the displacement change during the response between unloading points. It will be observed that the principal changes in displacement from positive to negative, denoted there by the differential displacement, occur when the power is the greatest. The equilibrium position, presented in Fig. 2.8f, is the residual plastic offset at any point in time. This parameter can be predicted by dividing the difference of the positive resistance and

negative resistance hysteretic energies by the corresponding yield resistance.

The Fourier amplitude spectrum (amplitude versus frequency) is shown in Fig. 2.8g for the entire duration of the El Centro record. It will be noted that the principal amplitudes occur around 2 hz, which suggests that 2 hz systems would experience the greatest excitation from El Centro. To further examine this point, a FFT calculation was carried out using a Hamming Window Function, as illustrated in Fig. 2.8h, to taper the edges of selected segments the time history to preclude biasing of the results over the frequency range of interest. The results of this operation for a series of windows of approximately five seconds in length, with the window translated by about 2.5 seconds in each step, is shown in Fig. 2.8i, j, k, and l. It will be noted, in line with the previous discussion, that the first and second windows show the primary excitation in the 1-3 hz region, and thereafter, the windowing illustrates that the ground motion at later times is of less significance with regard to excitations observed.

The Fourier Amplitude data are summarized briefly in Table 2.3 wherein the results for the El Centro, Pacoima Dam, and Melendy Ranch earthquake records can be compared. Of interest in this table are the values of the four largest Fourier amplitude components and their frequency values, which are noted to change as the window is moved along the time axis in 2.5 second intervals. When the results for the three earthquake records are compared, the configuration of the acceleration time histories represented by these three earthquake records can be noted. Specifically, the robust consistent composition of El Centro can be compared with the high frequency composition of

Melendy Ranch and the frequency composition of Pacoima Dam that changes sharply with window position. Also contained in this table are the Fourier amplitude acceleration spectrum area values which would appear to suggest that larger damage potential might be associated with larger Fourier spectrum area. However, the link between the area of the Fourier amplitude spectrum and the resulting structural response was not readily identifiable or consistent in trend. A separate study of the effects on the structural response of changes in the frequency content of several of these seven records was performed and is summarized in Appendix C. The results of these studies, although confirmatory of information already known, did not serve to identify any new response trends applicable to these studies.

The results of damped structural response for a 2 hz structure with five percent damping are presented in Fig. 2.8m, n, o, and p. The effect of damping is generally to reduce the levels of structural response, with the displacement and velocity maxima reduced, although only slightly. The more significant effects are the reduction in the amount of hysteretic energy dissipated and the lower numbers of yield excursions and hysteretic cycles, which are reduced substantially over the undamped case. The effects of damping are particularly illustrated in Fig. 2.8p where the hysteretic energy is less than the input energy with the damping energy a substantial portion of the overall total energy.

The structural response curves resulting from the Pacoima Dam earthquake record are presented in Fig. 2.9. This record is interesting because of the large ground velocity that exists early in the record is not repeated in any form as a result of the large

acceleration amplitudes that occur later. The structural resistance time history contained in Fig. 2.9b also indicates the role of the ground velocity in driving the structural resistance during the early portion of this record. The energy time history, shown in Fig. 2.9e, also shows the strong response generated by the ground velocity. The large acceleration pulses are not particularly effective in causing response for low and middle range frequency structures. The low frequency composition, which causes the large ground velocity, is capable of dominating the structural response.

The response to Melendy Ranch is contained in Fig. 2.10. This record represents a short duration, large amplitude record that provides a short burst of input energy. The structural response results indicate that while Melendy Ranch has large acceleration amplitudes, the structural response levels reached are substantially lower than those obtained from El Centro and Pacoima Dam. Another aspect of this lower response is the reduced number of hysteretic yield excursions that occur during Melendy Ranch, in most cases the response is entirely elastic.

It was noted earlier herein for simple pulse-type excitation that the relationship between the maximum ductility and the yield resistance was highly predictable and consistent. For more random-type excitation, such as that of earthquakes, it would be expected that this same relationship may not be as predictable or consistent. In order to test this relationship, the data in Fig. 2.11a were plotted. In spite of the fact that some of the resistances and other model parameters are unrealistic from a practical point of view, the plot is illustrative of a similar trend between ductility and yield resistance for both the 2

and 5 hz structures with Pacoima Dam excitation. Note that in this case the ductilities presented were calculated directly from the deformation responses.

Another technique for estimating the ductility versus yield resistance relationship is that of dividing the total (final) hysteretic energy by the product of the yield resistance and yield displacement. Such plots for the same conditions as just noted are presented in Fig. 2.11b. It will be noted that the trends are the same as in Fig. 2.11a but clearly, because of the negative and positive features of the response and the multiple cycles, this procedure leads to an estimate of ductility that is extremely high and unreasonable. However, the important point is that the trend exists and lends confidence to the fact that one can use these relationships for parameter evaluation and prediction purposes.

The studies summarized in this chapter have centered around the effects of two types of excitation on the response of simple structures. Such a concise yet comprehensive understanding of loading versus response is essential to the development of damage measures that is the subject of the remaining chapters of this thesis.

CHAPTER 3

STRUCTURAL DAMAGE EVALUATION CRITERIA

3.1 Introduction

As a part of the process of developing better seismic design provisions for buildings there is a pressing need to obtain techniques for estimating and evaluating response that incorporate an accurate measure of the structural damage and margin of safety. Unfortunately, at present we have only rudimentary techniques for estimating damage or for assessing the margin of safety remaining after some degree of nonlinear deformation of the building as a whole.

Current methods of assessing damage have focused on the maximum displacement or, when normalized by the yield displacement, the maximum ductility. This approach is an outgrowth of the evaluation of elastic response where the maximum displacement provides the designer with the corresponding maximum structural resistance developed to oppose this motion and is considered to be all that is needed for design. Nonlinear response complicates the damage evaluation because the displacement and resistance no longer are linearly related but form hysteresis loops associated with the reversal of motions. The damage that results is a function of not only the maximum displacement but also the hysteresis pattern that lies within the maximum displacement envelope.

Analysis techniques such as pseudostatic, response time history and response spectrum methods generally focus on the single value of maximum displacement and provide information to gauge appropriately the response under elastic conditions only. The information provided by

these methods for inelastic response situations will in many cases lead to reasonable estimates of maximum response but is not adequate to assess the actual damage, or the amount of inelastic deformation, that has occurred. For example, design spectrum methods, which will be discussed in the next section, are simple and have been adapted for use in modern building codes. However, the design spectrum only provides information about the maximum acceleration, velocity, or displacement in the system; in current building codes (force type approaches) only the former item receives attention. The design spectrum does not provide any information as to the effects of duration on the response, the number of cycles of repeated response, the amount of hysteretic energy absorbed through the deformation process, or any good measure as to damage mechanisms or margins of safety.

The development of improved damage measures is the major thrust of this dissertation. Accordingly, in the next section there is presented a brief review of the existing techniques for describing damage associated with inelastic action. The following two sections contain new approaches for estimating the damage that is associated with the inelastic response to earthquakes; specifically these developments center around low-cycle fatigue concepts adapted to seismic building design. This adaptation includes such factors as the number of cycles of response, loading levels, the amount of hysteretic energy involved, and factors that address unequal hysteretic energy patterns in the response.

In contrast to previous studies of this type, a major consideration has been the development of an approach that can be used in practice. The development of the theory depends to some significant

degree on possessing knowledge about the response process, which in turn was the reason for the background work regarding excitation and response reported in the previous chapter. The development of the suggested application techniques, and the confirmation of the applicability of these techniques through comparison with experimental results, are presented in Chapter 4.

3.2 Summary of Existing Damage Criteria

The design methods currently in use involve evaluation of the maximum displacement of a structure and comparison of this value with an allowable or desired value. Refinements to this basic approach have included computation of the hysteretic energy dissipated during response or changes in member stiffnesses. These methods are described in the following paragraphs and represent the current state of damage evaluation. The advantages and limitations will be discussed briefly to put the new damage criteria developed in the following sections in perspective.

In the case of elastic response, no damage normally is expected except where some localized damage in the form of buckling, brittle fracture or other nonductile failures may occur. The value of maximum deformation provides the designer with the limiting value of the motion, and from the stiffness the corresponding value of structural resistance can be estimated. This information permits the structure to be evaluated for the dynamic loading because the maximum response value normally is sufficient for elastic design purposes. When the maximum elastic response is computed for a collection of structural

frequencies, a response spectrum can be plotted to obtain the maximum elastic response for the entire frequency range for a simple system.

The concept of the response spectrum has been further refined through the use of the design spectrum to tailor the spectrum to reflect the judgment of the designer and to reduce the computational effort needed to produce a spectrum. The Newmark and Hall design spectrum (50) utilizes the peak ground acceleration, velocity and displacement values, such as those obtained for a ground motion record, and amplifies these ground motion values through the statistically obtained amplification factors found in Table 3.1. An elastic design spectrum of the form shown in Fig. 3.1 results when plotted on tripartite axes.

Nonlinear structural response to earthquake ground motion may occur in several forms such as localized yielding in a specific location in an element, buckling, and generalized yielding in a framework. In a gross sense, the maximum deformation of the element may be employed as an index (in the same way as maximum stress) depicting the behavior. This approach has been borrowed from the evaluation of elastic response where the maximum deformation is the parameter of interest, and over the years has been used extensively in the blast dynamics field.

When the maximum displacement is divided by the yield displacement, the maximum ductility is defined, as illustrated in Fig. 1.2. In the context of monotonic loading, the ductility is a reasonable way to assess the damage caused by the deformation of the structural element because the ductility can be compared readily with

allowable or failure ductility values obtained through prior experience or laboratory tests.

In the case of oscillatory dynamic response, the cycles of deformation represent a challenge to the designer to properly evaluate the damage that has occurred during this motion. At the present time, the maximum ductility, based on the ratio of the maximum displacement in any direction divided by the yield displacement as shown in Fig. 1.2, is the primary means used to describe damage. The maximum ductility is employed implicitly in pseudostatic direct design methods such as those employed in the Uniform Building Code. Similarly, the ductility is implicitly included in the determination and evaluation of the maximum drift. Ductility also can be employed in the evaluation of the results of response time history calculations if desired. Inelastic response spectra also can be computed in which the specified maximum ductility value is used as the response criterion in that the yield displacement is adjusted, and the response recomputed, until the desired maximum ductility is achieved. Spectral plots of yield displacement for various specified ductilities as a function of structural frequency then can be produced. As described next, these calculations are the basis for so-called modified spectra that reflect inelastic action.

The resistance values attained during inelastic response are reduced from those values reached during elastic response. Veletsos and Newmark (69,70) observed that this reduction was a function of the specified maximum ductility and used the ductility factor as the scaling parameter to reduce the elastic design spectrum. The ductility factor serves a dual purpose in this procedure being used to reduce the

required structural resistance and also as the measure of damage. The reduction factors commonly in use are as follows (49,50),

$$\frac{1}{\mu} \quad \text{for the low and intermediate frequencies,}$$

and (3.2)

$$\frac{1}{\sqrt{2\mu-1}} \quad \text{for high frequencies.}$$

These factors are based on the observation that for low and intermediate frequencies, the maximum elastic and inelastic displacements are approximately equal, while in the higher frequency acceleration region the absorbed energies for elastic and inelastic systems are assumed to be about equal. The application of these factors is presented in Fig. 3.2 (50).

Another measure of the level of damage related to the ductility is the secant or reduced stiffness of a structure. As the ductility increases, the secant stiffness decreases and can be employed as a measure of damage (6).

The hysteretic energy has been proposed by some investigators as a more comprehensive means to represent the response so as to include the other, nonmaximum response cycles. Because the area under the resistance-displacement hysteresis curve equals the dissipated hysteretic energy, the hysteretic energy has been employed in some form as a measure of damage. Since all of the nonlinear excursions are represented in the area, the hysteretic energy is potentially a more descriptive measure of the overall damage process than a single value of maximum displacement or ductility. Several researchers have

published results of studies where the hysteretic energy alone was used in some form as a basis for damage evaluation (10,19,24,31,32,72).

There are advantages and limitations to all of these existing methods. The use of the maximum ductility as the damage measure ignores the effects of the other nonlinear excursions. Based on the maximum ductility, a structure responding once or many times to a value of maximum deformation would be assessed the same damage level. The maximum ductility is easy to use, however, and has been shown to be useful in computing modified spectra. The hysteretic energy concept is conceivably a more rational basis for damage determination but the level of allowable hysteretic energy is difficult to define at present, and for complex structures it is not easily estimated. Substantial experimental determination of allowable energy values would be required, or careful estimates of deformation modes based on existing knowledge, as well as revision of traditional design philosophy from an equilibrium to an energy approach.

Obviously other methods, or variations of the foregoing, must be developed to provide more information about the response in a convenient form for use in design. The following sections address two proposed approaches as a result of work undertaken as a part of this investigation. One damage measure is based on the equivalent hysteretic cycles computed from the response, the other measure stems from fatigue theory.

3.3 Structural Damage Measured as Equivalent Hysteretic Cycles

The number of hysteretic cycles that a structure undergoes while resisting earthquake ground motions can be employed as one form of

damage index. If the cycles were all identical in size, as shown by path **abcde** in Fig. 3.3, then the number of cycles actually counted during the response could constitute an index of the response strength. However, the response is often erratic resulting in partial hysteretic cycles, shown by path **abcfg** in Fig. 3.3, and full hysteretic cycles of different energy content shown by paths **abcde** and **abhie** in Fig. 3.3. Thus, the counted number of hysteretic cycles may be based on different cycle sizes and configurations. This difference from one cycle to another makes the actual counted number of cycles an inconsistent basis for damage evaluation.

One way to provide a more consistent measure of damage is to compute the number of equivalent, identical hysteretic cycles that would be needed to dissipate the actual total hysteretic energy. These equivalent cycles would be full cycles with identical configuration and energy content. The number of equivalent cycles would provide a quantitative measure of the cyclic nature of the hysteretic energy.

A displacement must be used, together with the yield resistance, to define the equivalent hysteretic cycle. Because no single displacement value was obviously superior to any other, three different equivalent hysteretic cycles based on different displacements were used as a part of this study. These displacements were the maximum displacement response, the yield displacement and the weighted displacement obtained from evaluation of the hysteretic energy pattern.

The maximum displacement obtained from the structural response calculations can be employed as the basis to define the equivalent hysteretic cycle, as proposed by Zahrah and Hall (72). The hysteretic energy content of this cycle is obtained by multiplying the yield

resistance by the difference of the maximum and yield displacements. The total hysteretic energy is obtained from the response calculations and represents the total area within the hysteresis loops. When the total hysteretic energy is divided by the energy in an equivalent hysteretic cycle, the number of Equivalent Maximum Deformation Hysteretic (EMDH) Cycles results,

$$\text{NUMBER OF EMDH CYCLES} = \frac{\text{TOTAL HYSTERETIC ENERGY}}{(R_{yield})(U_{max} - U_{yield})}, \qquad (3.2)$$

where R_{yield} is the yield resistance, U_{yield} is the yield displacement, and U_{max} is the maximum deformation. A "cycle" here is clearly for one-half of a full cycle and as will be noted later calculations are made for both positive and negative hysteretic energy. This equivalent hysteretic cycle is based on the maximum deformation response, a quantity that is readily obtained. However, this deformation may not be representative of the actual response. The maximum displacement may not have occurred in one cycle but may have resulted from plastic offset deformation from earlier response that added to deformations taking place later in the response. Thus, the maximum displacement value may not be the result of a single excursion, but the sum of several cycles. This situation will be evaluated in the following chapter.

A second equivalent hysteretic cycle definition investigated in this study was based on the energy corresponding to the yield displacement for the structure; the energy equals the elastic strain energy at yield. The number of Equivalent Yield Displacement Hysteretic (EYDH) Cycles were computed as,

$$\text{NUMBER OF EYDH CYCLES} = \frac{\text{TOTAL HYSTERETIC ENERGY}}{1/2\ (R_{yield})(U_{yield})} \quad . \tag{3.3}$$

The results of application of this equivalent cycle are presented in the following chapter. The yield displacement energy is a small value which results in a very large number of equivalent yield displacement cycles, much larger than the counted number of actual cycles. The difference between the number of equivalent and actual cycles made it difficult to relate this equivalent cycle to actual response. This equivalent cycle was found to be an unsatisfactory measure of response.

The third equivalent hysteretic cycle examined in this study is based on a weighted deformation intended to recognize the difference in damage caused by a lower number of large deformations versus a larger number of smaller deformations beyond yield. Furthermore, the weighted deformation also minimizes the effects of any plastic offset from prior response from biasing the size of the equivalent hysteretic cycle as is the case with the maximum deformation cycles. The weighted deformation was computed from the positive and negative deformation response as,

$$U_{wt} = \frac{\sum[(\text{HYSTERETIC ENERGY PER YIELDING EXCURSION}) * (\text{DEFORMATION PER YIELDING EXCURSION})]}{\text{TOTAL HYSTERETIC ENERGY}} \quad , \tag{3.4a}$$

to obtain separate positive and negative weighted deformation values with the number of Equivalent Weighted Deformation Hysteretic (EWDH) Cycles defined as,

$$\text{NUMBER OF EWDH CYCLES} = \frac{\text{TOTAL HYSTERETIC ENERGY}}{R_{yield}\,(U_{wt} - U_{yield})} \quad . \tag{3.4b}$$

Here again the "cycle" is based on independent calculations using positive and negative hysteretic energy so that the total hysteretic energy employed in Eq. (3.4) is either the total positive or total negative resistance hysteretic energy as appropriate.

These three equivalent cycle definitions were applied in the response calculation of structures subjected to various earthquake ground motions. The performance of this damage measure will be evaluated and discussed in the following chapter.

3.4 Structural Damage as Measured by Fatigue Criteria

3.4.1 Introductory Remarks

The deformation pattern of a structure responding to earthquake ground motions is composed of an oscillatory motion that is similar to the deformations that induce fatigue damage in metals. Therefore, it is reasonable to expect that the same types of conceptual models that have been helpful in predicting damage from fatigue might be applicable as a basis to assist in the development of a damage evaluation criterion for earthquake response. The following discussion addresses the general topic of fatigue damage and then a specific damage criterion for earthquake-induced damage is developed.

Several investigators have applied fatigue theory to evaluate the damage generated in structural response to earthquakes. These studies typically were not oriented towards producing design methods but were aimed at in-depth analytical studies of detailed input and response

time histories and the damage effects at specific local structural locations. Examples of these previous studies include Krawinkler (38) who applied fatigue theory to evaluate experimental data from tests of structural steel members and frames under reversing loads. Krawinkler compared the actual damage observed with that predicted by analytical models but did not develop a theory for design purposes. Suidan and Eubanks (66) applied fatigue theory to predict the damage sustained in a structure subjected to earthquake loading by employing the Rain Flow Method (17) to determine the exact strain cycle pattern. Their procedure is far too complicated for general design purposes. Other studies by Lashkan-Irvani (40), Fischer and Wolfe (18), Kasiraj and Yao (34) and Tang and Yao (67) employed fatigue theory in various forms to the structural response question.

These previous studies are important because the investigator recognized the similarity of the fatigue problem to damage accumulation in structures responding to seismic excitation. However, these studies did not present methods that could be used readily in design because the computational requirements were typically quite substantial and complex. Moreover, no application of fatigue theory to response spectra or other design applications were developed in these studies. Because response spectra are widely used in design, adaptation of fatigue concepts to the response spectra concept could be quite useful.

3.4.2 Fundamental Fatigue Damage Concepts

Basic fatigue information is obtained through extensive testing of structural elements. These tests involve applying perhaps many thousands or millions of identical, prescribed load cycles to the element until failure occurs. This process is repeated with a

replacement element, tested with a different load cycle amplitude, until the relationship between the amplitude of the load or stress cycle and the number of cycles required for failure is established for a wide range of amplitudes. This relationship is the S-N curve, an example of which is presented in Fig. 3.4. The S-N curve has gained wide acceptance and usage in fatigue application because of the information it provides and because of its simplicity.

If the individual stress cycles portrayed in the S-N curve for the high-cycle portion were examined, they would be found to be essentially elastic. Because each maximum stress amplitude would fall below the yield point, no perceptible damage would be caused by a single stress cycle. However, the material will be damaged and the structural element will fail when thousands or millions of identical stress cycles are applied. This type of fatigue is known as high-cycle fatigue, and occurs in situations involving many elastic stress cycles where each cycle incrementally damages the structure as is the case in machines, aircraft structures, and highway bridges. This type of fatigue clearly is not a source of damage resulting from seismic excitation.

During earthquakes the structural response is characterized by large, nonlinear displacements that occur over, at most, a few dozen to a hundred cycles. Obviously, in these situations, some type of damage process is at work stemming from deformation into the nonlinear region during each loading cycle, causing hysteretic energy generation and a greatly reduced fatigue life. This region, shown in Fig. 3.4, is known as low-cycle fatigue. The damage sustained is a function of the plastic deformation that occurs over a small number of load cycles. As the number of cycles is decreased, the amount of deformation that can

be withstood is increased. In the limit, a monotonic tensile test represents a low-cycle fatigue test were the load is applied once in only one direction until failure occurs.

There have been several studies that have proposed rules for fatigue life prediction in the low-cycle region. Typical of such studies is one by Yao and Munse (71) who proposed a low-cycle fatigue theory, valid up to 1000 cycles, based on a series of tests of steel samples in axial fatigue. The basic form of this theory is

$$\sum_{i=1}^{n} \left[\left(\frac{\Delta\epsilon_t}{\Delta\epsilon_{t_1}}\right)^{1/m}\right]_i \leq 1.0, \tag{3.5}$$

where $\Delta\epsilon_t$ = cyclic tensile change in plastic strain, percent,

$\Delta\epsilon_{t_1}$ = cyclic tensile change in plastic strain for failure in a single load application, percent,

m = the slope of the log $\Delta\epsilon_t$ versus log N (cycles to failure) diagram,

1/m = 1-0.86r, where r is the relative strain ratio of compressive strain to tensile strain.

This equation relates the accumulation of plastic strains as a function of the plastic failure strain in monotonic loading. The exponent reflects the shape of the strain cycle and the slope of normalized strain versus load application curve. When the summation reaches one, the material is damaged. The theory by Yao and Munse is complex and not readily applicable to design situations involving seismic excitation because of the nature and form of the calculations required.

Another fatigue criterion of greater applicability in this case was proposed by Manson (42) and Morrow (44) based on the damage contribution of plastic strain reversals in the low-cycle region combined with elastic stress reversals in the high-cycle region. This theory can be adapted for seismic application because of its form. The statement of Morrow's damage theory is

$$\frac{\Delta\epsilon}{2} = \epsilon_f' (2N_f)^c + \frac{\sigma_f'}{E} (2N_f)^b, \tag{3.6}$$

where ϵ_f' = fatigue ductility coefficient,

σ_f' = fatigue strength coefficient,

b = strength exponent ranging from -0.7 to -0.12 for most metals,

c = ductility exponent ranging from -0.5 to -0.7 for most metals,

$2N_f$ = number of load reversals to failure,

$\frac{\Delta\epsilon}{2}$ = maximum total strain amplitude required for failure in $2N_f$ reversals,

E = Modulus of Elasticity.

Examination of Fig. 3.5 reveals the meaning of the terms of this equation. One complete load cycle ($2N_f$) is composed of two load reversals. The fatigue ductility coefficient, ϵ_f', represents the plastic strain amplitude that causes failure in monotonic loading. The fatigue strength coefficient, σ_f', when divided by the Modulus of Elasticity represents the intercept of the elastic strain amplitude curve for one load reversal. The coefficients b and c are the slopes of the high and low-cycle fatigue curves, respectively. The equation

is stated in terms of load reversals for convenience and direct application to complex loading histories.

The total maximum strain, $\Delta\epsilon$ in Eq. (3.6) is the elastic plus plastic strain that will cause failure in $2N_f$ load reversals. The maximum total strain amplitude, $\Delta\epsilon/2$, is presented as one-half of the total because the amplitude of the strain from zero to the maximum strain is one-half of the total range from maximum to minimum, as shown in Fig. 3.6. All of the loading cycles are assumed to cause identical strain cycles.

3.4.3 Structural Fatigue Damage as Defined in this Study

The fatigue concepts presented above may be adapted to the seismic damage problem as described next using Morrow's theory because of its simple form. Morrow's relationship will be converted into a more usable form for structural applications and will be employed in a Damage Index parameter to define damage levels resulting from earthquake excitation. However, prior to presenting the details of the development of this damage criterion, a brief overview is in order. The basic fatigue theory cited contains contributing components of low and high-cycle fatigue. In Morrow's equation, the high-cycle term becomes important only in applications where the load reversals are well above 1000. Most earthquakes, however, induce load reversals in structures that are well below 1000 reversals. Therefore, the low-cycle term controls the damage generation in this region and the minor contributions of the high-cycle fatigue terms of Eq. (3.6) can be ignored. The low-cycle components can be modified to accommodate the earthquake response application because earthquake response resembles a low-cycle fatigue situation. Part of this modification involves

developing equations in terms of ductility instead of strain, because ductility normally is more easily estimated as part of structural response analysis. Once the theory has been tailored to suit the earthquake problem, an evaluation method can be presented so the level of damage and margin of remaining strength can be estimated.

Accordingly the remaining low-cycle term of Morrow's Theory can be expressed as follows,

$$\frac{\Delta\epsilon^*}{2} = \epsilon_f' \, (2N_f)^{-0.6}, \tag{3.7}$$

where $\frac{\Delta\epsilon^*}{2}$ = plastic strain amplitude (single) during cyclic response,

ϵ_f' = fatigue ductility coefficient,

$2N_f$ = number of load reversals to failure.

This equation relates the plastic strain amplitude, the load reversals and the fatigue ductility coefficient. The fatigue ductility coefficient, ϵ_f', represents the amount of strain that can be tolerated in monotonic loading. It is the upper limit of the possible plastic strain that can be withstood before failure and is experimentally determined. The plastic strain amplitude, $\Delta\epsilon^*/2$, is the amplitude of the identical strain cycles that damage the material. For one load reversal, the plastic strain amplitude is equal to the fatigue ductility coefficient. As the number of reversals increases, the amount of strain that can be tolerated over each of these reversals drops. In this equation, a value of -0.6 for the exponent on the load reversals term was selected based on published test data (44); it represents an average for metals and is typical for most steels. Studies by other researchers, notably those by Coffin and Tavernelli

(16) and Benham and Ford (9), have reported similar low-cycle fatigue damage relationships to those proposed by Morrow.

The next step is to convert the plastic strain relationship from Morrow into a form employing ductility, a more useful parameter for structural applications. The total ductility, μ, conceptually can be thought of as containing elastic and plastic components. The elastic portion, μ_e, has a maximum value of 1.0 corresponding to a generally yielded element. The plastic ductility, μ_p, has a value that is zero during elastic response and is greater than zero during nonlinear excursions. The total displacement can be computed by multiplying the total ductility, μ, by the corresponding yield displacement, Δ_Y. The applicable expression is as follows,

$$\frac{\Delta_T}{\Delta_Y} = \mu = \mu_e + \mu_p \ . \tag{3.8}$$

This relationship is illustrated in Fig. 3.7 and is based on equal positive and negative hysteretic cycles.

On the assumption that the elastic portion of the response is not responsible for structural damage during earthquake response, Morrow's fatigue relationship, Eq. (3.7), can be converted from plastic strain into an equivalent expression depending only on the plastic component of ductility. Specifically, the Morrow theory can be written in terms of a hysteretic plastic ductility, μ^*, that would cause damage over $2N_f$ reversals equivalent to that caused by a monotonic plastic ductility, μ_p. Therefore, the low-cycle fatigue behavior can be described in terms of ductility as

$$\mu^* = \mu_p (2N_f)^{-0.6}, \tag{3.9}$$

where μ^* = hysteretic plastic ductility,

μ_p = monotonic plastic ductility,

$2N_f$ = number of reversals to failure.

A detailed proof of this conversion is presented in Appendix D.

The equation is illustrated in Fig. 3.8. The reversals term, $2N_f$, reflects the number of times the structural velocity changes sign when the structural velocity decreases to zero and the structure unloads in the opposite direction. The number of velocity reversals are equivalent to the number of load reversals in a structure where the load is directly applied. It can be noted from Fig. 3.8 that as the number of load reversals is increased from the monotonic case, the hysteretic plastic ductility necessary to cause equivalent damage is reduced. This behavior reflects the fact that the accumulation of damage that occurs when the structure is cyclically loaded is strongly dependent on the amount of nonlinear deformation in each cycle. Large nonlinear excursions quickly damage the structure while slight nonlinear deformations may require many cycles to completely damage the structure.

The relationship between the monotonic plastic failure ductility and the hysteretic plastic ductility required to cause failure after a number of reversals could be directly applied if all of the hysteretic cycles were of identical size, as required by this damage theory. However, an earthquake is composed of random amplitude acceleration pulses so the response deformation in each cycle may be different, a complexity that is addressed next.

If the deformation amplitudes are of equal size, then each cycle would produce an equal amount of hysteretic energy. Because the deformations are not equal, some cycles will produce more hysteretic energy than others. For purposes of damage assessment, however, it is the overall process that is important and not just one cycle. The large and small deformations may be averaged to produce a median deformation that produces the total hysteretic energy during the load reversals. Once the hysteretic energy required for a completely damaged structure is determined, it can be compared then to the actual hysteretic energy dissipated using a form of Miner's Rule.

The hysteretic energy corresponding to the hysteretic plastic ductility, μ^*, can be computed based on Eq. (3.10) as developed next. This plastic ductility produces a completely damaged structure after $2N_f$ velocity reversals. The total amount of hysteretic energy dissipated during this response is the area under one cycle of hysteretic response times the total number of cycles of response. The area under one-half cycle of response is the hysteretic plastic ductility, μ^*, times the product of the yield displacement and yield resistance. There are N_f cycles where each cycle contains two of these areas or a total of $2N_f$. This relationship is illustrated in Fig. 3.9 and can be stated as,

$$HYST = \mu^* R_Y U_Y (2N_f), \tag{3.10}$$

where HYST = total hysteretic energy for a fully damaged simple structure,

μ^* = hysteretic plastic ductility,

R_Y = yield resistance,

U_Y = yield displacement,

$2N_f$ = number of reversals to failure.

Once the amount of hysteretic energy that corresponds to a fully damaged condition is established, it can be compared to the hysteretic energy actually dissipated. When the actual hysteretic energy meets or exceeds the fully damaged value, the structure is completely damaged. Comparison of actual energy values may not be convenient or easily performed. Possibly, a better way to present the level of damage would be to form a normalized ratio of actual hysteretic energy to total hysteretic energy for a fully damaged condition, similar to Miner's Rule (33).

The immediate question, if a Miner's Rule type of damage evaluation is employed, is whether or not the normalized relationship is linear, as in Miner's Rule, or is nonlinear. Experimental data from several sources provides evidence that this energy ratio is not linear, particularly where multilevel or random deformation response histories are concerned. For example, Richart and Newmark (62) explored the cumulative damage process for loadings applied at several different stress levels. Their research indicated that the damage level was related to the cycle ratio, that is the ratio of the number of cycles at a given stress level to the total number of cycles for failure, in a form,

$$D = R^n \ , \tag{3.11}$$

where D = damage level, where 1.0 corresponds to a fully damaged condition,

R = ratio of cycles at a stress level to the total number of cycles for failure,

n = cycle ratio exponent.

This relationship is illustrated in Fig. 3.10. Richart and Newmark determined that for the steels tested, the damage accumulation was not linear but approximately quadratic, that is with a value of n of about two.

Morrow also studied the rate of damage accumulation in various materials on the basis of plastic strain energy. His results were presented as a ratio of the plastic strain energy per cycle to the monotonic plastic strain energy at failure. The data from Morrow (44) suggests that the relationship between the number of reversals and this ratio of plastic strain energy per cycle to the failure plastic strain energy is not linear but approximately quadratic as well, namely

$$2N_f = \left(\frac{\Delta w}{w'_f}\right)^{1/(b+c)}, \qquad (3.12)$$

where $2N_f$ = number of reversals to failure,

Δw = plastic strain energy per cycle,

w'_f = monotonic plastic strain energy at failure,

b = material constant equal to −0.10,

c = material constant equal to −0.60.

In another study on cumulative fatigue damage, Landgraf (39) applied the Morrow theory to damage processes resulting from random deformation cycles. The accumulated fatigue damage was approached through the ratio of plastic to elastic strain ranges in each reversal. This relationship indicates that the damage accumulates during each

reversal approximately as the square of the ratio of plastic to elastic strain range, or

$$\text{Damage/reversal} = (1/2N_f)\ \left(\frac{\Delta\epsilon_p}{\Delta\epsilon_e}\right)^{1/b-c}, \tag{3.13}$$

where b = material constant equal to −0.10,

c = material constant equal to −0.60,

$\Delta\epsilon_p$ = plastic strain range,

$\Delta\epsilon_e$ = elastic strain range.

The results from these studies indicate that the cumulative damage relationship is approximately quadratic, and is consistent with the findings of other researchers including Yao and Munse (71). The exact value is not important in this particular investigation and is probably a function of several parameters. For purposes of defining a plausible relationship for cumulative damage, a quadratic relationship was assumed. This approach corresponds to modifying Miner's Rule to the form

$$D = \sum\left(\frac{n_i}{N_i}\right)^2, \tag{3.14}$$

where D = damage level,

n_i = number of cycles at stress level i,

N_i = number of cycles required for failure at stress level i.

In this form the fraction of the fatigue life exhausted within a block of cycles at a discrete stress or strain range is computed, squared and added to the square of the other fractions.

The form of Eq. (3.14) could be employed directly if the earthquake response could be defined in terms of discrete strain blocks. However, the response amplitudes change in a random pattern and cannot be defined easily in the form needed with the modified Miner's Rule. This difficulty was overcome by assuming that the entire earthquake response represented one block of response, so the summation of Eq. (3.14) could be represented by a single quadratic term. Furthermore because the actual response is difficult to characterize in terms of deflection, the hysteretic energy was used to represent the level of response. The total hysteretic energy corresponding to the damage sustained at the specified monotonic plastic ductility can be computed from Eq. (3.10). The total hysteretic energy actually absorbed can be computed from the structural analysis as the sum of the positive and negative resistance hysteretic energies (Fig. 3.11). Based on these hysteretic energies, a Damage Index can be defined as

$$\text{Damage Index} = \left[\frac{\text{HYSP} + \text{HYSN}}{\text{HYST}}\right]^2, \tag{3.15}$$

where HYSP = Total Positive Resistance Hysteretic Energy,

HYSN = Total Negative Resistance Hysteretic Energy,

HYST = Total Hysteretic Energy for a fully damaged structure, Eq. (3.10).

This concept is illustrated in Fig. 3.11. When the Damage Index reaches 1.0, the structure is considered damaged to a level corresponding to the monotonic plastic ductility, μ_p, specified in Eq. (3.9).

An enhancement of this relationship can be made by observing that the level of damage also is a function of the balance between the

positive resistance hysteretic energy, HYSP, and the negative resistance hysteretic energy, HYSN. A structure that responds with unequal amounts of positive and negative resistance hysteretic energies will experience more residual drift, and thus more damage, than a building subjected to equal hysteretic energies as discussed in the previous chapter. For purposes of this study, a comprehensive Damage Index is proposed that addresses the total hysteretic energy as well as relative sizes of the positive and negative resistance hysteretic energies or

$$\text{Damage Index} = \left[\frac{\text{HYSP} + \text{HYSN}}{\text{HYST}}\right]^2 + \left[\frac{\text{HYSP} - \text{HYSN}}{\text{HYST}}\right]^2, \qquad (3.16)$$

where the terms are as defined earlier. When the Damage Index reaches 1.0, the structure is considered to be completely damaged; that is, damaged to an extent corresponding to the monotonic plastic ductility. The second term of Eq. (3.16) is nearly zero for most cases, except when HYSP and HYSN are significantly different in magnitude, representing the additional damage from unequal hysteretic energy distribution.

The margin of safety can be computed once the Damage Index is known. The total of the Margin of Safety and Damage Index must equal one, so the Margin of Safety can be defined as,

$$\text{Margin of Safety} = 1.0 - \text{Damage Index}. \qquad (3.17)$$

When the Damage Index reaches one, the structure is assumed to be completely damaged and the Margin of Safety is zero. This procedure

permits the designer to assess the margin in a quantitative manner and provides a basis for engineering judgment.

In summary, two damage criteria were presented in this chapter. One criterion (Section 3.3) was based on representing the total response to the earthquake, as obtained from the hysteretic energy, in terms of complete and identical hysteretic cycles. The second criterion (Section 3.4) is based on low-cycle fatigue and permits the designer to convert a monotonic plastic ductility into a hysteretic plastic ductility that causes equivalent damage under cyclic loading and to estimate of the margin of safety that remains.

The procedures defined in this chapter are design oriented. The relationships represent a philosophy that is consistent with the current emerging design philosophy such as that found in the fatigue provisions of the American Institute of Steel Construction steel specifications. As such, the methods proposed here are not as complicated to use as other procedures that have been previously developed and do not represent a significant compromise of accuracy. These procedures will be employed in the following chapter and compared to existing damage measures.

CHAPTER 4

EVALUATION OF STRUCTURAL DAMAGE CRITERIA

4.1 Introduction

The presentation in this chapter consists of a demonstration of the damage criteria developed in Chapter 3 and their applicability to the response of simple structures. The demonstration involves evaluation of the reasonableness of the criteria through their application to specific situations, especially laboratory results. As will be subsequently observed, the applications indicate that these criteria are good predictors of damage levels. As such they definitely have the potential for application to damage assessment procedures that may be incorporated in future building code provisions.

Specifically, this chapter contains material concerning the two damage criteria developed in the previous chapter. The next section contains a review and comparison of damage as described by the three equivalent hysteretic cycle definitions. The second section thereafter contains a comparison of the fatigue-based damage criterion with actual test data from experiments. This evaluation provides confirmation of the applicability of the damage theory by direct comparison of the predicted damage with that obtained by tests. As a by-product of the foregoing, specific design applications of these damage criteria are developed and discussed in the following chapter.

4.2 Evaluation of Performance of the Equivalent Hysteretic Cycles as a Damage Measure

The first damage measure to be evaluated is the equivalent hysteretic cycle concept wherein the total amount of hysteretic energy is converted into a number of identical, complete hysteretic cycles. The evaluation of this damage measure involves two factors, the first is the concept of an equivalent hysteretic cycle and its usefulness as a damage measure, and the second is the definition employed to define the size of the hysteretic cycle.

Three different definitions, as presented in Chapter 3, are employed to calculate the number of equivalent hysteretic cycles. These concepts center around the maximum displacement achieved during the response, the yield displacement and the weighted displacement; each one involves a definition of the cycle size and the amount of hysteretic energy content per standard cycle. The number of cycles is obtained by dividing the total amount of hysteretic energy dissipated by the energy content per cycle.

The evaluation in the case of the hysteretic cycles as a damage measure was carried out for earthquake records only. One may wonder why this evaluation method was not employed for uniform cyclic excitation; the reason is that in this case the number of cycles can be obtained directly by counting and in fact this is part of the evaluation process for the experimental data studied in subsequent sections. Accordingly, the hysteretic cycle concept was applied only in the earthquake case.

As noted in Chapter 2, detailed studies were made for seven earthquakes with the key results for three earthquakes, El Centro,

Pacoima Dam and Melendy Ranch, summarized therein. Similarly, in this chapter the detailed studies employing hysteretic cycles as a damage measure were carried out for all seven earthquakes and a detailed summary of these studies is contained in Appendix B. For purposes of illustrating the trends exhibited by these detailed calculations, a sampling of results for El Centro, Pacoima Dam and Melendy Ranch are presented in Table 4.1. The table entries include the total positive and negative resistance hysteretic energies, the number of counted yield excursions and the computed numbers of equivalent hysteretic cycles based on the three cycle definitions. Results are presented for structural frequencies of 0.5, 2.0, and 5.0 hz with zero percent damping.

The values of hysteretic energy are approximately symmetric between the positive and negative resistances and are a function of both the structural frequency and the excitation. It is to be recognized that the tabulated hysteretic energy can vary from being a small fraction of the total input energy to accounting for nearly all of the input energy; such comparisons can be made from the data in the appendix. The important thing to note here is that the hysteretic energy is the component related to damage. Larger values of hysteretic energy indicate more severe response and a greater potential for damage to the structure than smaller hysteretic energies.

However, present design philosophy is not oriented towards energy-based design, in time such methods may enter building codes as the phenomenon is better understood. Irrespective of that observation, in order to convert this response into a more usable form to provide the designer with information regarding the cyclic nature of the response,

the number of equivalent hysteretic cycles can be computed from the three cycle definitions developed in the previous chapter. Typical results of this conversion to equivalent cycles are presented in Table 4.1 as is the number of counted yield excursions, which is the actual number of times the yield resistance value was attained. The number of counted yield excursions is normally larger than the number of equivalent hysteretic cycles because the actual hysteretic response is erratic, composed of cycles of different sizes that are not all complete. If all of the hysteretic cycles were complete and of equal size, then the number of counted yield excursions and the number of equivalent hysteretic cycles computed from the maximum or weighted deformation equivalent cycle would be the same; the results using the yield deformation would not compare because this cycle is not based on the actual response.

Moreover, the difference between the equivalent hysteretic cycles and the number of actual yield excursions is one measure of the random nature of the response. For example, large numbers of counted yield excursions together with low levels of hysteretic energy, indicate that the structural response was not forming complete hysteretic cycles. Conversely, low numbers of counted yield excursions occurring with large hysteretic energy values indicate that the hysteretic cycles were large and complete, and may well be more damaging to the structure than the former situation.

It will be noted that in general, as the number of yield excursions increases, the maximum deformation basis produces the smallest number of equivalent hysteretic cycles while the weighted deformation produces a more average number of cycles, one that

addresses the features of the response and is probably the more realistic equivalent cycle basis. The number of equivalent cycles computed employing the energy at the yield displacement normally produces a very large number of equivalent cycles that may exceed the actual number of yield excursions by a large margin, and in some cases may exceed one thousand. This equivalent cycle was not found to be a realistic basis with which to estimate the cyclic nature of the response. Accordingly, although the equivalent yield displacement hysteretic cycles are presented in Table 4.1 and again in Appendix B for the various cases, because of the unrealistic nature of this counting technique, no further discussion of this equivalent cycle is presented in this dissertation.

In summary, the computation of the hysteretic energy is one measure of the strength of the response. Computation of the number of equivalent hysteretic cycles provides the designer with a measure or estimate of the number of complete hysteretic cycles of response that may occur. The number of cycles permits the appropriate steps to be taken in the structural design to ensure that members and connections are able to withstand the commensurate amount of cyclic response.

Although this damage measure is not pursued further in this dissertation, it is believed that it will have a place in the future as a part of the design procedures and philosophy contained in the next generation of building code provisions. The number of cycles of deformation, as well as hysteretic energy, are inherently a major factor in the nonlinear deformation process; accordingly the concepts must be reflected as a part of rationally developed procedures. The concept is not completely dismissed in the next development centered

around low-cycle fatigue theory in that the number of cycles and strength of each cycle are employed there, and are directly related to hysteretic energy. Thus, this type of damage measure is indirectly an important part of the following discussion as well.

4.3 Evaluation of Fatigue Damage Index Criterion Against Experimental Data

4.3.1 Introduction

The literature was reviewed to identify the previous experimental studies containing data that could be used to verify the accuracy of the proposed low-cycle fatigue damage criterion. Several studies were found in which structural steel specimens or complete steel members were tested under cyclic loading. In the following discussion, the term specimen will refer to small steel test samples or coupons removed from a full size steel member for fatigue testing. The results of these studies were compared against the predicted results obtained from the fatigue Damage Index criterion proposed herein. These comparisons are divided into three sections concerning data from fatigue tests of small steel specimens, data from tests of actual steel members and data from fatigue tests of steel members of large flange aspect ratio subject to local buckling behavior. In the majority of the reported experiments, the fatigue cycling was continued until a complete failure of the specimen or member occurred. Therefore, in the following discussion the term failure refers to a loss of load carrying capability of the member or a loss of functional capacity. Of course in design, this complete loss of capacity would not be acceptable and a

lower level of damage would have to be employed so that a margin of safety against complete failure would exist.

4.3.2 Evaluation Based on Data from Small Fatigue Test Specimens

The first group of experimental studies to be reviewed are those involving tests of structural steel specimens under cyclic loading. The comparison of the experimental results from Yao and Munse (71), where they proposed a comprehensive fatigue damage law based on low-cycle axial fatigue tests of steel specimens, with those predicted by the Damage Index concept from this study are shown in Table 4.2. The comparison reveals close agreement between the number of cycles to failure obtained experimentally with the predicted results from this study. It must be noted that under simple, cyclic loading of the type employed by Yao and Munse, the Damage Index, which becomes one at failure, is not needed in the analysis because all cycles are of equal size and shape and the low-cycle fatigue damage relationships can be applied directly.

Sawyer (64) presented data obtained from Welding Research Council-supported research into low-cycle fatigue behavior of typical structural steels. These experimental results are compared with the predicted values from this study in Table 4.3. As before, for complete damage using identical fatigue cycles, the fatigue damage relationships can be applied directly and the Damage Index attains a value of one for reasons just discussed. The results from experiment clearly follow the trends predicted by the fatigue damage criterion proposed in Chapter 3.

The next two tables concern the experimental work performed as a part of this study involving a small scale steel structure as summarized in Appendix A. In Table 4.4 there is presented the numbers

of cycles, each at a hysteretic plastic ductility value, μ^*, of 1.88, required for failure when plastic failure strain values varying from five to thirty percent are assigned. The actual monotonic failure strain was found by separate tensile test to be about twenty-four percent, which corresponds to about seven cycles of loading at this hysteretic plastic ductility.

In Table 4.5 there is presented the number of full cycles, each at a hysteretic plastic ductility value of 1.88, that produces the same damage as the various combinations of monotonic plastic ductilities, μ_p, and Damage Index values. As observed and expected, a larger monotonic plastic ductility results in a larger number of cycles to reach the specified damage level. Moreover, increases in the Damage Index value result in more cycles of response that can be absorbed for any monotonic plastic ductility. All of which are in support of the theory being evaluated and indicate that a ductile member is more capable of absorbing damage from cyclic motion than a brittle member.

4.3.3 Evaluation Based on Data from Actual Structural Members

The preceding data were developed from tests of small steel specimens representative of the material utilized in structures. This information is important, however, the behavior of actual steel members must be evaluated to ensure that this low-cycle fatigue theory correctly predicts the damage absorbed in actual structures. Any damaging effects arising from the arrangement and size of the member or its components, which are not significant in small steel specimens, are potentially prominent components of the behavior of steel members and elements under nonlinear behavior and must be included in the evaluation of this damage criterion. The results presented in this

section do not include local buckling, fatigue tests of members that experienced this behavior are the subject of the following section.

The literature was reviewed to identify experimental studies where actual steel members were cyclically loaded to failure, that is loaded until either the load capacity was lost or the member became functionally unacceptable. ASCE (1), Beedle (8) and Hodge (22) provided a useful foundation for this investigation. This search was difficult in that frequently not enough data were provided by the authors, or the test procedure was not adequate, to permit a proper evaluation against the damage theory developed in this study. In general, the agreement between the experimental and theoretical results is good. This conclusion can be confirmed by reviewing Tables 4.6 to 4.12 and the brief discussion of these tables that follows.

The data from Popov and Pickney (59,60), summarized in Tables 4.6 and 4.7, involved fatigue tests of cantilever wide-flange sections and is helpful because the testing was preceded by a nearly monotonic test of a similar section. The data are evaluated in Table 4.6 based on the results of three and one-half cycles of loading, with all of the displacement cycles occurring in one direction, rather than fully reversed loading. The results reveal that the equivalent monotonic loading can be computed using the Damage Index concept together with the fatigue theory. A total tip deflection of 9.5 in. imposed during loading, unloading, and reloading in the same direction generates about 100 in-kips of hysteretic energy. This loading pattern produces damage equivalent to 456 in-kips of hysteretic energy if the beam had been loaded in one direction monotonically.

The equivalent monotonic hysteretic energy was utilized in Table 4.7 as the basis to evaluate the other tests conducted by Popov and Pickney (59,60). These tests involved alternating load cycles of constant amplitude until fatigue failure occurred. The last two columns of this table reveal the comparison of the experimental results with the theoretical predictions. Here, the ratio of the hysteretic energy dissipated under cyclic loading to the hysteretic energy dissipated in monotonic loading is compared to the ratio of hysteretic to monotonic plastic ductilities predicted by theory. It can be seen that the theory closely predicts the actual behavior of the section under the load reversals. The damaging effects of the load reversals on the structure can be observed as the fraction of monotonic capacity drops with increasing numbers of load reversals.

Popov and Stephen (61) tested two different sizes of wide-flange beams connected to column stub assemblies where the beams were loaded cyclically until a fatigue failure occurred. A summary of the evaluation of this data is contained in Table 4.8. The actual hysteretic energy dissipated during testing was computed from the experimental results and was used to determine the number of hysteretic cycles of identical size required to dissipate this energy. Hysteretic cycles of either 2.0 or 2.5 in. total displacement were assumed for calculational purposes. From this assumed displacement and the yield load, the number of reversals, $2N_f$, can be computed as shown in the table (see Appendix D for background theory). For the assumed total displacement amplitude, an equivalent hysteretic plastic strain, ϵ^*, can be computed using plastic hinge theory as shown in Note 7 of the table. The equivalent monotonic plastic strain can be computed using

the fatigue theory as shown in Note 8. These results indicate that the computed monotonic plastic strain is a realistic value in the range of 10-20 percent, depending on the section. This analysis procedure is typical of the evaluation of experimental data when no firm monotonic plastic failure values are provided, but must be inferred from the results. Plastic strain values were used here but are essentially equivalent to ductility values as shown in Appendix D; strain was utilized because of the ease of calculation of plastic hinge rotations for this data.

Another study of interest is one performed by Krawinkler and Zohrei (37) which involved testing of cantilevered W4 x 13 steel sections under cyclic loading until failure occurred. The experimental results suggest a Morrow-Manson type relationship for failure,

$$N_f = 0.0198(\Delta\epsilon_p)^{-2.12} ,$$

where N_f is the number of cycles to failure, $\Delta\epsilon_p$ is the plastic strain range in each cycle and the constants were found from the experimental data. This result can be converted into a relation similar to that presented herein in terms of reversals and plastic strain amplitude as

$$2N_f = 0.0396(\Delta\epsilon_p)^{-2.12} ,$$

or by multiplying by $(\frac{2}{2})^{-2.12}$ and simplifying, the final result is obtained

$$\frac{\Delta\epsilon_p}{2} = 0.109(2N_f)^{-0.470}.$$

This result is similar to that obtained by Manson-Morrow and adapted for use in this study. The relationship shows the close link between the results from steel specimen tests and those from tests of actual steel members.

Popov and Bertero (58) reported separate test results for W24 x 76 beams attached as cantilevers to stub columns, and as simply supported beams with 7.5 ft. columns attached at the beam midspan position. In both test series, the beams were cyclically deformed until a fatigue failure occurred. No monotonic failure data was provided; thus in Table 4.9 a plastic hinge analysis was employed to convert an assumed value of maximum monotonic strain into a monotonic deflection that could be used in the fatigue analysis. The results presented in this table clearly indicate that the analysis procedures provide theoretical predictions of fatigue life that are quite close to the experimental values. It must be noted that because the loading cycles were identical, the Damage Index criterion was not needed and the fatigue damage relationship could be applied directly. Moreover, the analysis uses both strain and ductility terms because the ratio of hysteretic to monotonic plastic strain is equal to the ratio of hysteretic to monotonic plastic ductility.

A similar study was reported by Bertero, Popov and Krawinkler (12) in which beam and column assemblies were cyclically loaded through the column producing plastic hinge rotations in the beams. The evaluation of this data is contained in Table 4.10. No monotonic failure results

were provided so a maximum monotonic plastic strain of twenty percent was assumed and the corresponding hinge rotation was computed. By using the fatigue damage criterion, the number of identical hysteretic cycles required to equal the damage from the assigned monotonic plastic strain was calculated. The results from theory correlate well with the experimental results.

Similar results are presented in Table 4.11 based on tests performed on beam-column assemblies by Popov et al. (56). These evaluations follow the same procedures as before where monotonic strain values were assumed because no monotonic failure values were provided. Popov measured the amount of deflection caused by shear strain in the beam panel zone. For this particular section orientation, the shear deflection could not be ignored and was subtracted from the overall deflection so the correct fatigue results could be obtained. The test reported in Table 4.11a involved constant amplitude cyclic loading so the fatigue theory could be applied directly. The second test summarized in Table 4.11b involved variable amplitude cyclic testing and thus required the calculation of the hysteretic energy dissipated and an equivalent hysteretic plastic ductility required to dissipate the same amount of hysteretic energy over the assigned number of 18 reversals. The analytical results for both tests are in close agreement with the results provided by Popov.

Krawinkler et al. (38) compiled data from various sources regarding the cyclic behavior of various steel members. Two particular test series involving the cyclic testing of W4 x 13 sections were presented in the form of a low-cycle fatigue relationship as

$$N_f = 0.0304(\Delta\epsilon_p)^{-1.99},$$

where N_f is the number of cycles to failure and $\Delta\epsilon_p$ is the plastic strain range per cycle. This equation can be converted to an expression of reversals and plastic strain amplitude of the form

$$(2N_f) = 0.0608(\Delta\epsilon_p)^{-1.99},$$

or by multiplying by $(\frac{2}{2})^{-1.99}$ and simplifying, the final result is obtained as

$$\frac{\Delta\epsilon_p}{2} = 0.1224(2N_f)^{-0.502}.$$

This result is similar to the fatigue criteria reported by Morrow for steel specimens tested under fatigue loading. Thus, the application of the Morrow theory as a design basis for structural members subject to fatigue appears reasonable.

Additional data from Krawinkler (38) can be evaluated using the fatigue theory developed in this study. One particular test series in this study involved various W4 x 13 sections loaded montonically and other sections subjected to cyclic testing to failure. These sections did not undergo local buckling during the testing. The first set of results was evaluated in Table 4.12 where a monotonic plastic strain of 25 percent was computed, corresponding to the maximum monotonic tip deflection of 12 in. actually applied.

Krawinkler tested the other sections to failure under constant maximum deflection amplitude cyclic loading, where the maximum amplitude was different for each separate test. This change in deflection amplitude resulted in different fatigue lives for these test

specimens as reflected in the numbers of reversals to failure. For comparison purposes, various values of monotonic plastic strain ranging from 20 to 40 percent, and including the actual value of 25 percent computed from the monotonic data, was employed to compute the corresponding monotonic plastic ductility, μ_p. These values of monotonic plastic ductility were used then to compute the values of hysteretic plastic ductility, μ^*, corresponding to the number of reversals involved. The results noted in Table 4.12 indicate that a monotonic plastic strain value of 25 percent would correspond to a conservative value of hysteretic plastic ductility that would induce an equivalent damage level over the number of reversals. A value of 30 percent would more closely match the data.

Based on the different studies that have been evaluated, the design approach developed in this study has every appearance of providing a reasonable basis for assessing the damage caused by cyclic loading of steel members. The difference in behavior between steel test specimens and full-size steel members has been found to be small and can be ignored. Thus, the Morrow-based fatigue damage criterion for small steel specimens can be used to predict the degradation of actual structural members subjected to cyclic loading. Moreover, in situations where variable amplitude cycles are involved the Damage Index concept, which is based on hysteretic energy, was found to predict adequately the behavior and fatigue life of these members.

4.3.4 Evaluation Based on Data from Actual Structural Members Where Local Buckling Occurred

One major problem that occurs in actual members is local buckling of the flanges. The previous studies involved actual members of small

flange aspect ratio, b/t, so that failure occurred through fatigue of the material with no significant complications from local buckling. Yet, local buckling can occur and must be evaluated against the fatigue-based design procedure developed herein. However, one should note in those cases in earthquake engineering where adequate provisions have been taken for strong cyclic response, smaller flange aspect ratios are employed so the possibility of local buckling is reduced.

Several studies were identified where slender wide-flange members were loaded cyclically and where local buckling was observed. These tests were continued after the onset of local buckling until failure occurred by fatigue. The presence of flange buckling obviously changes the member behavior and the damage accumulation under the cyclic loading. The question is whether or not the proposed design method adequately represents the material behavior when fatigue is aggravated by local buckling.

Krawinkler et al. (38) published data for W6 x 9 sections that were cyclically loaded. These sections possessed a larger flange aspect ratio than did the W4 x 13 sections discussed earlier and experienced severe local buckling during the tests. The results of the tests in terms of cycles or reversals to failure, are contained in Table 4.13 together with the predicted results from the fatigue-based theory. Two W6 x 9 sections were monotonically loaded to 6.1 and 8.5 in. corresponding to a monotonic plastic ductility ranging from 19 to 27. When this value of the monotonic plastic ductility is employed in the fatigue theory to predict the number of reversals to failure, the computed number of reversals are higher than the test data. This situation suggests that additional damage is caused by local buckling

resulting in a faster rate of degradation than occurs without local buckling. If the monotonic plastic ductility is reduced to 16, in recognition of the effect of local buckling, a result reasonably close to the data is obtained. A further reduction of the monotonic plastic ductility to a value of 10 produces results that match the smallest hysteretic plastic ductility value and conservatively underestimate the others. Clearly, the addition of local buckling changes the relationship between damage and the number of reversals; the most probable change is in the value of the exponent on the reversals term which changes the slope of the reversals-ductility relationship. However, the proposed method can be used to estimate the effects of cyclic loading on members subject to local buckling so long as adequate care is exercised to specify a monotonic plastic ductility value that results in conservative results for all cyclic loading cases.

The results of tests by Popov and Pickney (59,60) were evaluated previously in Table 4.6. The experimental results indicating the reversals to failure relationship was found to be closely predicted by the fatigue damage theory developed in this study. These sections were observed during the testing to locally buckle to some degree at a tip deflection of about two inches. During the cyclic loading, the flange buckles were straightened and re-buckled until failure occurred. Obviously, the effects of the local buckling on this particular test series was not severe enough to affect the overall fatigue behavior and the close agreement between the test data and the fatigue damage relationship.

As a cross check of the overall procedure using plastic hinge theory, the reported 2 in. tip deflection was employed and the flange

strains were determined to verify that this strain would be sufficient for local buckling. As shown in Table 4.14, the predicted strain of 2.37 percent is sufficient to cause local flange buckling as reported by ASCE (1).

This result can be further confirmed by test data from Bertero and Popov (11) where 4M 13 sections were mounted as cantilevers and subjected to fully reversed cyclic loading. These sections were slender with flange aspect ratios that varied from 8.8 to 12.7. The beams were loaded to specified values of flange strain that varied from 1.0 to 2.5 percent as measured at the fixed end. Separate plots of the number of cycles for the onset of local buckling and for the onset of total failure as a function of the maximum flange strain were produced. The data can be converted into a fatigue life equation for local buckling and fatigue failure as follows for local buckling failure,

$$N_f = 2.8 \times 10^{-6} (\Delta\epsilon_p/2)^{-3.5},$$

and for fatigue failure,

$$N_f = 2.9 \times 10^{-4} (\Delta\epsilon_p/2)^{-3.0}.$$

Both of these relationships are in terms of the complete cycles to failure, N_f, the plastic strain amplitude per cycle, $\Delta\epsilon_p/2$, and the constants from the data. These expressions can be converted into a similar form to that employed in this study by transforming the expressions from cycles to reversals, $2N_f$. This transformation results in new expressions for the local buckling failure,

$$(\Delta\epsilon_p/2) = 0.0316(2N_f)^{-0.286},$$

and for fatigue failure,

$$(\Delta\epsilon_p/2) = 0.0834(2N_f)^{-0.333}.$$

Both expressions are of the same form as that proposed in this study. The reversals term in these expressions, when raised to powers of -0.286 and -0.333, results in a larger value than that obtained from the reversals term from this study which uses an exponent of -0.6. Thus, the results from the proposed fatigue damage criterion would be conservative even though local buckling was not specifically addressed.

On the basis of the material presented in this section the fatigue damage criterion has been demonstrated to be an extremely effective approach for incorporating the effects of cyclic response of a structure subjected to earthquake motion. The fatigue relationship employed was originally based on material tests of steel specimens but was found to accurately predict the fatigue life of structural members and thereby could be employed as a damage measure. The effects of local buckling were found to change the experimental behavior in some cases, but the fatigue damage concept can be used to predict the overall fatigue life without significant error. Moreover, it is to be appreciated that well-designed structures preclude local buckling for these limited strain values. The tests where variable amplitude loading was employed permitted the Damage Index to be used and verified against the experimental results. The Damage Index and its hysteretic

energy basis were demonstrated to be a sound criterion and resulting in accurate prediction of fatigue life under complex loading.

In conclusion, fatigue damage and the Damage Index theory based on Morrow's work were found to be effective techniques to evaluate cyclic response and structural damage. There is every reason to believe that this type of approach will form at least one basis in the next generation of building codes for arriving at consistent design procedures for building structures subjected to earthquakes. More specifically, it is to be noted that design will not be made to the same damage level but instead the design will be made in such a manner that if damage does occur, it is predictable and thus accounted for, hopefully explicitly, as part of the design procedure. Techniques such as this when applied to frame structures will go along way towards providing a higher degree of reliability for carrying loads and less uncertainty in predicted response.

4.4 Conclusions About the Damage Criteria Evaluation

The results and comparisons presented in this chapter reveal that the damage criteria developed in Chapter 3 are accurate, effective means of quantifying damage. These procedures enable the designer to obtain a more complete description of the resulting damage from an earthquake than that provided by traditional means. The equivalent hysteretic cycles permit the conversion of the hysteretic energy into a measure of the strength of the cyclic response, thus enabling the engineer to address this response in the design of the members and connections.

A perhaps more useful damage criterion is provided by the Damage Index and its low-cycle fatigue basis. This criterion permits the well-used ductility concept to be accurately modified to account for the significant damage caused by nonlinear cyclic response. The resulting hysteretic plastic ductility reflects the entire response, not just the peak response value. The experimental results confirm that the structural damage obtained in the laboratory can be correctly predicted by the Damage Index. Moreover, this procedure is easily applied and can be useful in design situations.

These results point to the improvements that can be made in design methods and philosophy. More than peak values of response must be addressed in design if more predictable and controlled response is the goal. The damage criteria evaluated in this chapter illustrate that improved methods can be accurate and readily usable in a design environment. This topic is explored in greater detail in the following chapter where design applications are explored.

CHAPTER 5

DESIGN APPLICATIONS OF THE DAMAGE CRITERIA

5.1 Introduction

The ultimate goal of any research aimed at improved design methods is to produce new procedures that can be readily applied to design and yet lead to more accurate and efficient final products. The damage criteria were shown in the previous chapter to be accurate measures of the damage sustained by simple structural elements in response to earthquake excitation. The question may be asked as to how these criteria could be employed in the design of structures. The purpose of this chapter is to illustrate three possible applications of these criteria.

Structures can be analyzed and designed using response time history analysis, response spectra concepts or pseudostatic building code procedures. The sections that follow contain application of the damage criteria for each of these three types of analysis. The equivalent hysteretic cycles and Damage Index concepts will be employed to evaluate hysteretic energy results from response time history results. The Damage Index will be used as a basis to construct inelastic response spectra. Finally the Damage Index, and its fatigue basis, will be employed to illustrate the development of a proposed maximum drift criterion to supplement present drift limits found in building codes.

These applications represent demonstrations of the possible ways that the concepts developed here can be applied to structural design. With additional development, these methods can be extended to the more

complex structural systems commonly used. It is not the intent of this study to examine all of the possible applications, but rather to provide a sound foundation to permit development of these new procedures.

5.2 Application of the Damage Criteria to the Evaluation of Response Time History Results

The hysteretic energy computed during response time history analysis has been shown to be a useful description of the behavior. This energy parameter provides the designer with a measure of the overall severity of the inelastic response. Because the hysteretic energy is representative of the nonlinear response, this parameter is more characteristic of the response history than the single maximum displacement or ductility value.

The hysteretic energy has a drawback in that there are no allowable energy values, nor any design or analysis procedures which presently can utilize hysteretic energy. Because of this lack of information, hysteretic energy has been used primarily in research where it provides valuable insight into nonlinear response. However, through application of the damage criteria developed in this study, the hysteretic energy can be adapted to the design process. This application of hysteretic energy can be accomplished in two ways.

The first application involves the use of the equivalent hysteretic cycle definitions to convert the energy into a measure of the severity of the cyclic response. The computed number of equivalent hysteretic cycles can be employed to ensure that members and connections have adequate ductility capacity to withstand the cyclic

response. This evaluation would serve to provide increased safety in the structural design because not only the deformation was addressed but also the estimated number of cycles that could occur. The results of this type of evaluation were discussed earlier in conjunction with Table 4.1.

The second way to adapt the hysteretic energy for design purposes is through application of the Damage Index. The procedure developed in Chapter 3 allows the monotonic plastic ductility corresponding to a fully damaged condition to be converted into a hysteretic plastic ductility that accounts for the number of reversals sustained and the damage caused by these reversals. This hysteretic ductility was utilized in the computation of the hysteretic energy corresponding to the plastic ductility value occurring over a specified number of reversals. The Damage Index was presented to compare this computed value with the actual dissipated hysteretic energy.

To illustrate the use of these concepts, the response data discussed in Chapter 2 was reviewed and the results for damped response to the El Centro and Pacoima Dam records were selected for evaluation. The actual hysteretic energies were compared against computed hysteretic energies corresponding to specified monotonic plastic ductilities; the Damage Index was computed as a result. The computations are presented in Tables 5.1 and 5.2 for the El Centro and Pacoima Dam records, respectively.

The results show that the Damage Index can be employed to provide a comparison energy value for evaluation purposes. Without the comparison hysteretic energy value, the parameter HYST in these tables, the energy values are illustrative of the response but are not in a

form that a designer could use. By comparing the dissipated values to the HYST value, the Damage Index provides the designer with a basis for estimating how much of the capacity of the member has been used in responding to the earthquake.

The actual values presented in Tables 5.1 and 5.2 reflect the amount of response computed as a function of the record and of the structural frequency. The yield resistances were all set to 100 lb and the damping was five percent throughout. The monotonic plastic ductilities ranged from 0.5 to 5.0 which are realistic values. The resulting Damage Index values are illustrative of the fact that the damage levels vary strongly with frequency and with the monotonic plastic ductility value. Moreover, in some cases the structures would be heavily damaged, as in the higher frequency structures with lower monotonic plastic ductilities. Lower damage levels are sustained for structures with larger values of monotonic plastic ductility, which corresponds to the classic definition of a ductile structure.

The next step in the design process would be to vary the yield resistance, or yield displacement, and compute the Damage Index, repeating this process until a desired level of damage is reached. This procedure is discussed in the next section in conjunction with construction of inelastic response spectra based on the Damage Index concept.

5.3 Application of the Damage Index to the Construction of Inelastic Response Spectra

The purpose of this section is to apply the Damage Index to the computation and construction of inelastic response spectra. As

discussed in earlier sections, the traditional response spectrum is a plot of the maximum value reached during response of a simple system to ground excitation. These plots are quite useful in assessing the overall envelope of response and particularly helpful in evaluating the maximum deformation and the maximum structural drift. However, as illustrated in the prior chapter, the damage processes are a function of not only the maximum values of response such as deformation but also of the cyclic nature of the response.

The evaluation of the Damage Index and its low-cycle fatigue basis has revealed that this concept correctly predicts the accumulation of damage during cyclic deformation. Moreover, this damage concept correctly addresses the factors such as the deformation amplitude and the number of velocity reversals that have been shown to strongly influence the damage level in a structure. The application of this damage theory to the construction of inelastic response spectra is a logical next step in the demonstration of this theory, and something that previously has not been possible for lack of adequate data of the type developed herein.

The first spectra that are presented for comparison purposes are produced using traditional maximum ductility methods by computing the actual response, adjusting the yield displacement and recomputing the response until the specified maximum ductility value is obtained. The spectra, shown in Fig. 5.1, are based on the response of a simple system with five percent damping to the El Centro record with specified maximum ductility values of 1.0 (elastic), 1.5, 2.0, 3.0, 5.0, and 10.0; the overall shapes of these curves are quite irregular as expected. In general, one can see that the increase in the specified

ductility causes an increase in the maximum displacement as shown in Fig. 5.1a. This ductility increase necessitates a decrease in the yield displacement value, Fig. 5.1b. The hysteretic energy spectrum presented in Fig. 5.1c has a shape that is smoother than the other spectra because this curve is based on the overall hysteretic response rather than just the single maximum displacement value. As with the other curves, the changes in the maximum ductility value shifts the energy spectrum curves accordingly.

The spectra presented in Fig. 5.1 are based on actual computed response and require many calculations to complete. As discussed in Chapter 2, an elastic design spectrum can be constructed based on statistically obtained amplification factors and the features of the maximum ground motion (50). This spectrum assumes constant displacement, velocity and acceleration regions which are approximations to the actual behavior but permit the rapid construction of the design spectrum. In Fig. 5.2a there is presented the ground motion and elastic design spectra for the El Centro record.

The elastic design spectrum can be reduced to estimate the effects of nonlinear behavior using a deamplification factor based on the ductility. The overall shape is still trapezoidal, however, the resulting velocity and acceleration values are reduced by the deamplication factor to reflect the lower response values as shown in Fig. 5.2b. The displacements are essentially equal to the elastic deflection except in the higher frequency region. The assumption in this method is that the displacements resulting from nonlinear response will be approximately equal to the elastic displacements. This assumption was partially verified in Chapter 2.

Comparison of the actual maximum displacements from Fig. 5.1 with the predicted values from Fig. 5.2b reveals the approximate nature of the modified spectrum. Because the irregular features of the computed spectrum are not carried over to the modified spectrum, there is an over estimation of displacement in some cases and an under estimation in other cases. Thus, the ductility factor is not a totally reliable factor to be employed in constructing these design and modified spectra. This fact was pointed out by Mahin and Bertero (41).

The objective of the design and modified spectra must be kept in mind. These spectra are approximations to the actual response spectra and are not intended to be completely in agreement with actual spectra. The effort required to construct one of these spectra is much less than that required to actually compute a spectrum for a specific earthquake ground motion record. Thus, a compromise between level of accuracy and level of effort was clearly made and is justified.

The real issue here is not the difference in values predicted between computed and modified spectra. Rather the issue is whether or not the ductility factor is a reasonable means to employ to describe damage and to construct a spectrum. As described earlier, the Damage Index was found to be a more accurate way to describe the damage caused by cyclic deformations than methods based on maximum response alone. The application of the Damage Index to the El Centro record is presented in Fig. 5.3. Each spectrum contains lines of constant damage of 0.0 (elastic), 0.25, 0.50, 0.75 and 1.0 (fully damaged) fractions of the damage level corresponding to the specified monotonic plastic ductility. In the case of Fig. 5.3, the specified monotonic plastic ductility was 0.5 indicating that a member monotonically deflected to a

total ductility of 1.5, thus a plastic ductility of 0.5, would represent a completely damaged condition. This assigned damage level was used to compute actual damage levels, adjust yield displacements and recompute response until the desired damage level was reached.

The maximum displacement spectrum, Fig. 5.3a, reveals relatively smooth curves that are close to the elastic curve. As frequency increases, the constant damage lines run slightly above the elastic line as expected. The yield displacement spectrum, Fig. 5.3b, also is smooth with lines of constant damage that run parallel to the elastic curve and slightly below; the reduction in displacement being a function of the level of damage desired. The important fact to notice is the smooth nature of these curves as compared to the yield spectrum based on maximum ductility presented in Fig. 5.1b.

Maximum ductility values, presented in Fig. 5.3c, are not excessive and generally are at or below 2.0 over most of the frequency range. It is important to note that the Damage Index is based on the ratio of the amount of hysteretic energy dissipated to the hysteretic energy corresponding to the specified monotonic plastic ductility as modified in Eq.(3.10). When this concept is used, the response is controlled by the overall hysteretic energy dissipated versus that permitted, and is not based on one of the displacement peaks. Thus, the result is more reflective of the overall response. This fact is illustrated in Fig. 5.3d wherein the hysteretic energy spectrum is presented. The smooth shape of the curves reflects the more consistent basis for the spectrum as compared to the irregular maximum ductility spectrum shown in Fig. 5.1c.

One may ask what happens if the specified monotonic plastic ductility is increased. This ductility increase would permit more damage to occur and thus smaller yield displacements would be expected. As shown in Fig. 5.4a when the specified monotonic plastic ductility is increased to 2.0, the yield displacements are reduced. Similarly, in Fig. 5.4b there is presented the maximum ductility spectrum which reflects ductility values that are larger than before, ranging between 2.0 and 10.0. As with the previous results, the curves are smooth and are nearly parallel to one another. When the specified monotonic plastic ductility is set at 4.0, the yield displacement spectrum is reduced further and the maximum ductility spectrum is increased as shown in Fig. 5.4c and d, respectively.

The same trends are evident in Fig. 5.5 wherein the yield displacement and maximum ductility spectra for damped response to Pacoima Dam are presented for specified monotonic plastic ductilities of 0.5 and 4.0. This record has large ground acceleration and velocity values and causes large levels of response. The nature of the curves is similar to that of El Centro revealing the consistent basis for these spectra. The Pacoima Dam record requires somewhat larger yield displacements to limit damage to the specified levels as compared to El Centro. Moreover, the resulting maximum ductilities are larger than for El Centro, also reflecting this large response to the excitation. The more consistent nature of the Damage Index prevents these isolated large ductility excursions from controlling the overall damage evaluation. Rather, these maximum ductilities are one point of response that are important, but not the sole criterion to judge response. Moreover, the actual maximum ductility values are not

excessive ranging from 3.0 to about 20.0 for the 4.0 specified monotonic plastic ductility.

Similar spectra are presented for the Melendy Ranch record in Fig. 5.6 for these same two specified monotonic plastic ductilities. This record induces modest response that is reflected in lower maximum ductilities and lower yield displacements necessary to induce the desired level of damage.

In conclusion, the inelastic response spectrum is an important analysis tool that has traditionally been based on the maximum ductility. This basis is not a consistent method to employ in construction of a spectrum because all of the nonmaximum cycles of response are ignored. These nonmaximum responses are important and lead to structural damage that accumulates with each cycle. The Damage Index has been shown to correctly predict the damage accumulation in the laboratory from the entire cyclic response history. The results presented in this section illustrate that the Damage Index also can be employed as a basis for construction of inelastic response spectra.

5.4 Application of the Damage Index to Building Code Provisions

5.4.1 Overview of Code Provisions for Design

Present building code provisions such as those found in UBC (68), ATC-3 (3) and NEHRP (14) are based on strength and maximum deflection criteria intended to ensure adequate member strength capacity while limiting deflections to reasonable values for stability and to preclude damage as much as practical. In these Codes, the strength criterion is evaluated through the use of response spectra, pseudostatic or response time history methods to determine the forces acting on, and generated

within, the structure. Once these forces are determined, the members can be evaluated for adequacy to resist these loads.

The displacement or drift criterion is evaluated through calculation of the estimated maximum displacement and by checking to insure that this value is within the code drift limit. There are no provisions in the drift limit, as presently defined, to include any of the structural or ground motion parameters that have been observed to be important factors in the inelastic deformation process. The drift limit is based solely on the story height and in some cases on the general nature of the structure. Accordingly, the purpose of this section is to propose a supplemental drift limit criterion for use in code analysis procedures that is based on the low-cycle fatigue damage theory developed earlier.

This proposed drift limit accounts for the fatigue damage aspects of the response by limiting the amplitude of the oscillation to levels that can be withstood over the number of total load reversals. This criterion is a supplemental limit, not intended to replace the existing drift limit that accounts in part for stability considerations. The latter consideration is a separate, important and complex issue that is not addressed here, and that incidently deserves much additional study, especially for combined translational and torsional type behavior.

Any new drift criterion should be of the same form as presently employed wherein a minimum amount of calculation is required. Parameters must be employed that are representative of the response and damage factors while at the same time are easily incorporated into the design procedure. Moreover, any such criterion must be conservative in

the sense of ensuring an adequate margin of safety, because the exact behavior is represented by a simplified model.

The present code provisions are based on assumed structural and ground motion models, as can be seen by examining the pseudostatic procedures for calculating the base shear. For example the UBC procedure for computing the base shear is

$$V = ZIKCSW, \tag{5.1}$$

where Z is the Seismic Zone Coefficient ranging from 3/16 to 1.0, I is the Occupancy Importance Factor ranging from 1.0 to 1.5, K is the Horizontal Force Factor ranging from 0.67 to 1.0, C is the Structural Period Factor, S is the Soil Structure Interaction Coefficient, and W is the total weight of the structure. The product CS need not exceed 0.14.

The ATC-3/NEHRP base shear is determined by computing a coefficient, C_s, and multiplying the structural weight by this parameter, or

$$V = C_s W,$$

where

$$C_s = \frac{1.2A_v S}{RT^{2/3}}, \tag{5.2}$$

and A_v is the Effective Peak Velocity Coefficient ranging from 0.1 to 0.4, S is the Soil Structure Interaction Coefficient ranging from 1.0 to 1.5, R is the Response Modification Factor that accounts for the structure type and implicitly the allowable level of nonlinear

behavior, and T is the Structural Period. ATC-3/NEHRP states that C_s need not exceed 2.5 A_a/R where A_a is the Effective Peak Acceleration Coefficient.

Both building codes distribute the total shear force over the stories of the building based on an assumed, approximate first mode deflected shape. The story shears then can be employed by the analyst to check the adequacy of the member design strengths.

The UBC and the ATC-3/NEHRP provisions implicitly assume that the details of the structural design will permit, if necessary, a limited amount of nonlinear behavior during response to earthquakes. The UBC provisions incorporate major allowance for nonlinear behavior implicitly into the K factor to reduce the member design loads, while the ATC-3/NEHRP provisions reduce the design loads using the R factor. Both of these factors are based on the anticipated performance of the specific building type during ground motion excitation.

Because the structure is assumed to act inelastically, both codes provide a maximum drift or deflection criterion to limit horizontal movement to control damage and insure stability. The UBC requires that the elastic deflection must be computed using the story loads as determined above. The total design drift is found then by multiplying the elastic deflection by the factor (1.0/K); the resulting deflection must be less than or equal to 0.005 times the story height. ATC-3/NEHRP requires that the elastic deflection, computed using the story forces determined above, must be multiplied by the Deflection Amplitude Factor, C_d. This C_d factor is a deflection amplifier similar to the ductility factor used to amplify spectral displacements while reducing the structural forces. The factor ranges in value from 1.25 for

masonry to 6.5 for reinforced concrete. In any event the total drift normally must be less than 0.015 times the story height for most structures.

These provisions are similar in form to the modified spectrum wherein the design loads are reduced from the elastic values by dividing by the ductility factor; it is to be appreciated that other factors than just inelastic behavior are involved in selecting a modified design spectrum, such as the assessment of risk, economics, importance of the structure, consequences of failure, etc. The maximum spectral deflections are estimated by multiplying the elastic deflection from the reduced loads by the ductility factor.

When the building code drift limits are converted into an equivalent ductility, the results illustrate the level of ductility permitted by the codes. Examination of typical values shown in Table 5.3 reveals that the ductility allowed in a building undergoing primarily shearing behavior is in the range of 1.2 to 14.5 depending on the member size and story height. These results illustrate that a level of nonlinear behavior is allowed that must be addressed by the designer in proportioning members and detailing of connections, especially if acceptable behavior is to occur under overload conditions.

Clearly, the effects of cyclic motion of the structure can compound the nonlinear behavior as has been demonstrated earlier herein. Any improved drift criterion should protect the structure from the accumulated damage caused by repeated cycling through large deformation amplitudes. The question is whether or not the level of ductility permitted by the codes is too large, thus allowing excessive

damage to occur when the structure cyclically responds to an earthquake. Moreover, the previous damage results indicate that several structural and ground motion parameters are important to the generation of damage. These parameters should be considered for inclusion in any improved drift or damage criterion.

5.4.2 Proposed Drift Criterion

The results of the previous chapters have shown that the number of reversals is a key factor in the structural damage accumulation. To determine how the number of reversals is affected by the structural and ground motion parameters, a study was performed using the El Centro, Pacoima Dam and Melendy Ranch earthquake records to excite structures of various frequencies and different specified maximum ductilities. As illustrated in Fig. 5.7a, when the first 40 seconds of the El Centro record was employed to excite structures of frequencies from 0.1 to 10.0 hz, the number of reversals was approximately a linear function of the frequency. The results indicate that the number of reversals is essentially a function of only the structural frequency and the duration of shaking. Moreover, note that changes in the specified maximum ductility, and therefore in the yield resistance value, did not affect the number of reversals to a large extent. Other earthquake records were employed and found to induce a similar number of reversals.

Furthermore, the duration of excitation was found to be an important parameter in causing reversals. As shown in Fig. 5.7b, elastic structures underwent about the same number of reversals when subjected to 20 seconds of El Centro and Pacoima Dam, a value approximately one-half of the number of reversals induced by 40 seconds

of excitation as reported in Fig. 5.7a. Similarly, when Melendy Ranch was employed, the 15 second duration induced three-quarters of the 20 second values from El Centro and Pacoima Dam. From these results, it can be seen that the number of reversals is independent of the particular earthquake record involved and is primarily a function of the structural frequency and the duration of ground excitation. These interesting observations need to be studied further for a wide range of earthquakes.

Based on this information, the number of reversals that a structure undergoes during earthquake response can be estimated without having to perform response time history analysis. Thus, the fatigue-based damage criterion developed in Chapter 3 can be employed to compute the hysteretic plastic ductility value accounting for the number of reversals that occur and more closely reflecting the true damage state of the structure.

Any new drift or ductility limit must address the important parameters involved in the generation of damage. The limit should include the estimated number of reversals as well as the natural frequency and type of structure. Moreover, the design level of the earthquake must be defined to determine the amount of conservatism employed. A large earthquake, such as that associated with UBC zone 4, would cause strong response and should have limits adjusted accordingly.

The parameters of structural frequency, building type, and excitation duration were combined with the fatigue-based damage criteria to produce a possible new drift limit that includes the important features of the damage process. The drift limit is in the

form of a total ductility criterion, that is a ductility that reflects the total overall displacement normalized by the yield displacement. Thus, both elastic and inelastic components of the deformation are included in this criterion which has the form of

$$\mu_a = 1.0 + (2C_d[(f_n)^{1.4} + (1/f_n)^{0.5}] (\frac{REV}{Q})^{-0.6}), \qquad (5.3)$$

where μ_a is the allowable maximum total ductility, C_d is the NEHRP Deflection Amplification Factor, f_n is the fundamental natural frequency of the structure, REV is the number of reversals obtained from Fig. 5.7c. The Q symbol is a duration coefficient that varies as follows, for UBC zone 4, Q equals 1.0; for UBC zone 3, Q equals 1.33; for UBC zone 2, Q equals 1.67; and for zone 1, Q has a value of 2.0. This proposed criterion provides the designer with the value of maximum ductility that can be tolerated as a maximum deformation during the cyclic response of a structure based on the duration of shaking, structural frequency and the building type.

The results presented in Table 5.4 show that the allowable total ductility values generally are comparable to, if not less than, the present ductility values from the Codes discussed earlier. The relative size depends in large part on the building type that is involved. Typical results are presented in Fig. 5.8 where the proposed criterion is plotted on a maximum ductility spectrum produced using the Damage Index concept. The results indicate that this simplified procedure falls slightly below the actual computed maximum ductility curves. The conservatism indicated would be desired in an approximate design tool of this type because the actual behavior is not computed,

rather a simplified representation is employed. This equation contains the important parameters that should be included in the drift evaluation. Adjustments in the individual terms might be required following detailed study, however, the basic trends are evident as depicted in Fig. 5.8.

The conclusion to this section is that the drift limits found in UBC, ATC-3, and NEHRP, when viewed from a fatigue perspective, may be too large. A ductility value of 7.5 reached once will cause a different level of damage than the same ductility level reached many times. The results presented herein indicate that the Code drift limits may exceed the levels required for complete damage; reduction of these drift limits should be considered to account for the damage accumulation caused by the cyclic response, however, more study of this question is required.

CHAPTER 6

OBSERVATIONS

6.1 Introduction

The important results and findings of this investigation are summarized in the sections that follow. The chapter concludes with a section devoted to possible future applications of this research in structural design practice as well as the research needed to answer questions posed by this study.

6.2 Observations Regarding the Parameter Study of Structural Response to Ground Motion

The first phase of this research involved the identification of the parameters responsible for strong response through detailed study of the response of simple structural systems. The structural response in terms of deformation, resistance, and energy time histories was computed and the effects of parameter changes were observed. A variety of ground motions were employed, ranging from simple pulse-type excitation to selected actual earthquake records. These analytical computations were supplemented by a small series of experiments involving a simple structure subjected to pulse-type excitation.

The response was found to be a function of several parameters; overemphasis of one parameter and the exclusion of other parameters can lead to erroneous assessments of the potential of an earthquake to cause strong structural response. A summary of the important findings includes the observation that the peak ground acceleration, when

employed by itself, is a poor response predictor; peak acceleration can be associated with high frequency excitation that will not induce strong response in typical structures as has been observed herein and in actual earthquakes. In contrast, the ground velocity, which is related to the impulse area of the acceleration record, was found to be a good indicator of the response potential of a record.

Individual pulse characteristics also can affect the response, particularly where a large area unbalance exists between the positive and negative acceleration sides of the record. This unbalance can cause the structure to respond more in one direction than the other potentially resulting in a larger residual plastic offset. Such effects are not reflected in current earthquake design criteria.

Finally, the overall duration of excitation was found to cause displacements to increase with time in structures close to the ground motion frequency. In these cases, elastic structures responded with increasing displacement amplitudes limited only by damping. Elastoplastic structures responded with increasing displacements until controlled by hysteretic action; longer excitation duration in these structures resulted only in increased numbers of hysteretic cycles.

This observation confirms the well-known fact that the structural frequency is an important factor in causing strong response when its value is close to the ground motion frequency; as a rule structures strongly respond to excitation that is no more than twice the structural frequency. High frequency excitation, significantly higher than the structural frequency, results in inertial accelerations of small impulse area that do not cause large response. Another important structural parameter is the damping that is relatively ineffective in

reducing peak displacement and velocity values as compared to hysteretic energy dissipation. However, the damping does dissipate energy and thereby often leads to reduced numbers of yielding excursions and lower hysteretic energy levels.

The complex combination of ground motion and structural parameters means that the effects of an earthquake cannot be predicted on the basis of a single parameter such as peak ground acceleration. Instead, this research indicates that other techniques, such as energy calculations, can be employed effectively to describe the ground motion and structural response interaction in a more complete manner than is possible with present methods. Future improvements in building analysis and design will depend in part on the application of information such as that presented herein to the development of these new procedures that need to address the entire range of parameters shown to play an important part in generating response. For example, the concepts studied may well lead to design criteria guidelines that force the designer to consider the zones or regions in a structure where yielding or deformation is to be concentrated; such design planning will lead to safer structures.

6.3 Observations Regarding the Proposed Damage Criteria

Two damage criteria were proposed, one based on equivalent hysteretic cycles and the other founded on low-cycle fatigue concepts. Computation of the number of equivalent hysteretic cycles, the first damage criterion studied, provides a way to convert the total hysteretic energy into a quantitative measure of the cyclic response strength, which can be employed as an indicator of damage as well as

part of the design basis for structural members and connections. Three standard hysteretic cycle definitions were developed. The weighted and maximum deformation cycle definitions were found to provide useful representations of the cyclic response; in contrast, the strain energy at yield was evaluated and not found to be an adequate cycle definition.

A second damage criterion was developed from low-cycle fatigue theory, modified so as to describe the structural damage accumulated during the erratic cyclic response to earthquakes. This damage measure converts a specified monotonic plastic ductility, required to completely damage a structural element in monotonic deformation, into a hysteretic plastic ductility that accounts for the additional damage caused by cyclic deformation. This fatigue-based damage criterion was compared against experimental data from a variety of cyclic tests reported in the literature and found to accurately predict the damage state in actual structural members.

Major improvements in the ability to design for earthquake excitation in the future depend in part on developing methods to evaluate the damaging effects of repetative, cyclic deformations during response. Present ductility methods are at best approximate because they examine only the maximum response value and ignore the other nonmaximum cycles of response. The two damage criteria developed in this dissertation represent significant improvements in damage evaluation because they are reasonably accurate for simple systems and they are in a form that can be readily adapted to conventional design methods.

6.4 Observations Regarding Design Applications of the Damage Criteria

Applications of the damage criteria developed in this study to three different damage evaluation problems were presented to demonstrate the use of these procedures in design situations. The cases presented included the evaluation of hysteretic energy dissipated in response, the construction of inelastic response spectra and the development of a new drift criterion for building code provisions. In the first application, the two damage criteria developed in this research provided a comparison basis for dissipated hysteretic energy values to permit this energy parameter to be directly employed in design. The equivalent hysteretic cycles produce a quantitative measure of the cyclic nature of the inelastic response that can be employed in the design of structural elements. Furthermore, the low-cycle fatigue and Damage Index concepts can be employed to convert a specified monotonic plastic ductility into a corresponding hysteretic energy that can be compared against the actual hysteretic energy dissipated.

The second application of the Damage Index was as a basis for the construction of nonlinear response spectra. The Damage Index nonlinear spectra reflect the entire response history including the maximum and nonmaximum cycles, as compared to conventional nonlinear spectra where only the maximum ductility is employed and damage from nonmaximum cycles is ignored. The Damage Index nonlinear spectra contain nearly parallel spectral lines that are smoother and more consistent in shape than the irregular spectra produced based on the maximum ductility. Moreover, the actual maximum ductility values permitted by the Damage Index nonlinear spectra are comparable to, and in some cases slightly

larger, than those ductility values obtained from maximum ductility spectra, these results reflect the fact that the damage is a function of all of the deformation cycles of response and not just the single maximum deformation. The inclusion of all of the response cycles in effect averages the peak response with the other values, de-emphasizing the peak response so that a structure frequently can absorb more damage, as measured by the Damage Index, than would be permitted during response limited to a maximum ductility value. This observation agrees with actual post-earthquake damage surveys where structural failure, or even severe damage, frequently does not occur following large displacement excursions that would exceed usual maximum ductility limits.

A third design application concerned a proposed drift criterion, based on low-cycle fatigue concepts together with a new representation of the effects of the earthquake ground motion, in terms of numbers of response reversals occurring in the structure. This limit provides a comprehensive means to control the amplitude of the oscillatory motion so the damage that accumulates over the total number of reversals will be acceptable. Existing drift criteria generally are based on stability as well as other considerations and will be supplemented by this proposed criterion; in most cases the new limit is more restrictive than present drift limits. The results from application of this new criterion are promising, indicating that a rigorous drift limit that addresses the features of the ground motion and response, can be developed for building code implementation. If it can be shown that such drift control leads to reduced damage and acceptable margins of safety following response, the economic impact could be substantial.

The applications presented in this dissertation indicate that these damage criteria reflect the damage from the entire response history and are developed in such a way that they can be readily employed in design. This result is fortunate because the additional damage that occurs from cyclic deformation of structural elements is not predicted or addressed by present maximum ductility-based methods. Improvement in design procedures will first require improved techniques to predict damage. The application of comprehensive methods of the type developed in this study represent a feasible way to accomplish this goal.

6.5 Observations on Future Applications of this Research

Successful structural design requires some form of response prediction and evaluation of this response to ensure that the resulting displacements will occur in a controlled and acceptable manner. The designer must have a sound understanding of the structural resistance as a function of displacement as well as a knowledge of what is acceptable for functional use or overall safety, and the implications of the adequate or inadequacy of the remaining margins of strength. These details of nonlinear behavior are not well addressed in current design guidelines, for most designs are carried out in the elastic domain. As limit design concepts are developed and adopted often permitting limited inelastic response, a great deal more research in the area of structural resistance behavior will be needed, if rational improvements in the building code criteria are to be adopted and enforced.

The results of this research point to new approaches in evaluating the damage potential of earthquake ground motion as well as ways to evaluate damage from cyclic structural response.

Clearly other applications and extensions of this work can be envisioned. For example, research into the design of complex frames and building systems employing comprehensive techniques such as hysteretic energy is continuing; progress has been substantial in recent years. Application of the damage concepts concerning SDOF systems from this dissertation will assist in development of new design criteria for such frameworks. Another area of potential application is in post-earthquake evaluation of buildings to determine why certain buildings performed well and others collapsed. The damage measures from this study permit evaluation of the response and corresponding damage from a new perspective which should aid in future damage surveys and the attendant assessment of adequacy of the surviving structures. After an earthquake, difficult decisions must be made about certifying a structure as adequate for future use, authorizing necessary repairs, or requiring that the structure be demolished because the structural damage is too severe. At present we have no rational methods for making such assessments.

The overall conclusion to this study is that comprehensive measures are needed to evaluate the hazard posed by earthquake ground motion on a structure as well as the resulting damage. The methods proposed in this study represent a starting point for further development of design and building code provisions to better predict structural response and damage than is possible with present approaches.

TABLES

Table 2.1 Summary of Effects of Damping on Response to Pulse-Type Excitation

Ground Motion Amplitude: ±0.5g
Balanced Simple Pulse

Structural Frequency, hz	Pulse Duration, sec	Maximum Deflection, in. Damping			Input Energy, in-lb Damping			Hysteretic Energy, in-lb Damping		
		0%	1%	5%	0%	1%	5%	0%	1%	5%
	0.1	-0.2	-0.2	-0.2	1.1	1.2	1.6	0.0	0.0	0.0
1.0	0.3	-1.7	-1.6	-1.6	83.4	85.1	91.5	0.0	0.0	0.0
	0.5	-3.4	-3.4	-3.2	452.8	457.9	475.8	91.6	86.1	66.0
	0.1	-0.2	0.2	-0.2	4.4	4.6	5.2	0.0	0.0	0.0
2.0	0.3	-1.1	0.1	-1.1	174.8	176.5	182.2	47.6	45.3	37.8
	0.5	-2.3	-2.2	-2.0	480.8	482.4	481.6	308.2	301.7	274.9
	0.1	-0.1	-0.1	-0.1	18.1	18.3	19.0	3.6	3.4	2.5
5.0	0.3	-0.6	-0.6	-0.5	150.0	149.2	141.6	116.4	113.2	98.9
	0.5	-1.3	-1.2	-1.0	320.3	309.2	263.9	278.4	261.2	205.8

Table 2.2 Earthquake Data

Earthquake and Station	Magnitude and Intensity, MMI	Maximum Ground Acceleration, in/sec^2, at Time, sec	Maximum Ground Velocity, in/sec, at Time, sec	Total Duration, sec	Duration Used in this Study, sec
Imperial Valley, CA May 18, 1940 El Centro (SOOE)	6.7 X	-134.5 at 2.1	-13.2 at 2.2	41.8	20.0
San Fernando, CA Feb. 9, 1971 Pacoima Dam S16E	6.4 XI	452.0 at 7.7	44.6 at 3.0	53.7	20.0
Bear Valley, CA Sept. 4, 1972 Melendy Ranch N29W	4.7 VI	-199.3 at 1.8	5.9 at 1.73	23.8	15.0

NOTES:

1. All information from Ref. 72.

2. Duration employed is the first number of seconds indicated which includes most of the strong motion.

Table 2.2 (continued)

Earthquake and Station	Magnitude and Intensity, MMI	Maximum Ground Acceleration, in/sec^2, at Time, sec	Maximum Ground Velocity, in/sec, at Time, sec	Total Duration, sec	Duration Used in this Study, sec
Morgan Hill, CA April 24, 1984 Coyote Lake Dam, 285	6.2 VIII	-447.97 at 3.70	30.06 at 3.63	59.98	10.24
Morgan Hill, CA April 24, 1984 Coyote Lake Dam, 195	6.2 VIII	251.87 at 4.68	-20.64 at 3.46	59.98	10.24
Morgan Hill, CA April 24, 1984 Halls Valley, 240	6.2 VIII	120.38 at 10.64	-15.74 at 10.54	59.98	15.00
Kern County, CA July 21, 1592 Taft-Lincoln School Tunnel, S69E	7.2 XI	-69.27 at 3.70	6.98 at 3.56	54.38	20.00

NOTES:

1. Information on Morgan Hill earthquake from Ref. 15; information on Kern County from Ref. 72.

2. Duration employed is the first number of seconds indicated which includes most of the strong motion.

Table 2.3 Complete Record and Short Time FFT Results in the Form of the Four Largest Fourier Amplitudes and Corresponding Frequency for Three Different Time Window Positions

Earthquake	Complete Record		Window at 0.0 - 5.12 sec		Window at 2.56 - 7.68 sec		Window at 5.12 - 10.24 sec	
	Amplitude in/sec	Frequency hz	Amplitude in/sec	Frequency hz	Amplitude in/sec	Frequency hz	Amplitude in/sec	Frequency hz
El Centro	99	1.46	38	0.98	28	1.37	28	1.37
	89	1.17	37	1.17	26	1.17	26	3.32
	67	1.56	34	1.76	26	2.15	26	1.56
	65	1.76	26	2.15	24	0.59	24	1.95
	(554)*		(336)		(264)		(264)	
Pacoima Dam	140	4.78	92	0.78	50	3.32	98	2.34
	139	2.54	86	0.98	49	0.59	77	2.54
	133	2.30	75	0.59	49	2.54	80	4.69
	132	0.98	56	1.17	46	3.12	76	2.15
	(1282)		(464)		(494)		(821)	
Melendy Ranch	43	5.57	30	5.66	7.6	5.47	2.7	2.54
	41	5.52	25	5.86	6.7	3.12	2.6	0.98
	40	5.62	24	4.49	6.5	5.27	2.5	3.71
	38	5.66	23	6.06	5.5	3.32	2.3	2.98
	(360)		(285)		(62)		(24)	

*The values in parenthesis are the computed areas under the Fourier Amplitude Spectrum for the record portion indicated.

Table 3.1 Elastic Design Spectrum Amplification Factors (49)

Damping, Percent of Critical	Cumulative Nonexceedance Probability, Percent: 84.1 (One Sigma) A	V	D	50 (Median) A	V	D
0.5	5.10	3.84	3.04	3.68	2.59	2.01
1.0	4.38	3.38	2.73	3.21	2.31	1.82
2.0	3.66	2.92	2.42	2.74	2.03	1.63
5.0	2.71	2.30	2.01	2.12	1.65	1.39
10.0	1.99	1.84	1.69	1.64	1.37	1.20
20.0	1.26	1.37	1.38	1.17	1.08	1.01

A = Acceleration factor

V = Velocity factor

D = Displacement factor

Table 4.1 Summary of Undamped Hysteretic Response to El Centro, Pacoima Dam and Melendy Ranch

Earthquake Record	Structural Frequency, hz	Total Hysteretic Energy, in-lb(1)		Number of Counted Yield Excursions		Equivalent Hysteretic Cycles - Computed From Energy in Single Cycles of: Maximum Deformation		Weighted Deformation		Yield Deformation(2)	
		+R	-R	+R	-R	+R	-R	+R	-R	+R	-R
El Centro	0.5	138	110	2	1	1.9	1.6	2.0	1.4	0.3	0.2
	2.0	500	526	13	9	3.7	3.9	5.5	5.6	15.8	16.6
	5.0	126	111	24	25	5.6	4.9	9.2	9.6	24.8	21.8
Pacoima Dam	0.5	882	639	2	2	1.6	1.2	1.4	1.4	1.7	1.3
	2.0	1760	1545	12	11	2.8	2.5	2.7	4.3	55.6	48.8
	5.0	1608	1548	42	38	4.3	4.1	4.6	8.2	317.3	305.5
Melendy Ranch	0.5	0	0	0	0	0.0	0.0	0.0	0.0	0.0	0.0
	2.0	2	3	1	2	1.0	1.6	1.0	2.0	0.1	0.1
	5.0	69	49	7	6	1.8	1.3	2.6	3.1	13.6	9.7

Notes:

1. The +R and -R abbreviations refer to response during the positive or negative resistance phases, respectively.

2. The energy corresponding to the yield deformation also is known as the strain energy at yield, equal to one-half the product of yield displacement and yield resistance.

Table 4.2 Comparison of Failure Strain Values for Specified Fatigue Lives Obtained from Yao and Munse (71) with the Predicted Values from the Proposed Criterion

Ratio of Hysteretic Plastic Strain, ϵ^*, to Plastic Strain at Failure in Monotonic Loading, ϵ_p, in percent:

Number of Cycles to Failure, N_f(1)	Yao and Munse, ϵ^*/ϵ_p, % (2,3)	This Study, ϵ^*/ϵ_p, % (4,5)
1	66.0	66.0
10	19.5	16.6
100	5.5	4.2

NOTES:

1. Each hysteretic cycle contains two reversals, therefore the number of reversals is twice the number of cycles or $2N_f$.
2. All hysteretic cycles are identical in this comparison.
3. Hysteretic cycles are produced by identical triangular strain pulses in which the strain is fully reversed, corresponding to a relative strain ratio of r = -1 from Yao and Munse data, Fig. 7, Ref. (71).
4. Ductility is defined as $\mu = \epsilon/\epsilon_y$ where ϵ_y is the yield strain.
5. Sample Calculation using the design concepts from this study:

Hysteretic Plastic Ductility	=	Monotonic Plastic Ductility	x	Reduction Coefficient
μ	=	μ_p	x	$(2N_f)^{-0.6}$

but $\mu = \epsilon/\epsilon_y$

$$\epsilon^*/\epsilon_y = (\epsilon_p/\epsilon_y)\ (2N_f)^{-0.6}$$

or

$$\epsilon^* = \epsilon_p(2N_f)^{-0.6}$$

Let N = 1.0 cycles or 2.0 reversals

$$\epsilon^* = \epsilon_p\ (2.0)^{-0.6} = 0.66\ \epsilon_p$$

or

$$\epsilon^*/\epsilon_p = 0.66 = \underline{66.0\%}$$

Table 4.3 Comparison of Low-Cycle Fatigue Data Presented by Sawyer (64) with the Predicted Values from the Proposed Criterion

Sawyer summarized low-cycle fatigue data from Welding Research Council studies on various steels subjected to cyclic loading. These failure results can be compared to the predicted results from this study:

Number of Reversals, $2N_f$	WRC Data Total Strain Range for Failure, % (1)	Strain Range Predicted from this Study for Failure, % (2)
1	100.0	100.0
10	38.0	25.1
100	13.0	6.3
1000	4.0	1.6
10000	1.1	0.4

NOTES:

1. Total strain range is twice the strain amplitude in any cycle. The monotonic plastic strain was found to be 1.0 or 100% for these steels. The strain range required for failure was found to be a lower value as the number of reversals increases as shown.

2. Failure strain is the hysteretic plastic strain computed from

$$\Delta\epsilon^* = \Delta\epsilon_p(2N_f)^{-0.6}$$

where $\Delta\epsilon_p$, the monotonic plastic strain was set equal to 100 percent.

Table 4.4 Computation of Damage from Hysteretic Response Using Experimental Results from Appendix A

From experimental results:
- Yield Displacement = 1.04 in.
- Maximum Displacement = 3.00 in.
- 3 Complete Hysteretic Cycles Applied
- Modulus of Elasticity, E = 29,555 ksi
- Failure Strain ≈ 24.2%

Assigned Monotonic Plastic Failure Strain, ϵ_p, % (1)	Corresponding Monotonic Plastic Failure Displacement, Δ_p, in. (2)	Corresponding Monotonic Plastic Failure Ductility, μ_p, (3)	Applied Hysteretic Plastic Ductility, μ^*, (4)	Number of Cycles to Failure, N, Corresponding To This Assigned Monotonic Failure Strain, (5)
5	2.0	1.92	1.88	0.52
10	4.0	3.85	1.88	1.64
15	6.0	5.77	1.88	3.23
20	8.0	7.69	1.88	5.21
25	10.0	9.62	1.88	7.57
30	12.0	11.54	1.88	10.25

NOTES:
1. Separate tensile testing indicated a failure plastic strain of approximately 24% for this material in monotonic loading.
2. Corresponding plastic failure displacement computed as

$$\text{Monotonic Plastic Failure Strain } \epsilon_p = \frac{[\text{Hinge Rotation}_{\theta}] * [\text{Section Height}_{h}]}{[\text{Hinge Length}_{a}]}$$

$$\text{Plastic Displacement } \Delta_p = \theta L = \frac{\epsilon_p a L}{h} = \frac{\epsilon_p (1.0)(17.5)}{0.4375}$$

where "h" is equal to 0.4375 in., the height of the reduced area, "L" is 17.5 in., the length of the bar and the parameter "a" equals 1.0 in., the length of the reduced area section of the bar.

3. Plastic ductility computed as $\mu_p = \Delta_p/1.04$ in. where 1.04 in. is the yield displacement.
4. Applied hysteretic ductility is $\mu^* = 3.0 - 1.04/1.04$ where 3.0 in. is the maximum displacement and 1.04 in. is the yield displacement.
5. Number of cycles computed from theory as

$$\mu^* = \mu_p (2N_f)^{-0.6} \quad \text{or} \quad N_f = 1/2[\frac{\mu^*}{\mu_p}]^{-1/0.6}$$

where $\mu^* = 1.88$ and μ_p is the assigned failure value for monotonic loading.

Table 4.5 Computation of Required Numbers of Hysteretic Cycles to Match the Assigned Damage Index Values for Various Monotonic Plastic Ductility Values Using Appendix A Data

Assigned Damage Index, percent	Number of identical cycles at 1.88 maximum hysteretic plastic ductility, μ^*, resulting in the assigned damage index value, for the monotonic plastic ductility values of: (1)				
	$\mu_p = 2$	$\mu_p = 4$	$\mu_p = 6$	$\mu_p = 8$	$\mu_p = 10$
100	0.55	1.75	3.44	5.56	8.07
90	0.52	1.66	3.27	5.28	7.65
80	0.49	1.57	3.08	4.98	7.22
70	0.48	1.52	2.98	4.82	6.99
60	0.43	1.36	2.67	4.31	6.25
50	0.39	1.24	2.44	3.93	5.71
25	0.28	0.88	1.72	2.78	4.03
10	0.17	0.55	1.09	1.76	2.55

NOTES:

1. The number of cycles required to reach the specified damage index level is computed as:

$$HYSP = HYSN = N(R_Y)(U_Y)\mu^*$$

where N = number of cycles

R_Y = yield resistance

U_Y = yield displacement

μ^* = maximum hysteretic plastic ductility

$$\text{Damage Index} = \left[\frac{HYSP + HYSN}{2N_f R_Y U_Y \mu^*}\right]^2 + \left[\frac{HYSP - HYSN}{2N_f R_Y U_Y \mu^*}\right]^2$$

$$\text{Damage Index} = \left[\frac{(2N)R_Y U_Y \mu^*}{(2N_f)R_Y U_Y \mu^*}\right]^2 + 0 =$$

(continued)

Table 4.5 (continued)

Damage Index = $[2N/(2N_f)]^2$

where $(2N_f)$ is the number of reversals required for failure at the assigned ductility value or

$$\mu^* = \mu_p(2N_f)^{-0.6}$$

$$1.88 = \mu_p(2N_f)^{-0.6}$$

$$[\frac{1.88}{\mu_p}]^{-1/0.6} = (2N_f)$$

Substitute into Damage Index = $[2N/(2N_f)]^2$

$$2N = (2N_f)\sqrt{DI}$$

$$= [\frac{1.88}{\mu_p}]^{-1/0.6}(\sqrt{DI})$$

$$N = 1/2[\frac{1.88}{\mu_p}]^{-1.67}(\sqrt{DI})$$

Sample Calculation

For $\mu_p = 10$ and Damage Index = 100%

N = 8.07 cycles

Table 4.6 Computation of Monotonic Failure Parameters for Popov Data

Popov and Pickney (59) loaded sample F1-S in one direction until failure but this was not monotonic loading. Seven reversals were involved in 3.5 cycles when the specimen was unloaded and reloaded in the same direction. All hysteretic energy generated was from positive resistance causing unbalanced damage.

From data, full yield displacement, U_Y = 0.525 in.

full yield load, R_Y = 11.19 kips

Cycle No.	Total Deflection over this cycle, in.	Plastic Deflection, in.	Hysteretic Energy, in-kips
1	0.667	0.142	1.589
2	0.444	0.444	4.968
3	4.722	4.722	52.839
4(3½)	3.667	3.667	41.034
Total Tip Deflection	9.50 in.	8.975 in.	100.43 in-kips

From this study:

$$\text{Damage Index} = \left[\frac{HYSP + HYSN}{2N_f R_Y U_Y \mu^*}\right]^2 + \left[\frac{HYSP - HYSN}{2N_f R_Y U_Y \mu^*}\right]^2$$

where

Damage Index = 1.0 represents full damage

HYSP = 100.43 in-kips, loaded and re-loaded in one direction

HYSN = 0

N = 3.5 Cycles (7 Reversals)

R_Y = 11.19 kips

U_Y = 0.525 in.

μ^* = Hysteretic Plastic Ductility

These values can be substituted into the equation above and the value of μ^* can be found. (continued)

Table 4.6 (continued)

$$1.0 = \left[\frac{100.43 + 0}{2(3.5)(11.19)(0.525)\mu^*}\right]^2 + \left[\frac{100.43 - 0}{2(3.5)(11.19)(0.525)\mu^*}\right]^2$$

$$1.0 = 2\left[\frac{100.43 + 0}{2(3.5)(11.19)(0.525)\mu^*}\right]^2$$

$$\mu^* = \underline{3.45}$$

This is the hysteretic plastic ductility causing failure over 3½ cycles under the test conditions.

The hysteretic energy corresponding to this hysteretic plastic ductility is

hysteretic energy = 2(3.5)(11.10)(3.45)(0.525) = 142 in-kips

From the fatigue damage theory developed earlier:

$$\mu^* = \mu_p(2N_f)^{-0.6}$$

where

μ^* = hysteretic plastic ductility = 3.45

μ_p = monotonic plastic ductility

$2N_f$ = 7.0 Reversals

The monotonic plastic ductility is:

$$\mu_p = \frac{\mu^*}{(2N_f)^{-0.6}} = \frac{3.45}{(7)^{-0.6}} = \underline{11.10}$$

Thus, a monotonic plastic ductility of 11.10 causes the same damage as a hysteretic plastic ductility of 3.45 applied over 3½ cycles.

Corresponding Hysteretic Energy (142 in-kips) $\frac{11.10}{3.45}$ = <u>456.4 in-kips</u>

This value corresponds to a monotonic hysteretic energy value causing the same damage level as the actual damage induced by the seven reversals or 3½ cycles.

Table 4.7 Comparison of Monotonic and Hysteretic Failure Results Using Popov and Pickney Data (59)

Test Number	Number of Reversals, $2N_f$(1)	Total Dissipated Hysteretic Energy in-k (2)	Dissipated Hysteretic Energy Per Reversal in-k/reversal	Disspated Hysteretic Energy as a Fraction of Hysteretic Energy at Failure in Monotonic Loading (3)	Predicted Results From This Study, μ^*/μ_p, (4)
F1-S	7.0	456.4	456.4	1.0	1.0
F1-C2	45.0	2400.0	53.3	0.1168	0.1019
F1-C3	240.0	3700.0	15.4	0.0337	0.0373
F1-C4	79.0	2800.0	35.4	0.0776	0.0727
F1-C6	64.0	2600.0	40.6	0.0889	0.0825

NOTES:

1. The number of reversals, $2N_f$, is twice the number of cycles, N_f, because two reversals occur per cycle.
2. Dissipated hysteretic energy values obtained from Popov data, Ref. (59). Hysteretic energy for F1-S computed from Popov data in Table 4.6 in this study.
3. From Popov data: Sample Calculation for F1-C3:

$$\text{Dissipated Energy per Reversal} = \frac{\text{Hysteretic Energy}}{\text{Number of Hysteretic Reversals}} = \frac{3700.0}{240.0} = 15.4 \ \frac{\text{in-k}}{\text{reversal}}$$

$$\text{Dissipated Energy as Fraction of Monotonic Loading} = \frac{15.4}{456.4} = \underline{0.0337}$$

4. From the Fatigue Damage Theory, the ratio μ^*/μ_p is equal to the reduction coefficient $(2N_f)^{-0.6}$ and is a measure of the maximum plastic ductility in each hysteretic cycle employed by Popov in the experimental study.

For F1-C3: $\mu^*/\mu_p = (2N_f)^{-0.6} = (240)^{-0.6} = \underline{0.0373}$

Table 4.8 Evaluation of Experimental Data from Popov and Stephen (61)

Specimen and Section Size (1)	Yield Deflection Δ_Y, in.(2)	Full Yield Load, P, kips (3)	Total Hysteretic Energy in-k (4)	Assumed Maximum Displacement per cycle, in.(5) (6)	Computed Number of Reversals, $2N_f$	Hysteretic Plastic Strain, ε^*, % (7)	Monotonic Plastic Strain, ε_p, % (8)
1-W18x50	0.60	54.6	1188	2.5	11.45	3.36	14.51
2-W18x50	0.60	54.6	1776	2.5	17.12	3.36	18.47
4-W18x50	0.60	54.6	1679	2.5	16.19	3.36	17.86
8-W18x50	0.60	54.6	671	2.5	6.46	3.36	10.29
5-W24x76	0.36	86.2	2679	2.0	19.0	3.79	22.15
6-W24x76	0.36	86.2	1424	2.0	10.10	3.79	15.16
7-W24x76	0.36	86.2	2914	2.0	20.62	3.79	23.29

NOTES:

1. WF shapes were employed in this research.
2. Full yield deflection computed as $\Delta_Y = f\sigma_y L^2/3cE$ where f is the shape factor, σ_y is the yield stress, L is the moment arm, c is one-half of the section height, and E is the Modulus of Elasticity.
3. Full yield load computed as $P_y = f\sigma_y I/Lc$ where I is the moment of inertia.
4. Hysteretic energy computed from areas inside hysteresis loops of figures.
5. Damage index value set at 1.0, full damage, so

$$\text{Damage Index} = \left[\frac{\text{Actual Hysteretic Energy}}{\text{Allowable Hysteretic Energy}}\right]^2 = 1.0$$

6. Maximum displacement for a set of constant amplitude hysteresis loops required to compute the number of reversals.

$$\left[\begin{matrix}\text{Hysteretic}\\ \text{Energy}\end{matrix}\right] = \left[\begin{matrix}\text{Number of}\\ \text{Reversals}\end{matrix}\right] \left[\begin{matrix}\text{Full Yield}\\ \text{Load}\end{matrix}\right] \left[\begin{matrix}\text{Maximum}\\ \text{Displacement}\end{matrix} - \begin{matrix}\text{Full Yield}\\ \text{Displacement}\end{matrix}\right]$$

Sample calculation:

$$1188 = (2N_f)\ (54.6)\ (2.5 - 0.6)$$

$$2N_f = \underline{11.45 \text{ Reversals}}$$

(continued)

Table 4.8 (continued)

7. Hysteretic Plastic strain ε^* computed from

$\varepsilon^* = \frac{\theta(2c)}{a}$ where θ is plastic hinge rotation computed below, 2c is the section height, a is the plastic hinge length or $a = (\frac{f-1}{f})L$ where f is the section shape factor and L is the moment arm.

$\theta = \frac{\Delta_T - \Delta_Y}{L - \frac{a}{2}}$ where Δ_T is the total deflection and Δ_Y is the full yield displacement.

Sample Calculation: For $\Delta_T = 2.5$ in., $f = 1.133$, $\Delta_Y = 0.6$ in., $L = 96$ in.

$$\theta = \frac{2.5 - 0.6}{96 - (\frac{0.133}{1.133})(\frac{96}{2})} = 0.02103 \text{ radians}$$

$$\varepsilon^* = \frac{0.02103(18)}{\frac{0.133}{1.133}(96)} = 0.0336 = \underline{3.36\%}$$

8. Monotonic Plastic Strain, ε_p, computed from theory as

$\mu^* = \mu_p(2N)^{-0.6}$ or $\varepsilon^*/\varepsilon_y = \varepsilon_p/\varepsilon_y(2N)^{-0.6}$

$\varepsilon^* = \varepsilon_p(2N)^{-0.6}$ or $\varepsilon_p = \varepsilon^*/(2N)^{-0.6}$

Sample Calculation: $\varepsilon_p = 3.36(114.5)^{-0.6} = \underline{14.51\%}$

Table 4.9 Evaluation of Experimental Data from Popov and Bertero (58)

For Test Series No. 1

The beam is a W24 x 76 attached to a column stub

Moment Arm, L = 7.5 ft
Shape Factor, f = 1.136
Section Height, 2c = 23.92 in.
Modulus of Elasticity, E = 29000 ksi
Yield Stress, σ_y = 36 ksi

For this shape factor, the plastic hinge length is

$$a = \frac{0.136}{1.136}L = 0.1197L$$

Assume ϵ_{max} = 20%

$$\epsilon = \frac{\theta(2c)}{a} \Rightarrow \theta = \frac{\epsilon a}{2c} = \frac{0.20(0.1197)(7.5)(12)}{23.92} = 0.090 \text{ radians}$$

Deflection at fully yielded condition

$$\Delta_Y = f\frac{PL^3}{3EI} = \frac{fML^2}{3EI} = \frac{f\sigma_y L^2}{3cE} = \frac{1.136(36)(7.5)^2(12)^2}{3(23.92/2)(29000)} = 0.318 \text{ in.}$$

From plastic hinge theory, the rotation of the hinge is

$$\theta = \frac{\Delta_T - \Delta_Y}{L - a/2}$$

For this plastic hinge rotation, the total monotonic deflection, Δ_T, corresponding to a strain of 20% is:

$$\Delta_T = \theta(L - \frac{a}{2}) + \Delta_Y$$

$$= 0.090[7.5(12) - \frac{0.1197(7.5)(12)}{2}] + 0.318$$

$$= 7.615 + 0.318 = \underline{7.933 \text{ in.}}$$

From cyclic test data, maximum tip deflection, is Δ_{max} = 1.5 in., the plastic portion of this deflection is

$$\Delta^* = \Delta_{max} - \Delta_Y = 1.5 - 0.318 = 1.182 \text{ in.}$$

From the fatigue damage theory, the number of cycles at a plastic deflection of 1.182 corresponds to a damage level attained at a monotonic plastic deflection of 7.615 in. of:

$$\mu^* = \mu_p(2N_f)^{-0.6}$$ (continued)

Table 4.9 (continued)

$$\frac{\Delta^*}{\Delta_Y} = \frac{\Delta_p}{\Delta_Y}(2N)^{-0.6}$$

$\Delta^* = 1.182$; $\Delta_p = \Delta_T - \Delta_Y = 7.933 - 0.318 = 7.615$ in.

$$1.182 = 7.615(2N)^{-0.6}$$

$$2N_f = 22.30 \text{ reversals}$$

$$N_f = \underline{11.15 \text{ cycles for failure}}$$

From the Popov and Bertero data, the number of cycles to failure is about 10 cycles. This value is compared to the 11.15 cycles computed above and based on a maximum allowable strain of 20%. Lower values of allowable monotonic strain will drop the number of cycles accordingly.

For Test Series No. 2

From Popov and Bertero data, a simply supported W24 x 76 beam 15 feet long was attached to a column stub at midspan where the column was 3.75 feet long on either side of the beam.

Deflection of column end was 1.0 inch so rotation of hinge was

$$\theta = \frac{1.0}{[\frac{7.5}{2}](12)} = 0.0222 \text{ radians}$$

The beam hysteretic plastic strain, $\epsilon^* = \frac{\theta(2c)}{a}$

where $a = \frac{0.14L}{1.14}$ or $0.1228L$

The computed value of hysteretic plastic strain is

$$\epsilon^* = \frac{0.0222(24)}{0.1228(7.5)(12)} = 0.0482 \text{ or } 4.82\%$$

If $\epsilon_p = 20\%$ for monotonic loading

$$\mu^* = \mu_p(2N_f)^{-0.6}$$

$$\frac{\epsilon^*}{\epsilon_y} = \frac{\epsilon_p}{\epsilon_y}(2N_f)^{-0.6}$$

$$4.82 = 20.0(2N_f)^{-0.6}$$

$$2N_f = 10.714 \text{ Reversals}$$

$$N_f = \underline{5.36 \text{ cycles}}$$

This result compares well with the experimental data.

Table 4.10 Evaluation of Experimental Data from Bertero, Popov and Krawinkler (12)

This data concerns a beam-column assembly using a 14B22 section.

The following data was obtained:
Moment Arm, L = 6 ft.
Shape Factor, f = 1.14
Section Height, 2c = 13.70 in.
Modulus of Elasticity, E = 29000 ksi
Yield Stress, σ_y = 36 ksi

Total Deflection, Δ_T, from hinge rotation = 3.77 in.

The deflection corresponding to full yield is

$$\Delta_Y = \frac{1.14\sigma_y L^2}{3cE} = \frac{1.14(36)(72)^2}{3(13.70/2)(29000)} = 0.357 \text{ in.}$$

$$\text{Hinge Rotation } \theta = \frac{\Delta_T - \Delta_Y}{L - a/2} = \frac{3.77 - 0.357}{72[1 - \frac{0.14}{1.14}]} = 0.054 \text{ radians.}$$

This result agrees with Figure 8 of this reference.

The corresponding strain for this rotation is

$$\epsilon^* = \frac{\theta(2c)}{a} = \frac{0.054(13.70)}{\frac{0.14}{1.14}(72)} = 0.0837$$

$\epsilon^* = \underline{8.37\%}$ This is the hysteretic strain applied over each cycle.

If the monotonic plastic strain, ϵ_p, permitted is 20%, then from fatigue theory, $\mu^* = \mu_p(2N_f)^{-0.6}$

Then $$\frac{\epsilon^*}{\epsilon_y} = \frac{\epsilon_p}{\epsilon_y}(2N_f)^{-0.6}$$

$$\epsilon^* = \epsilon_p(2N_f)^{-0.6}$$

$$8.37 = 20.0(2N_f)^{-0.6}$$

$$2N_f = 4.27 \text{ Reversals}$$

$$N_f = \underline{2.14 \text{ cycles}}$$

This is a realistic result from theory and agrees with experimental results.

Table 4.11a Evaluation of Experimental Data from Popov et al. (56)

Popov et al. tested beam-column assemblies and obtained the following results:

For Specimen No. 1 W18 x 50 beam
Shape Factor, f = 1.120
Modulus of Elasticity, E = 29000 ksi
Yield Stress, σ_y = 46.4 ksi
Moment Arm, L = 5.4 ft.
Section Height, 2c = 18.0 in.
Maximum Cyclic Displacement, in. = 1.20 in.
Maximum Shear Strain in Panel Zone = 0.008
Loading is constant amplitude cycling

Deflection at fully yielded cross section:

$$\Delta_Y = \frac{1.12\ \sigma_y L^2}{3cE} = \frac{1.12(46.4)(64.75)^2}{3(18.0/2)(29000)} = 0.278 \text{ in.}$$

The maximum deflection, Δ_T, is 1.20 in. The deflection caused by the rotation of the plastic hinge, Δ_p, is the total deflection minus the fully yielded deflection and deflection caused by shear strain of panel zone.

$$\theta = \frac{\Delta_p}{L - \frac{a}{2}} = \frac{1.20 - 0.278 - 0.008(64.75)}{64.75[a - \frac{0.12}{2(1.12)}]} = 0.00699 \text{ radians}$$

The corresponding hysteretic plastic strain is

$$\epsilon_{max} = \frac{\theta(2c)}{a} = \frac{0.00699(18.0)}{(\frac{0.12}{1.12})64.75} = 0.0181 \text{ or } 1.81\%$$

$$\mu^* = \mu_p(2N_f)^{-0.6}$$

$$\frac{\epsilon^*}{\epsilon_y} = \frac{\epsilon_p}{\epsilon_y}(2n_f)^{-0.6}$$

$$\epsilon^* = \epsilon_p(2N_f)^{-0.6}$$

If the monotonic plastic strain is assumed to be 15%, then

$$1.81 = 15(2N_f)^{-0.6}$$

$$2N_f = 33.94 \text{ reversals}$$

$$N_f = \underline{16.97} \text{ cycles}$$

This result agrees with values reported in this reference.

Table 4.11b Evaluation of Experimental Data from Popov et al. (56)

For Specimen No. 7 W18 x 71 Beam
Shape Factor, f = 1.142
Yield Stress, σ_y = 43.5 ksi
Modulus of Elasticity, E = 29000 ksi
Yield Resistance = 85k
Moment Arm, L = 5.4 ft
Section Height, 2c = 18.71 in.
Maximum Cyclic Displacement, in. = 2.25 in.
Maximum Shear Strain in Panel Zone = 0.022
Number of Reversals = 18

Loading is variable amplitude thus requiring calculation of the total energy dissipated to apply the damage index approach.

The deflection at a fully yielded cross section is

$$\Delta_Y = \frac{1.142\sigma_y L^2}{3cE} = \frac{1.142(43.5)(64.75)^2}{3(\frac{18.71}{2})(29000)} = 0.265 \text{ in.}$$

The maximum deflection is 2.25 in. but many cycles at a smaller deflection were applied so the total hysteretic energy dissipated will be computed.

This value is the total deflection at the end of the beam. A portion of this displacement is caused by the shear strain in the panel zone. The net hysteretic energy dissipated in the plastic hinge in the beam is

net hysteretic energy = (total - shear strain) hysteretic energy

From Figures 27 and 28 of the reference, the following values were computed

Total hysteretic energy dissipated = 1716 in-kips

Shear strain hysteretic energy dissipated in the panel zone = 765 in-kips

Net hysteretic energy dissipated in the beam plastic hinge = 951 in-kips

The hysteretic plastic ductility required to dissipate this amount of hysteretic energy in uniform cycling can be computed from the total number of reversals and the net hysteretic energy.

$$\text{Damage Index} = \left[\frac{HYSP + HYSN}{2N_f R_Y U_Y \mu^*}\right]^2 + \left[\frac{HYSP - HYSN}{2N_f R_Y U_Y \mu^*}\right]^2$$

(continued)

Table 4.11b (continued)

where HYSP + HYSN = Total Actual Hysteretic Energy Dissipated

HYSP - HYSN = 0; The hysteretic cycles are symmetric

Yield Resistance, R_Y = 85k

Yield Displacement, Δ_Y = 0.278 in.

Number of Reversals, $2N_f$ = 18

Damage Index = 1.0

$$1.0 = \left[\frac{\text{Actual Hysteretic Energy}}{R_Y \Delta_Y 2N_f \mu^*}\right]^2 + 0$$

or taking square root of both sides and solving for μ^*

$$\mu^* = \frac{\text{Hysteretic Energy}}{[\frac{\text{Yield}}{\text{Resistance}}][\frac{\text{Yield}}{\text{Displacement}}][\text{Reversals}]} =$$

$$\mu^* = \frac{951}{(85k)(0.278)(18)} = 2.236 \quad \text{Hysteretic Plastic Ductility}$$

But this can be converted into a monotonic plastic ductility by the fatigue damage theory:

$$\mu^* = \mu_p (2N_f)^{-0.6} = \mu_p (18)^{-0.6} = 0.1765\ \mu_p$$

Therefore,

$$\mu_p = \frac{\mu^*}{0.1765} = \frac{2.236}{0.1765} = \underline{12.67}$$

This corresponds to a plastic deformation of 12.67(0.278) = 3.52 in. Thus, one plastic excursion of 3.52 in. would cause identical damage to 18 reversals at 2.25 in. of total (elastic plus plastic) deflection.

Table 4.12 Further Evaluation of Krawinkler et al. Data (38) for W4 x 13 Beams

Further evaluation of the Krawinkler data presented for tests of a W4 x 13 cantilever specimen reveals the relationship with theory presented herein.

The full yield displacement for this W4 x 13 member can be computed as

$$\Delta_p = \frac{f\sigma_y L^2}{3cE}$$

where f is the shape factor, σ_y is the yield stress, L is the moment arm, c is one-half of the section height and E is the Modulus of Elasticity.

For this section

Shape Factor, f = 1.15
Yield Stress, σ_y = 49 ksi
Moment Arm, L = 40 in.
Maximum Monotonic Deflection Δ_T = 12.0 in.
Section Height, 2c = 4.244 in.
Modulus of Elasticity, E = 29000 ksi

The deflection at a fully yielded cross section is

$$\Delta_Y = \frac{1.15(49)(40)^2}{3(2.122)(29000)} = 0.488 \text{ in.}$$

The plastic hinge rotation can be computed as

$$\theta = \frac{\Delta_T - \Delta_Y}{(L - a/2)}$$

where θ is the rotation in radians, Δ_T is the total deflection and the hinge length, a, is (0.15/1.15)L.

The specimen was monotonically loaded to 12 inches, this corresponds to a plastic hinge rotation of

$$\theta = \frac{12 - 0.488}{40[1 - \frac{0.15}{2(1.15)}]} = 0.3079 \text{ radians}$$

and a corresponding monotonic plastic strain of

$$\epsilon = \frac{\theta(2c)}{a} = \frac{0.3079(4.244)}{\frac{0.15}{2/26}(40)} = 0.250 \text{ or } 25\%$$

(continued)

Table 4.12 (continued)

This strain is equivalent to a monotonic plastic ductility of

$$\mu_p = \frac{12.0 - 0.488}{0.488} = 23.59$$

For comparison purposes, set the maximum monotonic plastic strain to other values.

Case Number	Monotonic Maximum Strain, ϵ_p, %	Total Deflection, Δ_T, in.	Plastic Deflection, $\Delta_T - \Delta_Y$, in.	Monotonic Plastic Ductility, μ_p(1)
A	20	9.68	9.19	18.83
B	25	12.00	11.51	23.59
C	30	14.28	13.79	28.26
D	35	16.58	16.09	32.97
E	40	18.87	18.38	37.66

The values of hysteretic plastic ductility, μ^*, causing failure over the specified number of reversals obtained from the data can be compared with the predicted results from theory.

Reversals $2N_f$	μ^* from data	Predicted μ^* for Case A	Case B	Case C	Case D	Case E
28	5.30	2.55	3.19	3.83	4.47	5.10
16	5.38	3.57	4.47	5.35	6.25	7.14
30	5.32	2.45	3.07	3.67	4.29	4.89
42	4.11	2.00	2.50	3.00	3.50	4.00
36	4.10	2.19	2.75	3.29	3.84	4.39
184	1.91	0.82	1.03	1.24	1.44	1.65
90	1.98	1.27	1.59	1.90	2.21	2.53

Based on the information presented in this table, the results from Case C with a corresponding maximum plastic strain of 30% would closely match the data.

NOTE:

1. $\mu_p = \frac{\Delta_T - \Delta_Y}{\Delta_Y}$

Table 4.13 Evaluation of Krawinkler et al. Data (38) for W6 x 9 Beams

Krawinkler reported data for a W6 x 9 cantilever loaded to failure. This data was expanded from that found in Ref. 37 and addressed slender members more prone to local buckling. The experimental results can be compared against the results predicted from the theory developed in this study.

The deflection of the fully yielded beam can be computed from

$$\Delta_Y = \frac{f\sigma_y L^2}{3cE}$$

where Δ_Y is the deflection for fully yielded cross section, f is the section shape factor, σ_y is the yield stress, L is the moment arm, c is one-half of the section height and E is the Modulus of Elasticity.

For this W6 x 9 member

$L = 36$ in.
$f = 1.12$
$E = 29000$ ksi
$\sigma_y = 53$ ksi
$c = 2.95$ in.

$$\Delta_Y = \frac{1.12(53)(36)^2}{3(2.95)(29000)} = 0.30 \text{ in.}$$

The cantilevers were loaded monotonically to 8.5 inches and 6.10 inches of total deflection in two separate tests. The corresponding monotonic plastic ductility can be computed as:

Monotonic plastic ductility for 8.50 in. total displacement $\quad \mu_p = \frac{8.5 - 0.3}{0.3} = 27.33$

Monotonic plastic ductility for 6.10 in. total displacement $\quad \mu_p = \frac{6.10 - 0.3}{0.3} = 19.33$

Averaging these values, $\mu_p = 23.33$. This value can be used in the fatigue damage theory to predict the hysteretic plastic ductility, μ^*.

Reversals $2N_f$	From Data μ^*	Predicted from Theory, μ^* with $\mu_p = 23.33$	Predicted from Theory, μ^* with $\mu_p = 16$	Predicted from Theory, μ^* with $\mu_p = 10$
27	2.25	3.23	2.21	1.38
31	2.32	2.97	2.04	1.27
43	1.44	2.44	1.68	1.05
49	0.95	2.26	1.55	0.97
22	2.30	3.65	2.50	1.57

where $\mu^* = \mu_p(2N_f)^{-0.6}$

Table 4.14 Further Evaluation of Experimental Data from Popov and Pickney (59) - Monotonic Results

For monotonic test F1-S, a total displacement of 9.5 in. was applied. The strain corresponding to this deflection can be computed as:

Section Data: Yield Stress, σ_y = 38.9 ksi
Modulus of Elasticity, E = 29000 ksi
Shape Factor, f = 1.144
Section Height, 2c = 8.26 in.
Moment Arm, L = 66 in.

The tip deflection at a fully yielded cross section is

$$\Delta_Y = \frac{f\sigma_y L^2}{3cE}$$

$$\Delta_Y = \frac{1.144(38.9)(66)^2}{3(8.26/2)(29800)} = 5.25 \text{ in.}$$

During the test, the maximum tip deflection was 9.5 in. From plastic hinge theory, the hinge rotation, θ is

$$\theta = \frac{\Delta_T - \Delta_Y}{L - a/2}$$

where θ = plastic hinge rotation in radians = $\frac{9.5 - 0.525}{66 - 8.316/2}$ = 0.1451 radians = 8.315°

Δ_T = total tip deflection, in., = 9.5 in. for this test

Δ_Y = tip deflection at full yield, in.

L = moment arm, in. = 0.525 in.

a = hinge length, in. = $\frac{0.144L}{1.144}$ = 0.126(66) = 8.316 in.

L = 66 in.

Test results indicate that local buckling was first observed at a tip deflection of 2.0 inches. The strain at a tip deflection of 2.0 inches can be computed from the plastic hinge rotation, θ or

$$\theta = \frac{2.0 - 0.525}{66 - (8.316/2)} = 0.02385 \text{ radians}$$

The corresponding strain is

$$\epsilon = \frac{0.02385(8.26)}{8.316} = 0.0237 = \underline{2.37\%}$$

(continued)

Table 4.14 (continued)

This result indicates that a strain of 2.37% existed in the flanges when local buckling occurred.

The computed strain can be checked using local buckling criteria from Ref. (1). From Fig. 6.13 from this source, local flange buckling would occur for $\frac{b}{t} = \frac{5.268 \text{ in.}}{0.378 \text{ in.}} = 13.94$, at a predicted value of buckling strain of approximately 2%. This result confirms the computed strain value of about 2 percent for a 2.0 in. tip displacement when local buckling was reported.

Table 5.1 Evaluation of the Hysteretic Response to El Centro Using the Damage Index Criterion

Structural Frequency hz(1)	Hysteretic Energy(2), in-lb HYSP	HYSN	Number of Reversals	Total Hysteretic Energy, HYST, and Corresponding Damage Index, DI, (3) for Specified Monotonic Plastic Ductilities, μ_p	μ_p=0.25	μ_p=0.50	μ_p=1.0	μ_p=2.0	μ_p=5.0
0.5	0	0	27	HYST=	947	1893	3787	7573	18933
				DI=	0	0	0	0	0
1.0	216	158	51	HYST=	305	610	1221	2442	6104
				DI=	1.54	0.38	0.096	0.024	0.004
2.0	257	326	81	HYST=	92	184	367	735	1836
				DI=	40.88	10.22	2.56	0.64	0.10
5.0	66	58	200	HYST=	21	42	84	169	421
				DI=	34.72	8.68	2.17	0.54	0.09
10.0	16	34	369	HYST=	7	13	27	54	135
				DI=	62.24	15.56	3.89	0.97	0.16

NOTES: 1. Results based on response reported in Appendix B. Yield resistance value set at 100 lb for all calculations; damping was five percent.

2. Hysteretic Energy values are reported for the Positive Resistance (HYSP) and Negative Resistance (HYSN) Hysteretic Energies.

3. Total Hysteretic Energy, HYST, is the energy value corresponding to a damaged condition based on the specified monotonic plastic ductility or

$$HYST = \mu^* R_Y U_Y (2N_f),$$

where $\mu^* = \mu_p (2N_f)^{-0.6}$, μ_p is the specified monotonic ductility, R_Y is the yield resistance, U_Y is the yield displacement and $2N_f$ is the total number of reversals.

The Damage Index, DI, is

$$DI = \left(\frac{HYSP + HYSN}{HYST}\right)^2 + \left(\frac{HYSP - HYSN}{HYST}\right)^2.$$

Table 5.2 Evaluation of the Hysteretic Response to Pacoima Dam Using the Damage Index Criterion

Structural Frequency hz(1)	Hysteretic Energy(2), in-lb HYSP	HYSN	Number of Reversals	Total Hysteretic Energy, HYST, and Corresponding Damage Index, DI, (3) for Specified Monotonic Plastic Ductilities, μ_p	μ_p=0.25	μ_p=0.50	μ_p=1.0	μ_p=2.0	μ_p=5.0
0.5	626	427	30	HYST=	987	1975	3950	7899	19748
				DI=	1.18	0.29	0.018	0.08	0.003
1.0	1165	1035	51	HYST=	305	610	1221	2442	6104
				DI=	52.14	13.03	3.26	0.81	0.13
2.0	1312	1154	102	HYST=	101	201	403	805	2014
				DI=	602.34	150.59	37.65	9.41	1.51
5.0	1050	1031	179	HYST=	20	40	81	161	404
				DI=	10641.86	2660.46	665.12	166.28	26.60
10.0	522	659	310	HYST=	6	13	25	560	126
				DI=	35814.19	8953.55	2238.39	50.26	89.54

See Table 5.1 for Notes 1, 2, & 3.

Table 5.3 Determination of the Ductility Values Corresponding to Code Drift Limits

For a Shear Building the maximum moment is $M = \frac{6EI\Delta}{L^2}$; this equation can be solved for deflection, or $\Delta = \frac{ML^2}{6EI}$. From ATC/NEHRP, the maximum allowable story drift is $\Delta_{max} = 0.015L$. This corresponds to a value of ductility, μ, times the yield displacement, Δ_Y, or $\mu\Delta_Y$. Equating the drift limit, Δ_{max}, to this multiple of the yield displacement, $\mu\Delta_Y$, and noting that at the yield point $M_Y = \sigma_y I/c$ where I is the moment of inertia, c is the distance from the neutral axis to the maximum tensile stress and σ_y is the yield stress. The following result is obtained:

$$0.015L = \mu[(\frac{\sigma_y I}{c})\frac{L^2}{6EI}] = \mu[\frac{\sigma_y L}{6cE}]$$

For typical values of yield stress, σ_y = 36 ksi, and Young's Modulus, E = 30,000 ksi, then the ductility is $\mu = 0.015[\frac{6c(30000)}{36L}] = 75c/L$ where c is one-half the section height and L is the story height.

For various values of c and L

c (in)	L (in)	μ	L (in)	μ	L (in)	μ
3	180	1.21	120	1.81	90	2.42
6	180	2.42	120	3.62	90	4.84
9	180	3.62	120	5.44	90	7.26
12	180	4.83	120	7.25	90	9.68
18	180	7.25	120	10.88	90	14.50

Ductility values corresponding to drift limits of 0.010L and 0.005L are 2/3 and 1/3, respectively, of the values above.

Table 5.4 Example of the Application of the Proposed Drift Criterion

Structural Frequency, hz	Number of Reversals	NEHRP Deflection Amplification Coefficient C_d	Duration Coefficient Q	Allowable Maximum Ductility μ_a
0.1	40	6.5	1.0	5.55
0.5	60	6.5	1.0	3.00
1.0	100	6.5	1.0	2.64
2.0	160	6.5	1.0	3.07
5.0	390	6.5	1.0	4.61
10.0	690	6.5	1.0	7.55
0.1	40	5.0	1.0	4.50
0.5	60	5.0	1.0	2.54
1.0	100	5.0	1.0	2.26
2.0	160	5.0	1.0	2.59
5.0	390	5.0	1.0	3.78
10.0	690	5.0	1.0	6.04
0.1	40	4.0	1.0	3.80
0.5	60	4.0	1.0	2.23
1.0	100	4.0	1.0	2.00
2.0	160	4.0	1.0	2.27
5.0	390	4.0	1.0	3.22
10.0	690	4.0	1.0	5.03
0.1	40	2.0	1.0	2.40
0.5	60	2.0	1.0	1.61
1.0	100	2.0	1.0	1.50
2.0	160	2.0	1.0	1.64
5.0	390	2.0	1.0	2.11
10.0	690	2.0	1.0	3.01
0.1	40	5.0	2.0	6.30
0.5	60	5.0	2.0	3.33
1.0	100	5.0	2.0	2.91
2.0	160	5.0	2.0	3.41
5.0	390	5.0	2.0	5.21
10.0	690	5.0	2.0	8.63

FIGURES

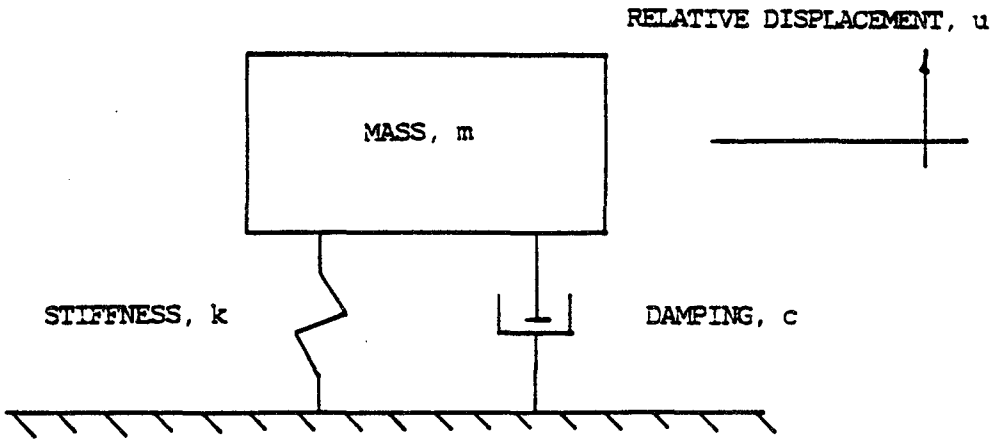

Figure 1.1 Single Degree of Freedom Structural System

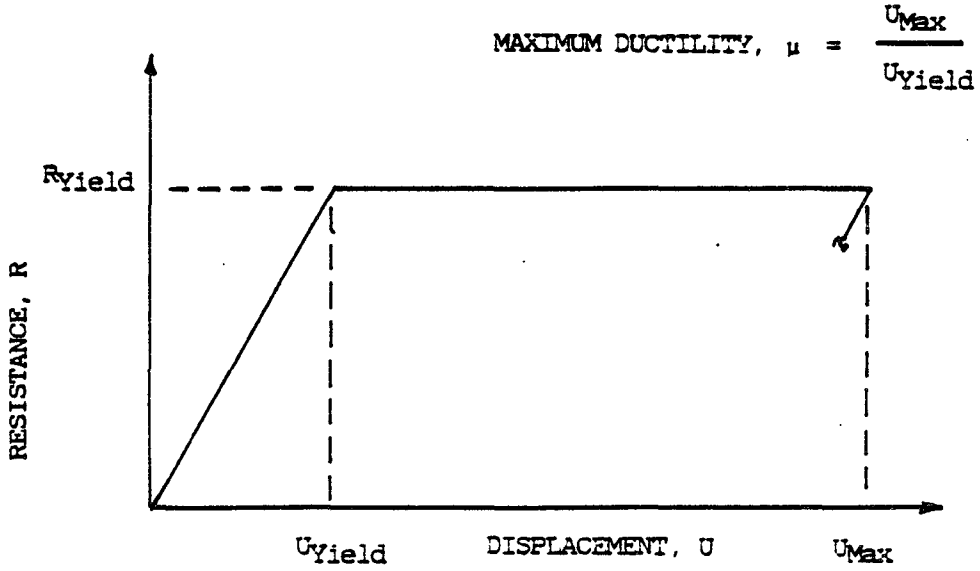

Figure 1.2 Definition of Maximum Ductility Based on an Elastoplastic Resistance Model

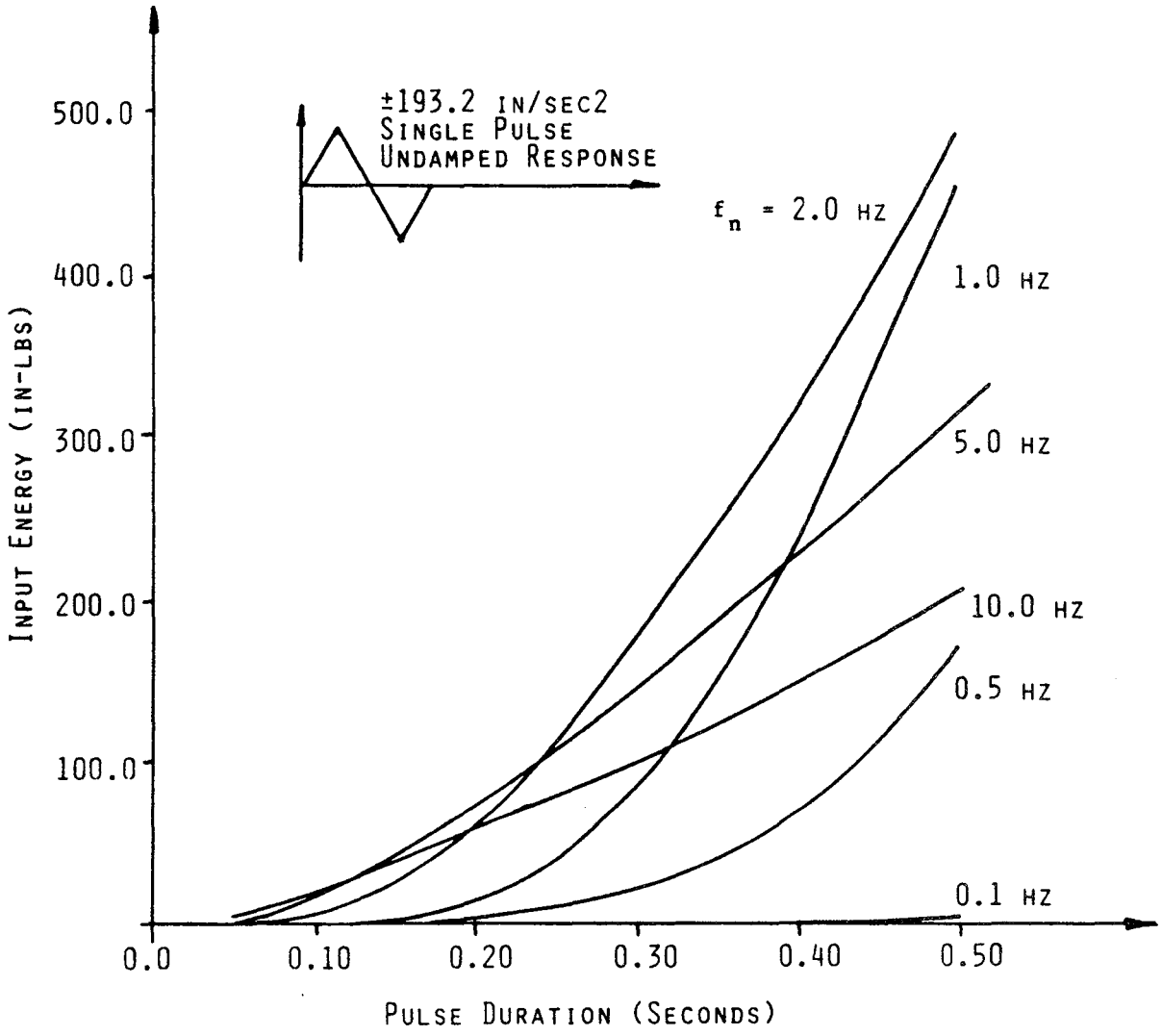

Figure 2.1a Input Energy Spectra for Undamped Structures Responding to a Balanced Simple Pulse

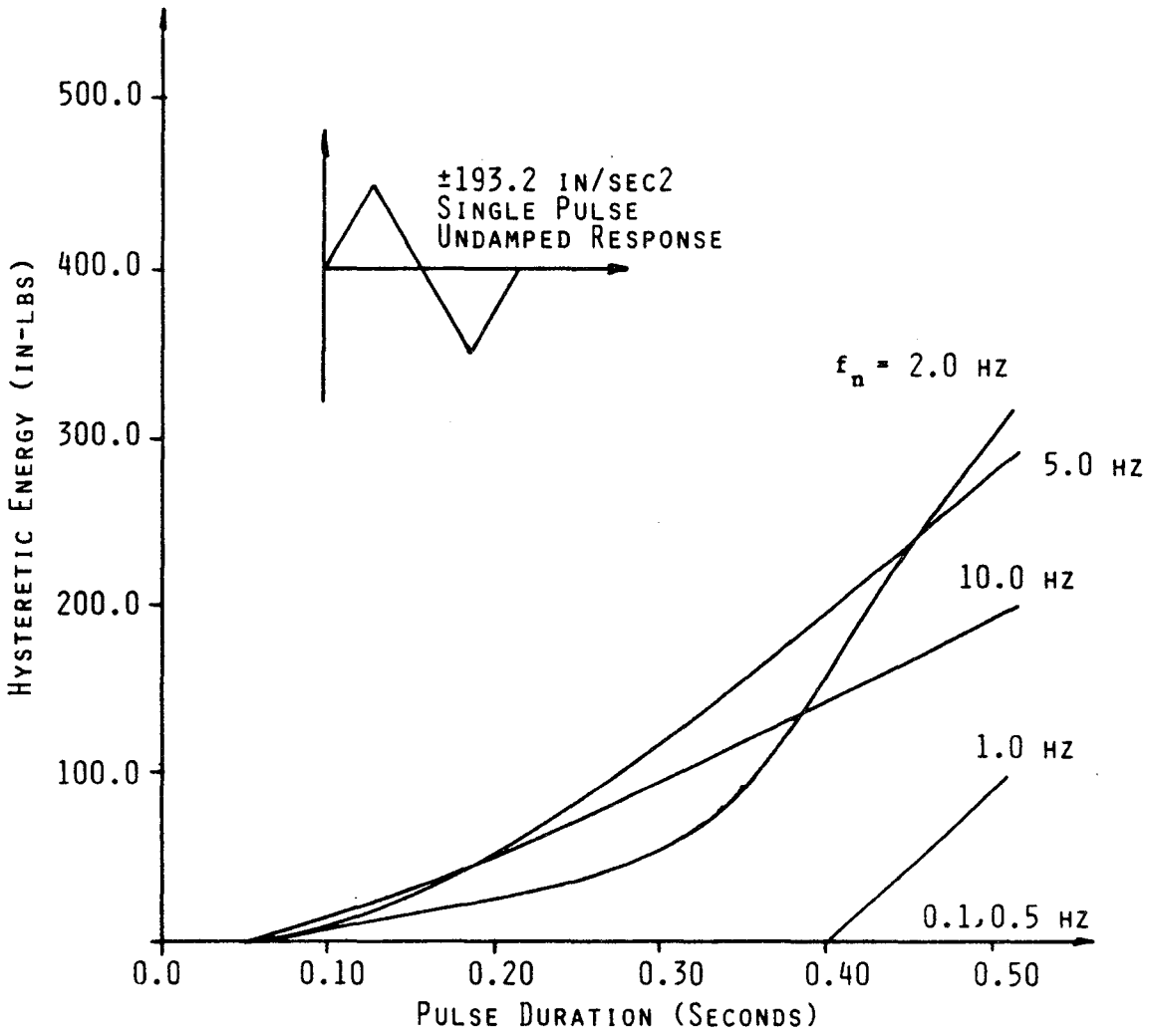

Figure 2.1b Hysteretic Energy Spectra for Undamped Structures Responding to a Balanced Simple Pulse

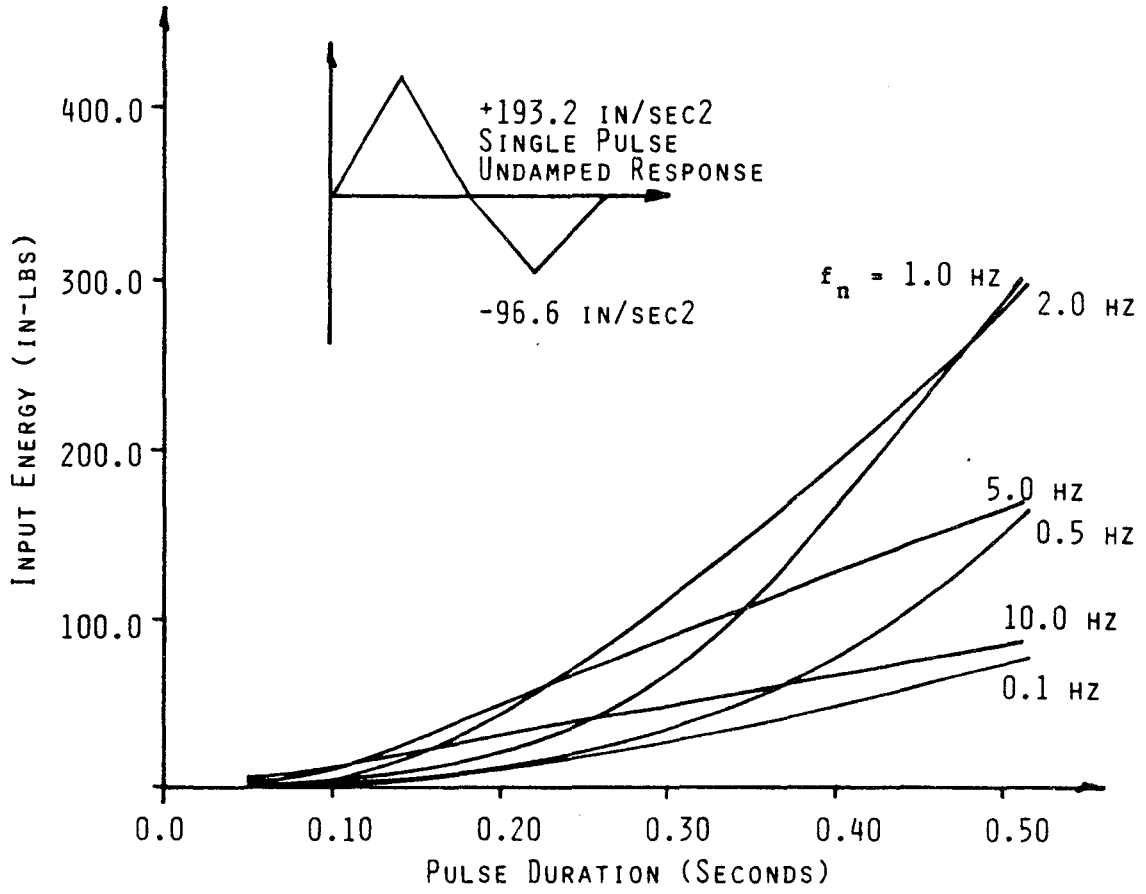

Figure 2.2a Input Energy Spectra for Undamped Structures Responding to an Unbalanced Simple Pulse

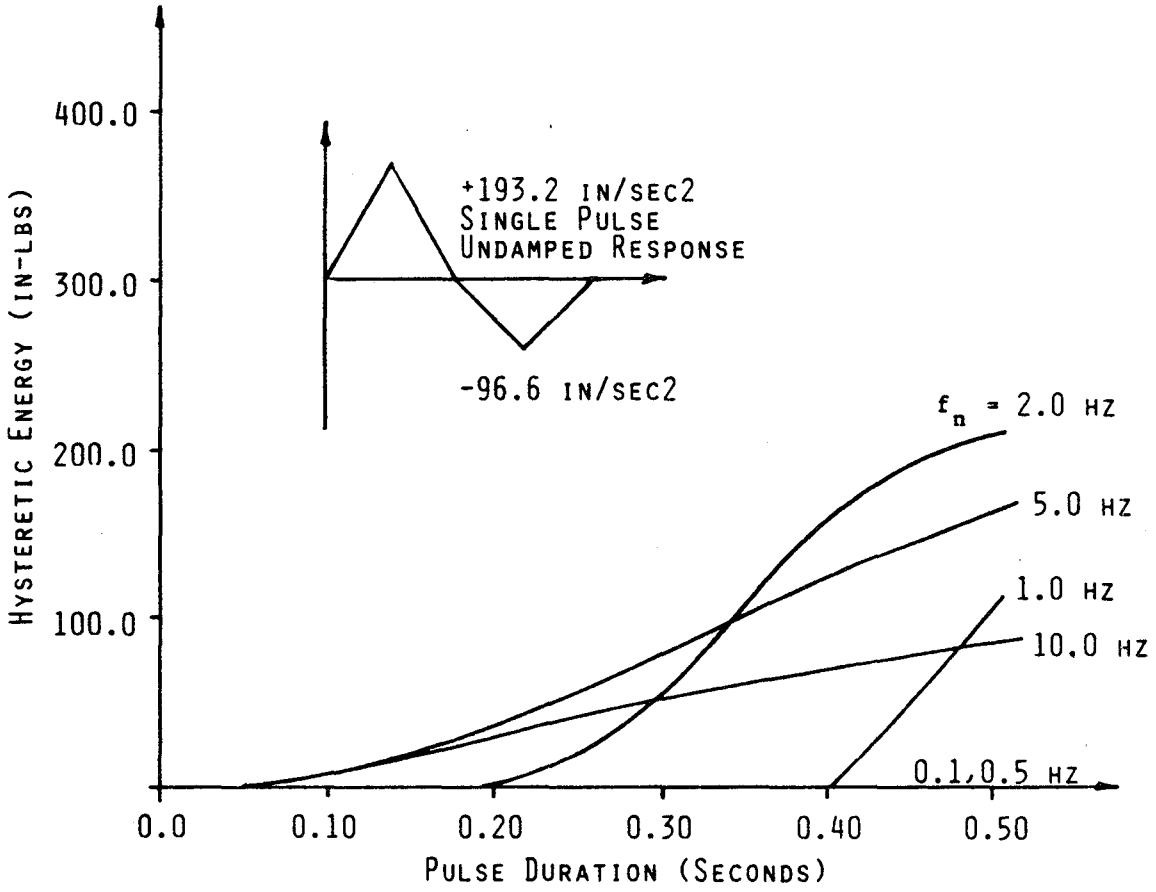

Figure 2.2b Hysteretic Energy Spectra for Undamped Structures Responding to an Unbalanced Simple Pulse

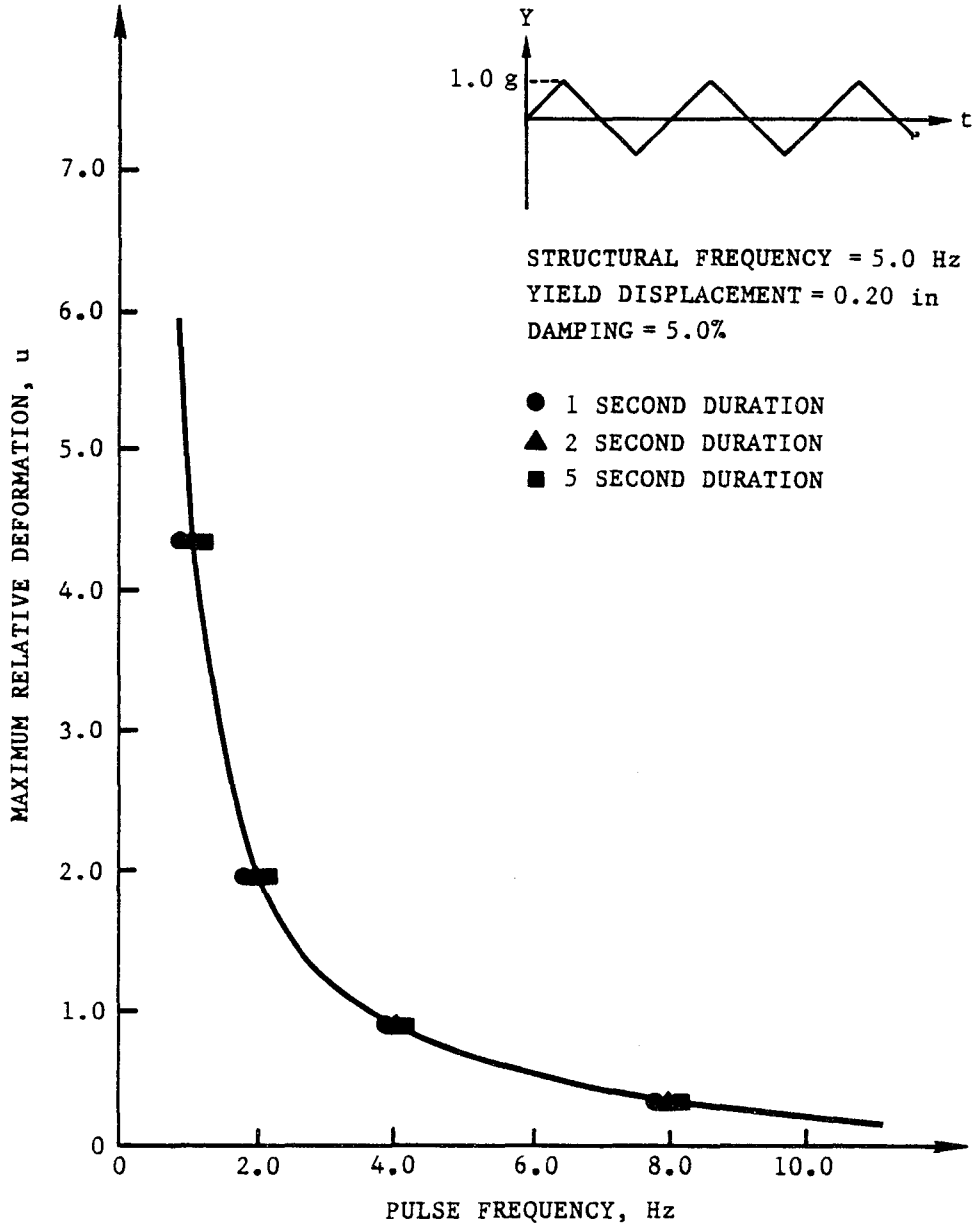

Figure 2.3 Maximum Input Energy of a 5 hz Structure Responding to a Repeated Simple Pulse of Various Duration and Frequency

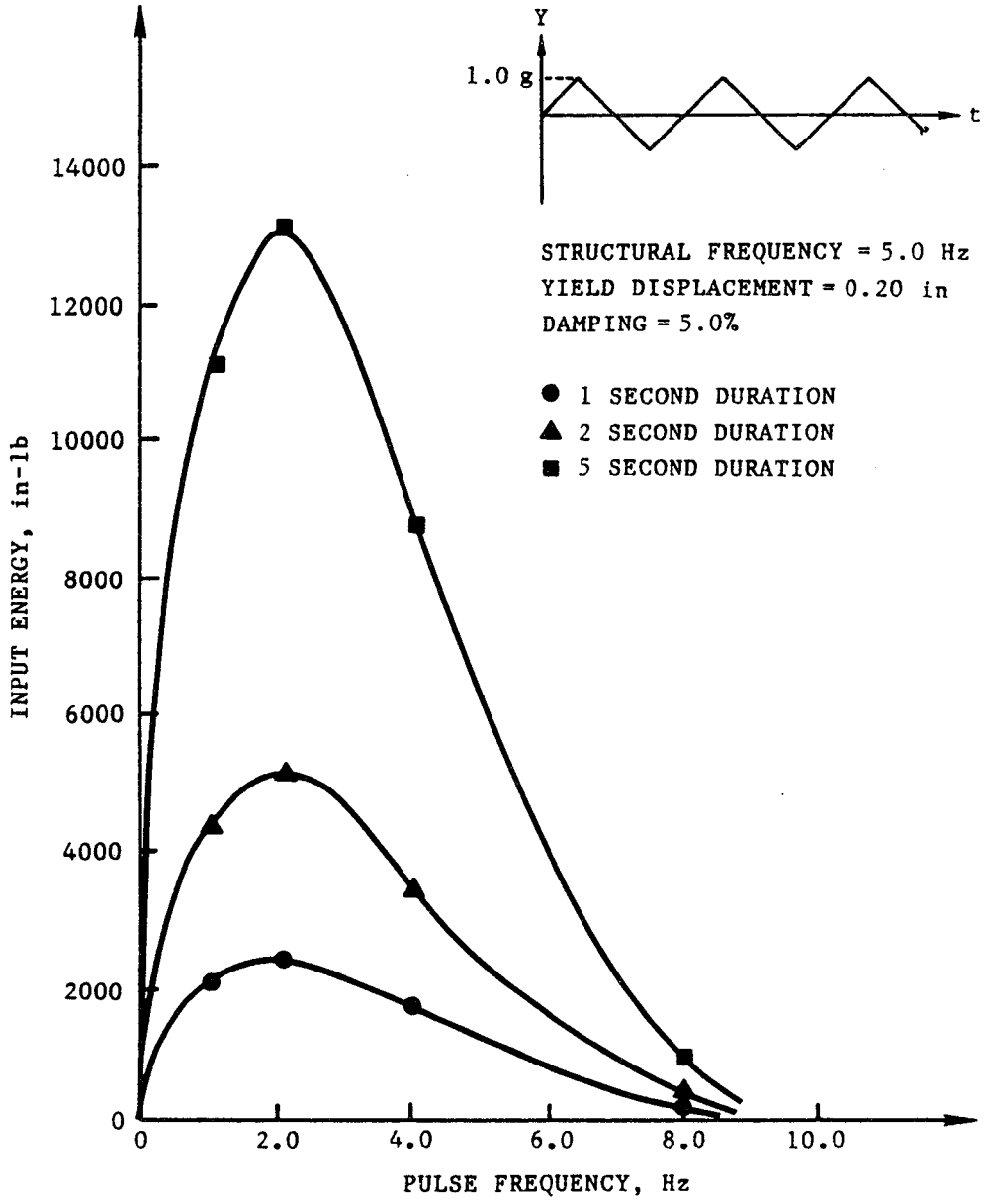

Figure 2.4 Maximum Input Energy of a 5 hz Structure Responding to a Repeated Simple Pulse of Various Duration and Frequency

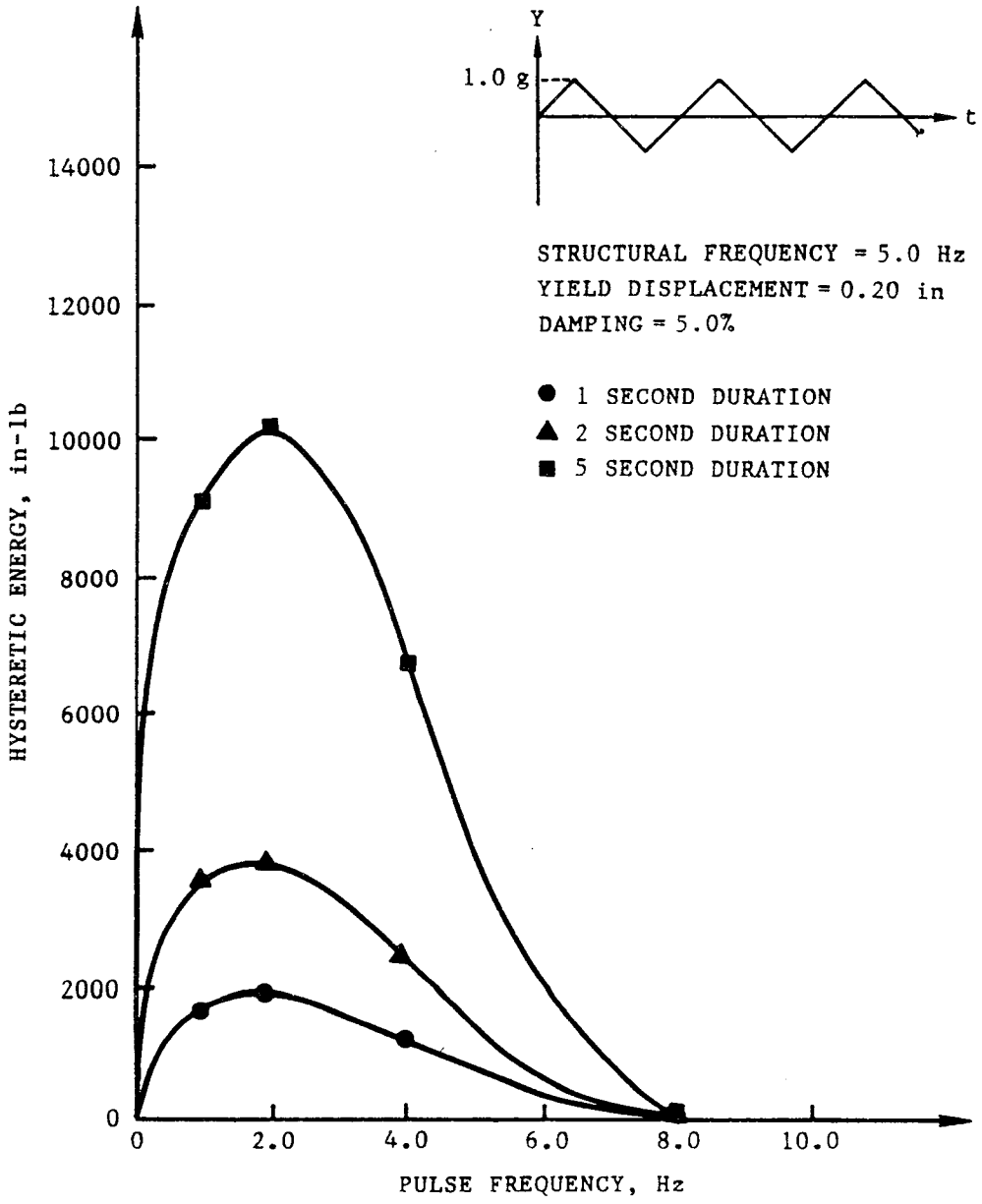

Figure 2.5 Dissipated Hysteretic Energy of a 5 hz Structure Responding to a Repeated Simple Pulse of Various Duration and Frequency

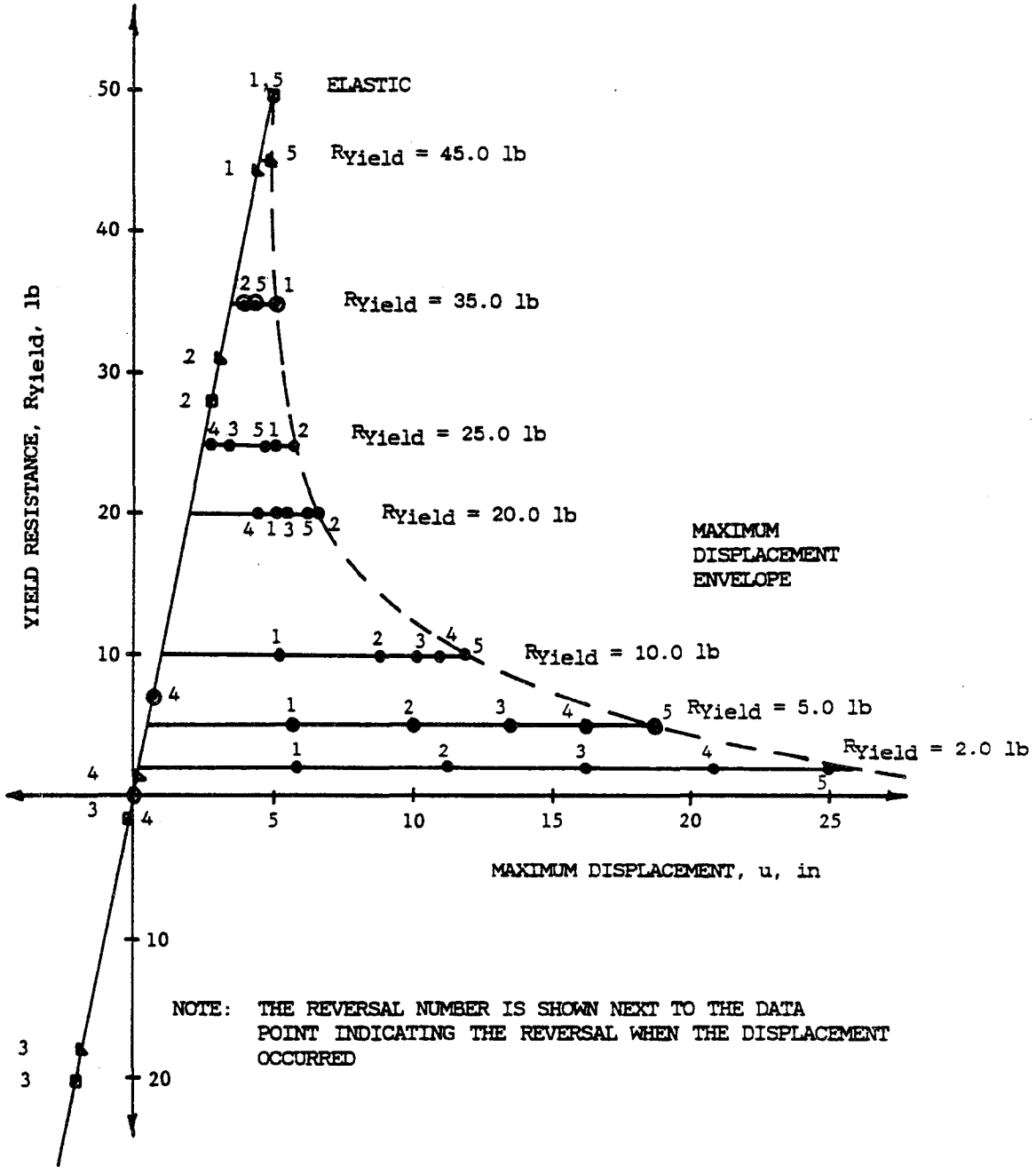

Figure 2.7c Maximum Displacement Versus Yield Resistance for Each of the First Five Reversals for Response of a 0.5 hz Undamped Structure to a 0.5g, 0.5 hz Repeated Pulse

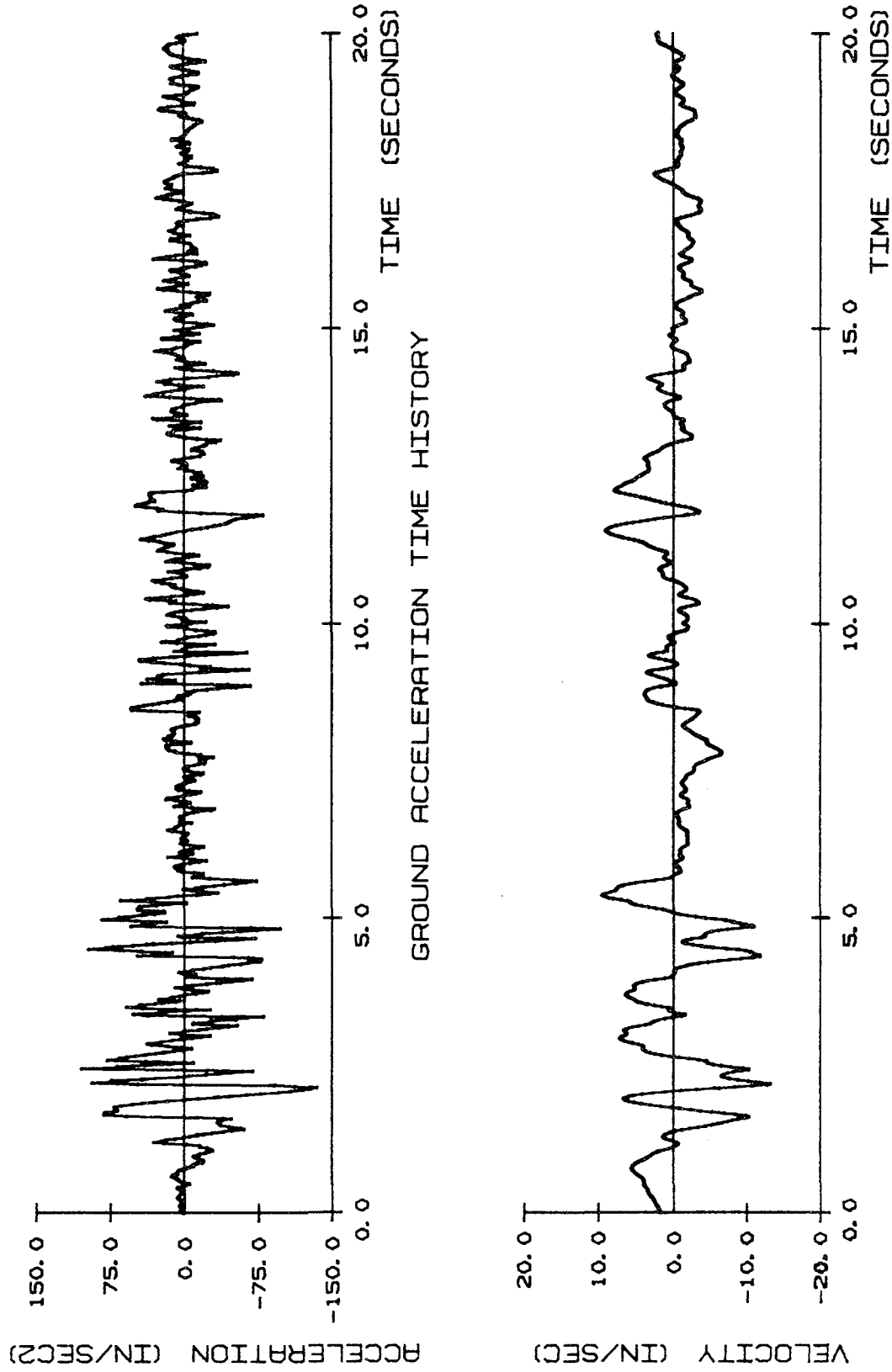

Figure 2.8a Ground Acceleration and Velocity Time Histories for the El Centro Record of May 18, 1940, S00E Component

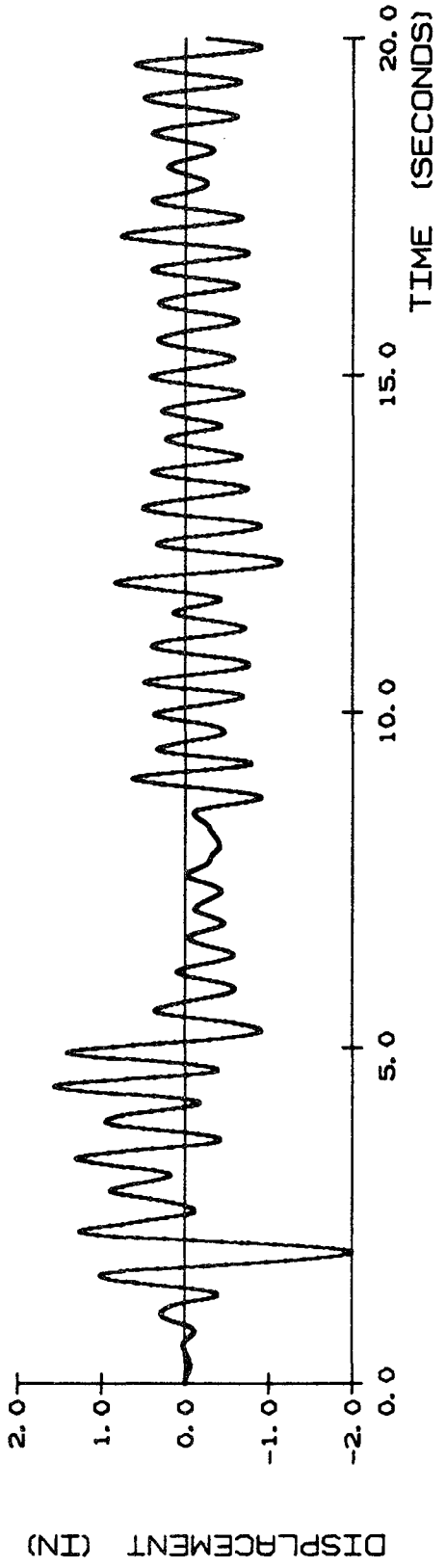

Figure 2.8b Relative Displacement Time History for a 2 hz Undamped Structure Responding to El Centro

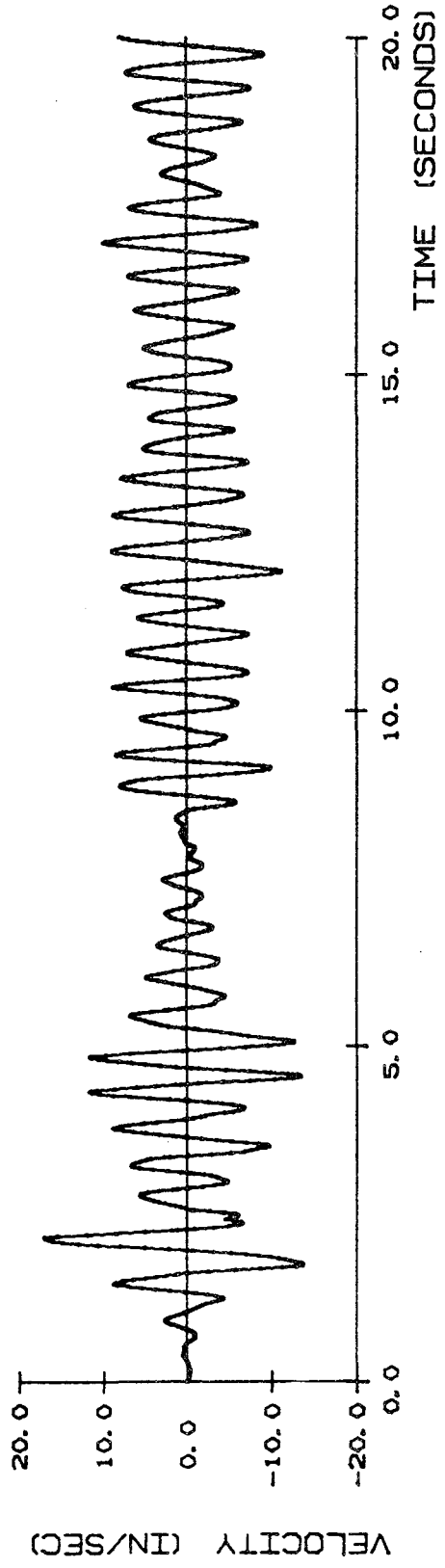

Figure 2.8c Relative Velocity Time History for a 2 hz Undamped Structure Responding to El Centro

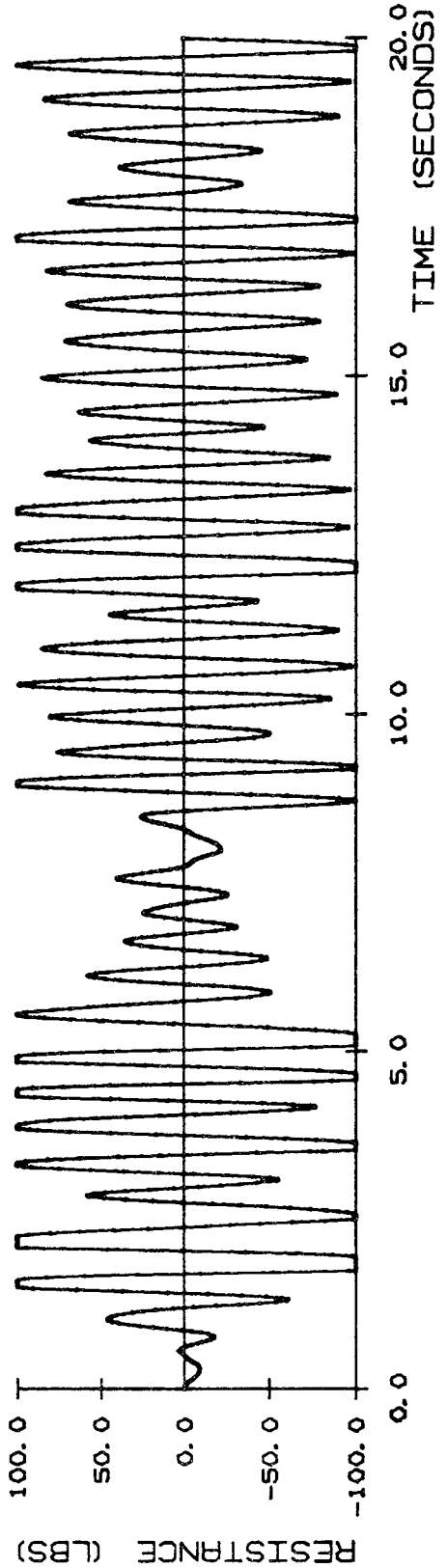

Figure 2.8d Resistance Time History for a 2 hz Undamped Structure Responding to El Centro

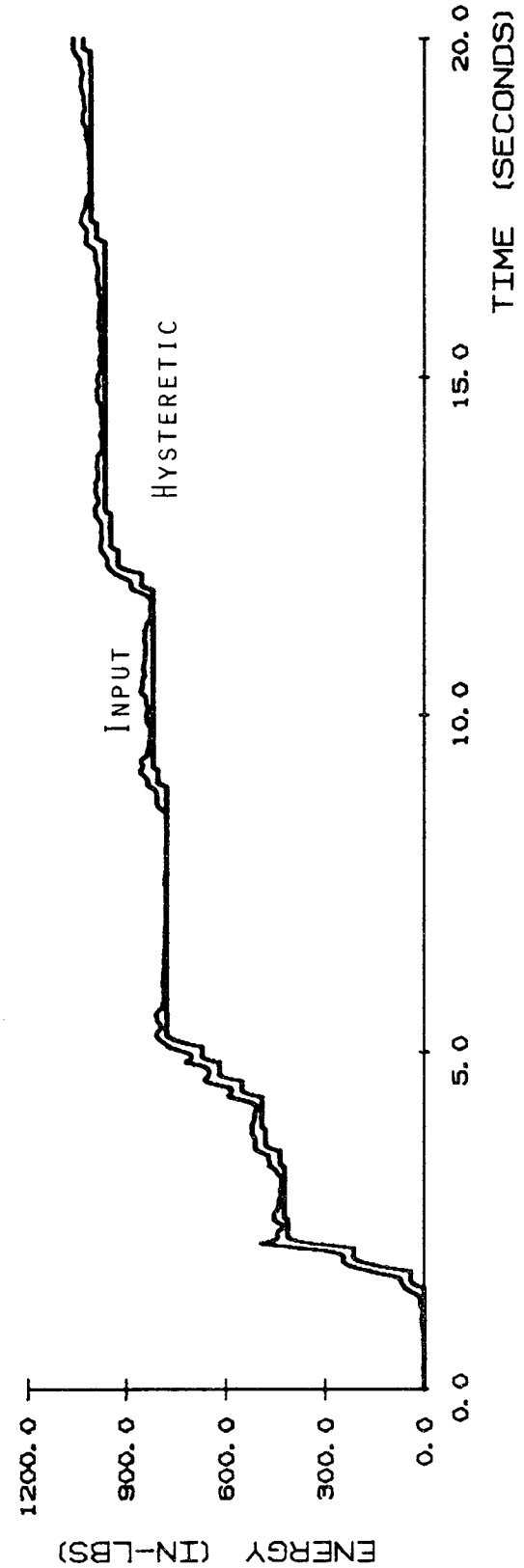

Figure 2.8e Energy Time History for a 2 hz Undamped Structure Responding to El Centro

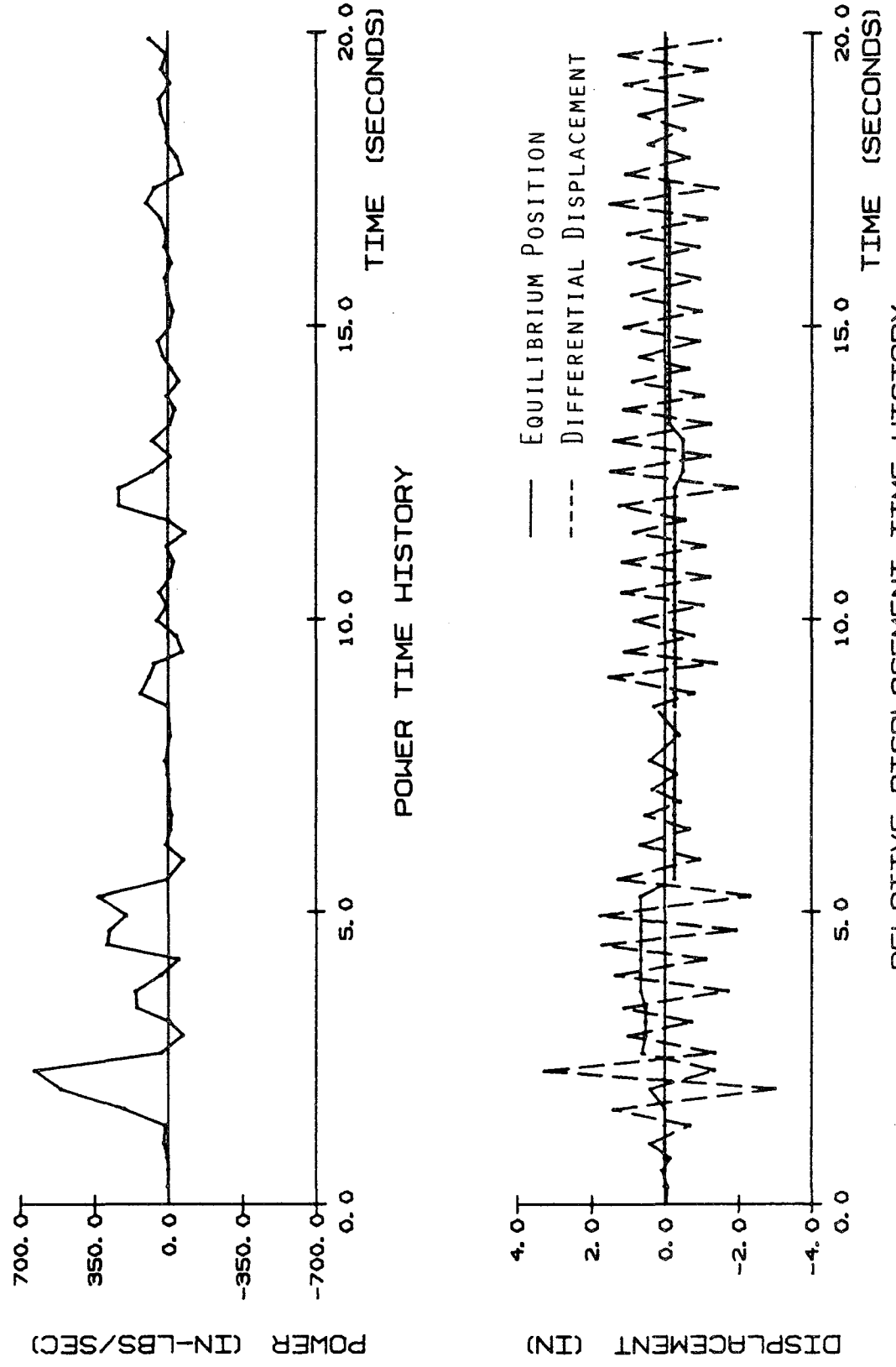

Figure 2.8f Structural Power and Displacement Time Histories for a 2 hz Undamped Structure Responding to El Centro

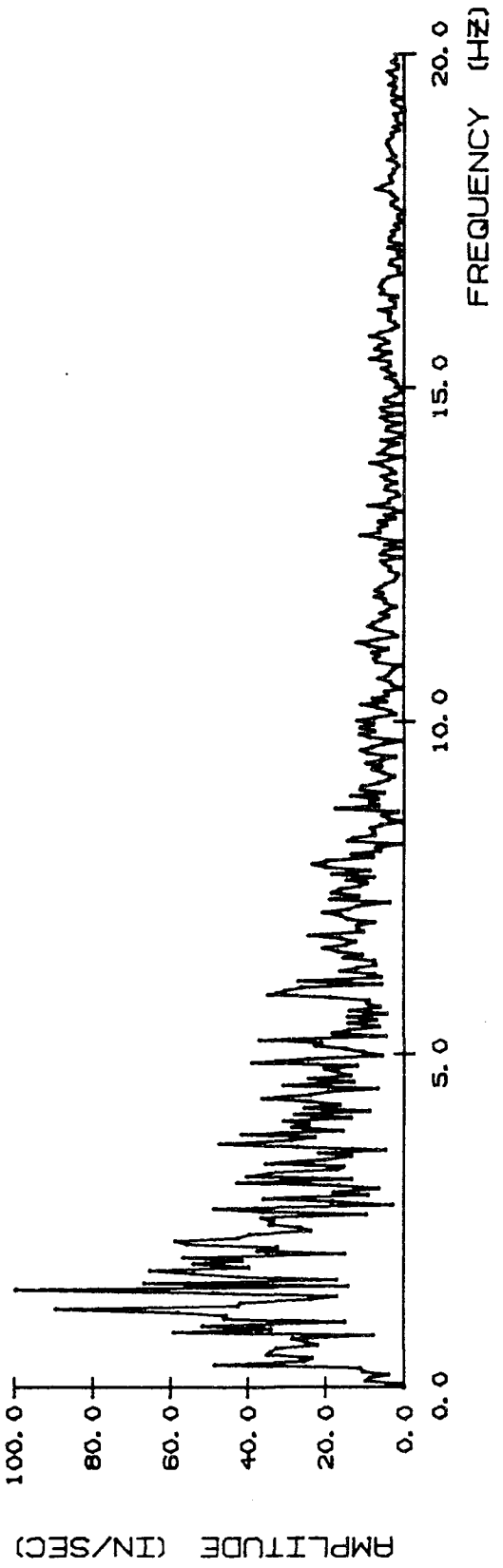

Figure 2.8g Ground Acceleration Fourier Amplitude Spectrum for El Centro

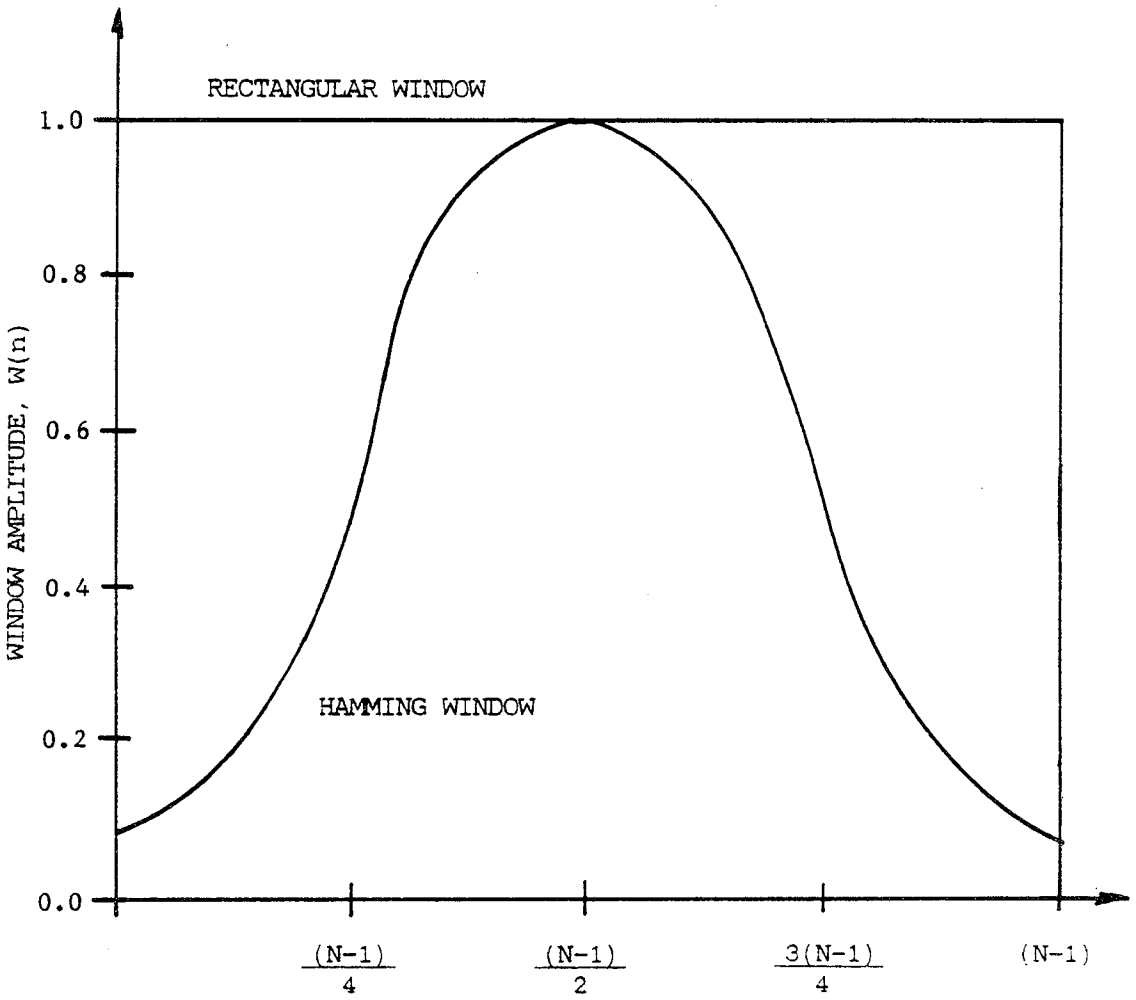

RECTANGULAR WINDOW $W(n) = 1.0; \quad 0 \leq n \leq N-1$

$0.0; \quad \text{ELSEWHERE}$

HAMMING WINDOW $W(n) = 0.54 - 0.46 \cos \frac{2\pi n}{N-1}; \quad 0 \leq n < N-1$

$= 0.0; \text{ ELSEWHERE}$

Figure 2.8h Time Window Functions

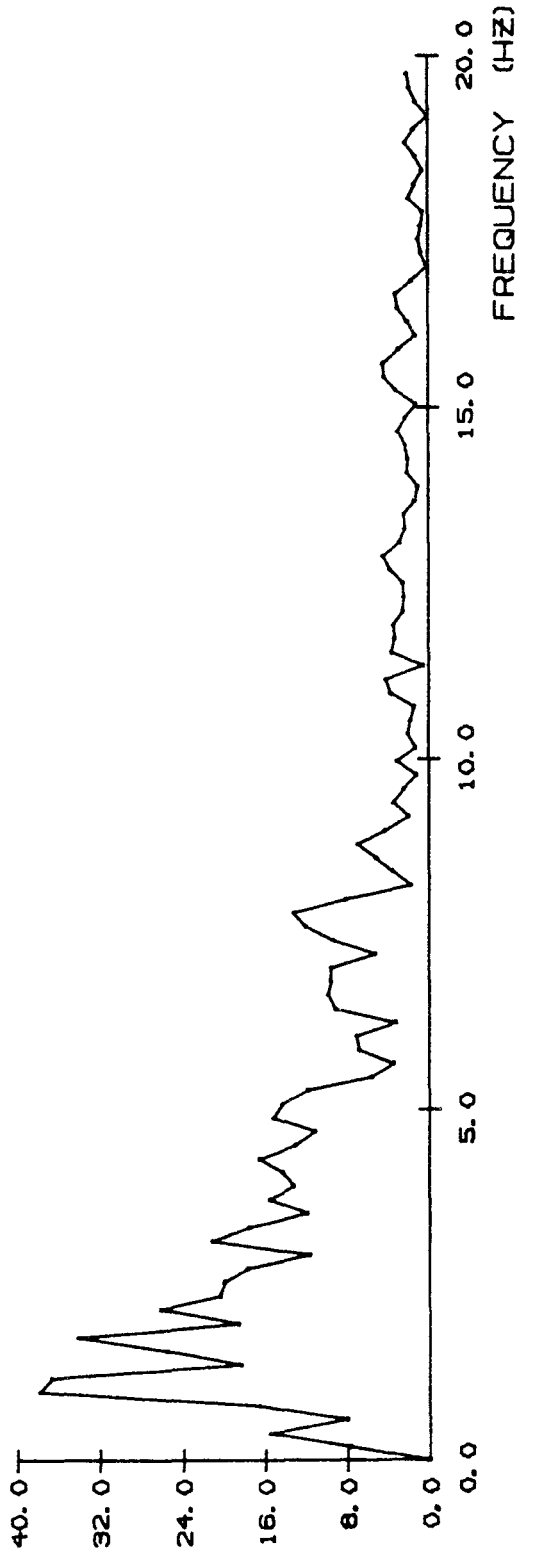

Figure 2.8i Fourier Amplitude Spectrum of the Ground Acceleration for the Time Window from 0.0-5.12 Seconds for El Centro

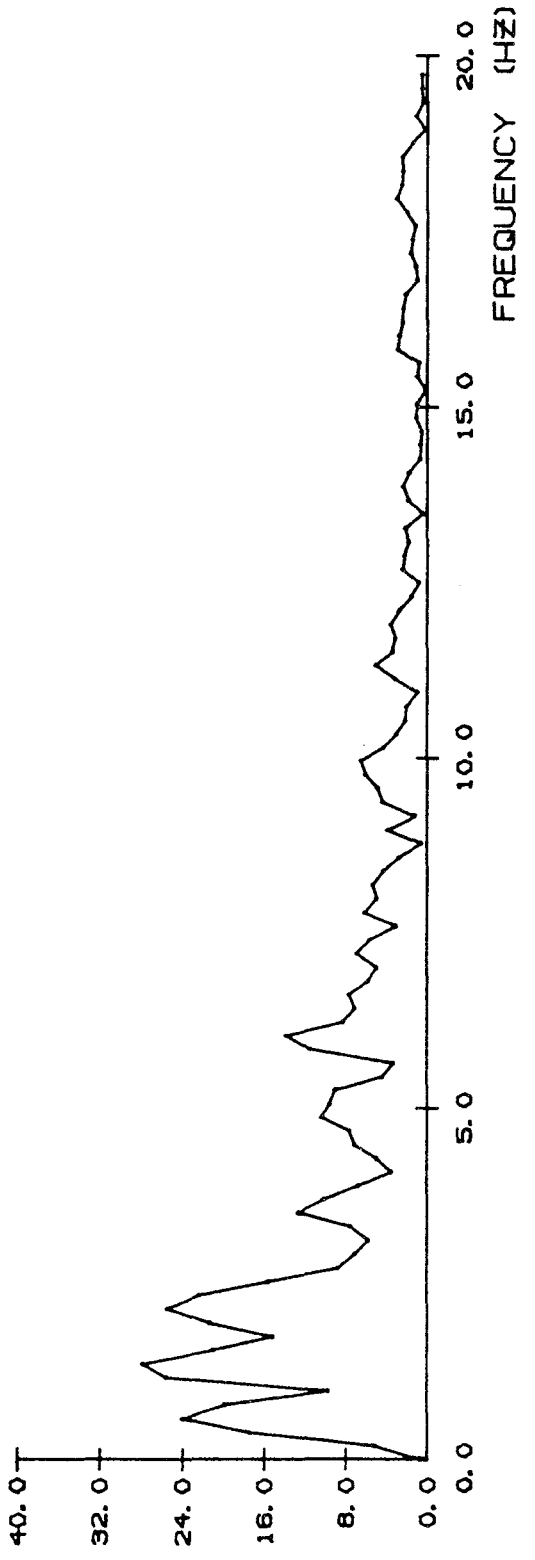

Figure 2.8j Fourier Amplitude Spectrum of the Ground Acceleration for the Time Window from 2.56-7.68 Seconds for El Centro

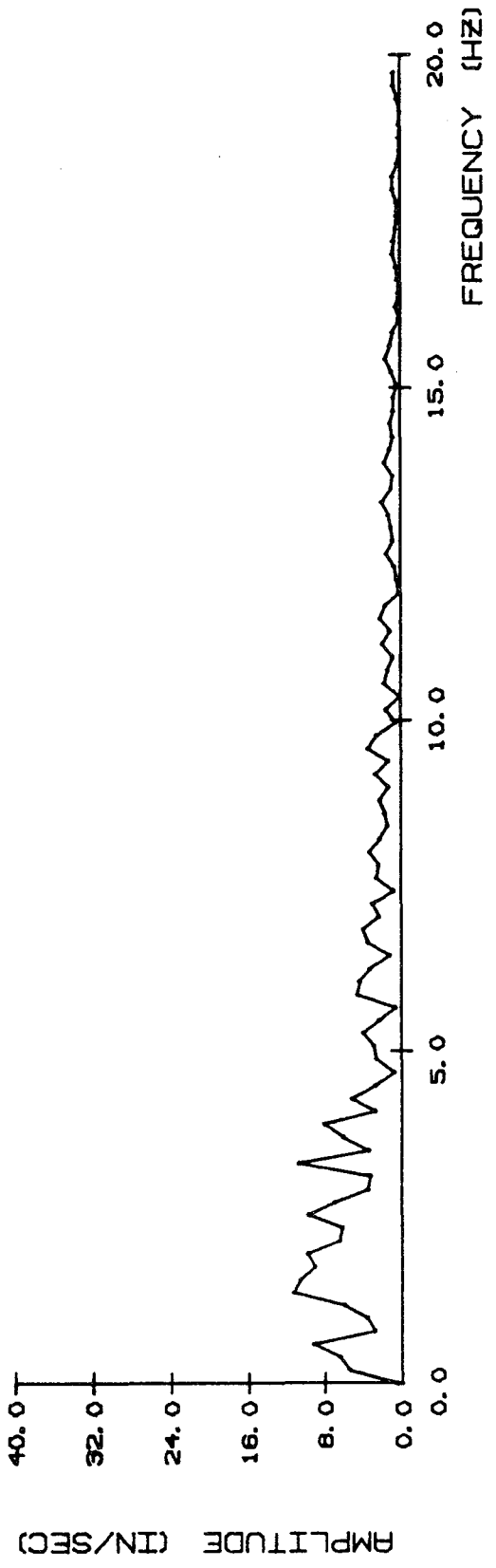

Figure 2.8k Fourier Amplitude Spectrum of the Ground Acceleration for the Time Window from 5.12-10.24 Seconds for El Centro

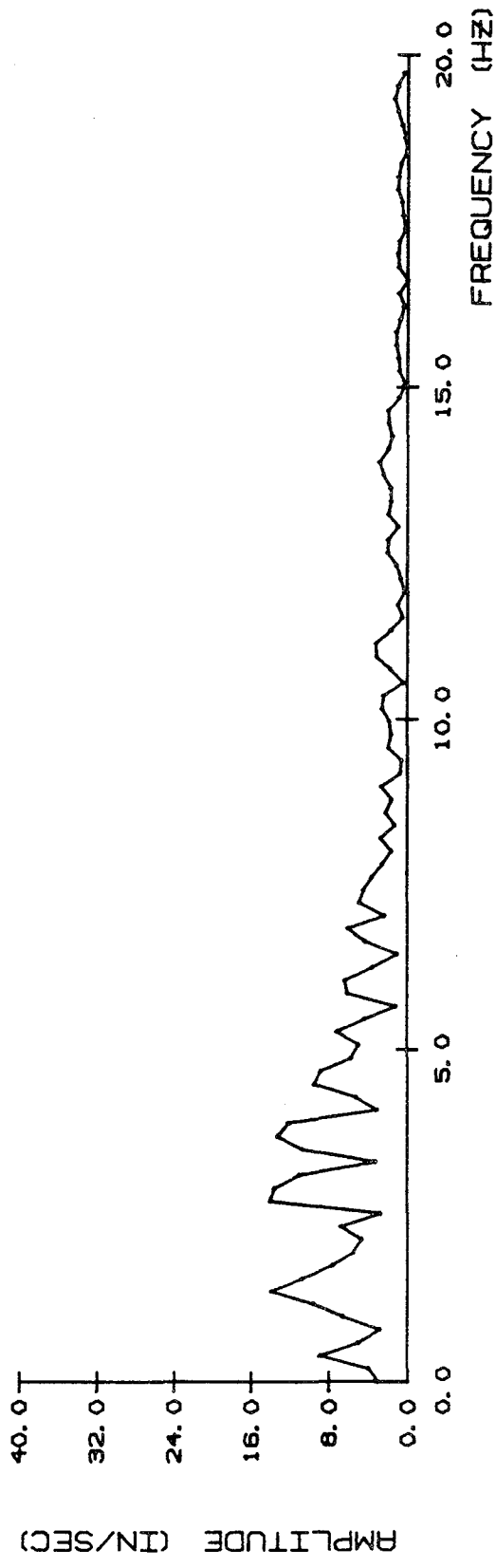

Figure 2.81 Fourier Amplitude Spectrum of the Ground Acceleration for the Time Window from 7.68-12.80 Seconds for El Centro

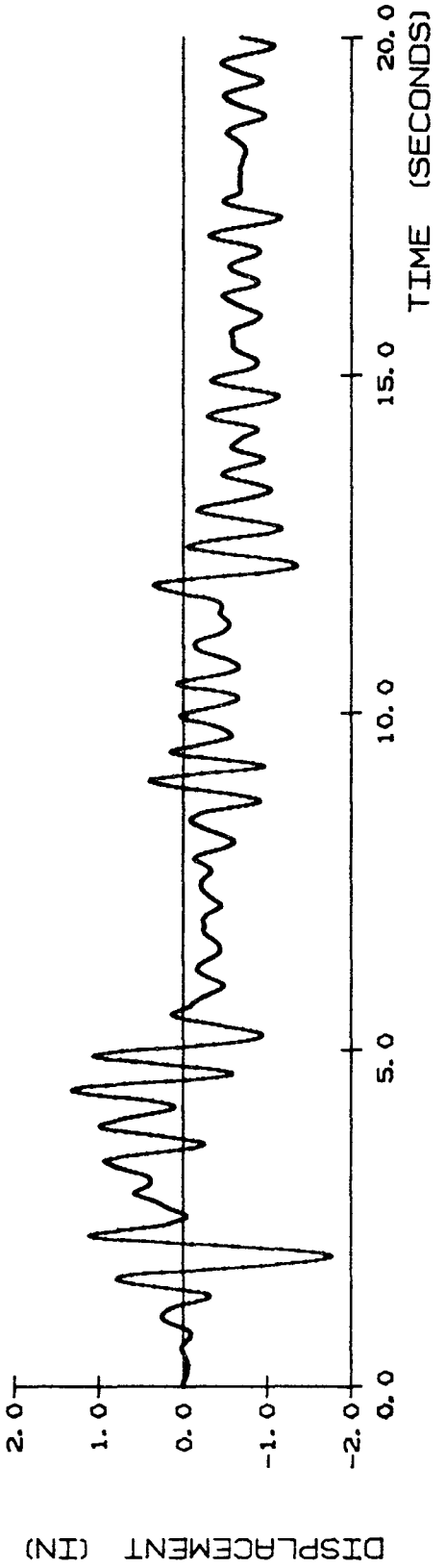

Figure 2.8m Relative Displacement Time History for a 2 hz, 5 Percent Damped Structure Responding to El Centro

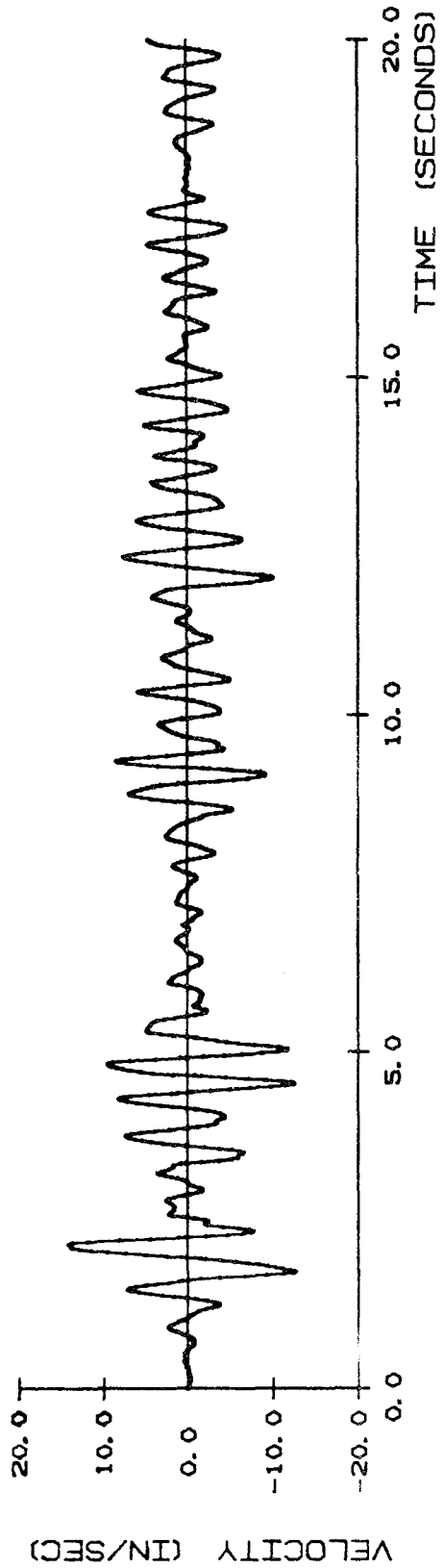

Figure 2.8n Relative Velocity Time History for a 2 hz, 5 Percent Damped Structure Responding to El Centro

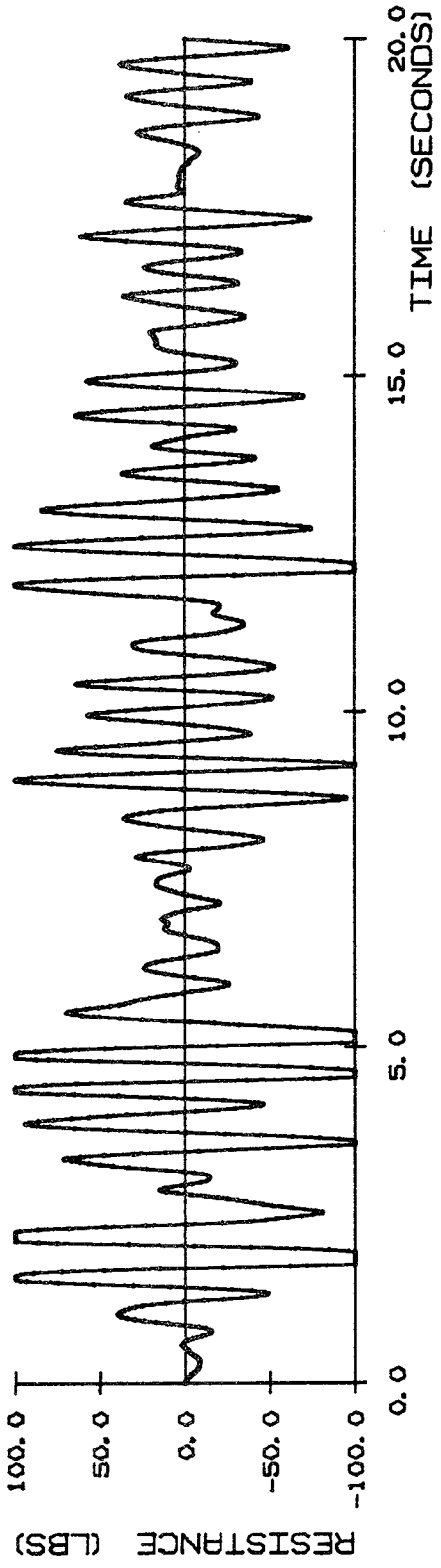

Figure 2.8o Resistance Time History for a 2 hz, 5 Percent Damped Structure Responding to El Centro

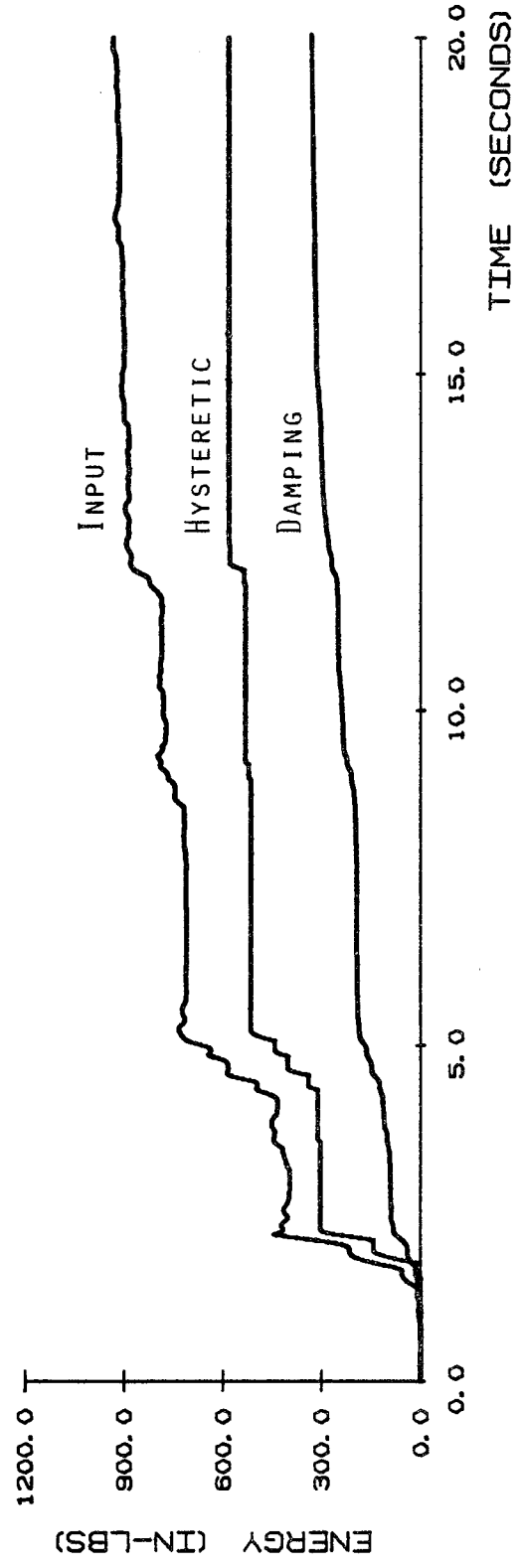

Figure 2.8p Energy Time History for a 2 hz, 5 Percent Damped Structure Responding to El Centro

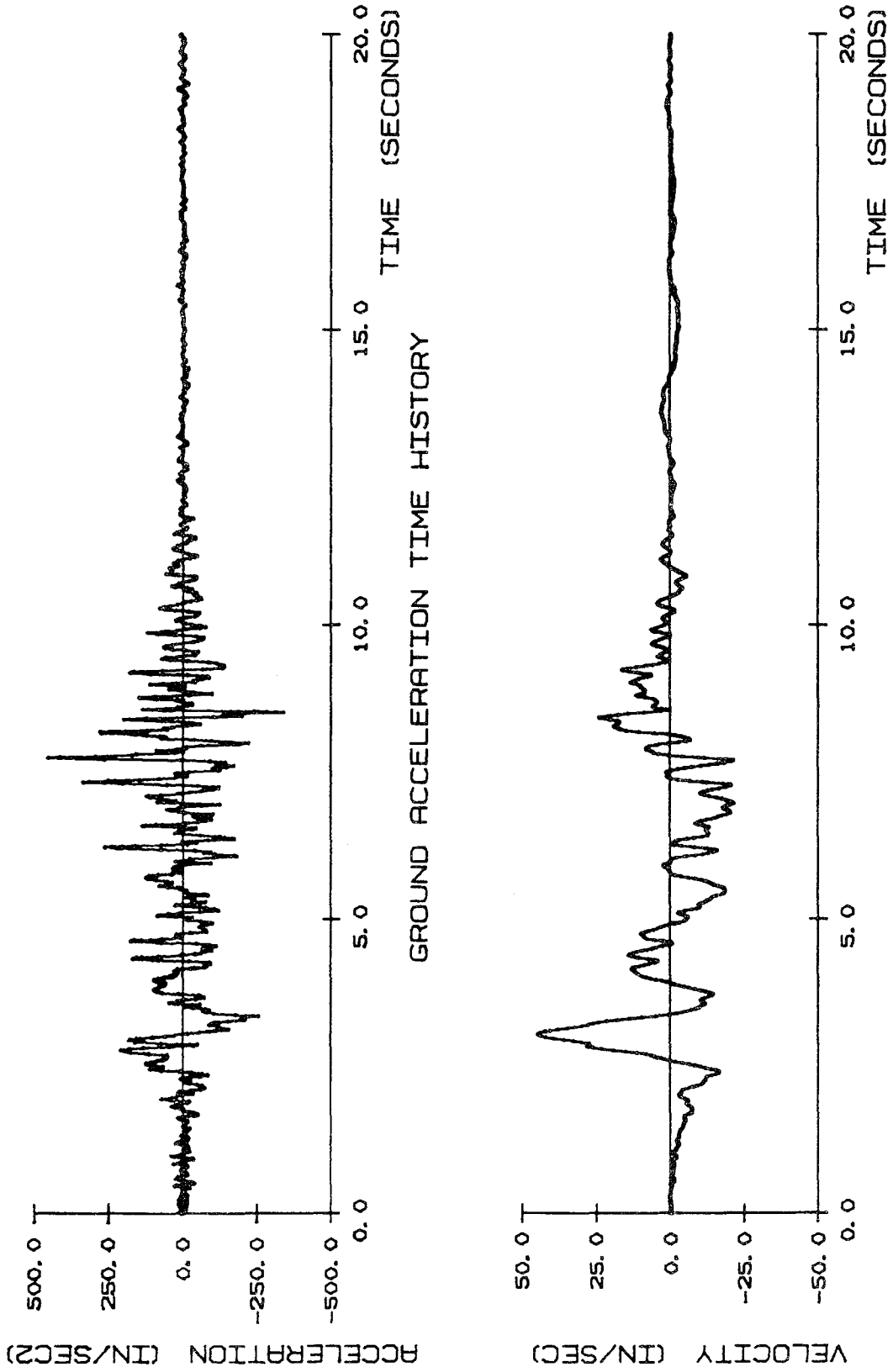

Figure 2.9a Ground Acceleration and Velocity Time Histories for the Pacoima Dam Record of February 9, 1971, S16E Component

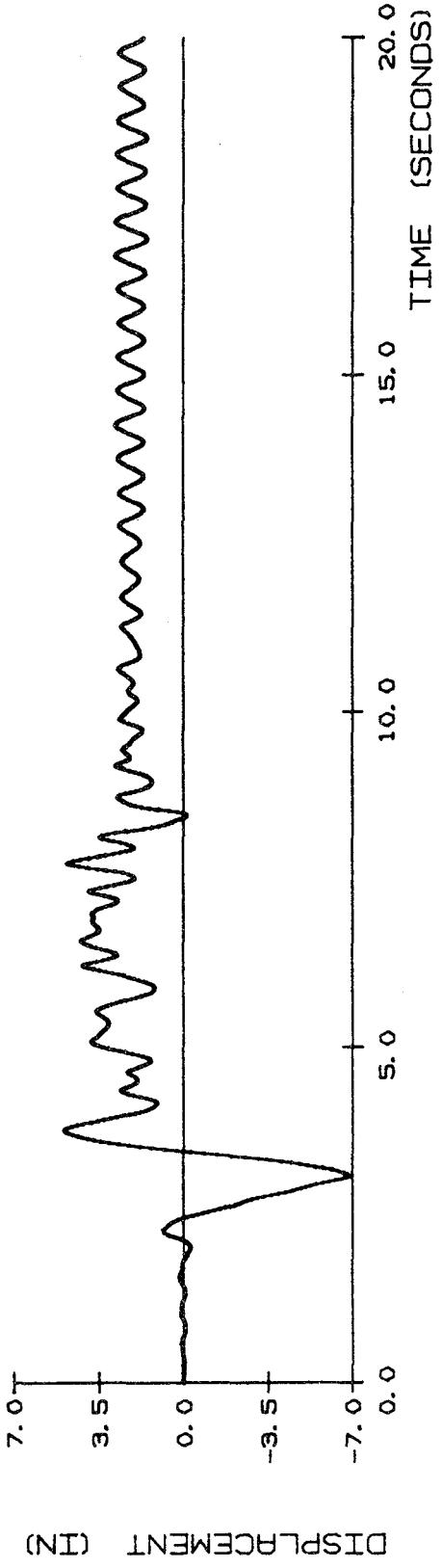

Figure 2.9b Relative Displacement Time History for a 2 hz Undamped Structure Responding to Pacoima Dam

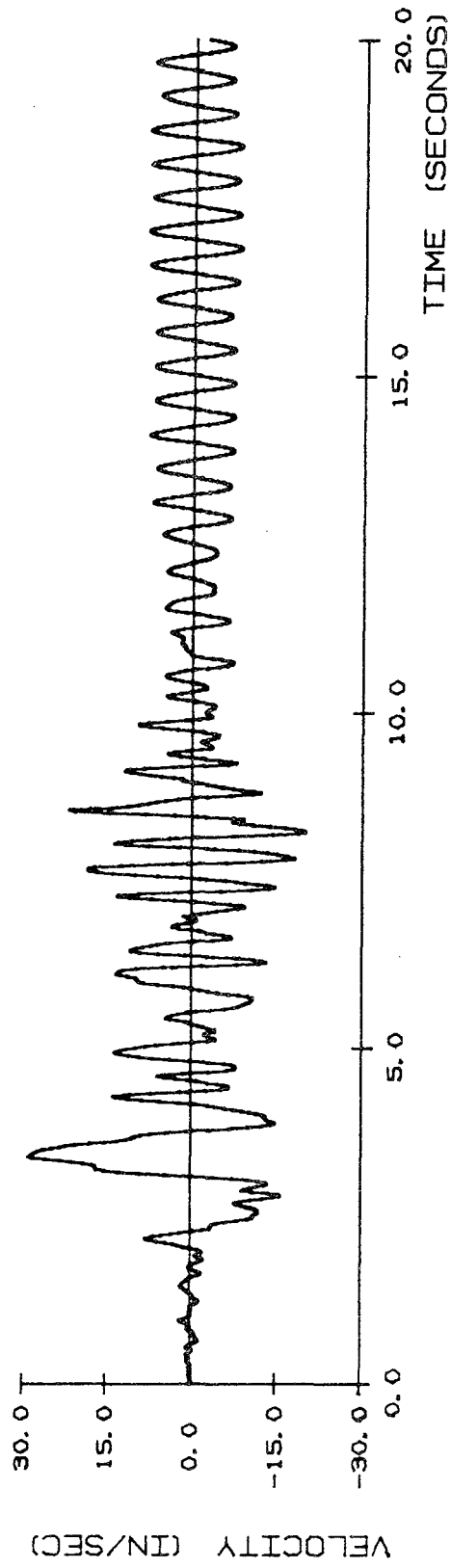

Figure 2.9c Relative Velocity Time History for a 2 hz Undamped Structure Responding to Pacoima Dam

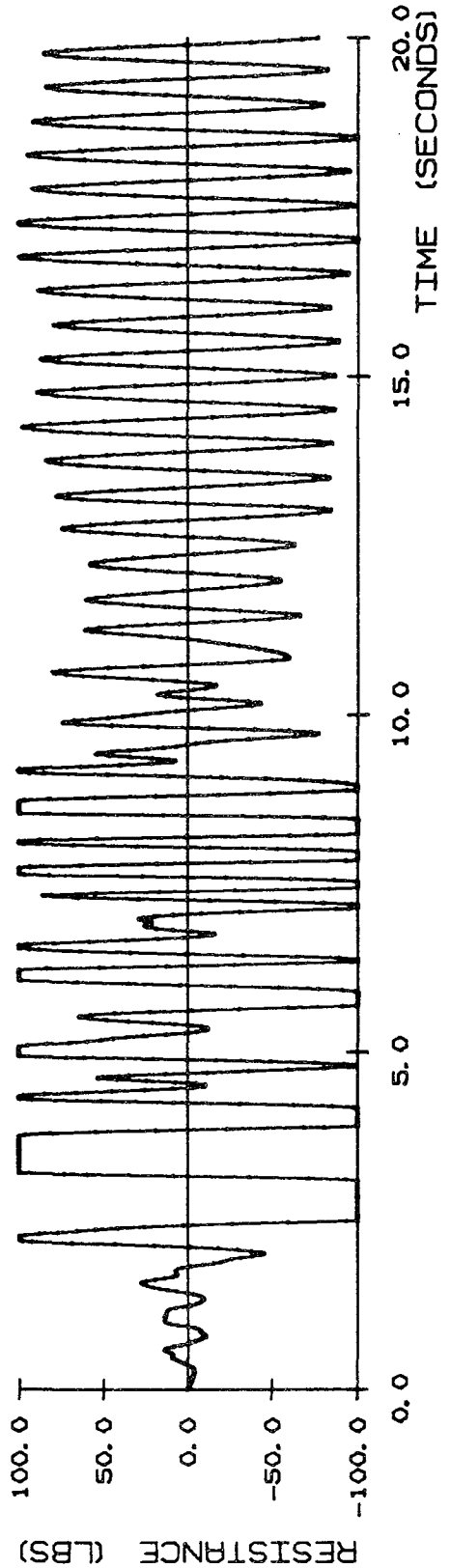

Figure 2.9d Resistance Time History for a 2 hz Undamped Structure Responding to Pacoima Dam

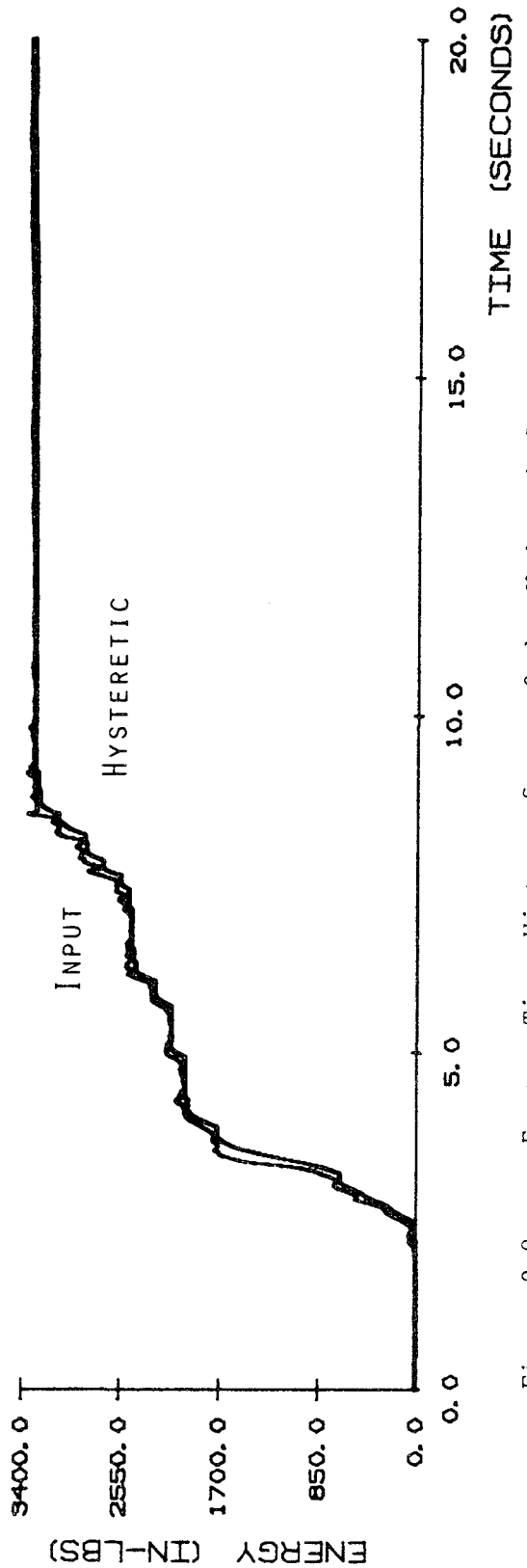

Figure 2.9e Energy Time History for a 2 hz Undamped Structure Responding to Pacoima Dam

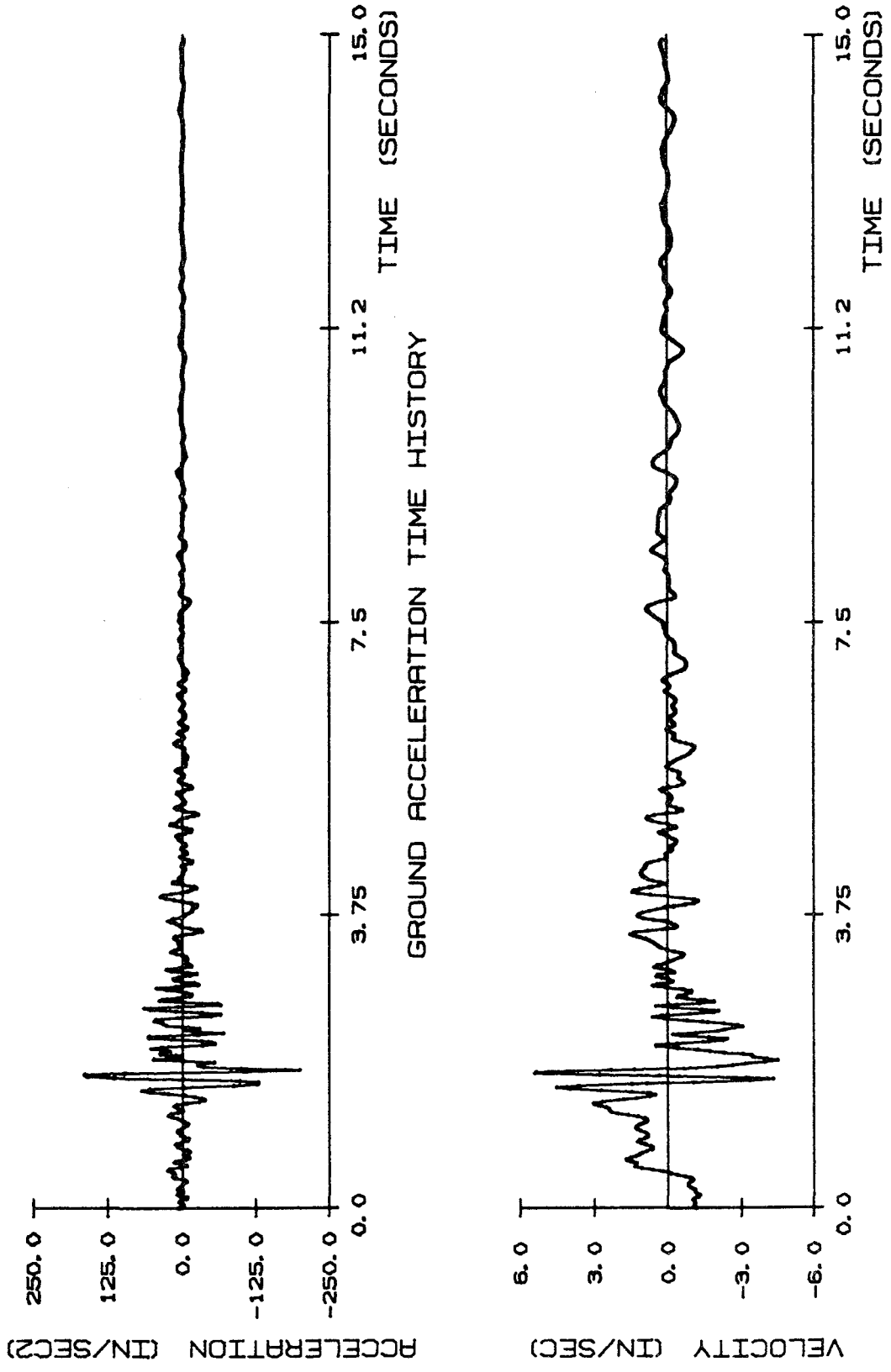

Figure 2.10a Ground Acceleration and Velocity Time Histories for the Melendy Ranch Record of September 4, 1972, N29W Component

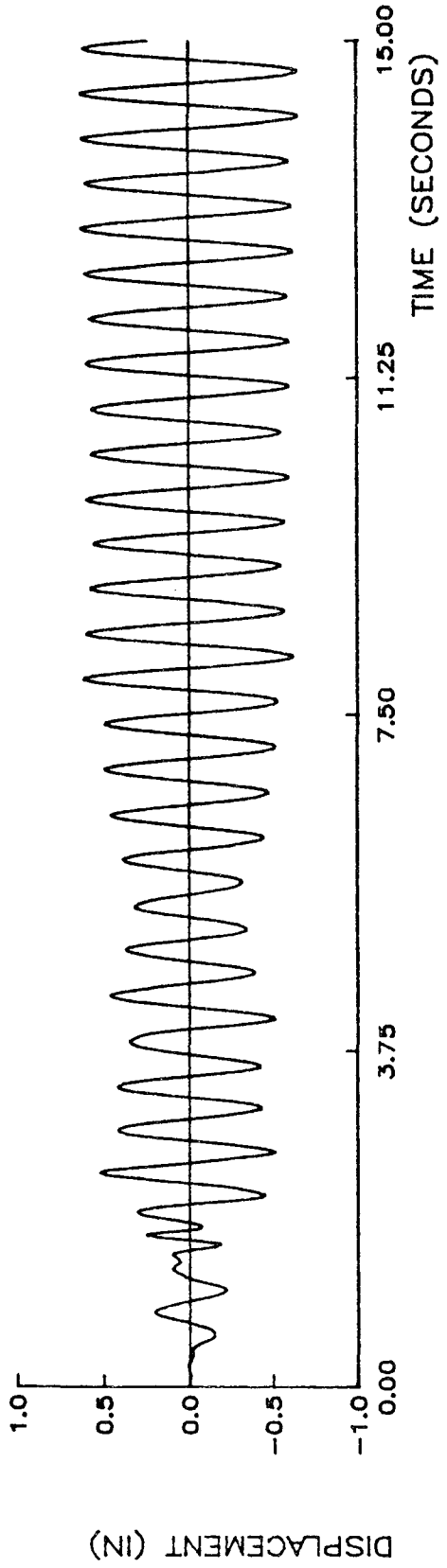

Figure 2.10b Relative Displacement Time History for a 2 hz Undamped Structure Responding to Melendy Ranch

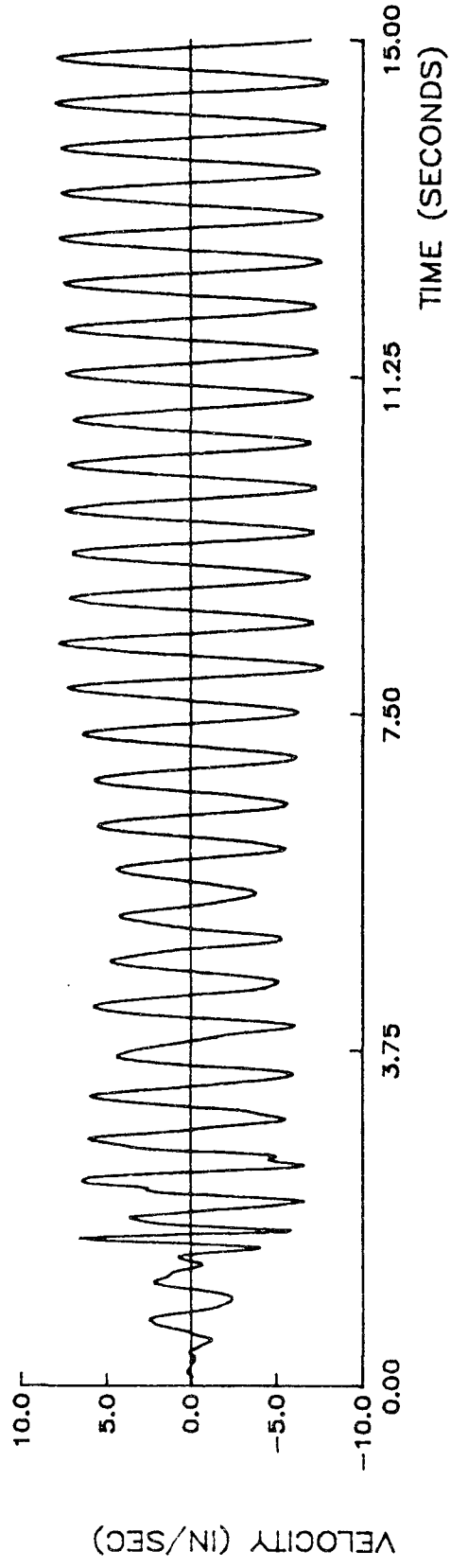

Figure 2.10c Relative Velocity Time History for a 2 hz Undamped Structure Responding to Melendy Ranch

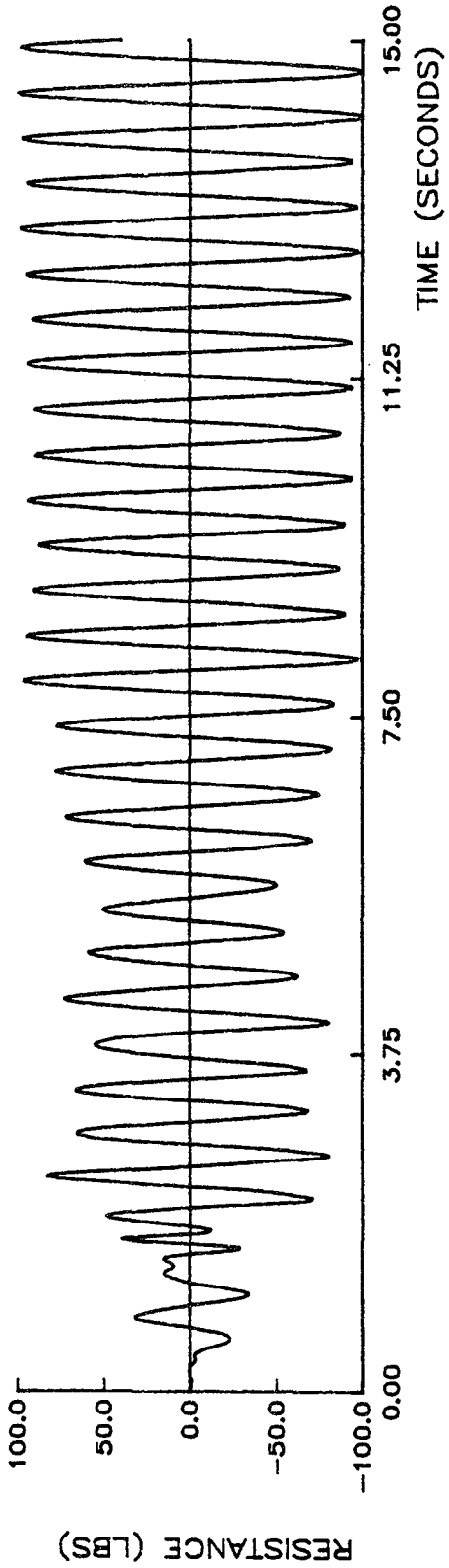

Figure 2.10d Resistance Time History for a 2 hz Undamped Structure Responding to Melendy Ranch

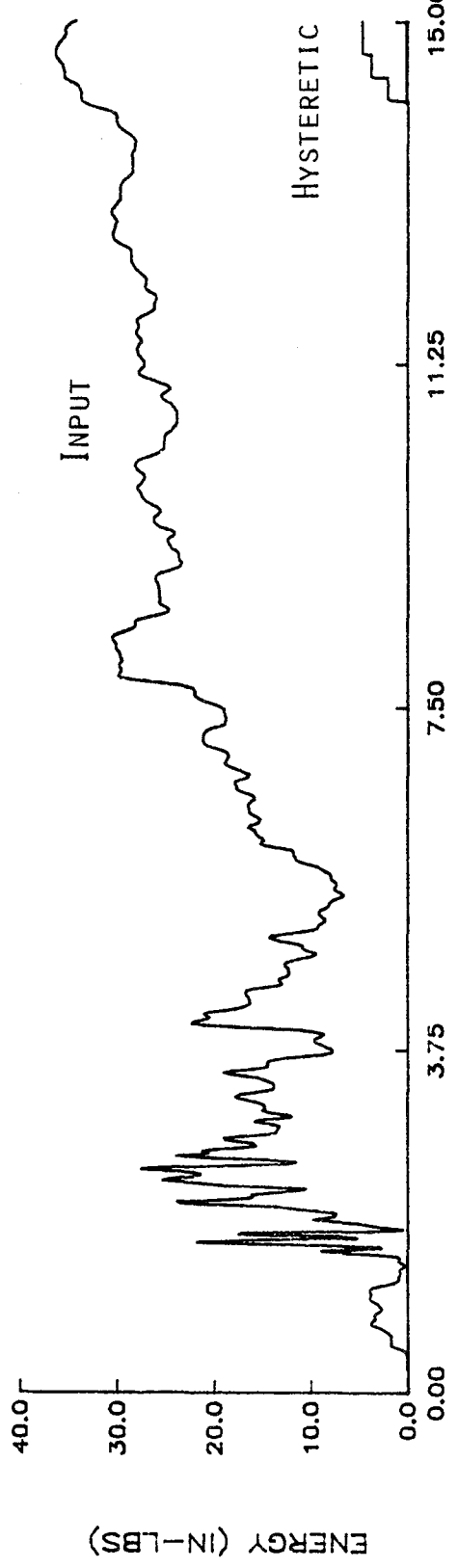

Figure 2.10e Energy Time History for a 2 hz Undamped Structure Responding to Melendy Ranch

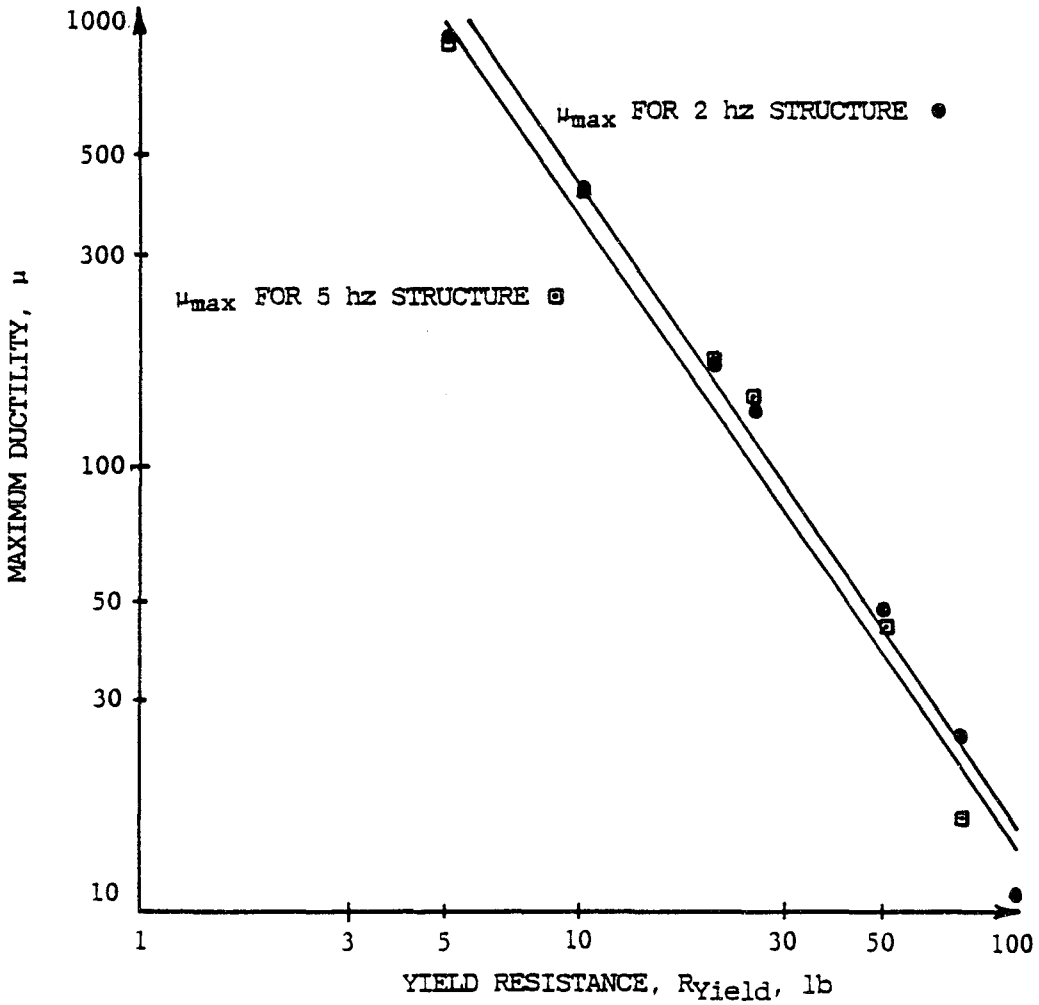

Figure 2.11a Maximum Ductility Versus Yield Resistance for Response to Pacoima Dam

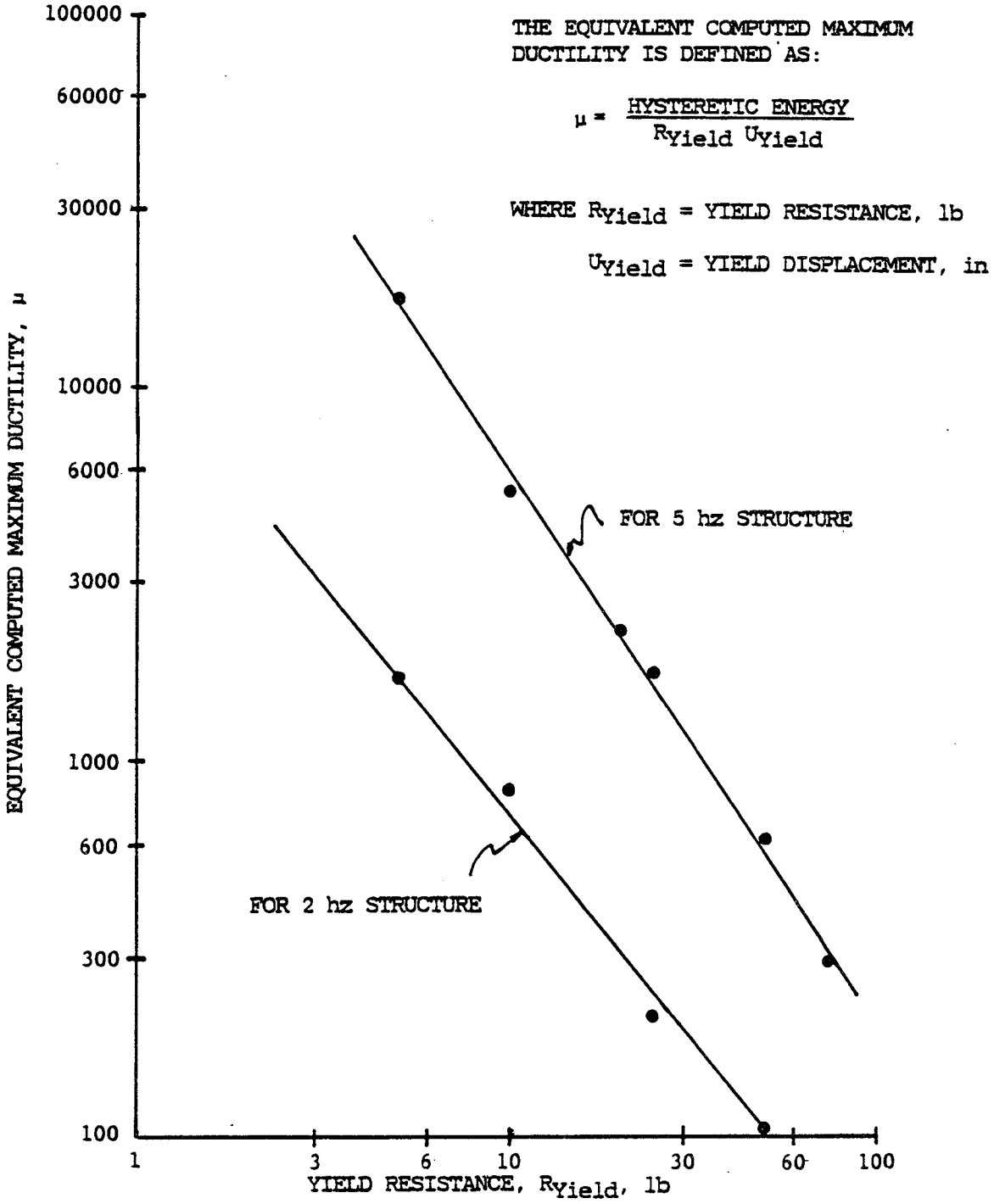

Figure 2.11b Equivalent Computed Maximum Ductility Versus Yield Resistance for Response to Pacoima Dam

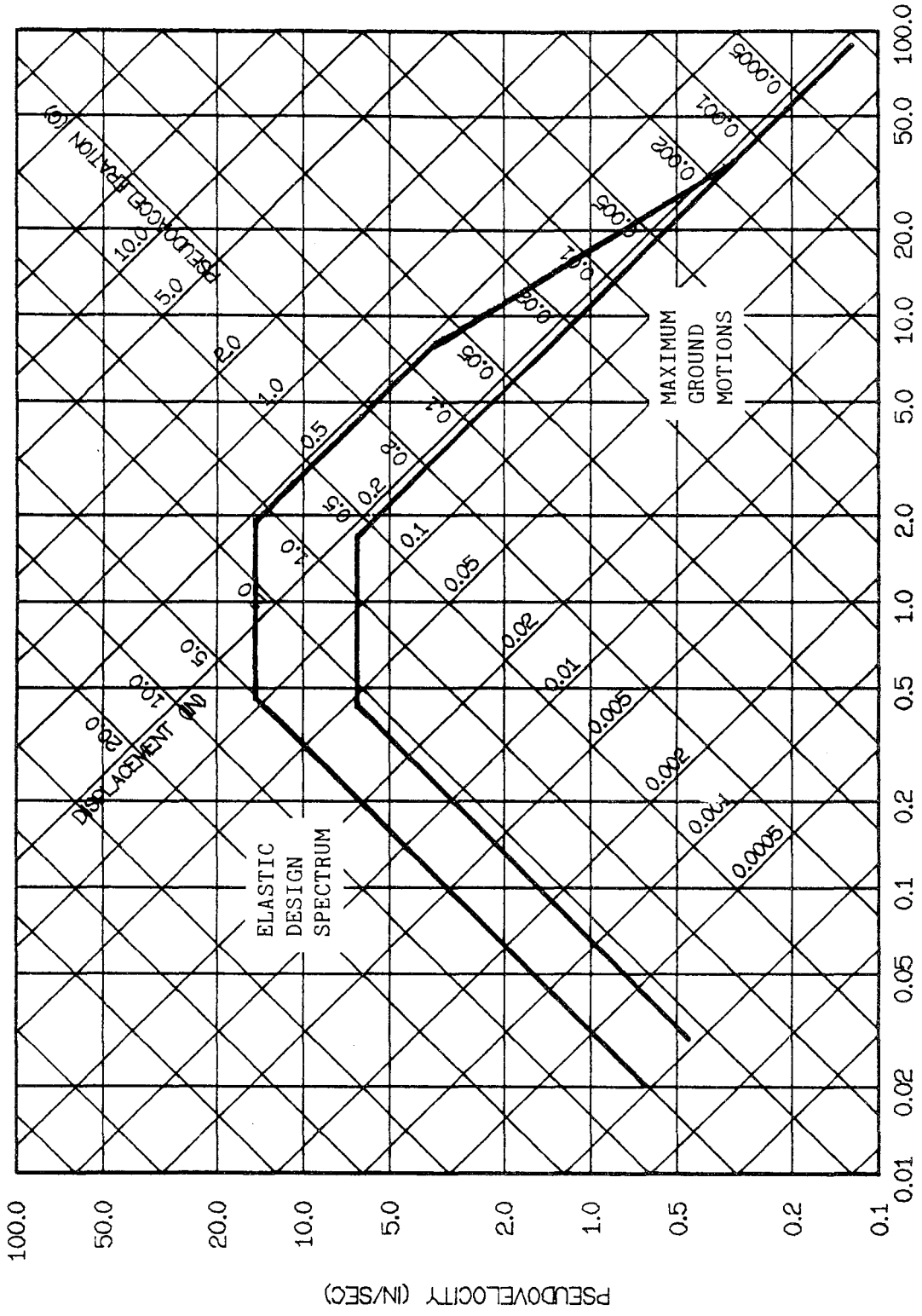

Figure 3.1 Elastic Design Spectrum Constructed Using the Newmark and Hall Procedure (49)

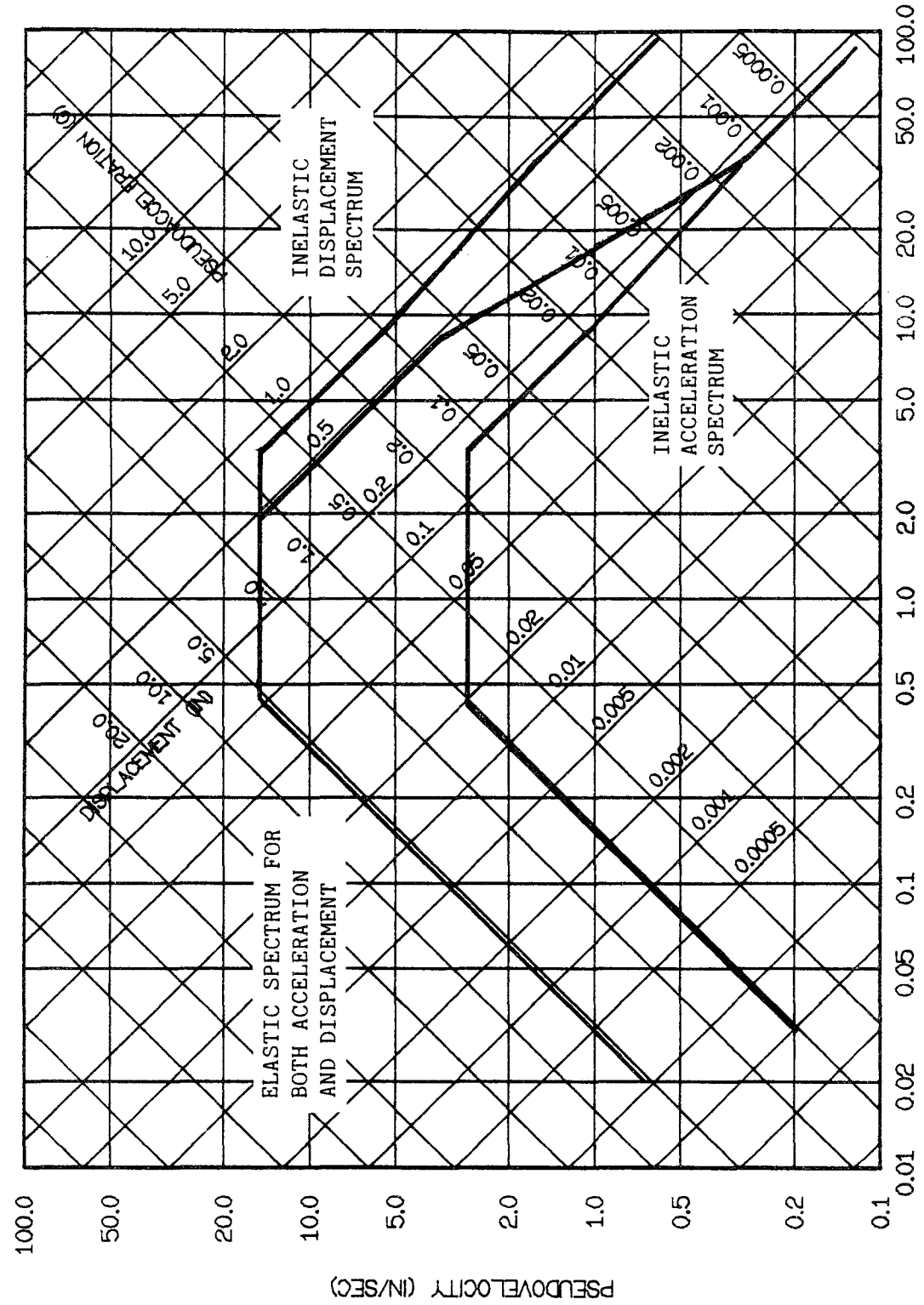

Figure 3.2 Modified Design Spectrum Constructed Using the Newmark and Hall Procedure (49)

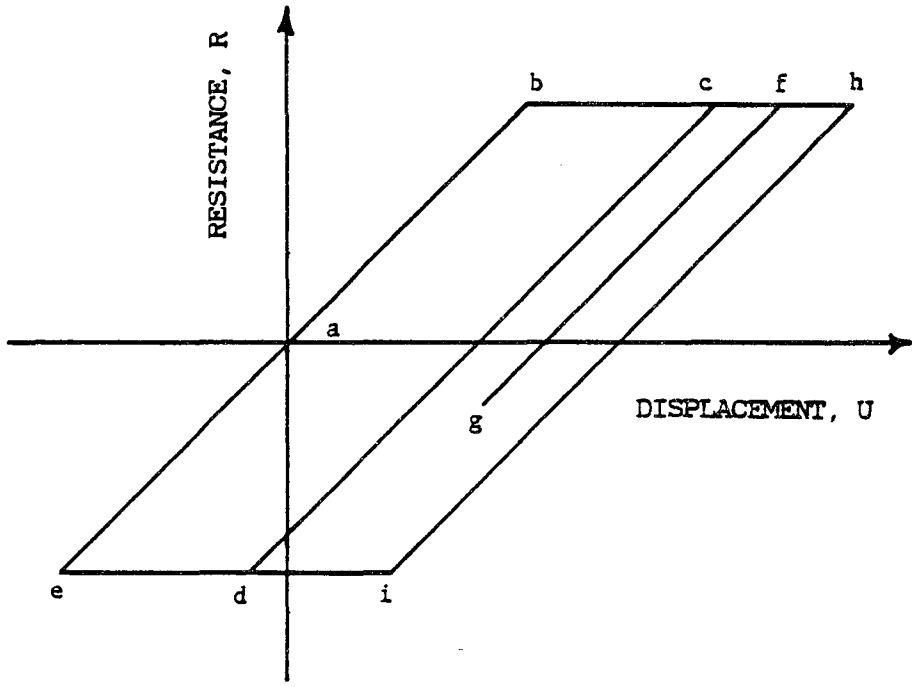

Figure 3.3 Hysteretic Cycle Paths

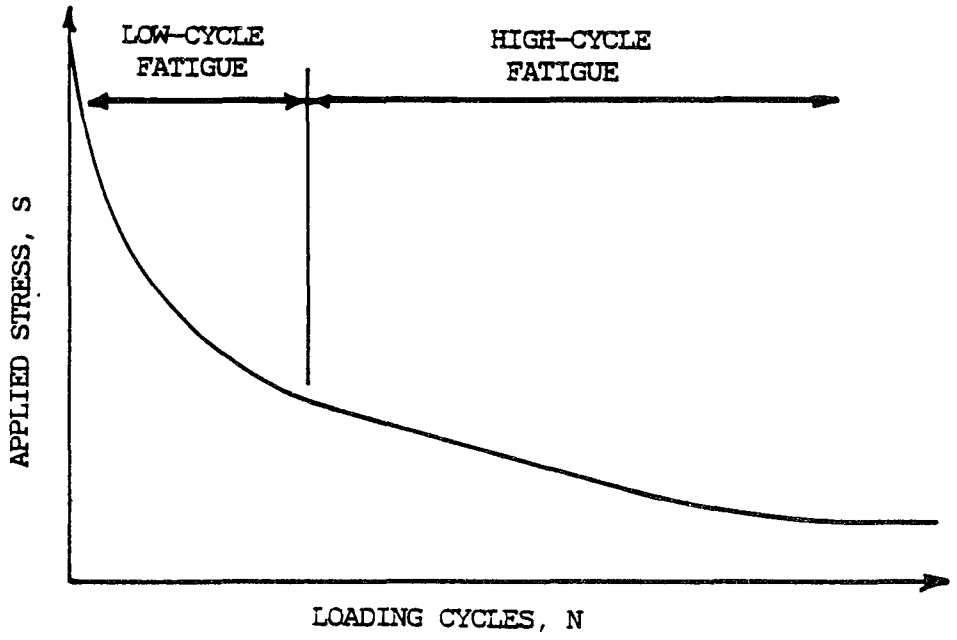

Figure 3.4 Definitions of Low- and High-Cycle Fatigue Using a Standard S-N Diagram

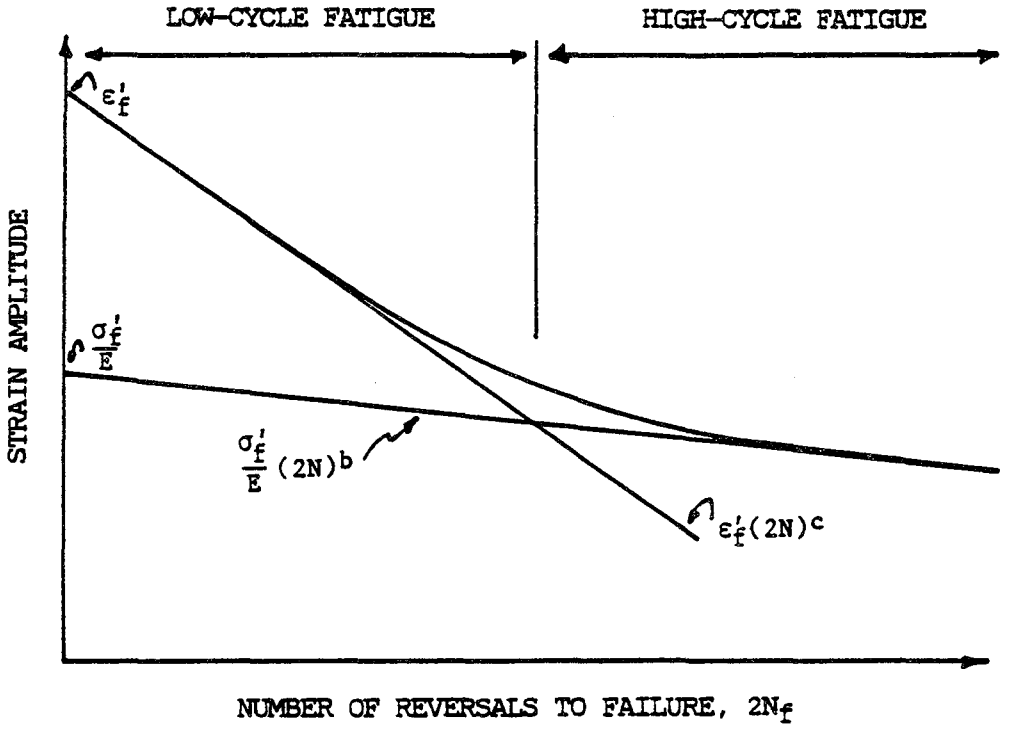

Figure 3.5 Morrow's Relationship for Low-Cycle Fatigue

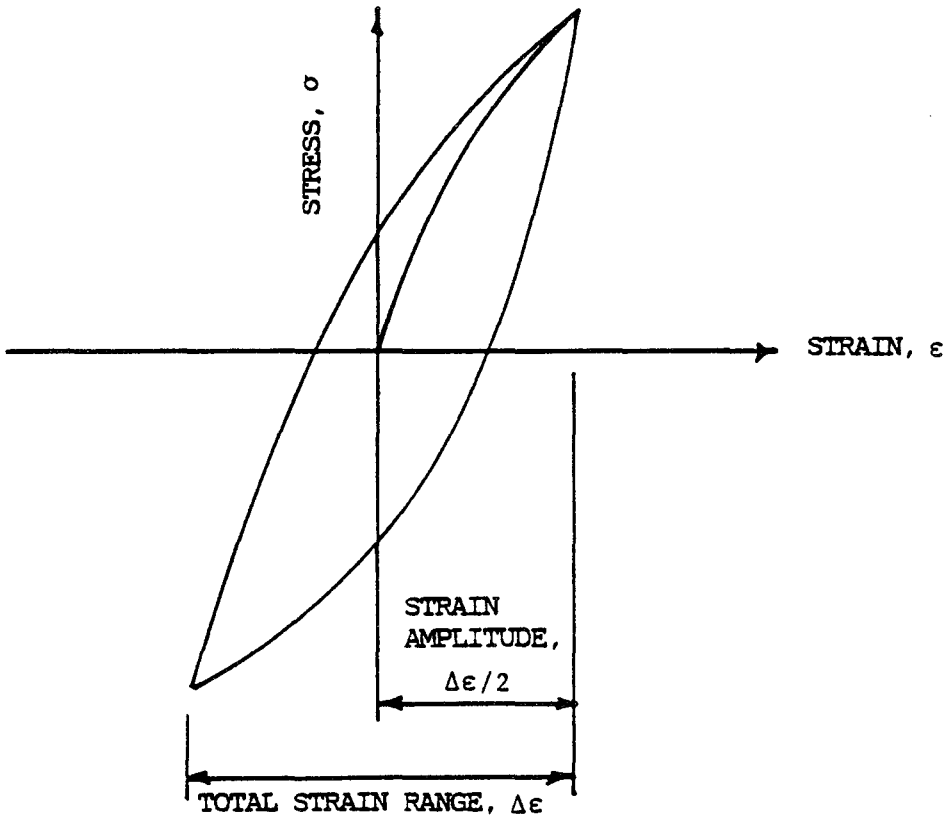

Figure 3.6 Definition of Strain Terms in Morrow's Low-Cycle Fatigue Relationship

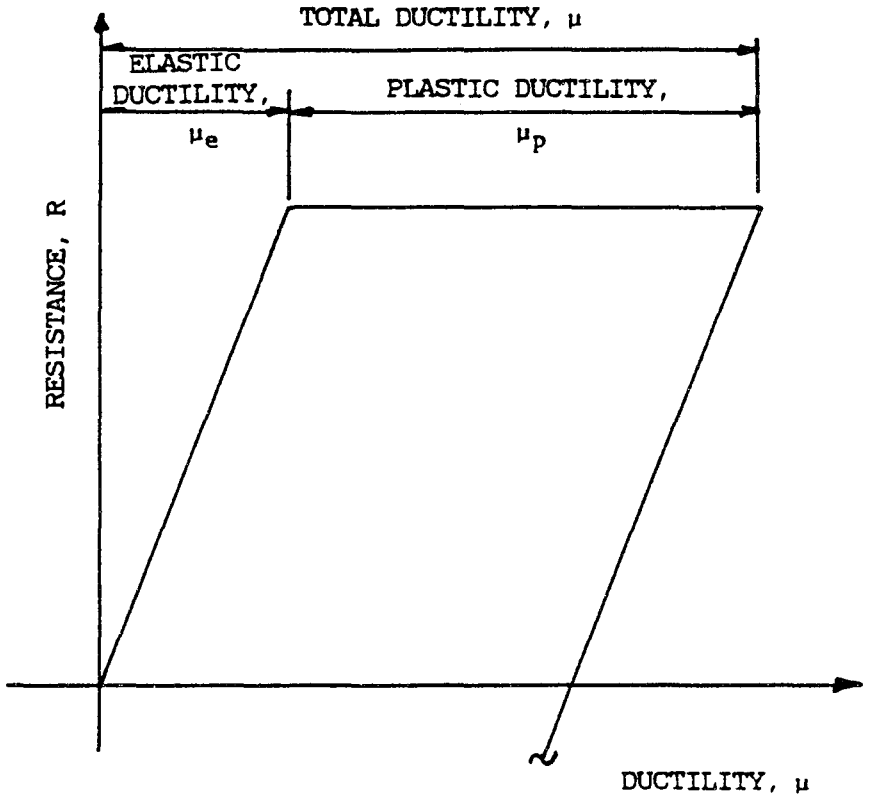

TOTAL DUCTILITY $\mu = \mu_e + \mu_p$

WHERE $\mu_e = 1.0$ FOR NONLINEAR RESPONSE

TOTAL DISPLACEMENT $\Delta_T = \Delta_Y + \Delta_p$

$\Delta_T = \mu_e \Delta_Y + \mu_p \Delta_Y$

BUT $\mu = 1.0$

THEREFORE $\Delta_T = \Delta_Y + \mu_p \Delta_Y$

Figure 3.7 Ductility Definitions

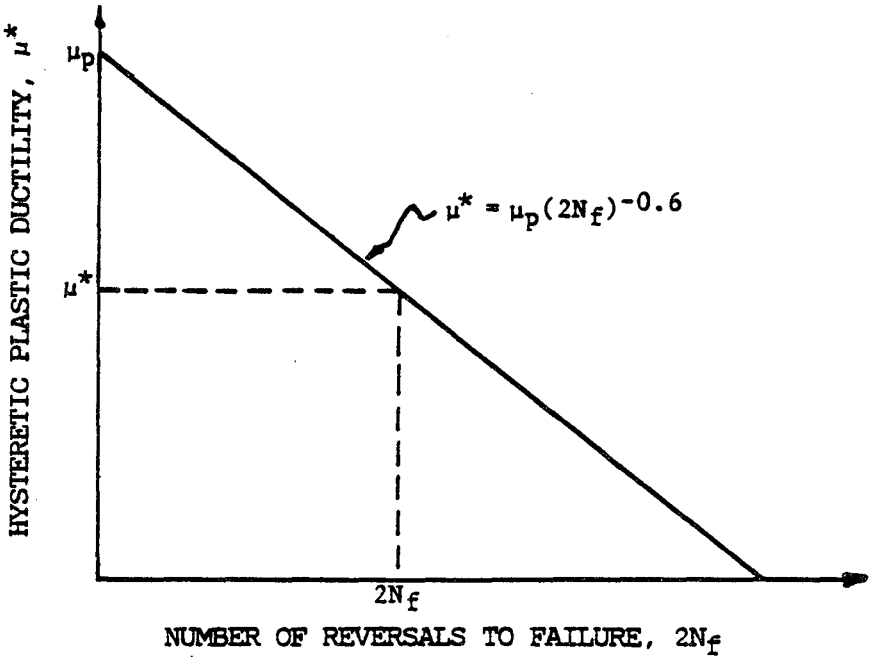

Figure 3.8 Definition of the Relationship Between Reversals and Ductility

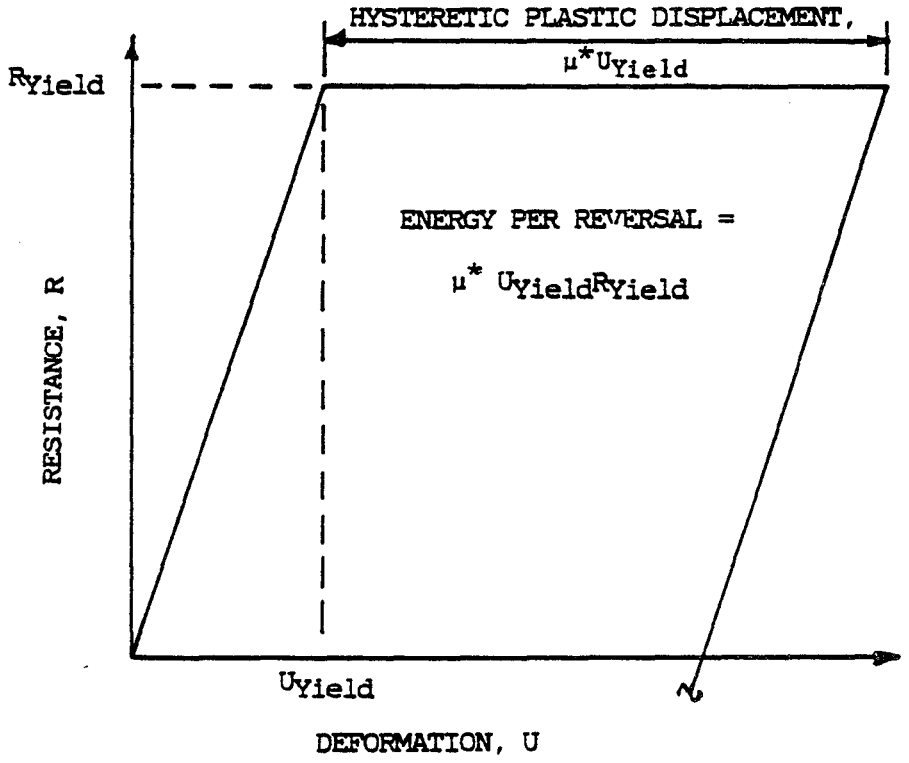

Figure 3.9 Hysteretic Energy Dissipated Over N Cycles or 2N Reversals

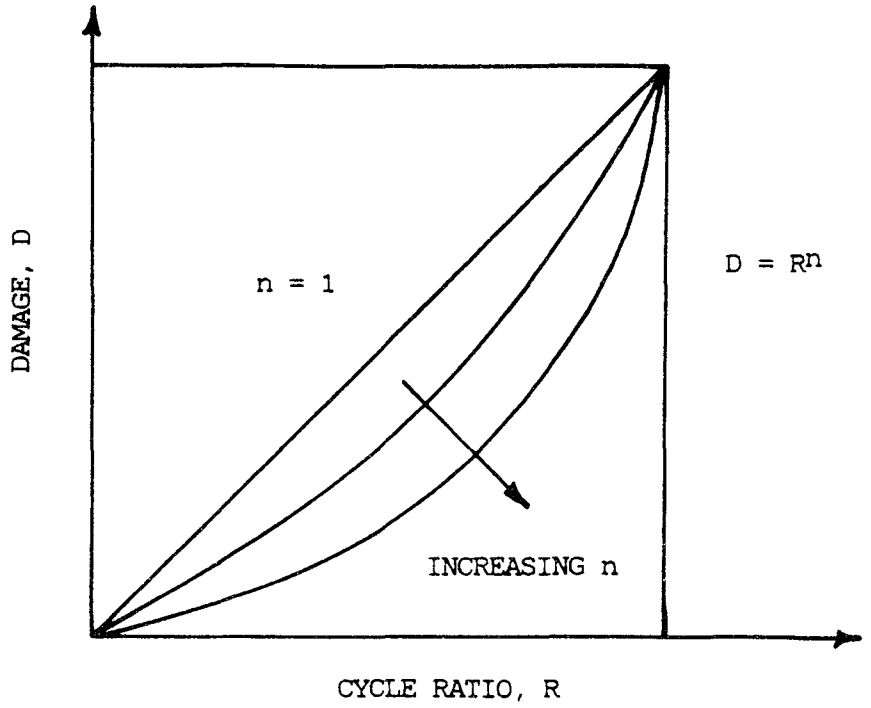

Figure 3.10 Damage-Cycle Ratio Relationship From Richart and Newmark (62)

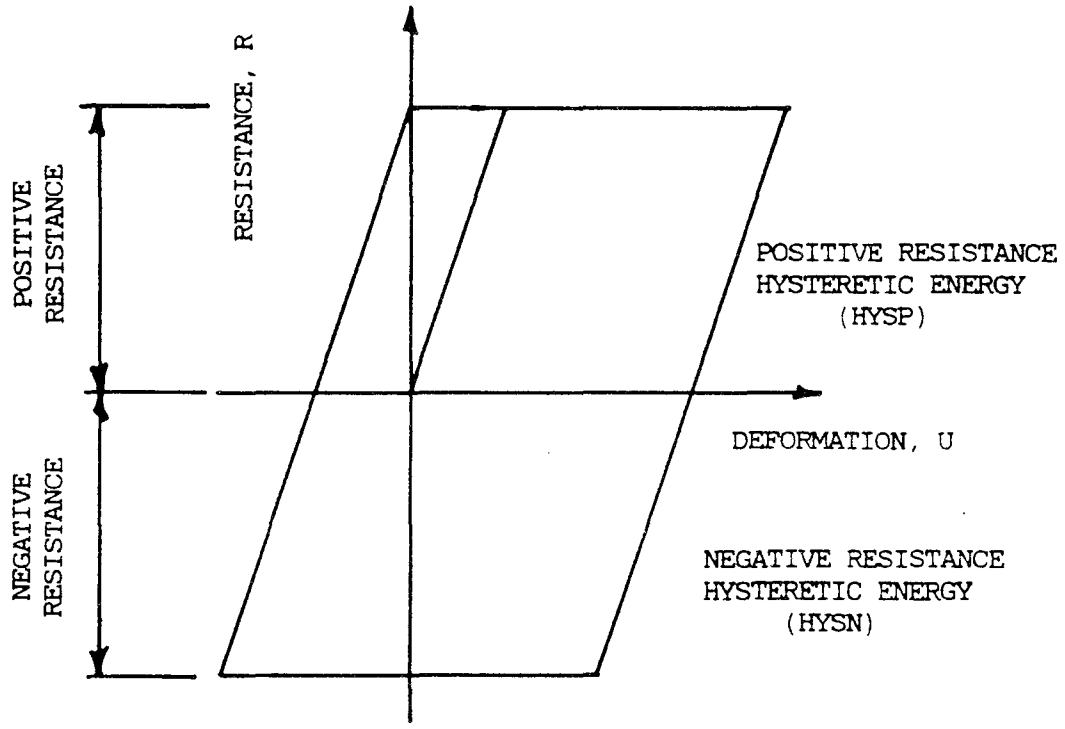

Figure 3.11 Definition of Positive and Negative Resistance Hysteretic Energy

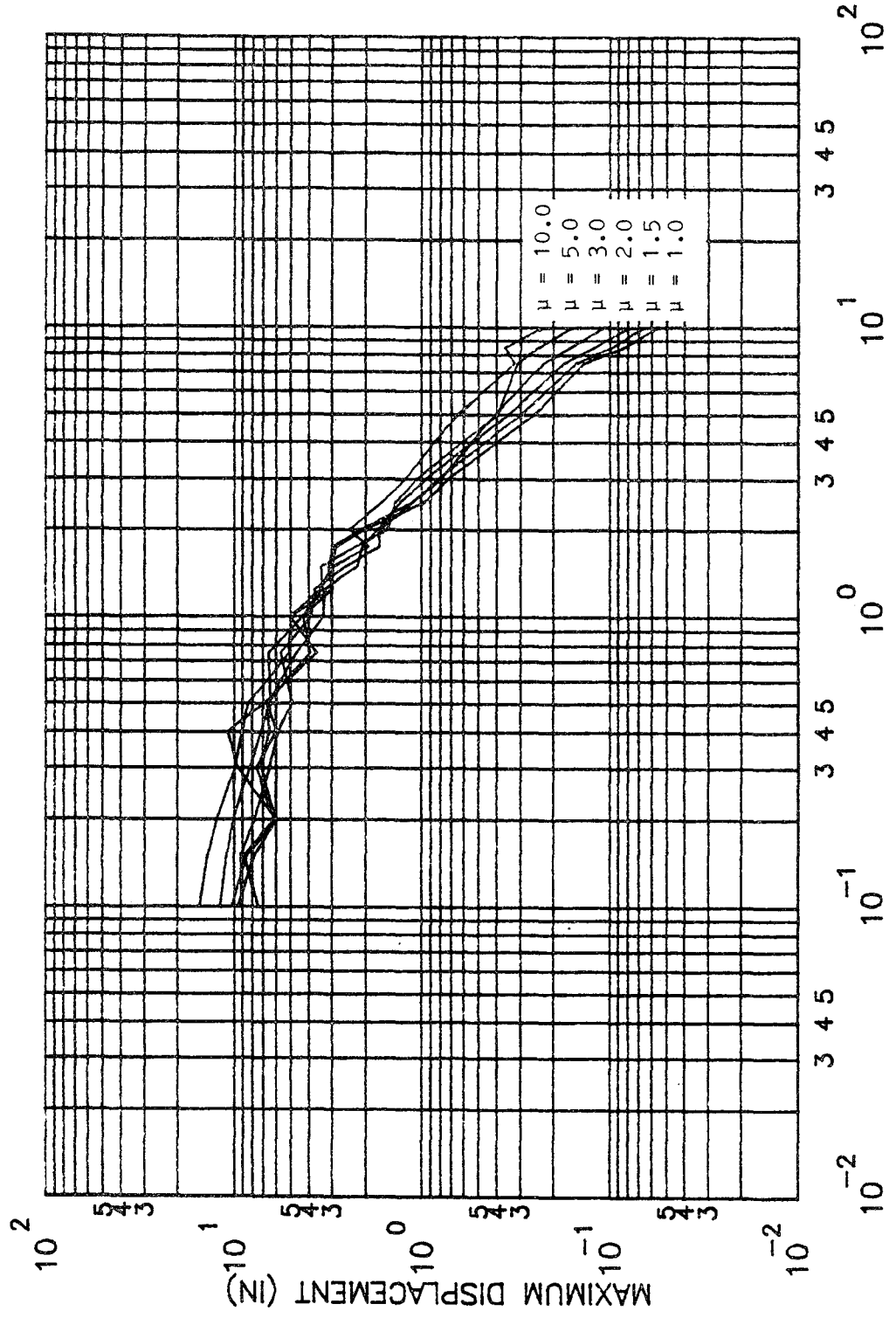

Figure 5.1a Maximum Displacement Spectrum Based on Computed Response to Specified Maximum Ductilities with 5 Percent Damping for El Centro

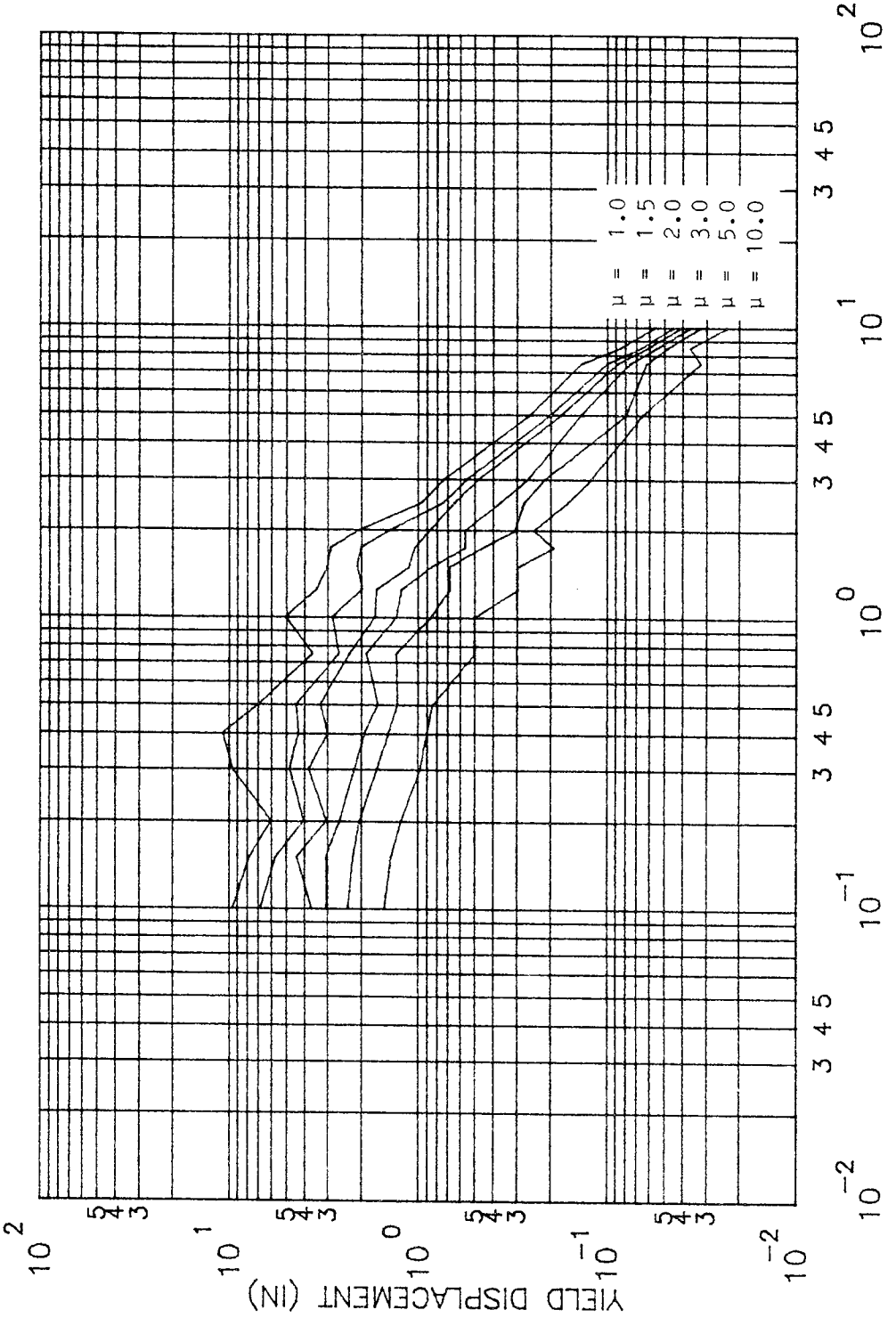

Figure 5.1b Yield Displacement Spectrum Based on Computed Response to Specified Maximum Ductilities with 5 Percent Damping for El Centro

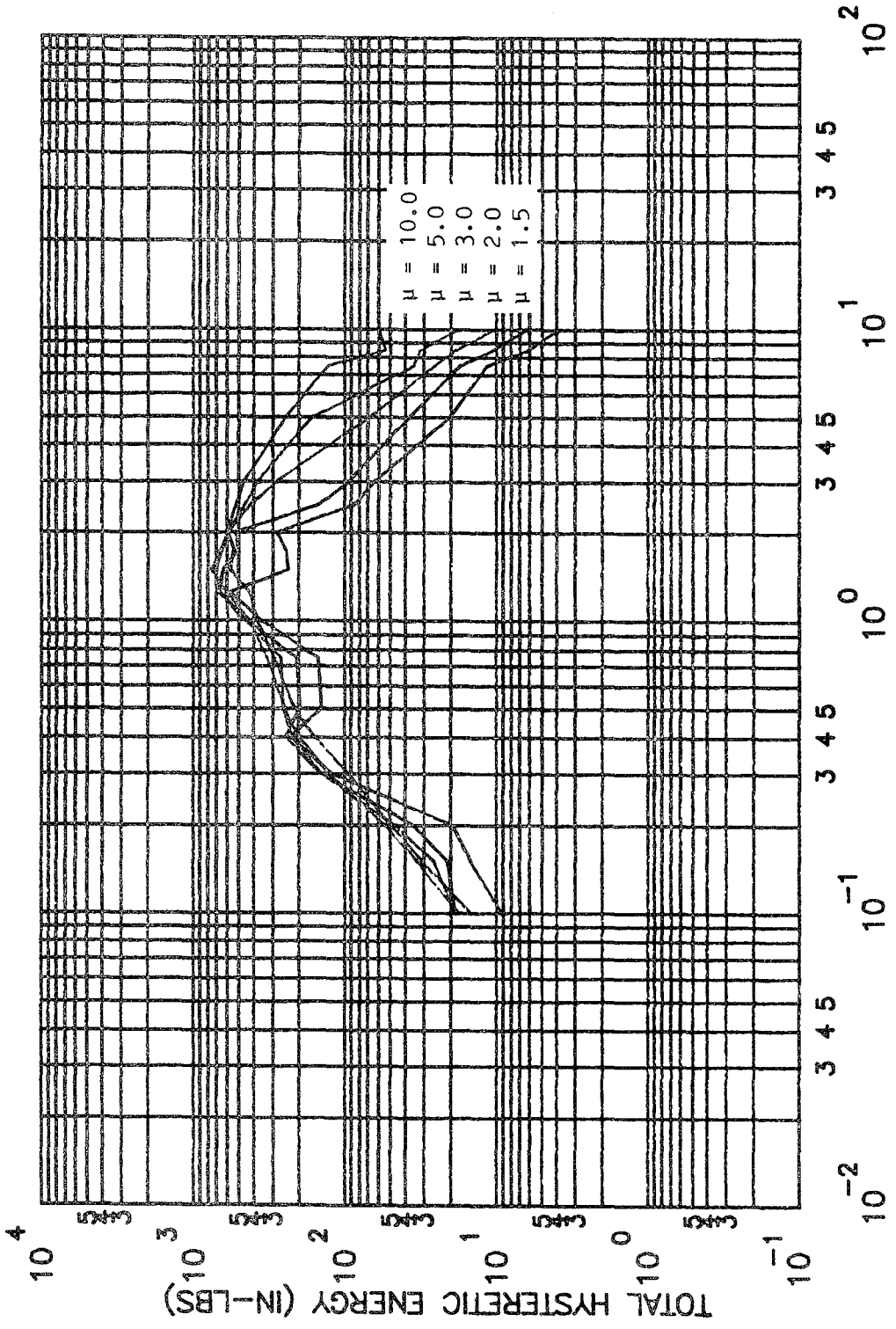

Figure 5.1c Total Hysteretic Energy Spectrum Based on Computed Response to Specified Maximum Ductilities with 5 Percent Damping for El Centro

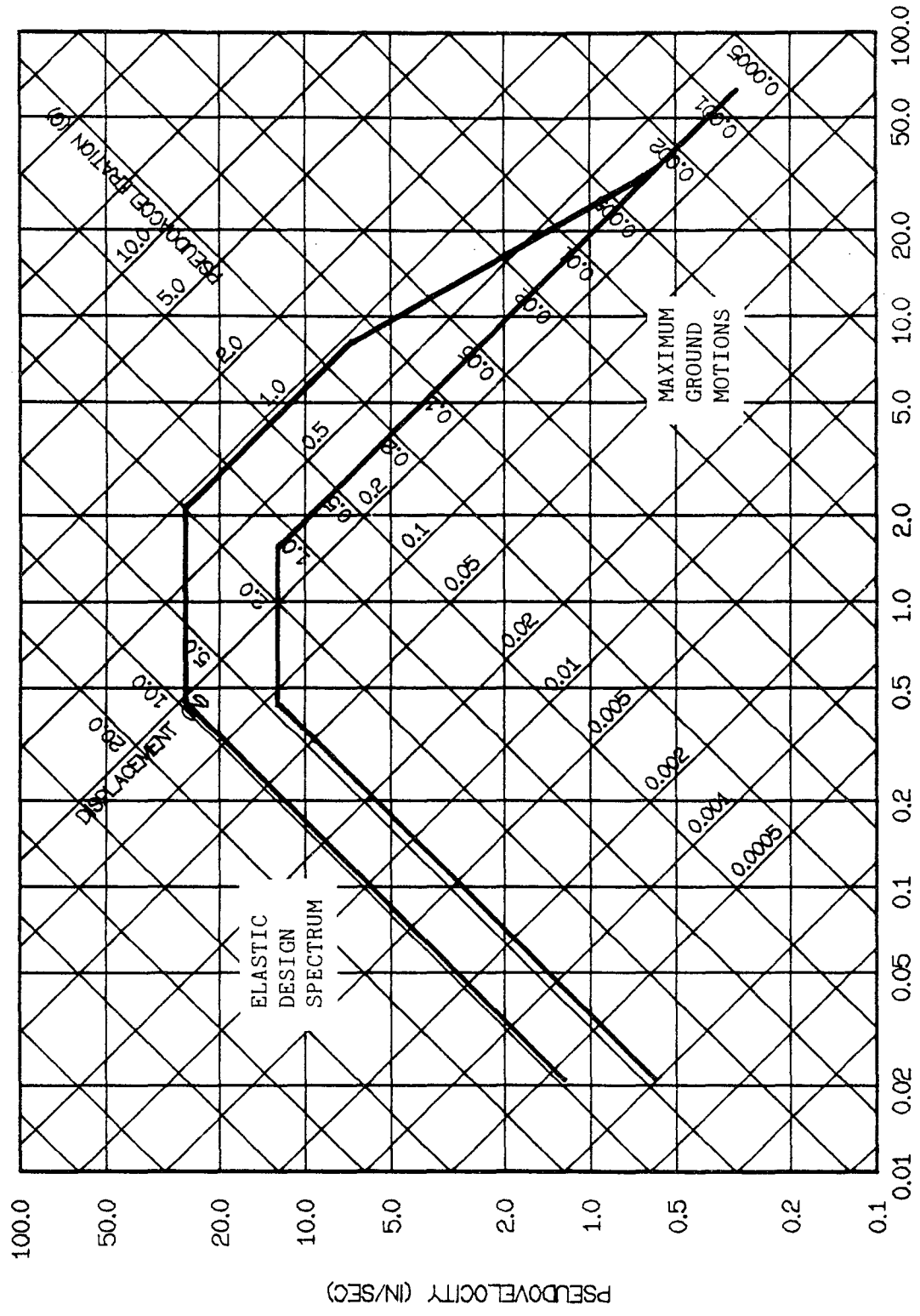

Figure 5.2a Elastic Design Spectrum Based on Newmark and Hall Procedure (50) with 5 Percent Damping for El Centro

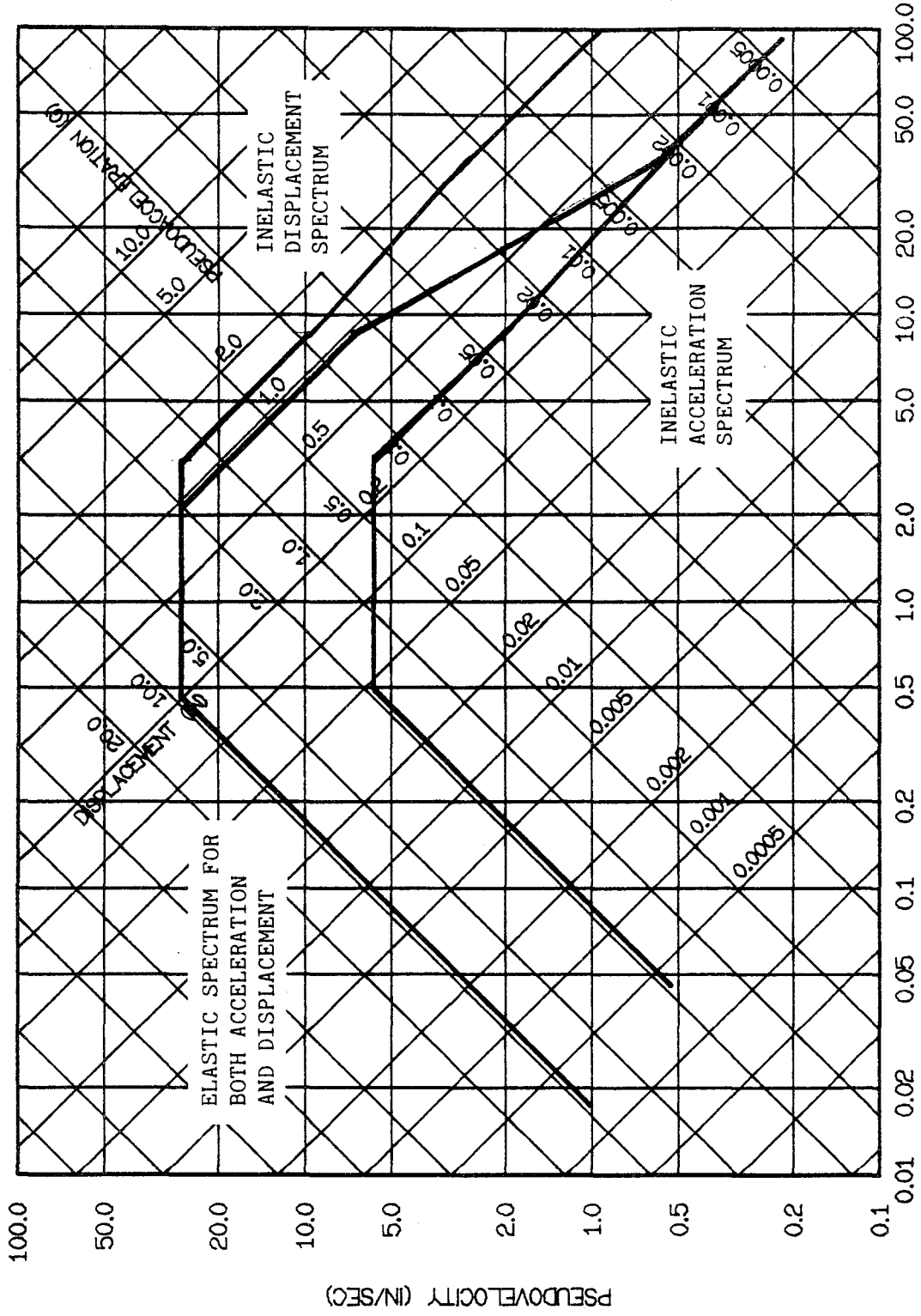

Figure 5.2b Modified Design Spectrum Based on the Newmark and Hall Procedure (50) for a Specified Ductility of 5.0 with 5 Percent Damping for El Centro

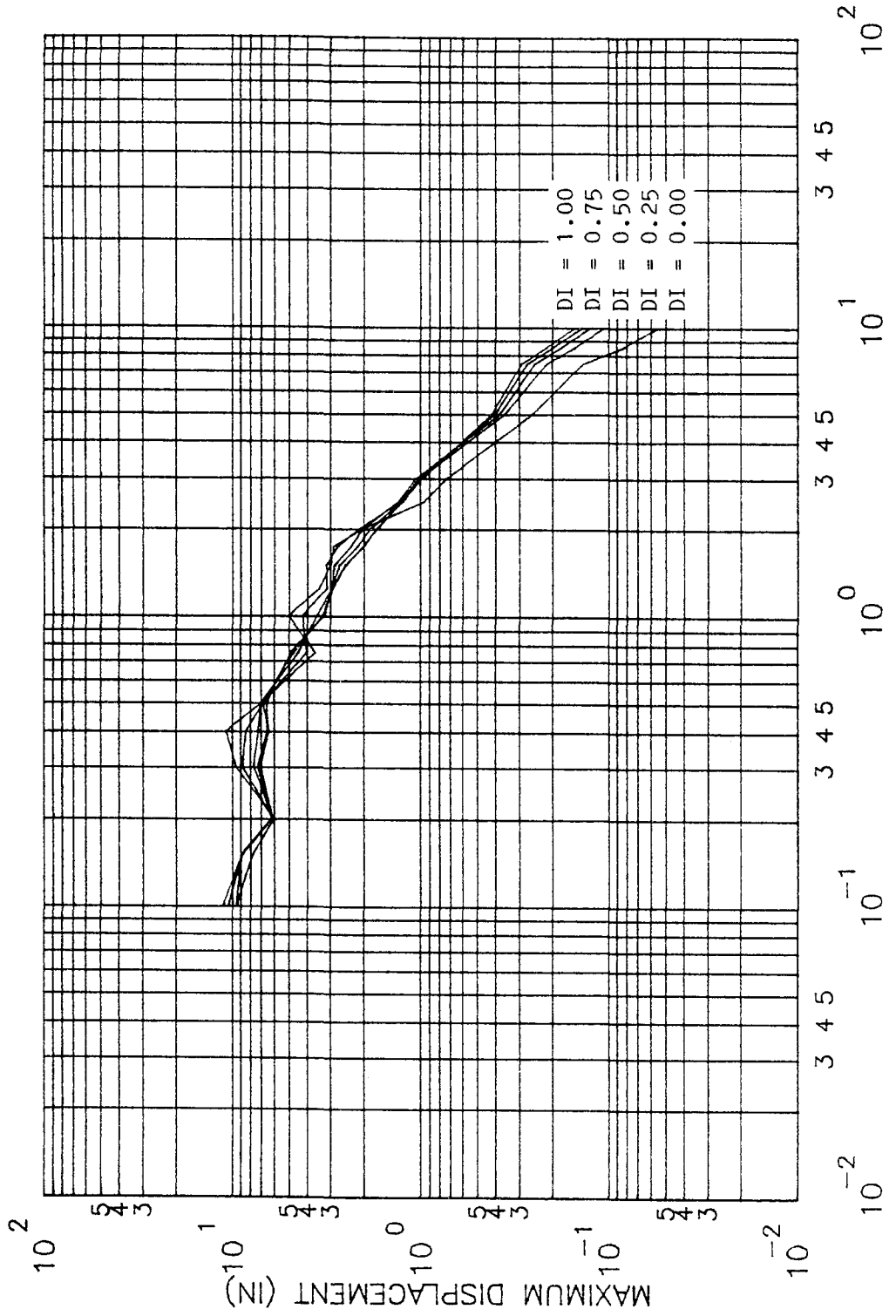

Figure 5.3a Maximum Displacement Spectrum for El Centro with 5 Percent Damping Based on the Damage Index with a Monotonic Plastic Ductility of 0.5

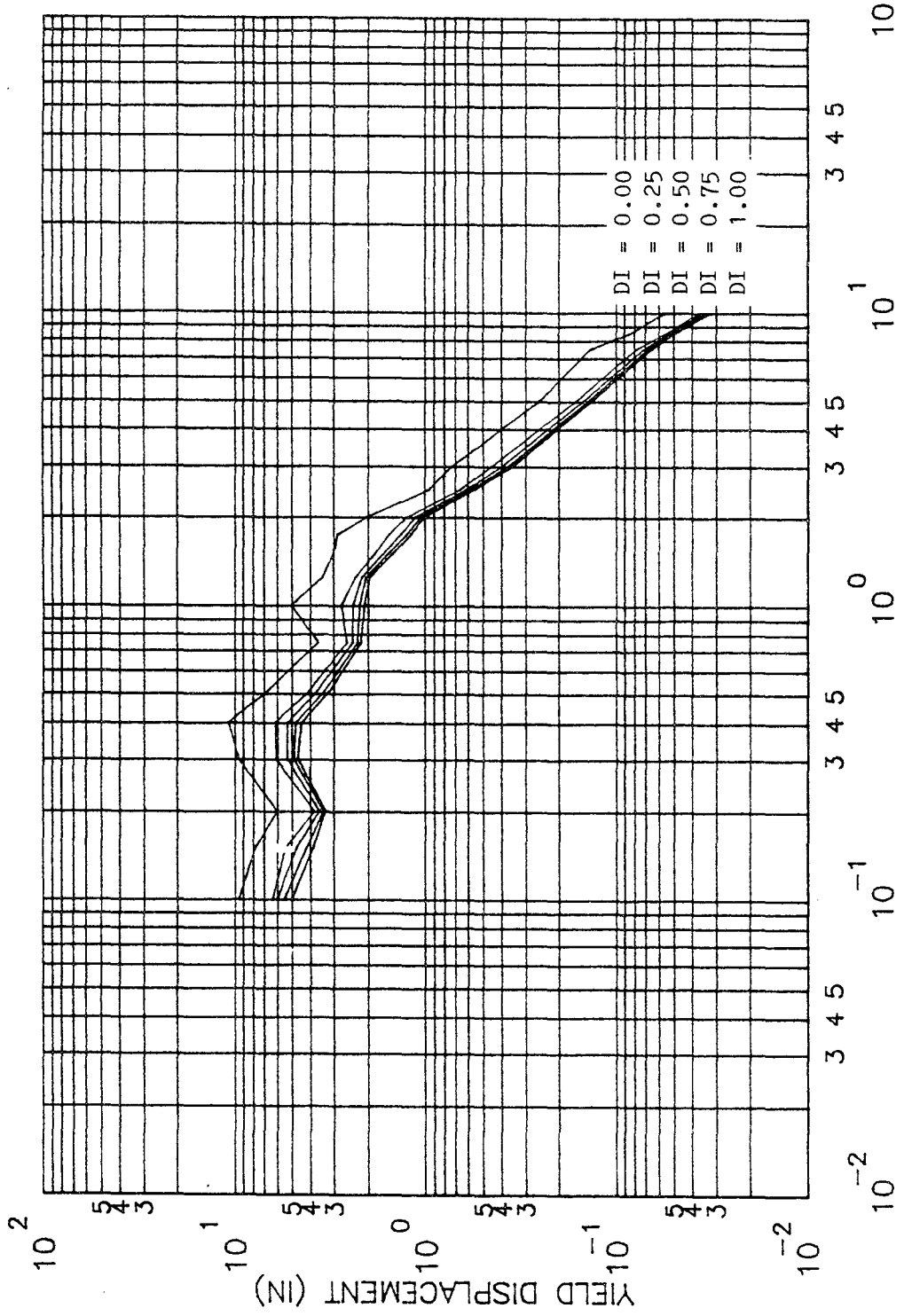

Figure 5.3b Yield Displacement Spectrum for El Centro with 5 Percent Damping Based on the Damage Index with a Monotonic Plastic Ductility of 0.5

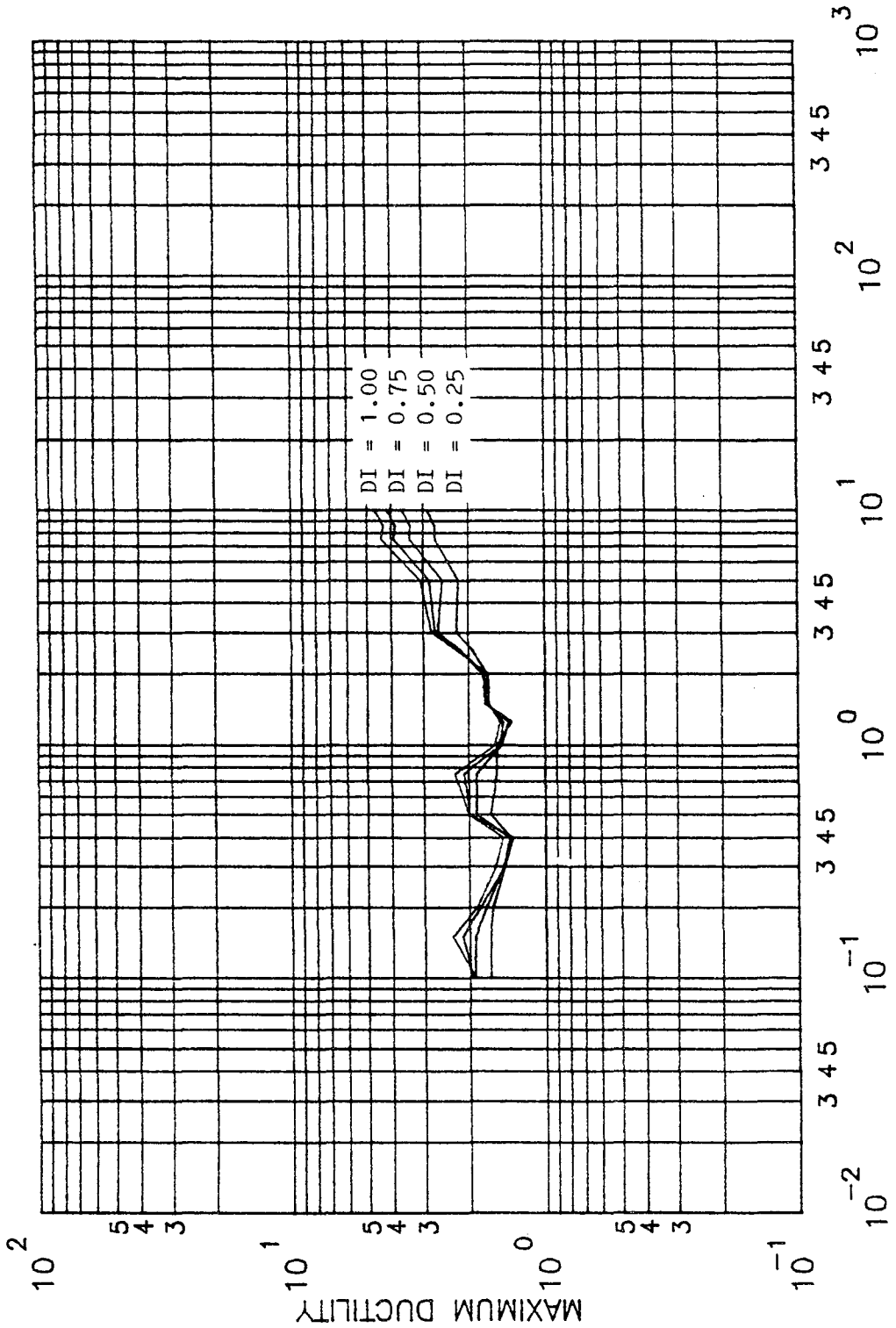

Figure 5.3c Maximum Ductility Spectrum for El Centro with 5 Percent Damping Based on the Damage Index with a Monotonic Plastic Ductility of 0.5

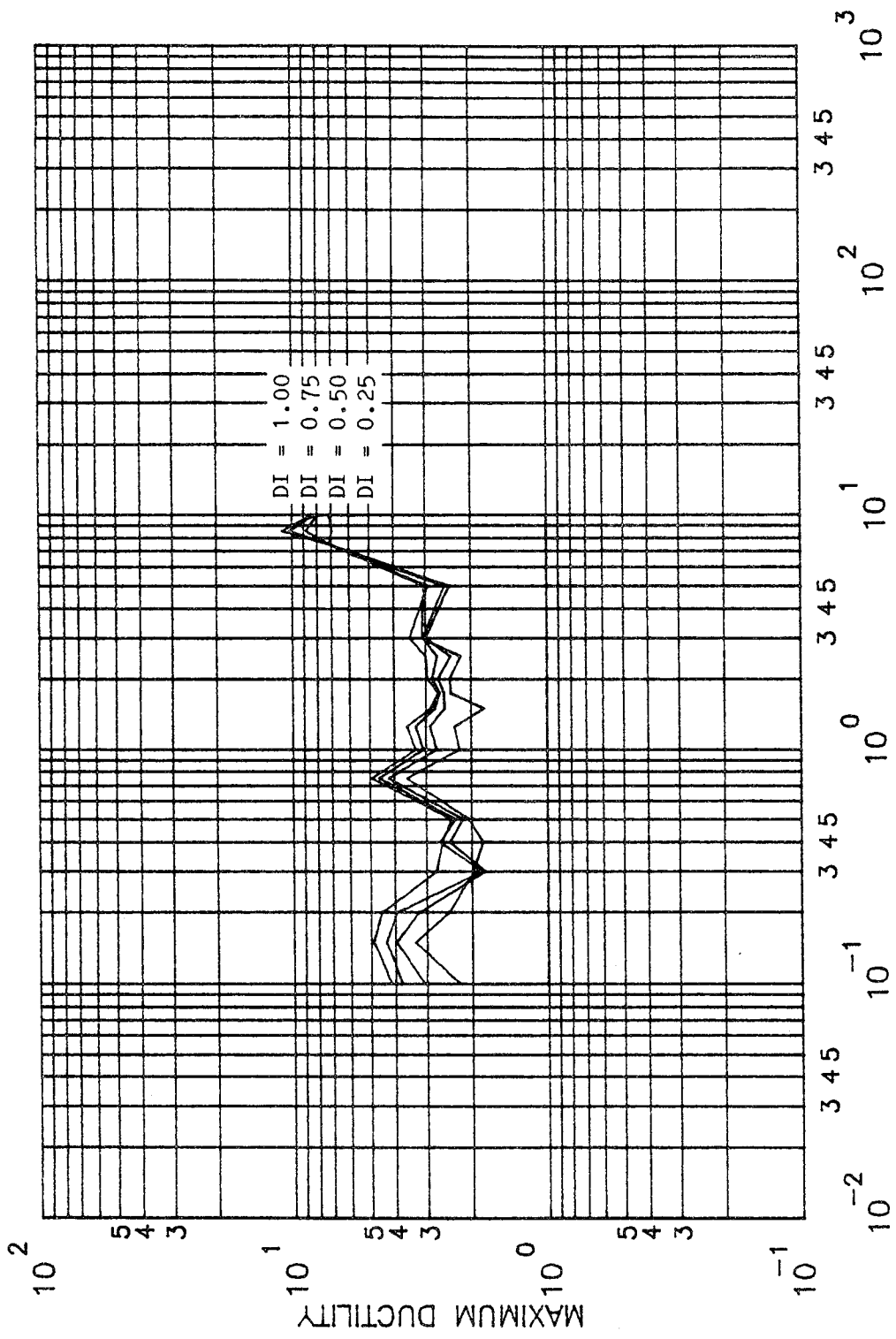

Figure 5.4b Maximum Ductility Spectrum for El Centro with 5 Percent Damping Based on the Damage Index with a Monotonic Plastic Ductility of 2.0

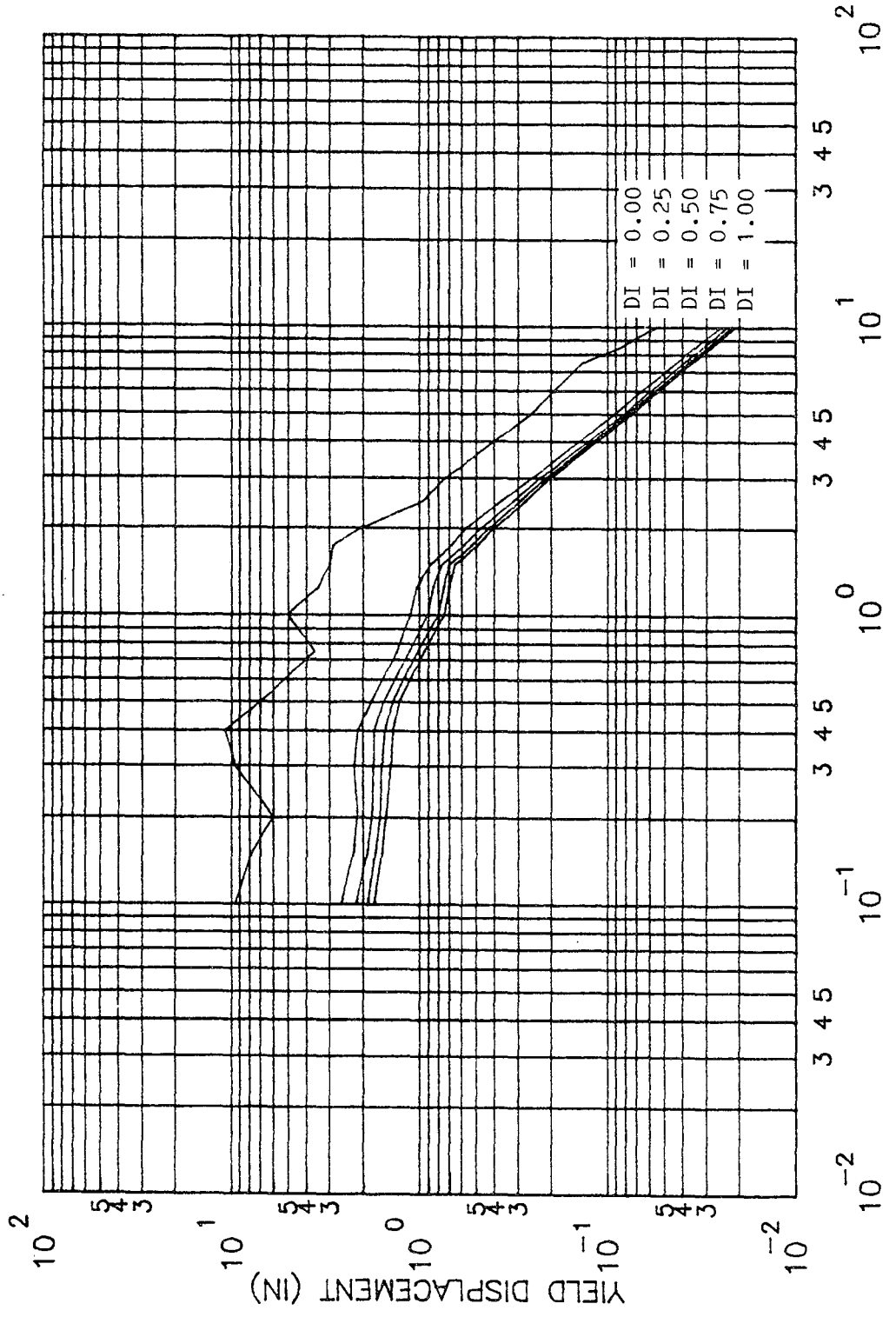

Figure 5.4c Yield Displacement Spectrum for El Centro with 5 Percent Damping Based on the Damage Index with a Monotonic Plastic Ductility of 4.0

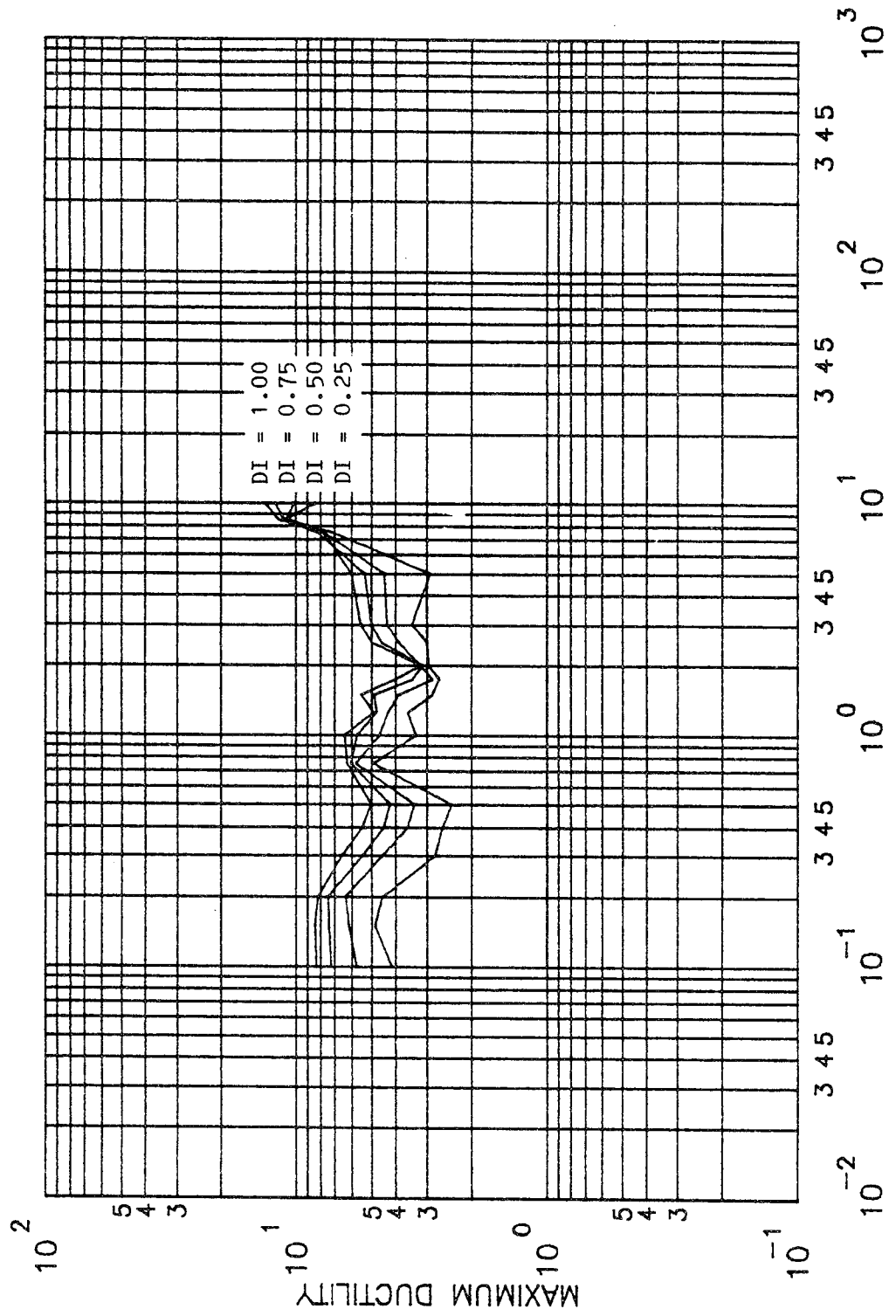

Figure 5.4d Maximum Ductility Spectrum for El Centro with 5 Percent Damping Based on the Damage Index with a Monotonic Plastic Ductility of 4.0

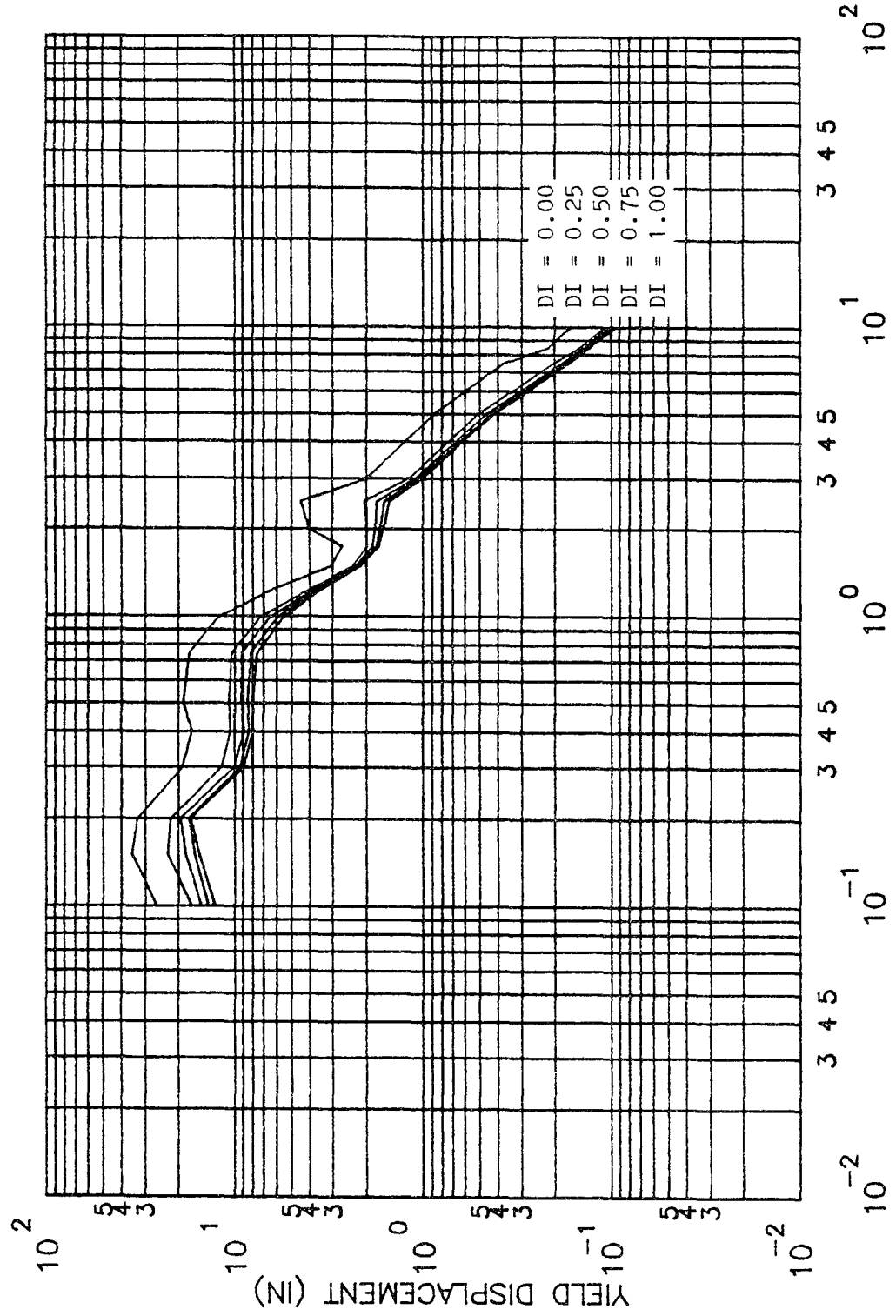

Figure 5.5a Yield Displacement Spectrum for Pacoima Dam with 5 Percent Damping Based on the Damage Index with a Monotonic Plastic Ductility of 0.5

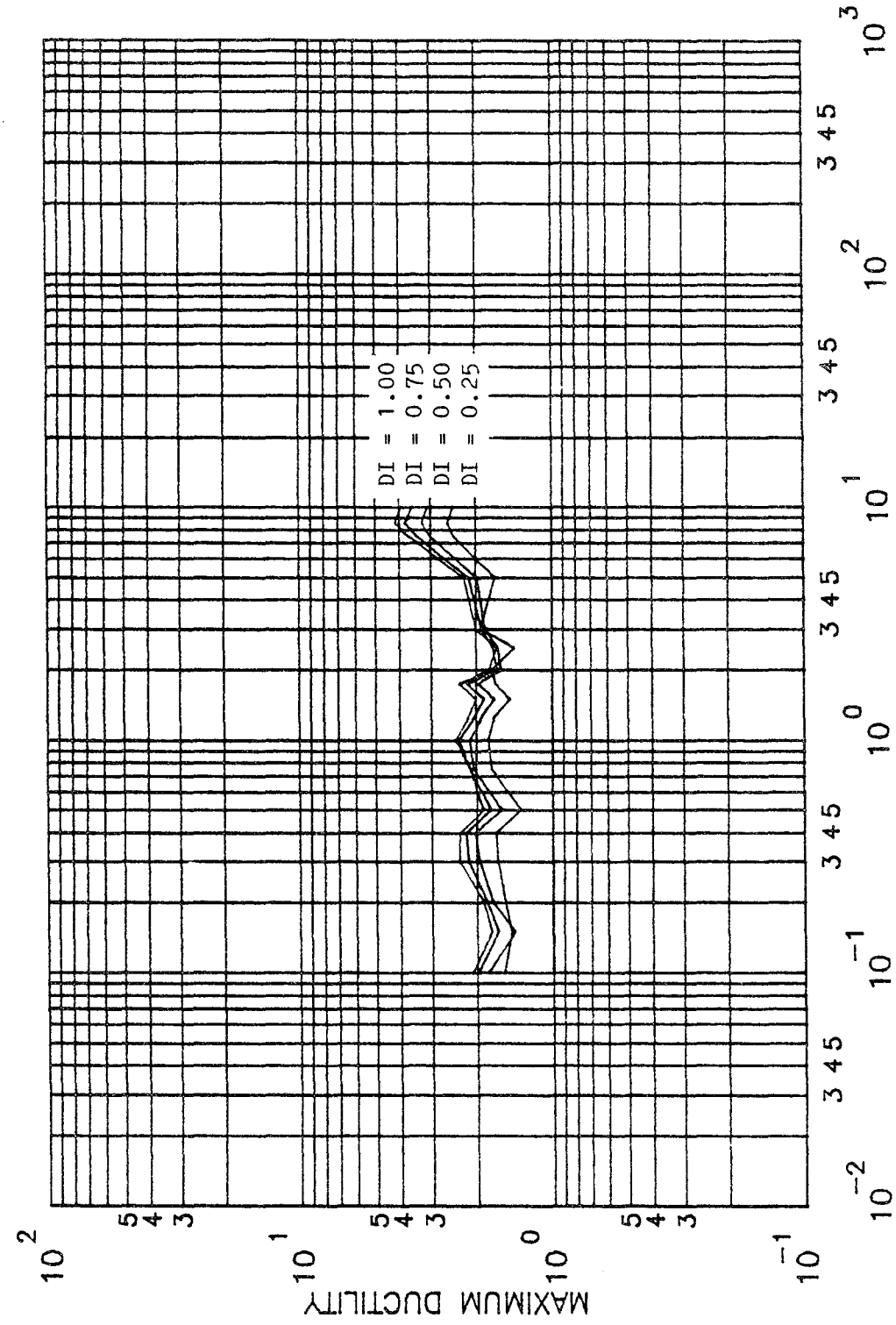

Figure 5.5b Maximum Ductility Spectrum for Pacoima Dam with 5 Percent Damping Based on the Damage Index with a Monotonic Plastic Ductility of 0.5

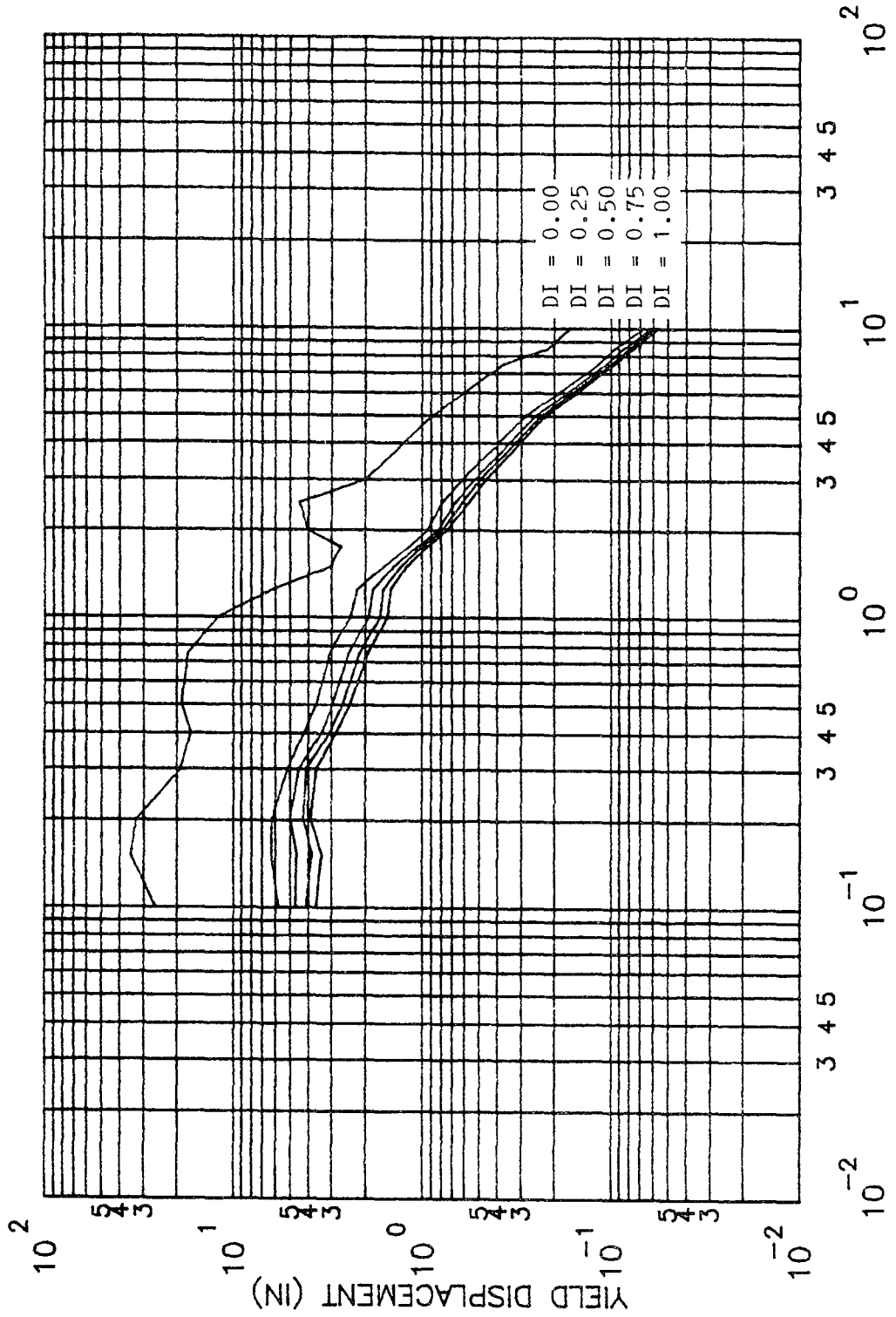

Figure 5.5c Yield Displacement Spectrum for Pacoima Dam with 5 Percent Damping Based on the Damage Index with a Monotonic Plastic Ductility of 4.0

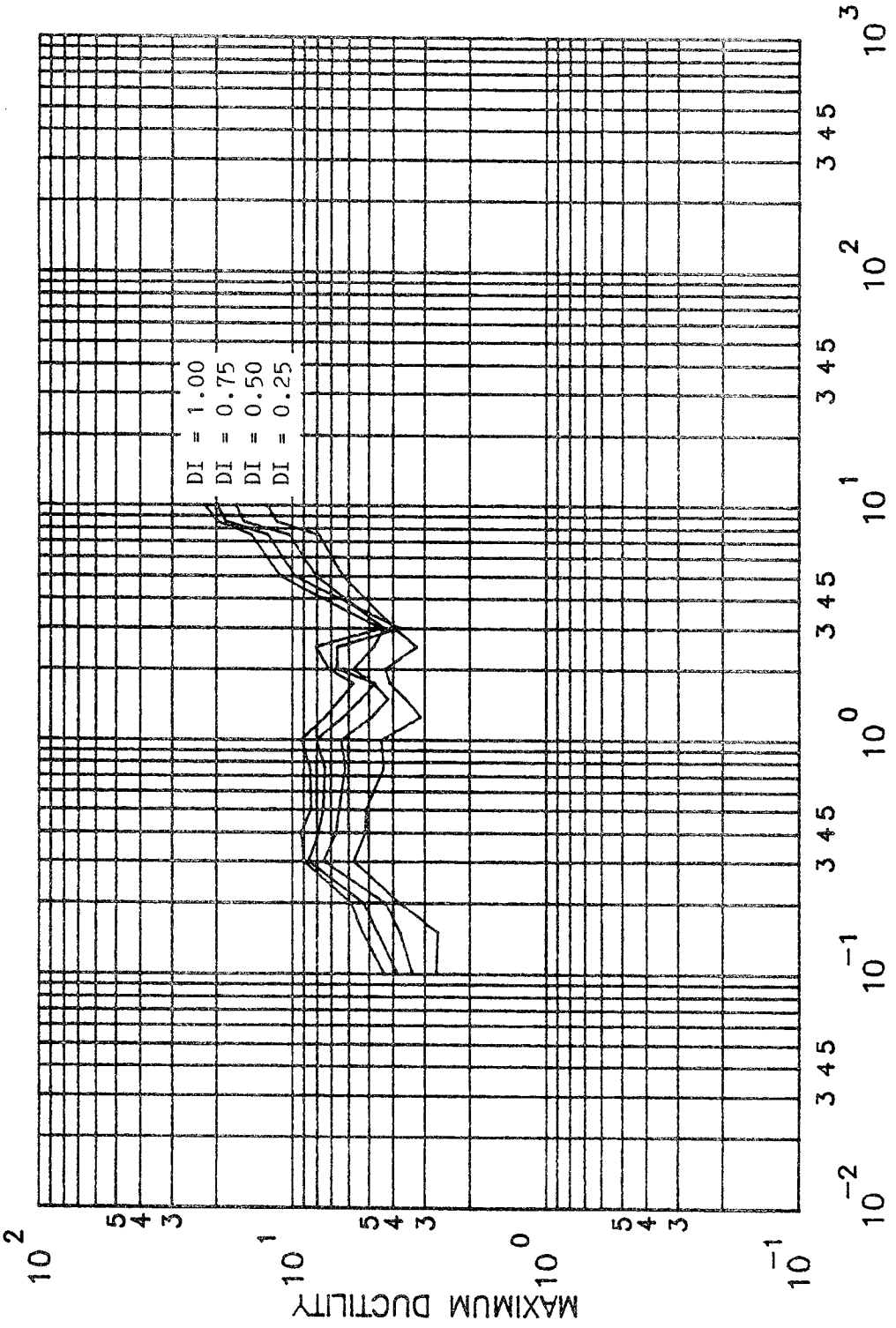

Figure 5.5d Maximum Ductility Spectrum for Pacoima Dam with 5 Percent Damping Based on the Damage Index with a Monotonic Plastic Ductility of 4.0

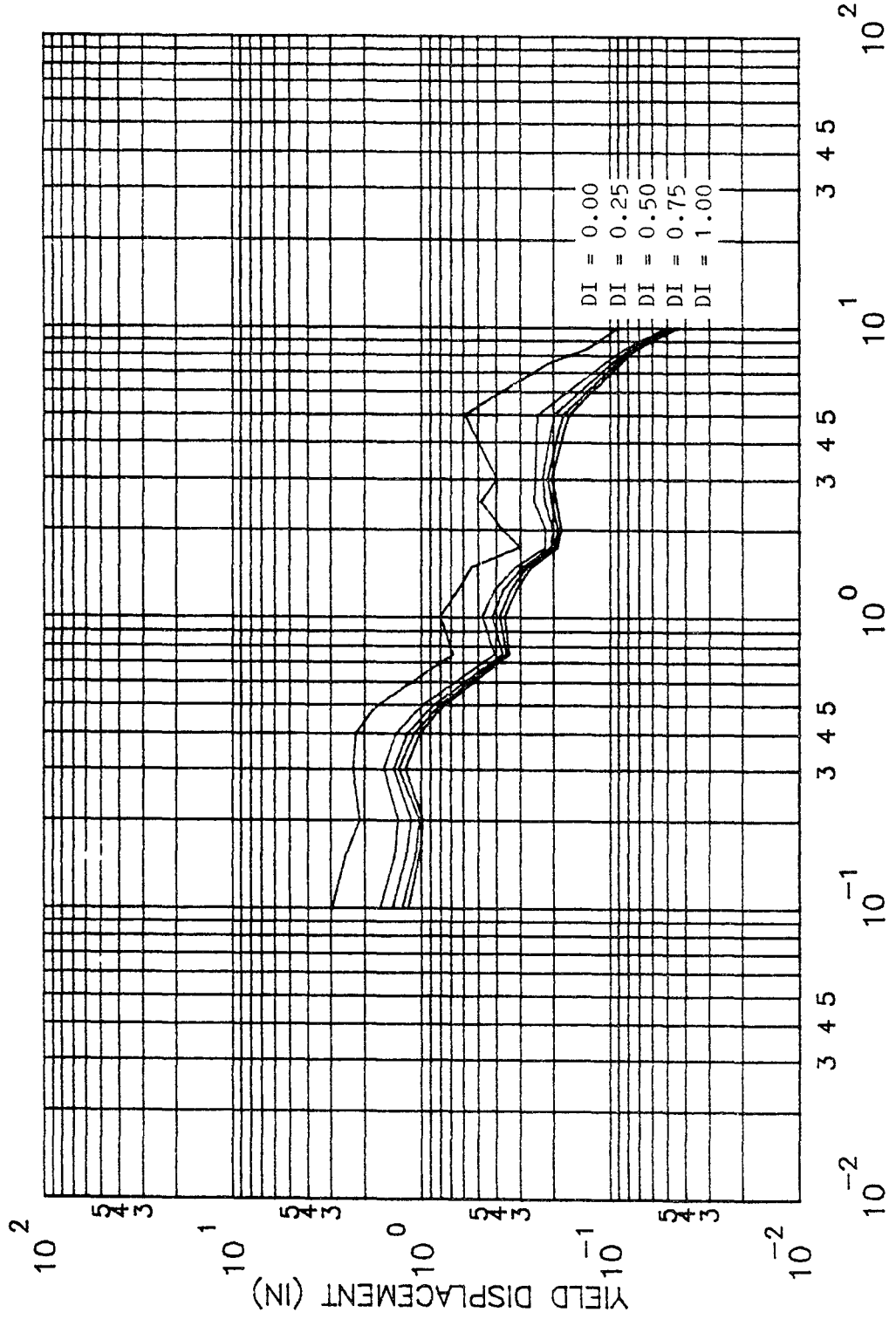

Figure 5.6a Yield Displacement Spectrum for Melendy Ranch with 5 Percent Damping Based on the Damage Index with a Monotonic Plastic Ductility of 0.5

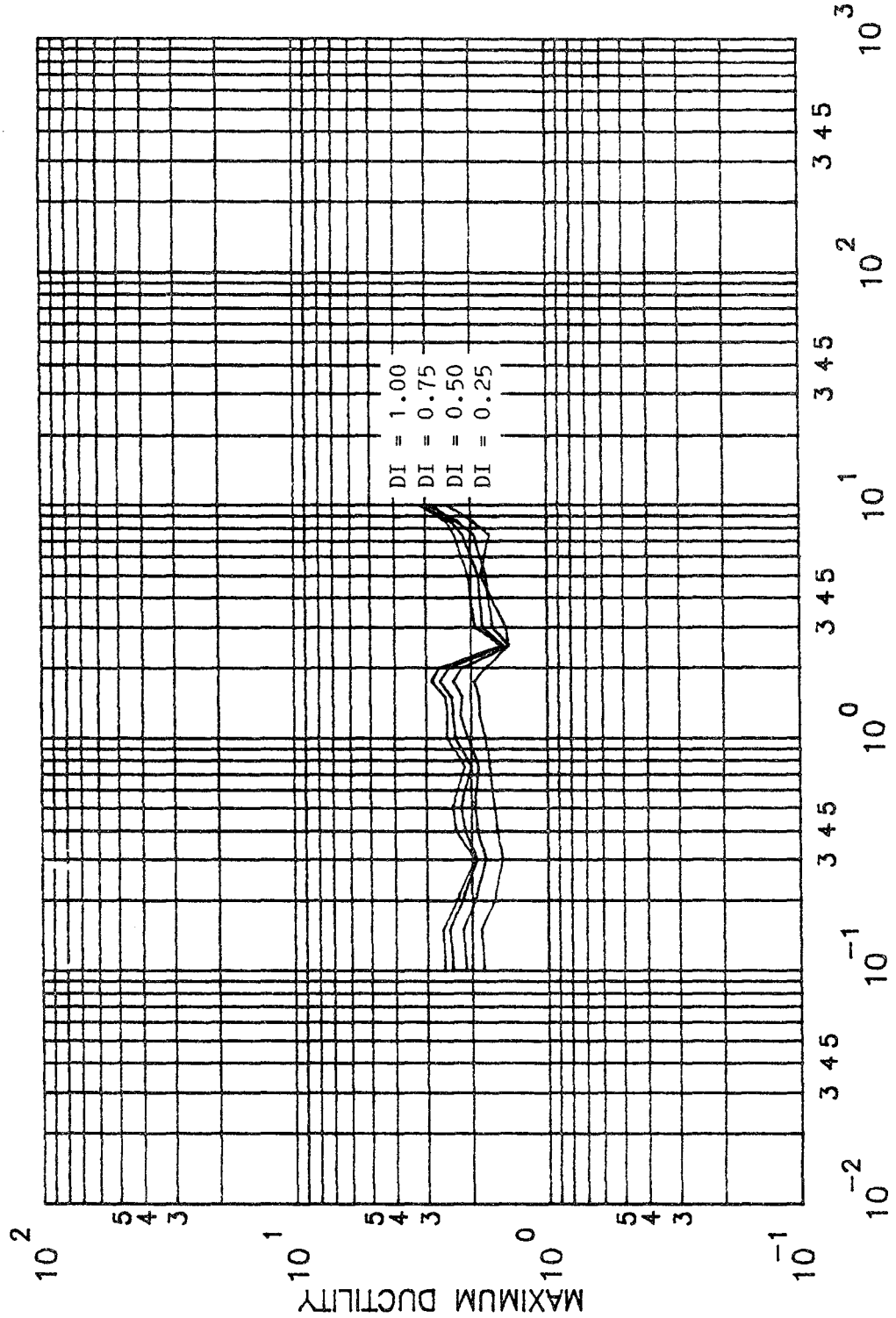

Figure 5.6b Maximum Ductility Spectrum for Melendy Ranch with 5 Percent Damping Based on the Damage Index with a Monotonic Plastic Ductility of 0.5

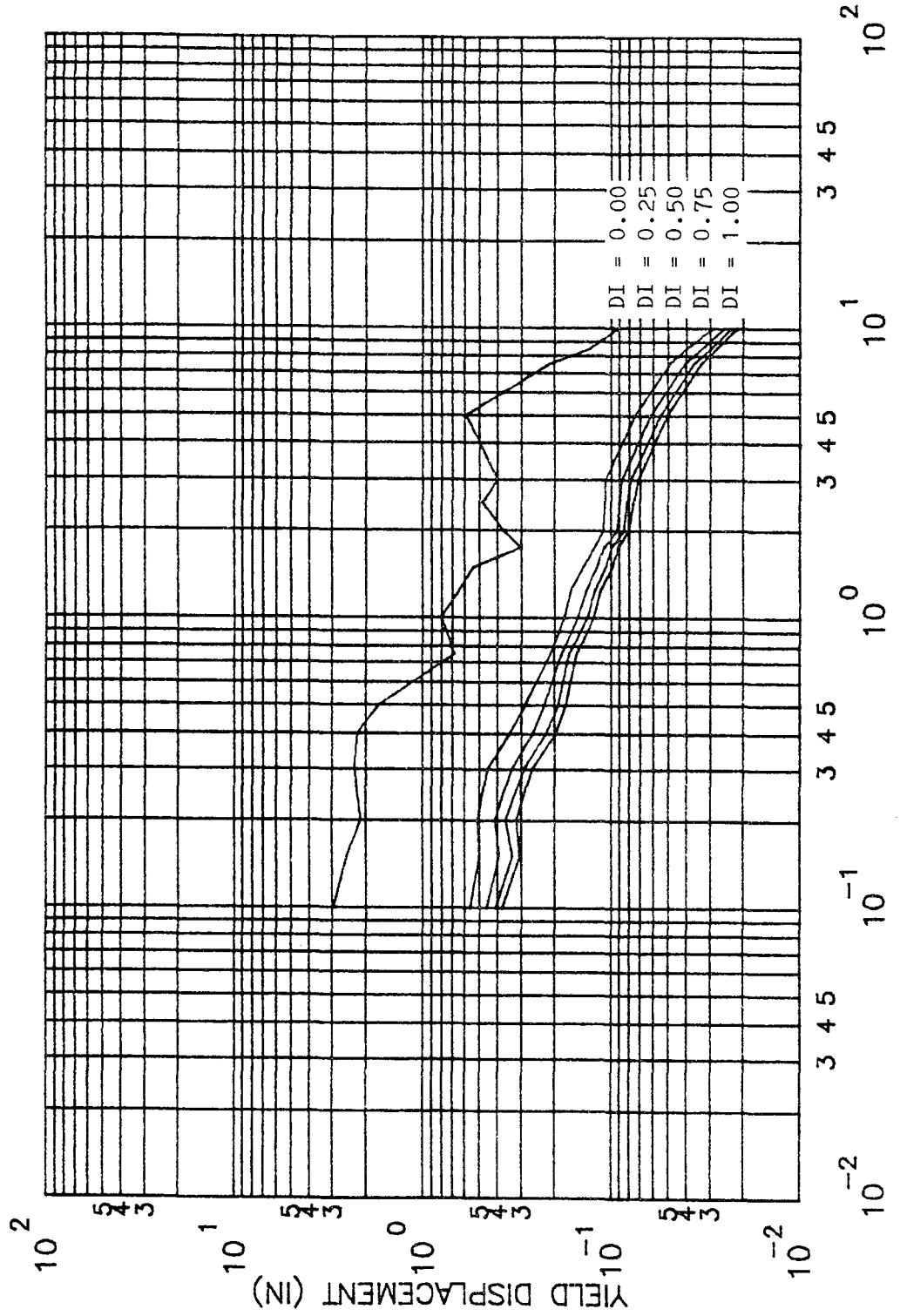

Figure 5.6c Yield Displacement Spectrum for Melendy Ranch with 5 Percent Damping Based on the Damage Index with a Monotonic Plastic Ductility of 4.0

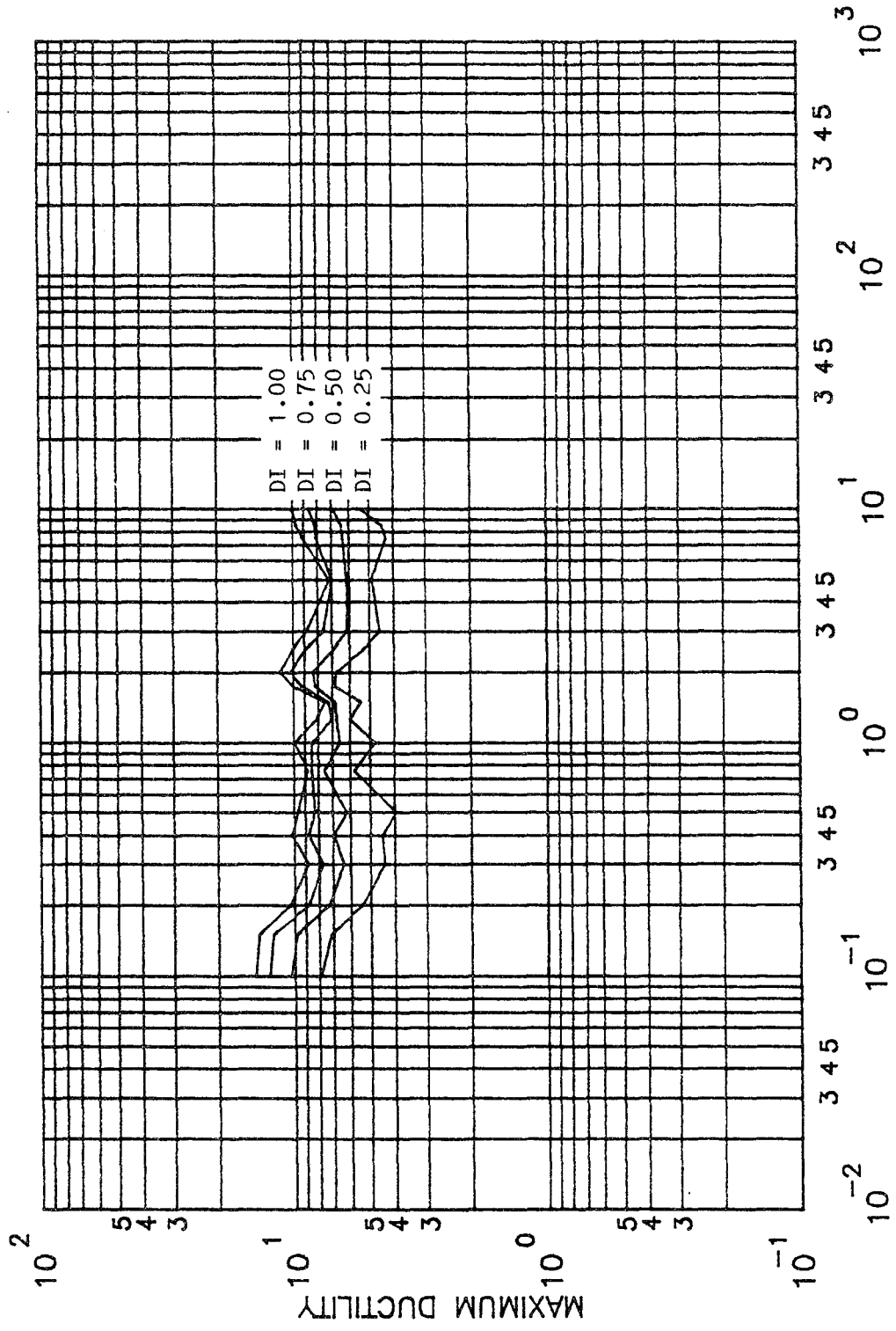

Figure 5.6d Maximum Ductility Spectrum for Melendy Ranch with 5 Percent Damping Based on the Damage Index with a Monotonic Plastic Ductility of 4.0

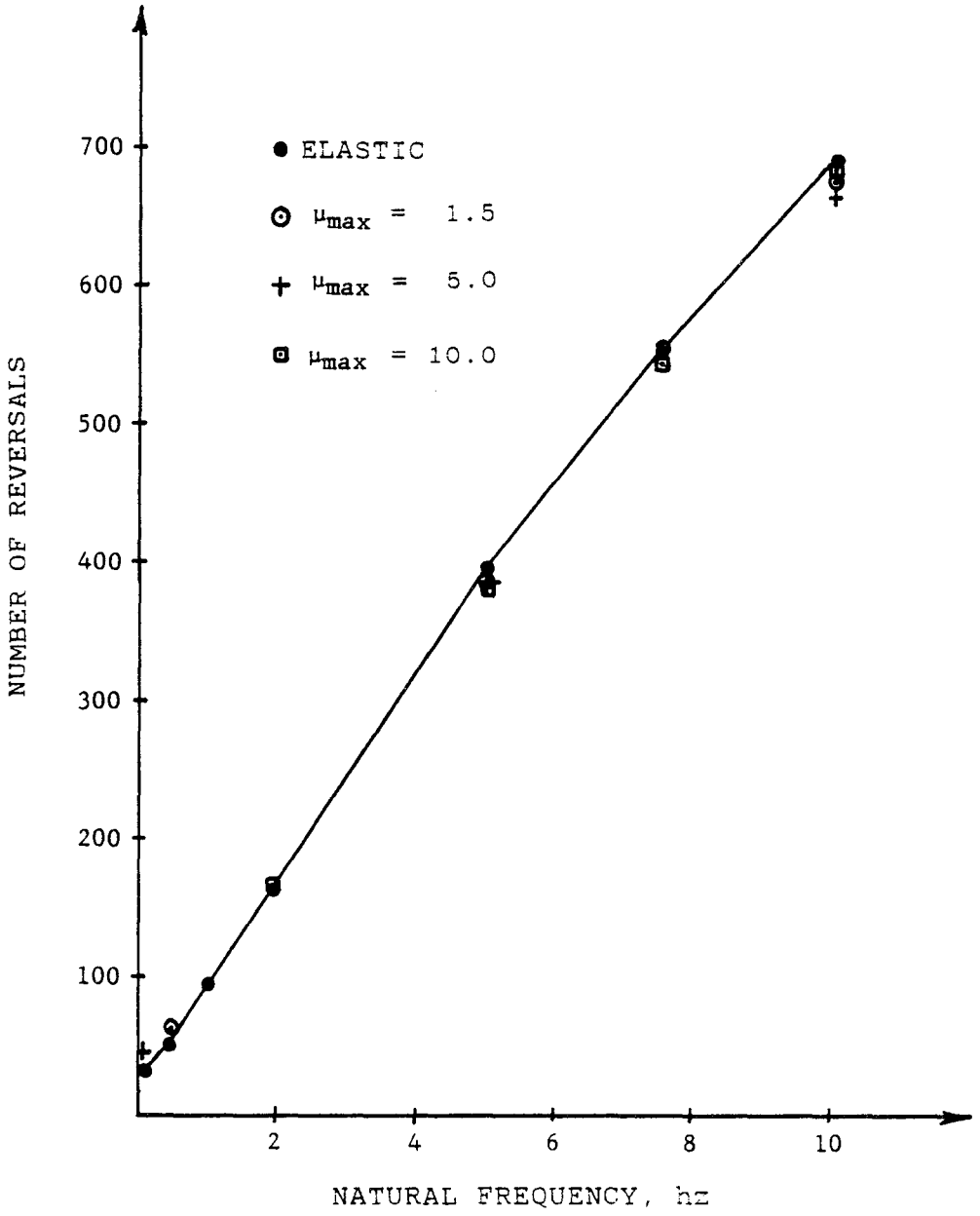

Figure 5.7a Effects of Changes in the Specified Maximum Ductility on the Number of Reversals Experienced by 5 Percent Damped Structure Responding to the First 40.0 Seconds of El Centro

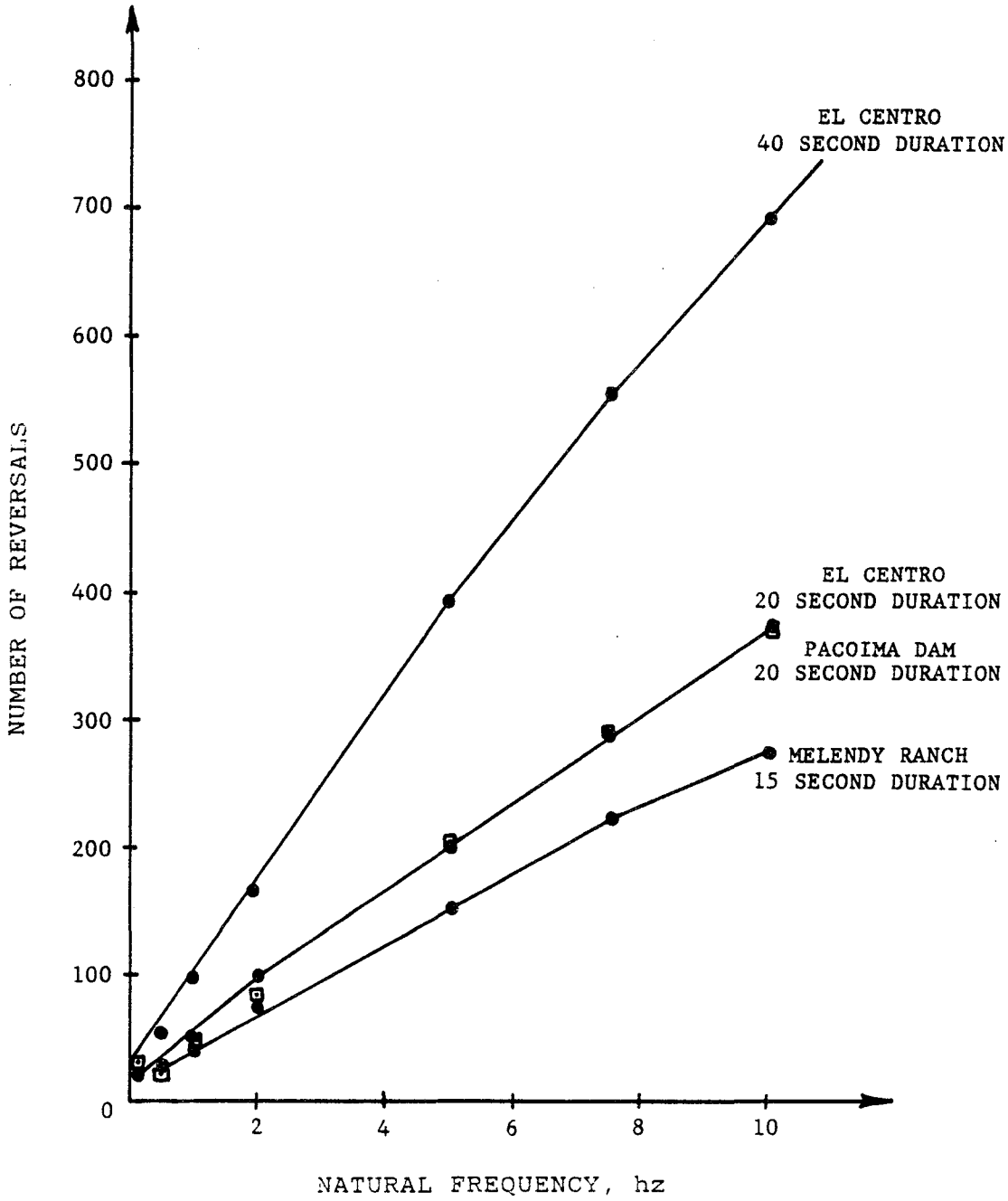

Figure 5.7b Effects of Changes in the Ground Motion Duration on the Number of Reversals Experienced by a 5 Percent Damped Structure Elastically Responding to El Centro, Pacoima Dam and Melendy Ranch

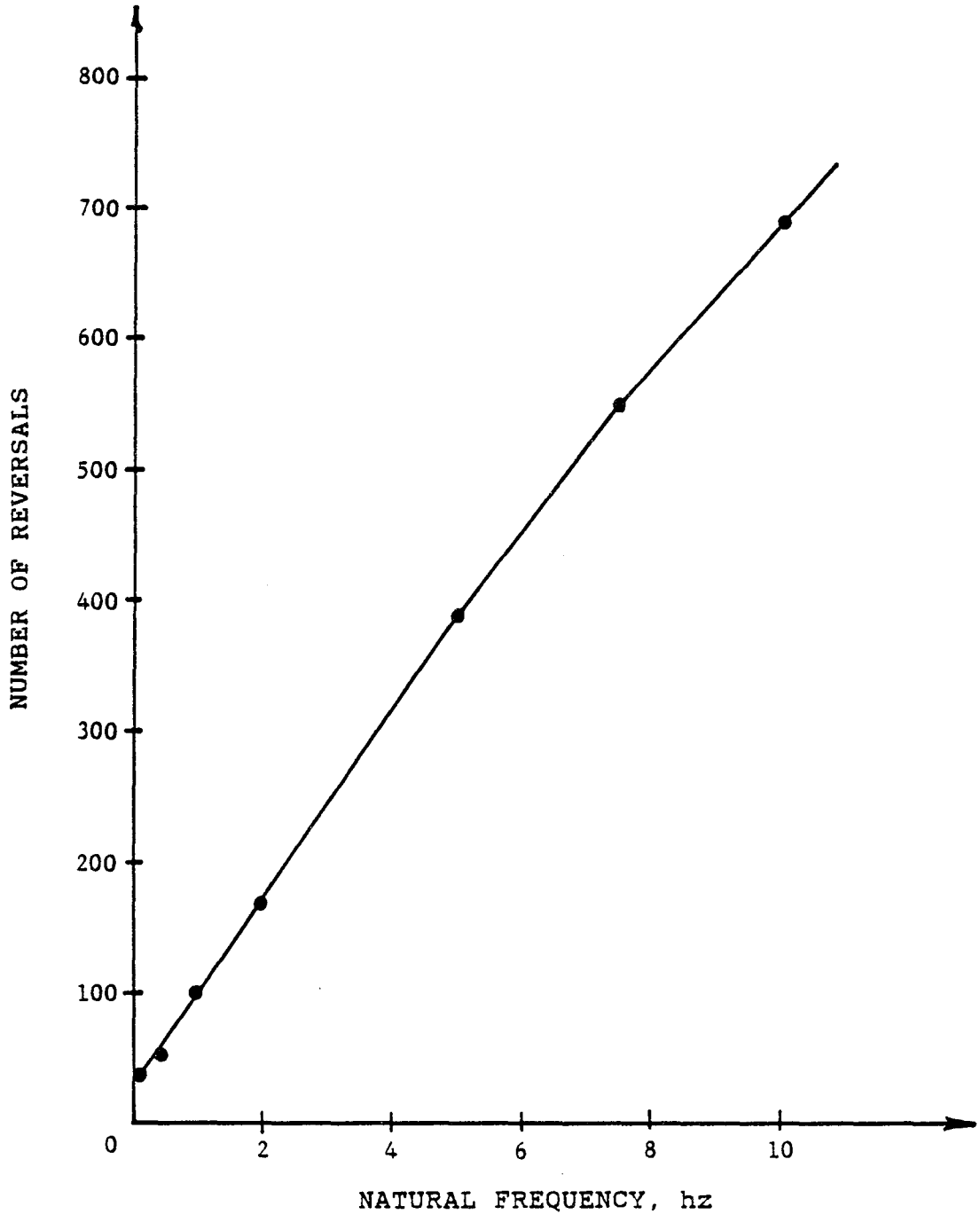

Figure 5.7c Design Curve for the Number of Reversals Experienced by a 5 Percent Damped Structure as a Function of Structural Frequency Based on the First 40.0 Seconds of El Centro

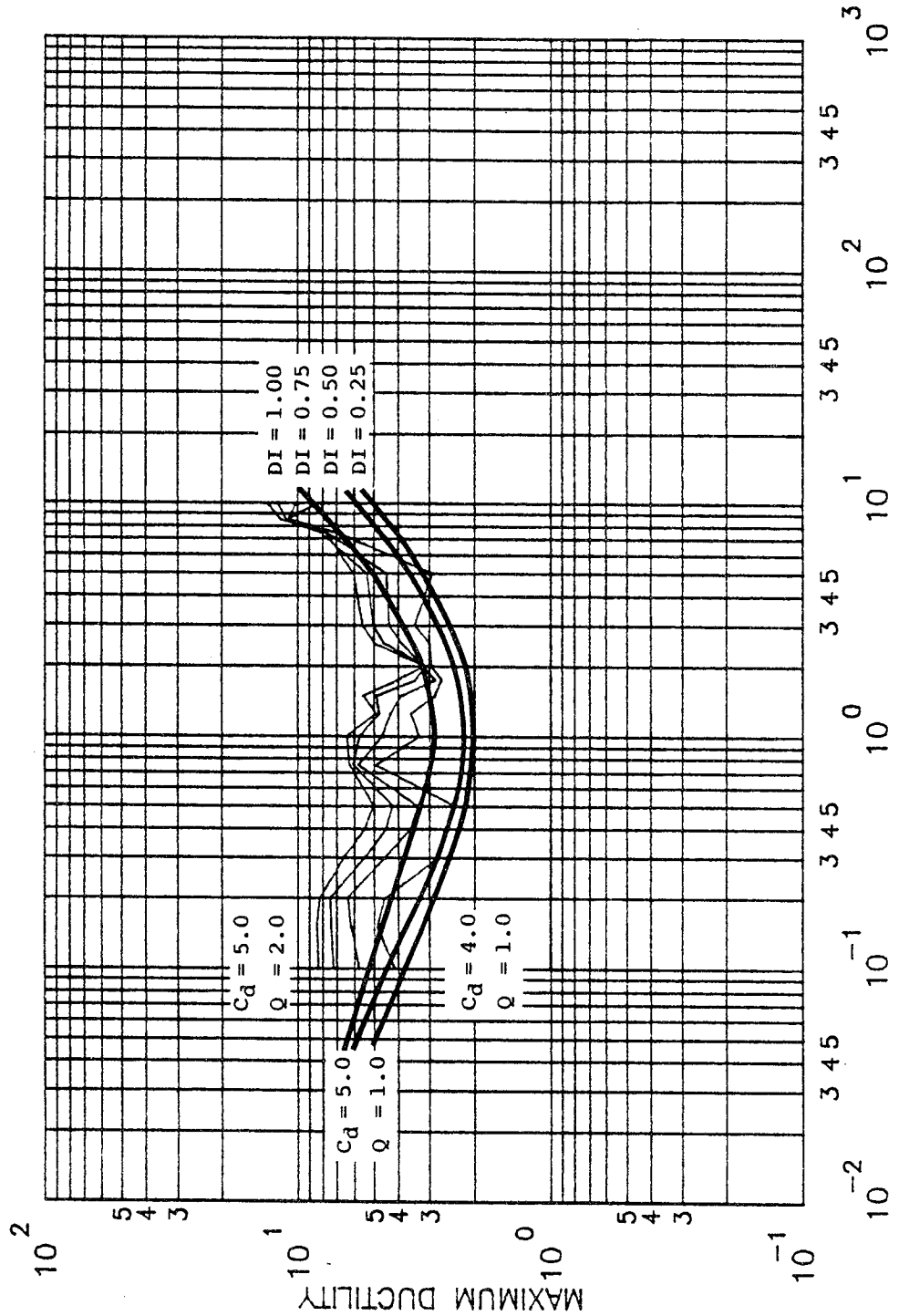

Figure 5.8 Comparison of the Maximum Ductility Values Obtained from the Proposed Drift Criterion with those Computed Using the Damage Index with a Monotonic Plastic Ductility of 4.0 in 5 Percent Damped Response to El Centro

APPENDICES

APPENDIX A

EXPERIMENTAL PROGRAM

A.1 Introduction

A short series of experiments was performed to verify several assumptions of the analytical work including the resistance model representation and to gain experimental perspective regarding structural response of simple systems to ground motion. The experimental work was designed to be simple, utilizing a single-degree-of-freedom (SDOF) structure subjected to pulse-type acceleration excitation similar to that described in Chapter 2.

Also of interest were the hysteretic energy calculations, specifically the area inside the hysteresis loops as compared to the elastoplastic hysteretic energy calculations. Another purpose of the experimental work was to obtain data as to how the relative frequencies of the structure and ground motion affected the level of nonlinear response and data regarding the overall sensitivity of the structure to frequency shifts in the input ground motion.

A.2 Test Configuration

A.2.1 Structure

The structure that was tested was a small SDOF structure with four legs supporting a steel plate as shown in Fig. A.1. Two of the legs were pinned at both ends while the other two legs were pinned at the bottom and fixed at the top. Pinned connections were obtained by attaching the columns to shafts that were held by ball bearings mounted in fixtures; fixed connections were approximated by using special

clamps attached to the plate. This configuration of four legs was selected to remove any significant rotational motion as might occur with a mass mounted at the end of a single pair of supports.

The legs were made of steel bar stock (1.0 in. x 0.5 in.). This simple cross section was selected so as not to introduce local buckling or other complications into the response. The tops of the two fixed-end bars had reduced areas (1.0 in. x 0.4375 in.) to ensure that the nonlinear action occurred at the clamp and not elsewhere. The stiffness of these bars was estimated by analysis to be 225 lb/in which resulted in a natural frequency for the structure of just above 3 hz.

A.2.2 Instrumentation

The structure was instrumented using linear variable differential transformers (LVDT's) to measure the displacement relative to the earthquake table. LVDT's were placed at the centerline of the steel plate and also on two of the support legs near the top of the two pinned connections at the plate level. The LVDT's had a 4.0 in. stroke and were positioned to be at their midpoint. Table displacement also was measured by an internal position transducer in the hydraulic ram.

Acceleration values were obtained by Endevco piezoresistive type accelerometers mounted on the earthquake table and plate centerline to obtain the table and structural accelerations. One accelerometer was located vertically at the center of the plate to measure vertical accelerations; two other accelerometers were placed transversely at the front and back of the plate between the two column rows to measure any torsional accelerations. The accelerometers had a 25g capacity, 1.0% linearity, 0-750 hz frequency response, a natural frequency of 2500 hz and 0.7 damping. All instrumentation was calibrated prior to testing.

A.2.3 Earthquake Simulator

Dynamic testing was performed using the University of Illinois earthquake simulator located in Newmark Civil Engineering Laboratory. The table is 12 ft square and allows one direction of translational motion only. The table is moved by a MTS hydraulic ram that is controlled via an analog displacement control system. The ram can generate 75,000 lb of force resulting in a maximum table acceleration of 7g's for small specimens, a maximum velocity of 15 in/sec and a maximum peak to peak displacement of 4 in.

Input ground motions can be displacement, velocity or acceleration time histories that are converted to an analog displacement signal. All table control and data acquisition is performed in the control room located on the mezzanine level of the laboratory.

A.2.4 Earthquake Excitation

A triangular acceleration input pulse of $\pm$0.5g and frequencies of 3.0, 3.5, 4.0 and 6.0 hz were used to observe the response changes with increasing frequency. Two additional tests at 3.0 hz and $\pm$0.75g and $\pm$1.0g also were performed to study the changes in response with amplitude.

The signal for the table was produced using a signal generator to produce an analog displacement signal directly to the table control system. A trial and error process was used to select a displacement function that would result in a triangular acceleration time history. The haversine function was selected because it produced the smoothest triangular acceleration pulse. The function is defined as

$$\text{hav}\ (A) = (1/2)[1 - \cos(A - \tfrac{\pi}{2})], \qquad (A.1)$$

where the function was shifted to have its maximum at time zero. The results of this operation are illustrated in Figs. A.2 and A.3 for the 3 hz case. Close examination of the table acceleration pulses show a slight distortion of the pulse caused by a higher frequency vibration that was part of the table motion. Attempts to remove this vibration completely were unsuccessful although it was reduced by using an analog filter to remove all frequencies above 10 hz.

A.2.5 Data Reduction Procedures

The data from the experiments, logged at 0.005 second intervals, was reduced using a DEC-LSI computer. Plots were generated using a Hewlett-Packard 7221A plotter. These plots include displacement and acceleration time histories as well as hysteresis loops. Calculated values of hysteretic energy with time were added to the respective values of kinetic and damping energy to obtain the total input energy.

During the data reduction for the 3 hz pulse frequency test, a problem was discovered in the data. A plot of resistance-deformation data produced a hysteresis curve that ran backwards indicating negative energy dissipation. Investigation of the table displacement and acceleration time histories revealed a time shift between the acceleration and displacement data points. With this simple ground motion, the displacement and acceleration peaks should have been exactly 180° out of phase.

The explanation as to how this shift occurred was difficult to ascertain. The data acquisition system was identical for both displacement and acceleration except for a filter used to remove frequencies above 10 hz from the accelerometer data. It was believed

that the filter led to the time shift. Accordingly, the data was adjusted by 0.030 sec to align the displacement and acceleration data appropriately. Such shifts are not unusual. Morrison and Sozen (43) noted a time shift present in this same test system on the order of 0.004 sec. Iemura and Jennings (29) also observed a time shift between measured acceleration and displacement during testing of the Millikan Library at the California Institute of Technology. Their observed shift was 0.04 to 0.06 sec. In summary, these observations point to the need for examination of the data for consistency.

A.3 Results

A.3.1 Static Tests

The load-deflection relationship was obtained by static tests using a 2500 lb capacity hydraulic actuator which applied force directly to the mass. Typical measured hysteresis behavior is shown in Fig. A.4. The hysteresis loops are interesting in the fact that a stiffness of 243 lb/in was measured which was quite close to the design prediction; also the first loop closely approximates an elastoplastic resistance model. The Bauschinger Effect is evident as indicated by the rounding of the loops and the slight rotation of the loops with cycling. The value of the Modulus of Elasticity for the bar steel was found to be 29,500 ksi from the recorded data and verified by separate test.

A.3.2 Dynamic Tests Results

The natural frequency of the structure was measured to be 3.15 hz by free vibration test, close to the design prediction. A typical

damping value of 2.5 percent of critical was determined through use of the log decrement method.

Typical structural displacement and acceleration time histories for the 3 hz pulse are presented in Figs. A.5 and A.6. Hysteresis curves are presented in Figs. A.7 through A.12 for all of the tests except the 1.0g, 3.0 hz pulse where the displacements exceeded the range of the LVDT's.

A summary of the calculated results from the data is presented in Table A.1. The following observations can be made about the results.

1. The experimental results show that the frequency of the pulse relative to the structural frequency is a very important factor in the overall response. Slight increases in the pulse frequency from 3.0 to 3.5 hz cause the maximum displacement and particularly the energy values to drop significantly for this 3.15 hz structure. Further frequency increases induce even lower response.
2. A duration of 5.0 seconds, as compared to 2.0 seconds, did not cause any increase in displacement response but the input energy, the hysteretic energy and the overall number of response cycles were increased almost linearly with duration.
3. The total hysteretic energy was found to be nearly balanced between energy dissipated on the positive and negative resistance sides.
4. Vertical and torsional acceleration values were found to be small relative to the horizontal values indicating that the motion was confined primarily to the single horizontal degree of freedom.

5. The hysteresis response curves are good indicators of the drop in response with increasing input frequency. The displacement values drop, as does the area of the loops with increasing pulse frequency. For example, the hysteresis area of the 6.0 hz pulse is minute.
6. The increase in amplitude to 0.75g for the 3 hz input pulse did not increase the displacement amplitude significantly. The total input energy was increased roughly in proportion to the acceleration amplitude increase. This observation shows the advantage of using the energy as a measure of response characteristics.
7. The hysteretic behavior observed during static and dynamic tests was noted to be quite similar confirming Hanson's results (21). Comparable displacements caused comparable areas for the static dynamic test results. The initial elastic stiffness obtained from the static and dynamic tests were essentially equal. Softening is observed in the unloading and loading phases after cycling resulting in a tangent stiffness of 190 lb/in.

A.3.3 Comparison to Analytical Results

The ground motion input pulses used in the experimental tests were used to excite a 3.15 hz structure analytically in order to compare the analytical results with the experimental observations. The ground motion was modeled as +0.52g and −0.48g rather than $\pm$0.5g because of the slight distortion of the acceleration pulses as noted earlier, with a 2.5 percent damping value and several values of stiffness and yield resistance for the elastoplastic material model. A variation of

parameters indicated that the values of 235 lb/in stiffness and 1.10 in. yield displacement provided reasonably good agreement with the experimental results. Typical results are presented in Table A.2.

The maximum deformations were generally close and consistently less than the experimental values. Hysteretic energies were comparable to the experimental values but again were lower possibly because of the slight difference in shape of a hysteretic cycle and the elastoplastic material model. The equivalent hysteretic cycles were close to the actual number of yield excursions during the tests with the weighted deformation cycles, defined in Chapter 2, being the best indicator.

A.4 Conclusions

The results of these simple tests indicate that the pulse input frequency is of great importance to the structural response. Slight mistuning greatly reduced the response as compared to response caused by closely matched frequencies. Increases in input amplitude did not cause a corresponding increase in displacement but did cause a similar increase in overall energy dissipation. Duration causes more hysteretic cycles but did not cause any increase in deformation response. For limited yielding, it was interesting to observe from the hysteretic loops how quickly the structure reached a steady state condition. It is apparent from these studies that the calculation of input and hysteretic energies, as well as kinetic and damping energies, can significantly aid in the evaluation of structural response.

Table A.1 Summary of Experimental Results

Ground Motion Pulse Frequency, hz	Ground Motion Pulse Duration, sec	Ground Motion Pulse Amplitude, g	Maximum Relative Displacement, in	Total Input Energy, in-lb	Total Kinetic Energy, in-lb	Total Strain and Hysteretic Energy, in-lb	Number of Response Cycles*
3.0	2.0	0.5	2.06	2440	216	2170	12
3.0	5.0	0.5	1.98	5620	66	5420	30
3.0	2.0	0.75	2.17	4294	236	3240	12
3.5	2.0	0.5	1.82	1120	116	962	14
4.0	2.0	0.5	1.37	375	116	230	16
6.0	2.0	0.5	0.47	38	7	23	23

* During these cycles of response, yielding may or may not have occurred.

Table A.2 Summary of Analytical Results

Ground Motion Pulse Amplitude: +0.52g/-0.48g
Pulse Duration: 2.0 seconds

Structural Stiffness: 235 lb/in
Yield Displacement: 1.10 in

Ground Motion Pulse Frequency, hz	Maximum Relative Displacement, in	Total Input Energy, in-lb	Total Hysteretic Energy, in-lb	Counted Velocity Sign Changes/ Yield Excursions	Equivalent Hysteretic Cycles Based On Maximum Displacement	Equivalent Hysteretic Cycles Based On Weighted Displacement
3.0	1.82	2451	1871	11 / 11	10.1	11.6
3.5	1.50	1595	934	13 / 11	10.8	10.9
4.0	1.28	314	46	15 / 2	1.0	2.3
6.0	0.36	36	0	23 / 0	0.0	0.0

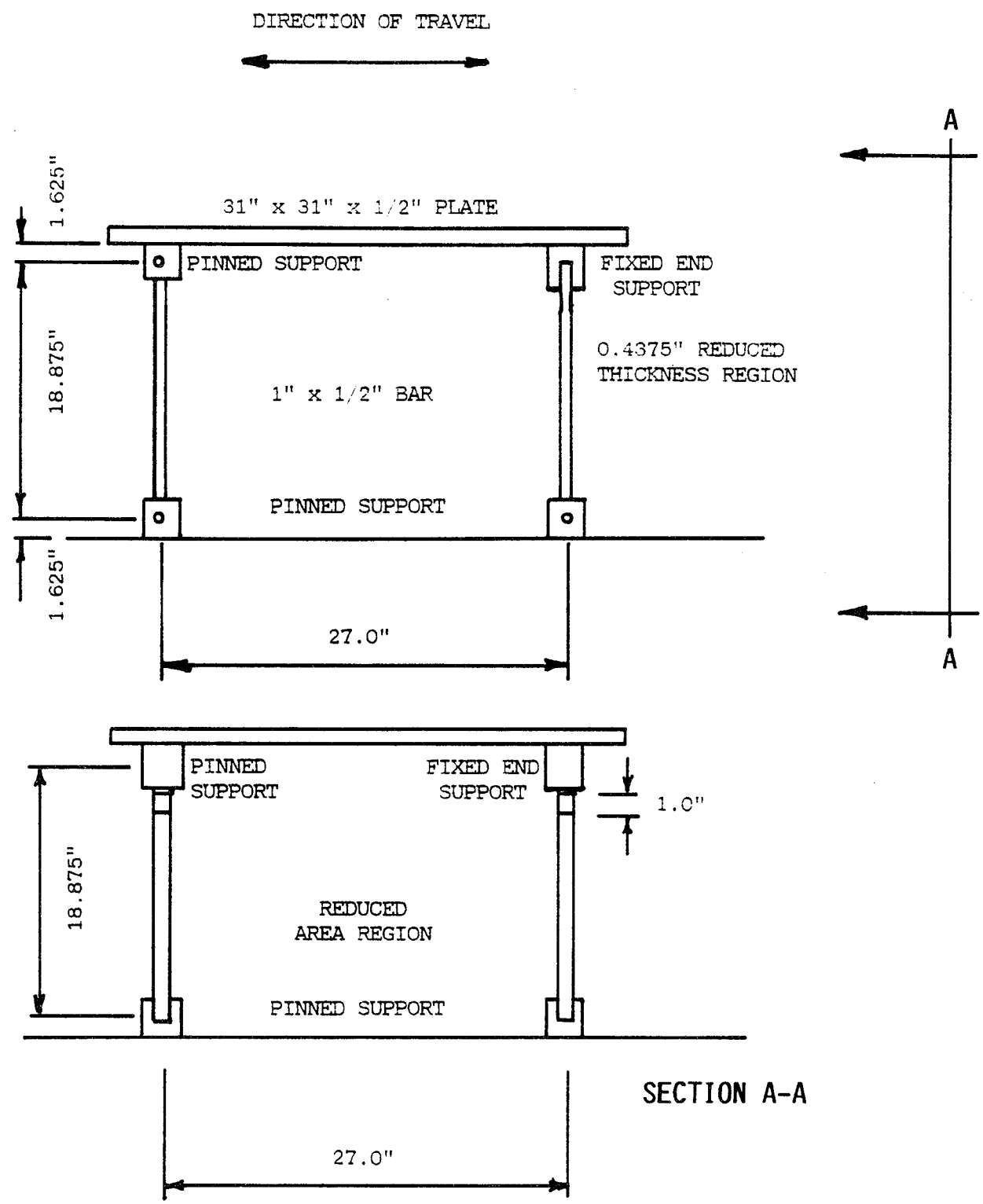

Figure A.1 Test Structure

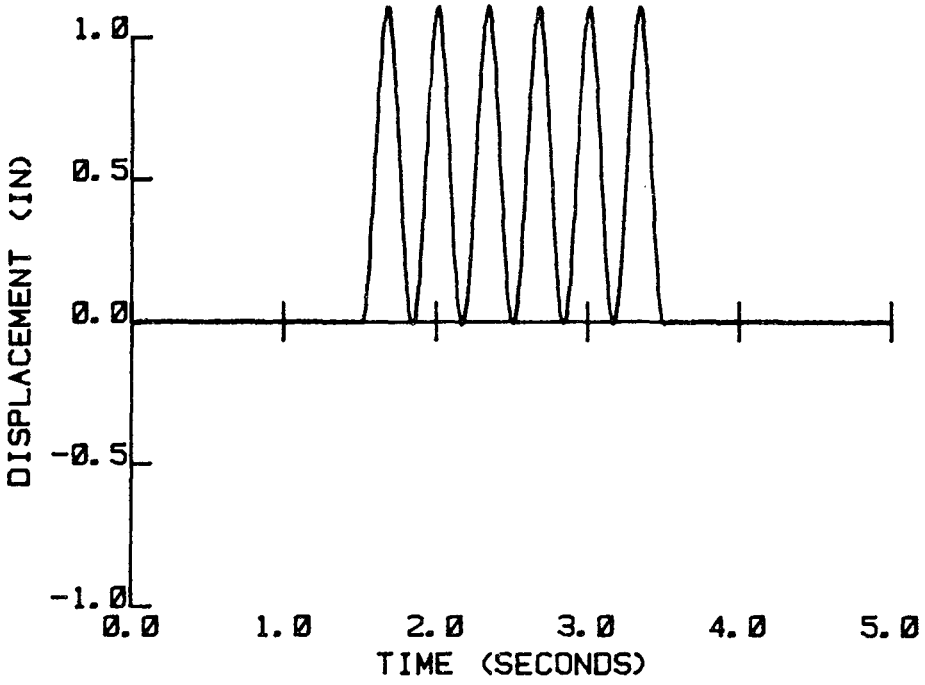

Figure A.2 Input Table Displacement Time History Causing a 3.0 hz Pulse, ±0.5g, 2.0 Second Duration, Test No. 1

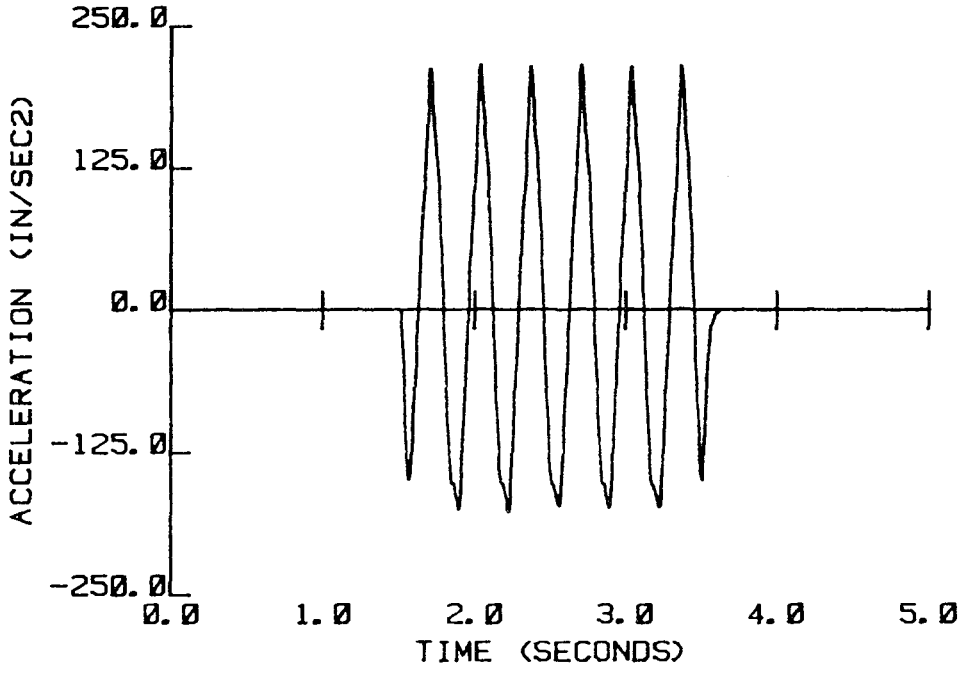

Figure A.3 Measured Table Acceleration Time History Resulting From Input Shown in Fig. A.2, Test No. 1

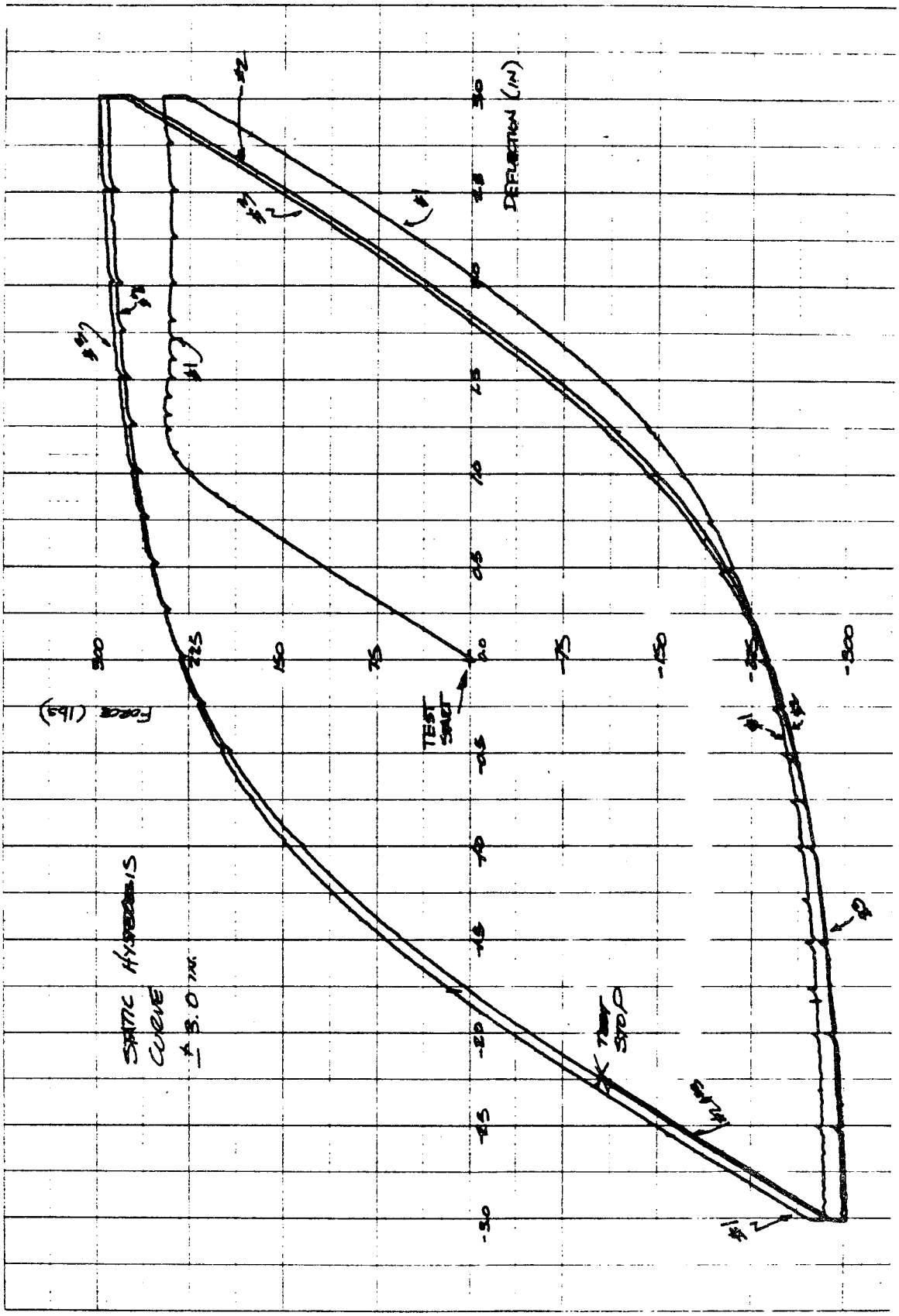

Figure A.4 Static Hysteresis Behavior

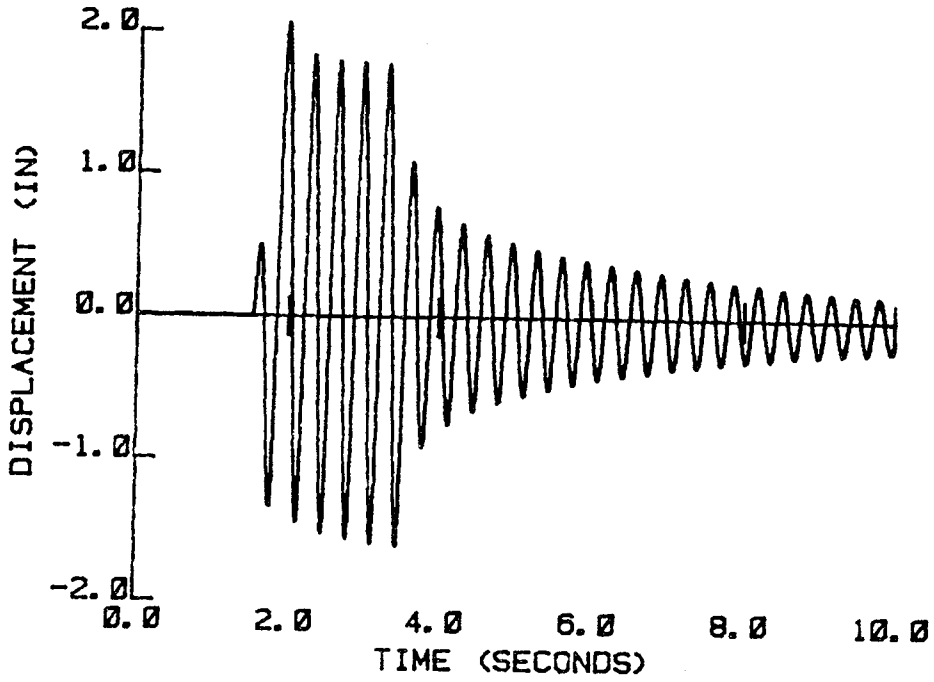

Figure A.5 Structural Displacement Time History-Response to a 3.0 hz Pulse, ±0.5g, 2.0 Second Duration, Test No.1

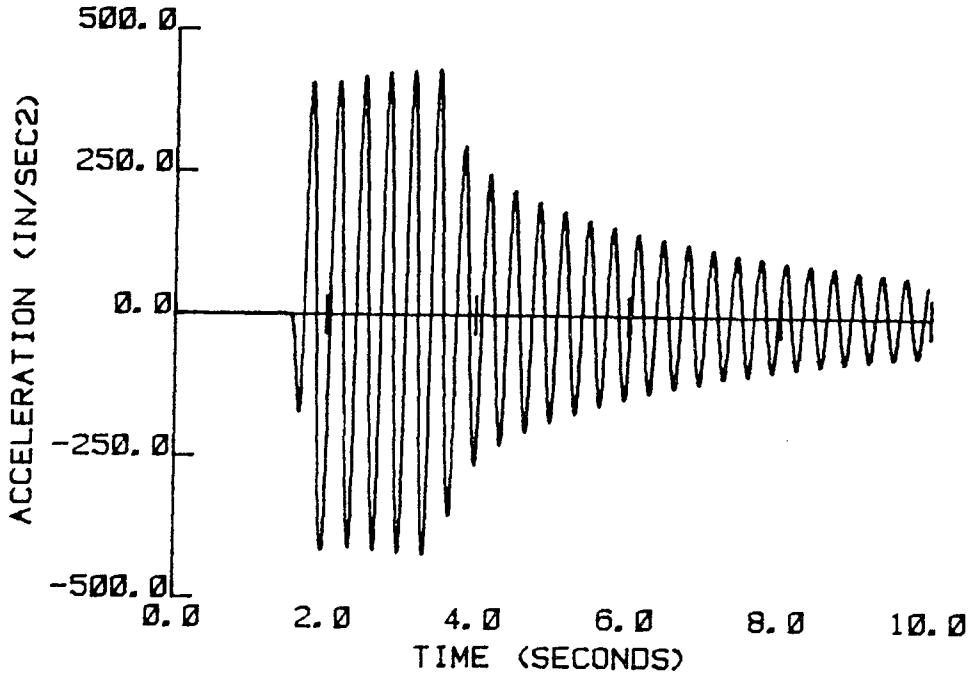

Figure A.6 Structural Acceleration Time History-Response to a 3.0 hz Pulse, ±0.5g, 2.0 Second Duration, Test No. 1

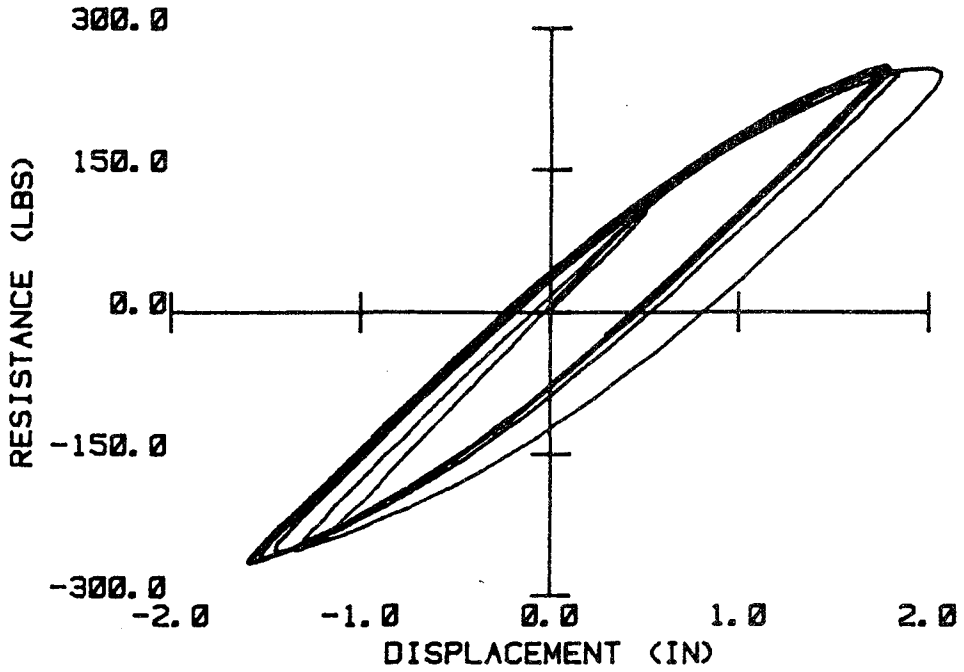

Figure A.7 Dynamic Hysteresis Behavior-Response to a 3.0 hz Pulse, ±0.5g, 2.0 Second Duration, Test No. 1

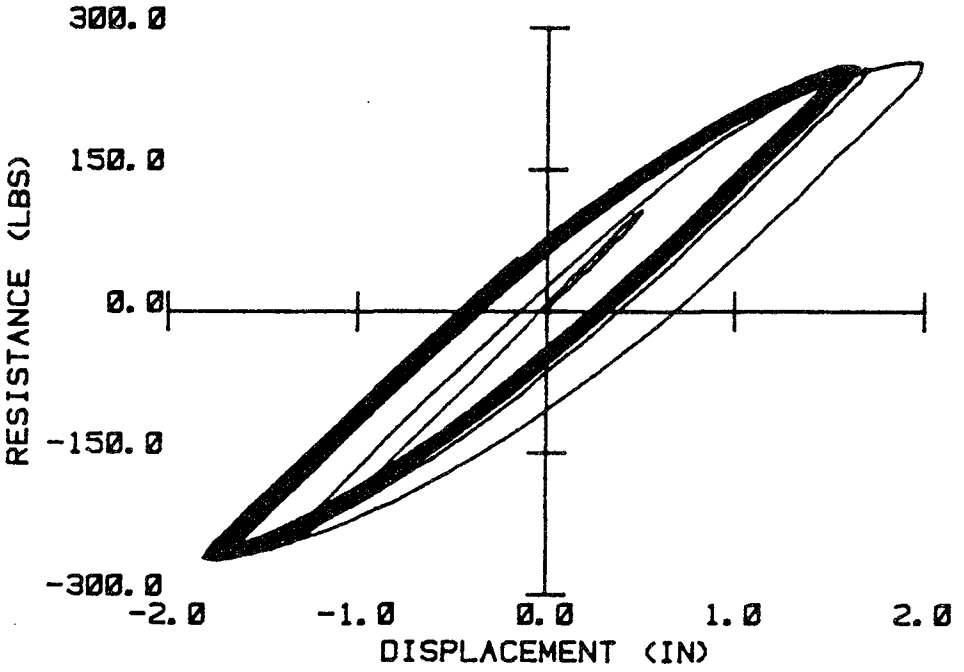

Figure A.8 Dynamic Hysteresis Behavior-Response to a 3.0 hz Pulse, ±0.5g, 2.0 Second Duration, Test No. 2

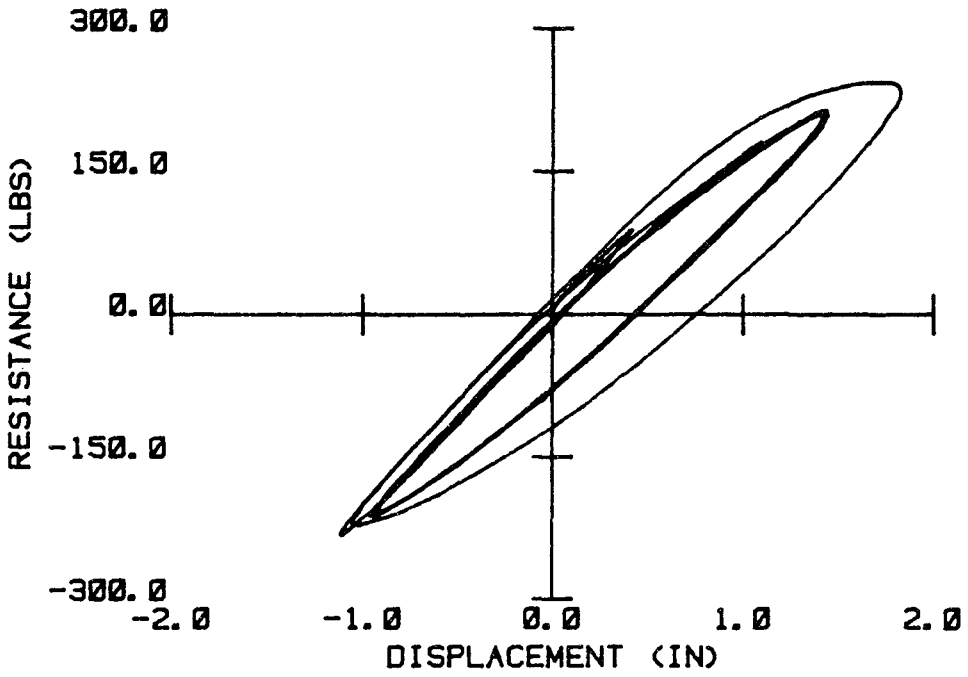

Figure A.9 Dynamic Hysteresis Behavior-Response to a 3.5 hz Pulse, ±0.5g, 2.0 Second Duration, Test No. 3

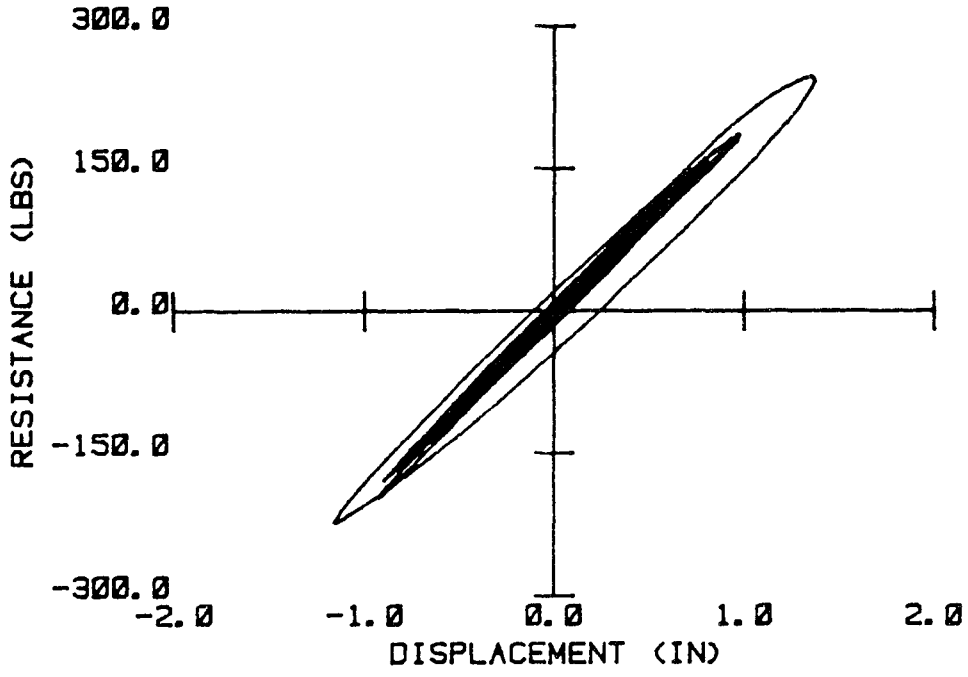

Figure A.10 Dynamic Hysteresis Behavior-Response to a 4.5 hz Pulse, ±0.5g, 2.0 Second Duration, Test No. 4

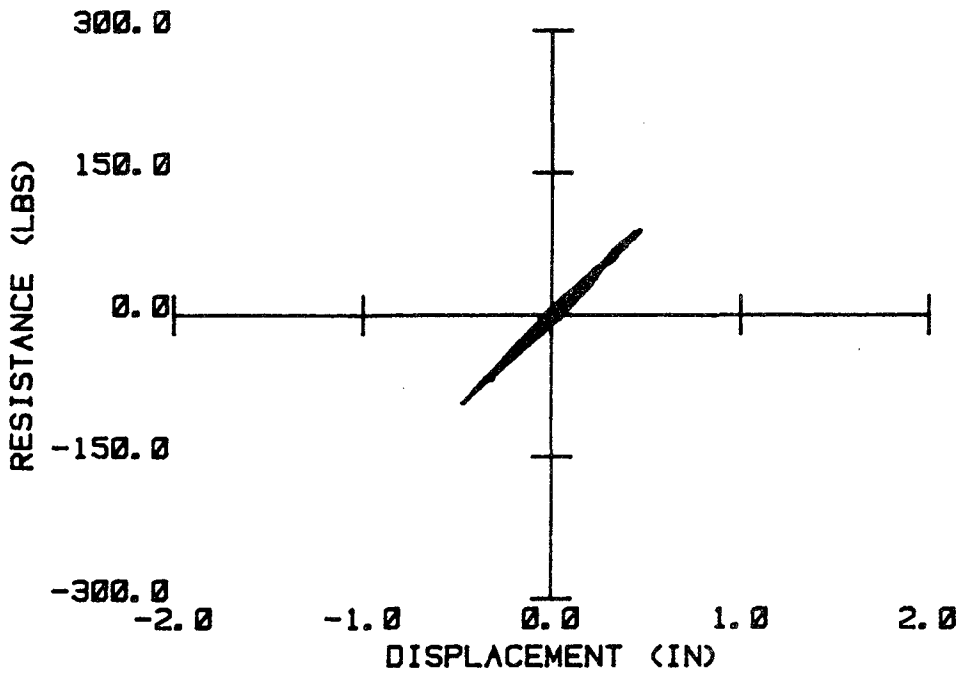

Figure A.11 Dynamic Hysteresis Behavior-Response to a 4.5 hz Pulse, ±0.5g, 2.0 Second Duration, Test No. 5

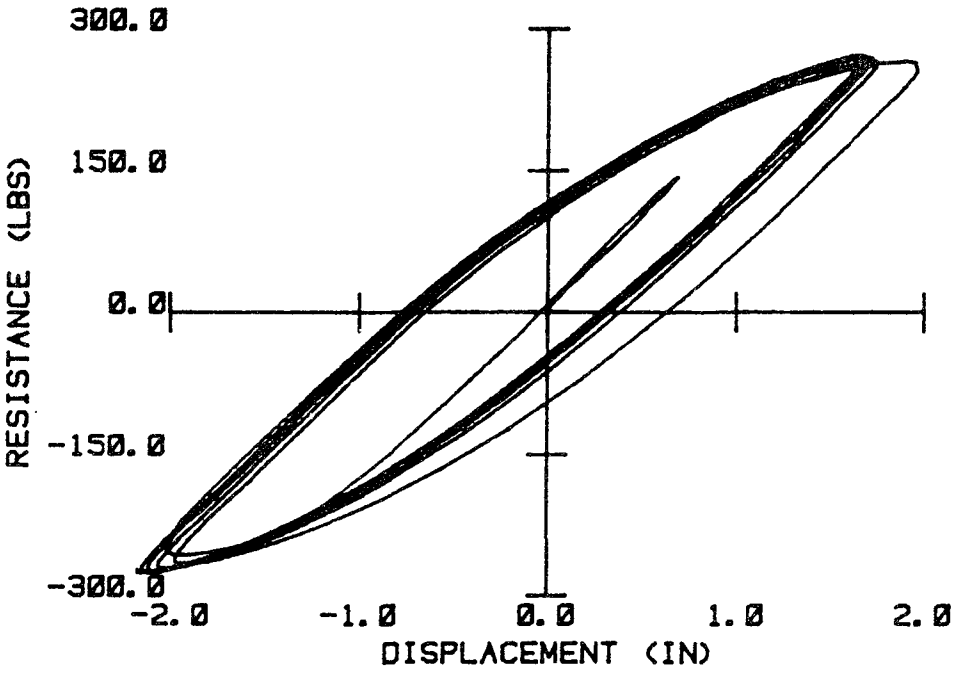

Figure A.12 Dynamic Hysteresis Behavior-Response to a 4.5 hz Pulse, ±0.5g, 2.0 Second Duration, Test No. 6

APPENDIX B

EVALUATION AND SUMMARY OF STRUCTURAL RESPONSE TO EARTHQUAKE GROUND MOTION

B.1 Introduction

The detailed evaluation and summaries of the undamped and damped structural response to seven earthquake acceleration time histories is presented in this appendix. The characteristics of the seven earthquakes are summarized in Table 2.2 of Chapter 2. The response summaries are contained in Tables B.1 through B.28 and in each case are given for zero and five percent damping.

The calculations summarized here were performed as part of the basic numeric studies presented in Chapter 2 of this dissertation where the results from three of these earthquakes, namely El Centro, Pacoima Dam and Melendy Ranch, were employed to demonstrate certain trends. Similarly in Chapter 4, pieces of this data were used to demonstrate trends in application to damage evaluation. It is for these reasons and for purposes of completeness that the results for all seven earthquakes are summarized in the tables that follow.

B.2 Evaluation of Results

It is appropriate to note certain other important trends that can be gleaned from this set of data. For example, in the response to El Centro and Taft, both recognized as being vigorous, sustained excitation, there is a significant difference in the input energy yet in each case the maximum deflections decrease with increasing frequency

and the maximum velocity values are largest in the midrange frequency range.

In the case of an earthquake characterized by a short burst of energy, like Melendy Ranch, in spite of the high peak acceleration the input energies are low as are the other response quantities. It will also be observed that the number of cycles of yielding are low and in some cases zero.

For other types of records, characterized by Pacoima Dam, Halls Valley and the two Coyote Lake Dam records, the later three representing localized earthquake excitation but with segments of excitation that are quite strong, like Pacoima Dam, the responses were significant but highly frequency dependent. In addition, depending on the severity of the short segments of strong excitation, a number of yield excursions were experienced as expected.

One obvious conclusion from the foregoing is that there is no generic earthquake and one cannot generalize the results that encompass all earthquakes.

Table B.1 Undamped Structural Response Summary - El Centro Record

Structural Damping: 0%
Yield Resistance: 100 lb
Record Duration: 20.0 seconds
Maximum Amplitude: 0.348g

Structural Frequency, hz	Maximum Relative Deformation, in, at time, sec	Maximum Relative Velocity, in/sec, at time, sec	Maximum Input Energy, in-lb, at time, sec	Total Input Energy, in-lb	Total Damping Energy, in-lb	Total Hysteretic Energy, in-lb	Total Number of Velocity Sign Changes
0.1	10.6 at 17.20	15.2 at 2.18	116.8 at 2.18	46.2	0.0	0.0	28
0.5	-10.8 at 11.28	41.0 at 11.88	1018.3 at 11.90	523.3	0.0	248.3	25
1.0	4.4 at 12.00	25.8 at 2.18	910.0 at 13.82	815.1	0.0	733.1	39
2.0	- 2.0 at 1.96	16.9 at 2.16	1058.5 at 20.00	1058.5	0.0	1026.5	75
5.0	0.3 at 10.34	- 5.5 at 2.24	241.4 at 19.68	239.3	0.0	236.3	192
10.0	- 0.3 at 14.10	- 2.9 at 2.45	109.3 at 18.73	108.3	0.0	108.0	383
25.0	0.1 at 2.18	1.9 at 2.15	21.5 at 11.82	21.3	0.0	21.3	982

Table B.2 Hysteretic Response Summary - El Centro Record
Based on Undamped Response Summarized in Table B.1

Structural Frequency, hz	Total Hysteretic Energy, in-lb		Number of Counted Yield Excursions		Equivalent Hysteretic Cycles - Computed From Energy in Single Cycles of: Maximum Deformation		Weighted Deformation		Yield Deformation	
	+R	-R	+R	-R	+R	-R	+R	-R	+R	-R
0.1	0.0	0.0	0	0	0.0	0.0	0.0	0.0	0.0	0.0
0.5	138.0	110.4	2	1	1.9	1.6	2.0	1.4	0.3	0.2
1.0	446.0	327.1	5	3	2.4	1.8	4.1	1.9	3.5	2.6
2.0	500.2	526.3	13	9	3.7	3.9	5.5	5.6	15.8	16.6
5.0	125.6	110.7	24	25	5.6	4.9	9.2	9.6	24.8	21.8
10.0	40.5	67.5	26	29	1.5	2.4	2.7	9.8	32.0	53.3
25.0	16.1	5.2	22	19	1.2	0.4	1.5	3.6	79.2	25.8

Table B.3 Damped Structural Response Summary - El Centro Record

Structural Damping: 5%
Yield Resistance: 100 lb

Record Duration: 20.0 seconds
Maximum Amplitude: 0.348g

Structural Frequency, hz	Maximum Relative Deformation, in, at time, sec	Maximum Relative Velocity, in/sec, at time, sec	Maximum Input Energy, in-lb, at time, sec	Total Input Energy, in-lb	Total Damping Energy, in-lb	Total Hysteretic Energy, in-lb	Total Number of Velocity Sign Changes
0.1	9.5 at 17.21	15.0 at 2.18	117.1 at 2.18	58.3	24.9	0.0	26
0.5	7.0 at 6.40	24.6 at 11.88	751.5 at 11.90	532.8	527.7	0.0	27
1.0	- 3.8 at 2.95	24.0 at 2.18	960.3 at 12.26	929.0	554.0	374.5	51
2.0	- 1.8 at 1.94	14.0 at 2.14	935.0 at 20.00	935.0	342.4	582.6	81
5.0	- 0.2 at 2.91	- 5.1 at 2.23	233.6 at 19.69	232.5	107.6	124.7	200
10.0	- 0.2 at 8.57	- 2.7 at 2.21	74.4 at 19.54	74.3	24.3	50.0	369
25.0	0.1 at 2.17	1.1 at 2.13	11.9 at 11.84	11.9	2.4	9.5	741

Table B.4 Hysteretic Response Summary - El Centro Record
Based on Damped Response Summarized in Table B.3

Structural Frequency, hz	Total Hysteretic Energy, in-lb		Number of Counted Yield Excursions		Equivalent Hysteretic Cycles - Computed From Energy in Single Cycles of: Maximum Deformation		Weighted Deformation		Yield Deformation	
	+R	-R	+R	-R	+R	-R	+R	-R	+R	-R
0.1	0.0	0.0	0	0	0.0	0.0	0.0	0.0	0.0	0.0
0.5	0.0	0.0	0	0	0.0	0.0	0.0	0.0	0.0	0.0
1.0	216.0	158.5	3	1	1.7	1.2	2.5	1.2	1.7	1.2
2.0	256.6	326.0	7	6	2.3	2.9	2.8	4.1	8.1	10.3
5.0	66.3	58.4	12	10	4.7	4.1	5.4	4.8	13.1	11.5
10.0	15.6	34.3	6	11	0.8	1.8	1.3	6.9	12.4	27.1
25.0	7.6	1.9	2	6	1.0	0.2	1.0	2.6	37.7	9.2

Table B.5 Undamped Structural Response Summary - Pacoima Dam Record

Structural Damping: 0%
Yield Resistance: 100 lb

Record Duration: 20.0 seconds
Maximum Amplitude: 1.171g

Structural Frequency, hz	Maximum Relative Deformation, in, at time, sec	Maximum Relative Velocity, in/sec, at time, sec	Maximum Input Energy, in-lb, at time, sec	Total Input Energy, in-lb	Total Damping Energy, in-lb	Total Hysteretic Energy, in-lb	Total Number of Velocity Sign Changes
0.1	28.1 at 7.76	- 47.7 at 3.04	1142.3 at 3.04	124.8	0.0	0.0	14
0.5	-15.7 at 3.21	57.3 at 3.54	2359.3 at 3.72	1783.1	0.0	1520.8	28
1.0	-12.4 at 3.16	42.1 at 3.39	2984.1 at 11.52	2903.0	0.0	2841.0	50
2.0	- 6.8 at 3.10	29.0 at 3.38	3354.0 at 9.14	3326.6	0.0	3305.3	92
5.0	3.8 at 3.71	20.9 at 3.38	3160.5 at 18.57	3155.9	0.0	3155.4	165
10.0	3.2 at 6.19	17.6 at 3.38	2213.6 at 20.00	2213.6	0.0	2212.3	314
25.0	2.5 at 6.18	-15.8 at 7.81	1557.6 at 9.96	1557.6	0.0	1557.4	770

Table B.6 Hysteretic Response Summary - Pacoima Dam Record
Based on Undamped Response Summarized in Table B.5

Structural Frequency, hz	Total Hysteretic Energy, in-lb		Number of Counted Yield Excursions		Equivalent Hysteretic Cycles - Computed From Energy in Single Cycles of: Maximum Deformation		Weighted Deformation		Yield Deformation	
	+R	-R	+R	-R	+R	-R	+R	-R	+R	-R
0.1	0.0	0.0	0	0	0.0	0.0	0.0	0.0	0.0	0.0
0.5	882.0	638.8	2	2	1.6	1.2	1.4	1.4	1.7	1.3
1.0	1515.5	1325.5	5	6	1.5	1.3	1.5	1.8	12.0	10.5
2.0	1760.3	1545.0	12	11	2.8	2.5	2.7	4.3	55.6	48.8
5.0	1607.5	1547.9	42	38	4.3	4.1	4.6	8.2	317.3	305.5
10.0	1098.4	1114.0	41	38	3.5	3.5	3.8	7.4	867.2	879.6
25.0	751.6	805.8	36	31	3.0	3.2	3.0	5.3	3708.9	3976.4

Table B.7 Damped Structural Response Summary - Pacoima Dam Record

Structural Damping: 5%
Yield Resistance: 100 lb
Record Duration: 20.0 seconds
Maximum Amplitude: 1.171g

Structural Frequency, hz	Maximum Relative Deformation, in, at time, sec	Maximum Relative Velocity, in/sec, at time, sec	Maximum Input Energy, in-lb, at time, sec	Total Input Energy, in-lb	Total Damping Energy, in-lb	Total Hysteretic Energy, in-lb	Total Number of Velocity Sign Changes
0.1	26.0 at 7.76	-47.4 at 3.04	1154.3 at 3.04	247.3	191.9	0.0	20
0.5	-14.4 at 3.18	55.6 at 3.54	2707.9 at 8.54	2447.4	1383.2	1055.0	30
1.0	-10.1 at 3.12	40.2 at 3.38	3404.2 at 11.52	3378.6	1177.5	2200.0	51
2.0	- 4.5 at 3.06	23.8 at 3.38	3280.3 at 10.72	3276.1	810.2	2465.8	102
5.0	2.1 at 3.74	-15.4 at 7.80	2729.3 at 19.74	2728.8	647.8	2080.7	179
10.0	- 2.3 at 8.43	-13.2 at 7.78	1619.4 at 19.16	1619.4	438.2	1181.2	310
25.0	- 1.4 at 8.42	- 9.2 at 7.77	851.4 at 9.95	851.3	311.3	540.0	487

Table B.8 Hysteretic Response Summary - Pacoima Dam Record
Based on Damped Response Summarized in Table B.7

Structural Frequency, hz	Total Hysteretic Energy, in-lb		Number of Counted Yield Excursions		Equivalent Hysteretic Cycles - Computed From Energy in Single Cycles of: Maximum Deformation		Weighted Deformation		Yield Deformation	
	+R	-R	+R	-R	+R	-R	+R	-R	+R	-R
0.1	0.0	0.0	0	0	0.0	0.0	0.0	0.0	0.0	0.0
0.5	626.1	429.0	1	1	1.5	1.0	1.1	1.2	1.2	0.8
1.0	1165.0	1034.9	3	5	1.5	1.4	1.2	1.8	9.2	8.2
2.0	1312.4	1153.4	10	9	3.4	3.0	3.0	5.5	41.4	36.4
5.0	1049.8	1030.8	26	28	5.3	5.2	6.8	10.2	207.2	203.5
10.0	522.2	659.0	31	33	2.3	2.9	5.8	8.3	412.3	520.3
25.0	227.6	312.3	29	28	1.7	2.3	4.8	7.0	1123.3	1541.3

Table B.9 Undamped Structural Response Summary - Melendy Ranch Record

Structural Damping: 0%
Yield Resistance: 100 lb
Record Duration: 15.0 seconds
Maximum Amplitude: 0.516g

Structural Frequency, hz	Maximum Relative Deformation, in, at time, sec	Maximum Relative Velocity, in/sec, at time, sec	Maximum Input Energy, in-lb, at time, sec	Total Input Energy, in-lb	Total Damping Energy, in-lb	Total Hysteretic Energy, in-lb	Total Number of Velocity Sign Changes
0.1	-3.1 at 1.78	- 5.8 at 1.72	18.4 at 1.72	0.8	0.0	0.0	23
0.5	-2.1 at 3.12	8.0 at 1.64	32.4 at 1.64	18.8	0.0	0.0	22
1.0	1.7 at 14.00	-10.6 at 14.24	56.9 at 14.18	52.9	0.0	0.0	34
2.0	- 0.6 at 14.16	8.0 at 14.28	36.4 at 14.65	34.3	0.0	4.7	66
5.0	0.5 at 1.67	- 7.8 at 1.72	124.4 at 2.58	121.9	0.0	117.9	150
10.0	0.2 at 1.65	- 5.6 at 1.72	99.8 at 7.78	99.7	0.0	98.6	291
25.0	- 0.2 at 1.75	- 3.5 at 1.72	41.9 at 2.60	41.7	0.0	41.7	727

Table B.10 Hysteretic Response Summary - Melendy Ranch Record
Based on Undamped Response Summarized in Table B.9

Structural Frequency, hz	Total Hysteretic Energy, in-lb		Number of Counted Yield Excursions		Equivalent Hysteretic Cycles - Computed From Energy in Single Cycles of: Maximum Deformation		Weighted Deformation		Yield Deformation	
	+R	-R	+R	-R	+R	-R	+R	-R	+R	-R
0.1	0.0	0.0	0	0	0.0	0.0	0.0	0.0	0.0	0.0
0.5	0.0	0.0	0	0	0.0	0.0	0.0	0.0	0.0	0.0
1.0	0.0	0.0	0	0	0.0	0.0	0.0	0.0	0.0	0.0
2.0	1.8	2.9	1	2	1.0	1.6	1.0	2.0	0.1	0.1
5.0	68.9	49.0	7	6	1.8	1.3	2.6	3.1	13.6	9.7
10.0	54.4	44.2	18	19	2.4	2.0	3.3	1.9	43.0	34.9
25.0	21.3	20.4	5	3	1.4	1.4	1.6	1.0	105.2	100.4

Table B.11 Damped Structural Response Summary - Melendy Ranch Record

Structural Damping: 5%
Yield Resistance: 100 lb

Record Duration: 15.0 seconds
Maximum Amplitude: 0.516g

Structural Frequency, hz	Maximum Relative Deformation, in, at time, sec	Maximum Relative Velocity, in/sec, at time, sec	Maximum Input Energy, in-lb, at time, sec	Total Input Energy, in-lb	Total Damping Energy, in-lb	Total Hysteretic Energy, in-lb	Total Number of Velocity Sign Changes
0.1	-2.9 at 1.78	-5.6 at 1.72	18.0 at 1.72	1.7	1.4	0.0	27
0.5	-1.7 at 3.12	7.6 at 1.64	30.8 at 1.64	19.4	19.1	0.0	22
1.0	0.8 at 1.98	7.1 at 1.64	30.6 at 11.72	29.9	29.5	0.0	36
2.0	0.4 at 2.38	-6.6 at 1.72	33.2 at 2.44	32.0	31.9	0.0	74
5.0	0.4 at 1.67	-7.4 at 1.71	146.0 at 15.00	146.0	54.4	91.6	149
10.0	0.2 at 1.65	-4.4 at 1.71	87.8 at 9.62	87.8	22.3	65.5	269
25.0	-0.1 at 1.74	2.3 at 1.77	30.1 at 2.61	30.0	6.1	24.0	210

Table B.12 Hysteretic Response Summary - Melendy Ranch Record
Based on Damped Response Summarized in Table B.11

Structural Frequency, hz	Total Hysteretic Energy, in-lb		Number of Counted Yield Excursions		Equivalent Hysteretic Cycles - Computed From Energy in Single Cycles of: Maximum Deformation		Weighted Deformation		Yield Deformation	
	+R	-R	+R	-R	+R	-R	+R	-R	+R	-R
0.1	0.0	0.0	0	0	0.0	0.0	0.0	0.0	0.0	0.0
0.5	0.0	0.0	0	0	0.0	0.0	0.0	0.0	0.0	0.0
1.0	0.0	0.0	0	0	0.0	0.0	0.0	0.0	0.0	0.0
2.0	0.0	0.0	0	0	0.0	0.0	0.0	0.0	0.0	0.0
5.0	56.0	35.7	4	5	1.8	1.2	2.5	2.2	11.0	7.0
10.0	36.7	28.8	7	4	2.5	2.0	2.8	1.3	29.0	22.8
25.0	13.7	10.2	2	1	2.0	1.5	1.6	1.0	67.6	50.5

Table B.13 Undamped Structural Response Summary - Coyote Lake Dam 285° Record

Structural Damping: 0%
Yield Resistance: 100 lb
Record Duration: 10.24 seconds
Maximum Amplitude: 1.159g

Structural Frequency, hz	Maximum Relative Deformation, in, at time, sec	Maximum Relative Velocity, in/sec, at time, sec	Maximum Input Energy, in-lb, at time, sec	Total Input Energy, in-lb	Total Damping Energy, in-lb	Total Hysteretic Energy, in-lb	Total Number of Velocity Sign Changes
0.1	4.7 at 4.94	-29.5 at 3.62	434.6 at 3.62	2.9	0.0	0.0	28
0.5	-7.7 at 3.76	-42.7 at 3.62	993.9 at 3.62	132.4	0.0	0.0	30
1.0	-8.5 at 3.72	-32.7 at 3.58	1712.7 at 8.32	1584.2	0.0	1542.8	29
2.0	-6.6 at 3.71	-25.5 at 3.58	1914.6 at 8.90	1913.6	0.0	1882.9	39
5.0	4.4 at 4.11	26.3 at 3.78	1667.6 at 10.02	1666.4	0.0	1662.6	91
10.0	6.2 at 4.77	26.2 at 3.78	1262.5 at 5.87	1261.5	0.0	1261.3	172
25.0	5.8 at 4.75	25.0 at 3.78	1026.9 at 5.31	1026.7	0.0	1026.7	410

Table B.14 Hysteretic Response Summary - Coyote Lake Dam 285° Record
Based on Undamped Response Summarized in Table B.13

Structural Frequency, hz	Total Hysteretic Energy, in-lb		Number of Counted Yield Excursions		Equivalent Hysteretic Cycles - Computed From Energy in Single Cycles of: Maximum Deformation		Weighted Deformation		Yield Deformation	
	+R	-R	+R	-R	+R	-R	+R	-R	+R	-R
0.1	0.0	0.0	0	0	0.0	0.0	0.0	0.0	0.0	0.0
0.5	0.0	0.0	0	0	0.0	0.0	0.0	0.0	0.0	0.0
1.0	618.6	924.2	5	5	1.0	1.6	2.2	2.3	4.9	7.3
2.0	702.7	1180.2	7	8	1.2	2.0	1.6	2.8	22.2	37.3
5.0	1001.4	661.1	24	17	2.3	1.5	1.7	2.8	197.7	130.5
10.0	933.1	328.1	19	21	1.5	0.5	1.4	2.5	736.8	259.1
25.0	804.7	222.0	8	10	1.4	0.4	1.2	1.7	3971.0	1095.7

Table B.15 Damped Structural Response Summary - Coyote Lake Dam 285° Record

Structural Damping: 5%
Yield Resistance: 100 lb
Record Duration: 10.24 seconds
Maximum Amplitude: 1.159g

Structural Frequency, hz	Maximum Relative Deformation, in, at time, sec	Maximum Relative Velocity, in/sec, at time, sec	Maximum Input Energy, in-lb, at time, sec	Total Input Energy, in-lb	Total Damping Energy, in-lb	Total Hysteretic Energy, in-lb	Total Number of Velocity Sign Changes
0.1	4.5 at 4.92	-29.5 at 3.62	446.0 at 3.62	28.0	26.0	0.0	30
0.5	-7.3 at 3.74	-40.6 at 3.60	975.1 at 3.62	311.8	290.5	0.0	30
1.0	-7.5 at 3.70	31.3 at 3.90	1973.1 at 8.70	1908.0	749.1	1149.2	31
2.0	-4.8 at 3.68	28.7 at 3.78	2057.7 at 8.88	2048.5	542.5	1498.0	41
5.0	3.2 at 4.77	24.3 at 3.77	1543.5 at 9.49	1543.3	450.2	1093.1	89
10.0	2.7 at 4.75	19.0 at 3.76	883.2 at 5.39	882.6	328.3	554.3	160
25.0	1.0 at 5.12	12.1 at 3.75	473.6 at 5.30	473.4	232.7	240.8	199

Table B.16 Hysteretic Response Summary - Coyote Lake Dam 285° Record
Based on Damped Response Summarized in Table B.15

Structural Frequency, hz	Total Hysteretic Energy, in-lb		Number of Counted Yield Excursions		Equivalent Hysteretic Cycles - Computed From Energy in Single Cycles of: Maximum Deformation		Weighted Deformation		Yield Deformation	
	+R	-R	+R	-R	+R	-R	+R	-R	+R	-R
0.1	0.0	0.0	0	0	0.0	0.0	0.0	0.0	0.0	0.0
0.5	0.0	0.0	0	0	0.0	0.0	0.0	0.0	0.0	0.0
1.0	433.3	715.9	1	3	0.9	1.4	1.1	2.0	3.4	5.6
2.0	653.9	844.1	3	4	1.6	2.0	1.2	2.7	20.6	26.7
5.0	692.5	400.6	14	11	2.2	1.3	1.9	2.9	136.7	79.1
10.0	404.7	149.6	15	16	1.5	0.6	1.6	2.2	319.5	118.1
25.0	170.6	70.2	5	7	1.7	0.7	1.6	1.6	841.9	346.3

Table B.17 Undamped Structural Response Summary - Coyote Lake Dam 195° Record

Structural Damping: 0%
Yield Resistance: 100 lb

Record Duration: 10.24 seconds
Maximum Amplitude: 0.652g

Structural Frequency, hz	Maximum Relative Deformation, in, at time, sec	Maximum Relative Velocity, in/sec, at time, sec	Maximum Input Energy, in-lb, at time, sec	Total Input Energy, in-lb	Total Damping Energy, in-lb	Total Hysteretic Energy, in-lb	Total Number of Velocity Sign Changes
0.1	5.4 at 3.62	21.3 at 3.46	229.1 at 3.46	1.8	0.0	0.0	45
0.5	4.9 at 4.48	-25.3 at 3.82	353.3 at 4.62	88.7	0.0	0.0	36
1.0	-6.5 at 3.96	-33.4 at 3.66	898.6 at 3.82	833.2	0.0	700.8	42
2.0	-5.4 at 4.50	-20.4 at 4.38	1066.3 at 4.62	1016.6	0.0	1012.3	47
5.0	-3.0 at 4.48	-13.5 at 4.39	922.6 at 8.76	919.1	0.0	917.5	100
10.0	-2.0 at 4.45	12.4 at 4.58	651.0 at 6.08	649.7	0.0	649.7	177
25.0	-2.0 at 4.45	10.9 at 4.59	440.2 at 5.06	440.0	0.0	440.0	442

Table B.18 Hysteretic Response Summary - Coyote Lake Dam 195° Record
Based on Undamped Response Summarized in Table B.17

Structural Frequency, hz	Total Hysteretic Energy, in-lb		Number of Counted Yield Excursions		Equivalent Hysteretic Cycles - Computed From Energy in Single Cycles of: Maximum Deformation		Weighted Deformation		Yield Deformation	
	+R	-R	+R	-R	+R	-R	+R	-R	+R	-R
0.1	0.0	0.0	0	0	0.0	0.0	0.0	0.0	0.0	0.0
0.5	0.0	0.0	0	0	0.0	0.0	0.0	0.0	0.0	0.0
1.0	184.7	516.0	4	3	0.5	1.3	2.7	1.1	1.5	4.1
2.0	294.3	718.1	5	4	0.6	1.5	3.8	2.5	9.3	22.7
5.0	366.6	550.9	16	16	1.3	1.9	3.7	3.3	72.4	108.8
10.0	290.8	358.9	25	26	1.4	1.8	2.6	3.4	229.6	283.4
25.0	177.6	262.4	12	9	0.9	1.3	1.4	2.5	876.4	1294.7

Table B.19 Damped Structural Response Summary - Coyote Lake Dam 195° Record

Structural Damping: 5%
Yield Resistance: 100 lb

Record Duration: 10.24 seconds
Maximum Amplitude: 0.652g

Structural Frequency, hz	Maximum Relative Deformation, in, at time, sec	Maximum Relative Velocity, in/sec, at time, sec	Maximum Input Energy, in-lb, at time, sec	Total Input Energy, in-lb	Total Damping Energy, in-lb	Total Hysteretic Energy, in-lb	Total Number of Velocity Sign Changes
0.1	5.4 at 3.60	21.0 at 3.46	227.8 at 3.46	15.0	13.6	0.0	41
0.5	-4.3 at 4.48	-24.9 at 3.82	402.6 at 4.62	170.0	157.8	0.0	36
1.0	-6.1 at 3.94	-32.5 at 3.66	899.4 at 4.42	886.0	357.5	494.2	42
2.0	-3.5 at 4.48	19.2 at 4.58	1082.8 at 9.18	1077.2	296.3	777.3	46
5.0	-2.2 at 4.46	11.6 at 4.56	872.5 at 9.21	871.6	215.7	655.7	99
10.0	-1.2 at 4.44	8.2 at 6.10	535.5 at 6.10	535.2	137.8	397.3	162
25.0	-0.7 at 4.42	4.7 at 4.54	261.3 at 5.07	261.1	85.4	175.7	210

Table B.20 Hysteretic Response Summary - Coyote Lake Dam 195° Record
Based on Damped Response Summarized in Table B.19

Structural Frequency, hz	Total Hysteretic Energy, in-lb		Number of Counted Yield Excursions		Equivalent Hysteretic Cycles - Computed From Energy in Single Cycles of: Maximum Deformation		Weighted Deformation		Yield Deformation	
	+R	-R	+R	-R	+R	-R	+R	-R	+R	-R
0.1	0.0	0.0	0	0	0.0	0.0	0.0	0.0	0.0	0.0
0.5	0.0	0.0	0	0	0.0	0.0	0.0	0.0	0.0	0.0
1.0	68.6	425.6	1	1	0.2	1.2	1.2	1.0	0.5	3.4
2.0	294.8	482.6	3	4	1.0	1.7	3.0	2.3	9.3	15.2
5.0	269.3	386.4	12	12	1.3	1.9	3.0	3.8	53.2	76.3
10.0	174.8	222.6	18	19	1.5	2.0	2.4	4.4	138.0	175.7
25.0	66.9	108.8	8	12	0.9	1.5	1.5	3.3	330.1	537.0

Table B.21 Undamped Structural Response Summary - Halls Valley Record

Structural Damping: 0%
Yield Resistance: 100 lb

Record Duration: 15.0 seconds
Maximum Amplitude: 0.312g

Structural Frequency, hz	Maximum Relative Deformation, in, at time, sec	Maximum Relative Velocity, in/sec, at time, sec	Maximum Input Energy, in-lb, at time, sec	Total Input Energy, in-lb	Total Damping Energy, in-lb	Total Hysteretic Energy, in-lb	Total Number of Velocity Sign Changes
0.1	-3.7 at 10.34	15.6 at 10.54	122.6 at 10.54	1.6	0.0	0.0	40
0.5	4.6 at 10.78	24.4 at 10.54	313.1 at 10.54	83.3	0.0	0.0	39
1.0	-3.8 at 11.06	21.4 at 11.30	643.4 at 12.74	550.3	0.0	503.0	37
2.0	-2.6 at 12.10	-15.6 at 10.68	697.9 at 14.94	697.8	0.0	666.0	59
5.0	0.4 at 10.42	4.3 at 2.72	139.3 at 12.01	135.0	0.0	134.2	148
10.0	0.2 at 10.43	2.2 at 1.85	24.0 at 11.18	23.0	0.0	22.7	293
25.0	-0.1 at 10.71	-0.7 at 10.67	4.5 at 10.71	4.3	0.0	4.3	703

Table B.22 Hysteretic Response Summary - Halls Valley Record
Based on Undamped Response Summarized in Table B.21

Structural Frequency, hz	Total Hysteretic Energy, in-lb		Number of Counted Yield Excursions		Equivalent Hysteretic Cycles - Computed From Energy in Single Cycles of: Maximum Deformation		Weighted Deformation		Yield Deformation	
	+R	-R	+R	-R	+R	-R	+R	-R	+R	-R
0.1	0.0	0.0	0	0	0.0	0.0	0.0	0.0	0.0	0.0
0.5	0.0	0.0	0	0	0.0	0.0	0.0	0.0	0.0	0.0
1.0	279.6	223.4	7	6	2.2	1.7	5.6	4.2	2.2	1.8
2.0	257.5	408.5	15	14	1.3	2.1	8.6	3.5	8.1	12.9
5.0	60.3	73.9	13	15	2.0	2.5	4.7	2.7	11.9	14.6
10.0	15.0	7.7	8	5	1.2	0.6	1.7	1.4	11.8	6.1
25.0	0.01	4.3	1	1	0.0	1.0	1.0	1.0	0.0	21.3

Table B.23 Damped Structural Response Summary - Halls Valley Record

Structural Damping: 5%
Yield Resistance: 100 lb
Record Duration: 15.0 seconds
Maximum Amplitude: 0.312g

Structural Frequency, hz	Maximum Relative Deformation, in, at time, sec	Maximum Relative Velocity, in/sec, at time, sec	Maximum Input Energy, in-lb, at time, sec	Total Input Energy, in-lb	Total Damping Energy, in-lb	Total Hysteretic Energy, in-lb	Total Number of Velocity Sign Changes
0.1	-3.6 at 10.34	15.8 at 10.54	129.5 at 10.54	7.8	6.6	0.0	40
0.5	3.9 at 10.75	22.2 at 10.54	289.2 at 10.54	101.1	83.5	0.0	41
1.0	3.2 at 10.62	-21.1 at 10.82	849.4 at 12.74	778.6	544.5	228.1	37
2.0	1.8 at 10.56	-14.8 at 10.68	662.6 at 15.00	662.6	284.4	369.8	61
5.0	-0.4 at 11.98	3.9 at 1.76	111.9 at 11.98	108.9	51.7	57.2	154
10.0	0.1 at 2.83	2.0 at 1.84	17.2 at 10.71	16.7	5.2	11.4	249
25.0	-0.1 at 10.70	-0.5 at 10.66	3.1 at 10.70	2.9	0.3	2.6	243

Table B.24 Hysteretic Response Summary - Halls Valley Record
Based on Damped Response Summarized in Table B.23

Structural Frequency, hz	Total Hysteretic Energy, in-lb		Number of Counted Yield Excursions		Equivalent Hysteretic Cycles - Computed From Energy in Single Cycles of: Maximum Deformation		Weighted Deformation		Yield Deformation	
	+R	-R	+R	-R	+R	-R	+R	-R	+R	-R
0.1	0.0	0.0	0	0	0.0	0.0	0.0	0.0	0.0	0.0
0.5	0.0	0.0	0	0	0.0	0.0	0.0	0.0	0.0	0.0
1.0	105.6	122.5	3	1	1.6	1.8	2.4	1.3	0.8	1.0
2.0	182.9	186.9	4	5	1.5	1.5	2.0	2.0	5.8	5.9
5.0	15.2	42.1	6	5	0.6	1.6	3.5	1.4	3.0	8.3
10.0	6.5	4.9	3	2	1.0	0.8	1.3	1.2	5.1	3.9
25.0	0.03	2.6	1	1	0.0	1.0	1.1	1.0	0.2	12.9

Table B.25 Undamped Structural Response Summary - Taft Record

Structural Damping: 0%
Yield Resistance: 100 lb
Record Duration: 20.0 seconds
Maximum Amplitude: 0.179g

Structural Frequency, hz	Maximum Relative Deformation, in, at time, sec	Maximum Relative Velocity, in/sec, at time, sec	Maximum Input Energy, in-lb, at time, sec	Total Input Energy, in-lb	Total Damping Energy, in-lb	Total Hysteretic Energy, in-lb	Total Number of Velocity Sign Changes
0.1	9.9 at 20.00	- 7.9 at 3.56	31.0 at 3.56	19.8	0.0	0.0	31
0.5	4.8 at 6.58	17.5 at 7.82	165.9 at 7.80	31.0	0.0	0.0	29
1.0	3.0 at 15.98	-17.5 at 16.24	257.1 at 16.24	209.7	0.0	117.8	48
2.0	- 1.2 at 17.62	- 9.3 at 10.04	225.7 at 19.20	217.4	0.0	191.7	88
5.0	0.3 at 9.12	4.3 at 9.06	127.6 at 19.91	126.4	0.0	122.6	197
10.0	0.1 at 17.35	1.7 at 17.32	5.3 at 17.35	4.8	0.0	4.0	398
25.0	0.0 at 3.71	0.1 at 8.62	0.1 at 3.71	0.0	0.0	0.0	946

Table B.26 Hysteretic Response Summary - Taft Record
Based on Undamped Response Summarized in Table B.25

Structural Frequency, hz	Total Hysteretic Energy, in-lb		Number of Counted Yield Excursions		Equivalent Hysteretic Cycles - Computed From Energy in Single Cycles of: Maximum Deformation		Weighted Deformation		Yield Deformation	
	+R	-R	+R	-R	+R	-R	+R	-R	+R	-R
0.1	0.0	0.0	0	0	0.0	0.0	0.0	0.0	0.0	0.0
0.5	0.0	0.0	0	0	0.0	0.0	0.0	0.0	0.0	0.0
1.0	75.2	42.6	2	2	1.6	0.9	2.7	3.0	0.6	0.3
2.0	71.4	120.3	10	9	1.2	2.1	13.2	8.4	2.3	3.8
5.0	68.4	54.1	23	22	2.8	2.2	13.8	12.7	13.5	10.7
10.0	2.6	1.5	10	5	2.3	1.3	7.6	4.5	2.0	1.2
25.0	0.0	0.0	0	0	0.0	0.0	0.0	0.0	0.0	0.0

Table B.27 Damped Structural Response Summary - Taft Record

Structural Damping: 5%
Yield Resistance: 100 lb

Record Duration: 20.0 seconds
Maximum Amplitude: 0.179g

Structural Frequency, hz	Maximum Relative Deformation, in, at time, sec	Maximum Relative Velocity, in/sec, at time, sec	Maximum Input Energy, in-lb, at time, sec	Total Input Energy, in-lb	Total Damping Energy, in-lb	Total Hysteretic Energy, in-lb	Total Number of Velocity Sign Changes
0.1	7.7 at 20.00	- 7.8 at 3.56	31.5 at 3.56	21.0	9.3	0.0	29
0.5	3.3 at 6.56	13.3 at 7.80	155.6 at 7.80	112.1	108.3	0.0	34
1.0	1.6 at 3.92	11.4 at 5.54	189.5 at 16.24	170.9	168.6	0.0	50
2.0	-0.9 at 6.74	- 8.6 at 6.64	253.8 at 19.20	250.1	224.6	24.1	88
5.0	0.2 at 9.11	3.7 at 9.05	104.1 at 19.40	103.6	75.8	27.6	201
10.0	-0.1 at 6.54	0.8 at 8.61	5.4 at 17.35	5.4	5.4	0.0	346
25.0	0.0 at 3.71	- 0.1 at 4.62	0.1 at 3.71	0.1	0.1	0.0	408

Table B.28 Hysteretic Response Summary - Taft Record
Based on Damped Response Summarized in Table B.27

Structural Frequency, hz	Total Hysteretic Energy, in-lb		Number of Counted Yield Excursions		Equivalent Hysteretic Cycles - Computed From Energy in Single Cycles of: Maximum Deformation		Weighted Deformation		Yield Deformation	
	+R	-R	+R	-R	+R	-R	+R	-R	+R	-R
0.1	0.0	0.0	0	0	0.0	0.0	0.0	0.0	0.0	0.0
0.5	0.0	0.0	0	0	0.0	0.0	0.0	0.0	0.0	0.0
1.0	0.0	0.0	0	0	0.0	0.0	0.0	0.0	0.0	0.0
2.0	0.0	24.1	0	1	0.0	1.0	0.0	1.1	0.0	0.8
5.0	17.1	10.5	9	4	1.7	1.0	4.6	3.8	3.4	2.1
10.0	0.0	0.0	0	0	0.0	0.0	0.0	0.0	0.0	0.0
25.0	0.0	0.0	0	0	0.0	0.0	0.0	0.0	0.0	0.0

APPENDIX C

STRUCTURAL RESPONSE TO FILTERED GROUND MOTION

C.1 Introduction

The frequency content of the ground motion is an important factor to the overall structural response. In order to explore further the effect of frequency content on structural response, a selected set of five records were filtered using the Fast Fourier Transform (FFT) to remove portions of the frequency content and the structural response to these adjusted records was calculated. By varying the width of the filter, the effects of changes in the frequency content was identified for the records and structures involved.

Four structural frequencies, 0.1, 1.0, 5.0, and 10.0 hz, were selected to span the frequency range of interest. Damping values of zero and five percent were used with an elastoplastic yield resistance of 100 lb.

Although studies were made on five different earthquake records, results are presented only for Melendy Ranch and Coyote Lake Dam 285°. These two records were selected because of their differences in frequency content within themselves and as compared to each other. The duration used in these calculations was selected to be compatible with the interval required by the FFT calculation technique while allowing the character of the ground motion to develop. It was desired to isolate smaller portions of the record to observe the effects of localized frequency content changes on the response accordingly, two sets of durations, 5.12 and 10.24 seconds, were used for these calculations, except for Melendy Ranch where only a 5.12 second

duration was found to cover the strong excitation. These durations were found to be sufficient to demonstrate the effects of frequency content changes on the response.

The selected record interval was decomposed into its frequency components through the use of the FFT technique. The frequencies that were outside the window were removed and set to zero while those inside the frequency window were left unchanged. The frequency window used was a Rectangular Window Function. As discussed in Chapter 2, abrupt ends of a window can cause errors in the FFT computations. To reduce any errors, the Rectangular Window was smoothed using the Fourier Transform of the Hanning Window Function that has frequency domain values of 0.25, 0.5, 0.25, for the preceding, present, and following frequency values (20). The Fourier Transform of the Hanning Window Function, when multiplied by the Rectangular Window, smoothed the edges, and rounded the corners to reduce the errors as shown in Fig. C.1.

The resulting frequency composition was inverted to obtain a new acceleration time history containing only those frequencies that were inside the window. The structural response to this altered record segment was computed and the results compared to similar results for other widths of frequency windows, as well as to the original unfiltered records.

C.2 Results

Some initial studies were made using a bandpass filter with a variable lower and upper frequency limit, the results indicated that removal of the lower frequencies greatly affected the level of

structural response. Various lower frequency limits were used and consistently showed that these lower frequencies were important in developing structural response. More so than observed in the simple pulse studies of Chapter 2.

Based on these results, the lower frequency limit was shifted to zero creating a consistent low pass filter in every case in order to determine the effects of the higher frequency components. Typical results are contained in Table C.1a-h for Melendy Ranch and one of the Coyote Lake Dam records. In these tables, the response to the original, unfiltered record is denoted as "Full," response to the other filtered records is indicated with the corresponding frequency composition.

The position of the upper frequency required to induce comparable levels of response to that of the unfiltered record was a function of the particular record and of the structural frequency involved. The results generally show that the frequencies above twice the natural frequency do not contribute in any significant way to the response. In general, the 0.1 hz structure required a 10 hz wide bandpass filter. The 1.0 hz structure required about 5-7 hz upper frequency bound to develop response while the 5 and 10 hz structures required an upper limit of about 10 hz.

While the upper limits required for comparable response were fairly sensitive, the bulk of the response was achieved generally within the frequencies at twice the structural frequency and below, with the exception of the 0.1 hz structure that was sensitive to frequencies above this limit. Although the damping clearly changes the

structural response it did not affect the frequency window widths required.

In conclusion, these calculations indicate that the frequency content of the record is of prime importance in the overall structural response. Lower frequency components affect the response and are especially important if their amplitude is large; high frequency components that are much higher in frequency than the structure do not induce large levels of response. The large response contributions are obtained from a region generally from 10 hz and below. It should be recognized that this window is a function of the structural frequency and the strength and composition of the ground motion.

On the whole, the results of these results using the FFT were confirmatory in nature. However, the FFT procedure was not particularly helpful in contributing to an understanding of parameters that contribute to response.

Table C.1a Structural Response to Filtered Ground Motion Records

Ground Motion Record: Melendy Ranch
Duration: 5.12 seconds

Structural Frequency: 0.1hz
Damping: 0%

Filter Bandwidth, hz	Maximum Relative Displacement, in, at time, sec	Maximum Relative Velocity, in/sec, at time, sec	Maximum Input Energy, in-lb, at time, sec	Total Hysteretic Energy, in-lb +R	Total Hysteretic Energy, in-lb -R	Number of Velocity Sign Changes	Equivalent Hysteretic Cycles
Full	3.1 at 1.78	5.8 at 1.72	18.4 at 1.72	0	0	21	0
0.0- 0.98	2.6 at 1.74	2.7 at 1.14	4.2 at 1.18	0	0	1	0
0.0- 1.95	2.5 at 1.71	2.9 at 1.35	4.8 at 1.37	0	0	6	0
0.0- 5.08	3.3 at 1.81	5.1 at 1.88	14.9 at 1.88	0	0	11	0
0.0- 7.62	3.2 at 1.79	5.3 at 1.54	15.7 at 1.73	0	0	13	0
0.0-10.16	3.1 at 1.78	5.8 at 1.72	18.3 at 1.72	0	0	17	0
0.0-12.50	3.1 at 1.78	6.1 at 1.73	20.1 at 1.73	0	0	21	0
0.0-15.04	3.1 at 1.78	6.1 at 1.73	20.4 at 1.73	0	0	21	0
0.0-20.12	3.1 at 1.78	6.2 at 1.73	21.1 at 1.73	0	0	21	0
0.0-25.00	3.1 at 1.78	6.2 at 1.73	21.1 at 1.73	0	0	21	0

Table C.1b Structural Response to Filtered Ground Motion Records

Ground Motion Record: Melendy Ranch
Duration: 5.12 seconds

Structural Frequency: 1.0 hz
Damping: 0 %

Filter Bandwidth, hz	Maximum Relative Displacement, in, at time, sec	Maximum Relative Velocity, in/sec, at time, sec	Maximum Input Energy, in-lb, at time, sec	Total Hysteretic Energy, in-lb +R	Total Hysteretic Energy, in-lb -R	Number of Velocity Sign Changes	Equivalent Hysteretic Cycles
Full	1.0 at 4.00	7.2 at 1.64	26.4 at 1.64	0	0	14	0
0.0- 0.98	0.2 at 2.50	1.2 at 2.20	1.2 at 2.50	0	0	8	0
0.0- 1.95	1.0 at 4.48	6.3 at 4.24	20.1 at 4.26	0	0	11	0
0.0- 5.08	1.0 at 3.99	7.0 at 1.88	30.8 at 1.88	0	0	16	0
0.0- 7.62	1.0 at 3.99	7.1 at 1.64	25.8 at 1.64	0	0	16	0
0.0-10.16	1.0 at 3.99	7.3 at 1.64	27.2 at 1.64	0	0	16	0
0.0-12.50	1.0 at 3.99	7.0 at 1.64	25.3 at 1.64	0	0	14	0
0.0-15.04	1.0 at 3.99	7.1 at 1.64	25.9 at 1.64	0	0	14	0
0.0-20.12	1.0 at 3.99	7.2 at 1.64	26.5 at 1.64	0	0	14	0
0.0-25.00	1.0 at 3.99	7.2 at 1.64	26.5 at 1.64	0	0	14	0

Table C.1c Structural Response to Filtered Ground Motion Records

Ground Motion Record: Melendy Ranch
Duration: 5.12 seconds

Structural Frequency: 5.0 hz
Damping: 0%

Filter Bandwidth, hz	Maximum Relative Displacement, in, at time, sec	Maximum Relative Velocity, in/sec, at time, sec	Maximum Input Energy, in-lb, at time, sec	Total Hysteretic Energy, in-lb +R	Total Hysteretic Energy, in-lb -R	Number of Velocity Sign Changes	Equivalent Hysteretic Cycles
Full	0.5 at 1.67	7.8 at 1.72	124.4 at 2.58	68.9	49.0	52	3.1
0.0- 0.98	0.0 at 1.62	0.0 at 2.06	0.0 at 1.62	0	0	50	0
0.0- 1.95	0.0 at 1.70	0.2 at 1.95	0.2 at 1.70	0	0	51	0
0.0- 5.08	0.4 at 1.91	5.9 at 1.82	141.0 at 3.56	76.3	59.6	49	4.2
0.0- 7.62	0.6 at 2.35	7.1 at 1.71	127.2 at 4.30	79.5	42.6	50	2.6
0.0-10.16	0.5 at 1.67	7.8 at 1.71	127.7 at 2.58	72.0	50.1	50	3.3
0.0-12.50	0.5 at 1.67	8.0 at 1.72	124.6 at 2.58	68.2	50.0	52	3.1
0.0-15.04	0.5 at 1.67	8.0 at 1.72	124.4 at 2.58	67.9	49.9	52	3.2
0.0-20.12	0.5 at 1.67	7.9 at 1.72	123.9 at 2.58	67.4	49.8	52	3.1
0.0-25.00	0.5 at 1.67	7.9 at 1.72	123.9 at 2.58	67.5	49.7	52	3.1

Table C.1d Structural Response to Filtered Ground Motion Records

Ground Motion Record: Melendy Ranch
Duration: 5.12 seconds

Structural Frequency: 10 hz
Damping: 0%

Filter Bandwidth, hz	Maximum Relative Displacement, in, at time, sec	Maximum Relative Velocity, in/sec, at time, sec	Maximum Input Energy, in-lb, at time, sec	Total Hysteretic Energy, in-lb +R	Total Hysteretic Energy, in-lb -R	Number of Velocity Sign Changes	Equivalent Hysteretic Cycles
Full	0.2 at 1.66	5.6 at 1.72	98.9 at 5.12	54.0	43.7	95	4.3
0.0- 0.98	0.0 at 1.71	0.0 at 2.04	0.0 at 1.71	0	0	101	0
0.0- 1.95	0.0 at 1.66	0.1 at 1.88	0.0 at 1.66	0	0	101	0
0.0- 5.08	0.0 at 1.84	0.9 at 1.88	2.0 at 1.84	0.7	0	88	1.0
0.0- 7.62	0.2 at 1.65	4.7 at 1.71	76.3 at 2.29	41.2	33.9	92	4.6
0.0-10.16	0.2 at 1.66	5.7 at 1.71	96.6 at 5.12	50.6	44.7	92	5.1
0.0-12.50	0.2 at 1.66	5.9 at 1.72	100.7 at 5.12	51.6	47.7	94	4.6
0.0-15.04	0.2 at 1.66	5.7 at 1.72	98.4 at 5.12	53.1	44.0	94	4.4
0.0-20.12	0.2 at 1.66	5.6 at 1.72	98.3 at 5.12	53.6	43.4	94	4.3
0.0-25.00	0.2 at 1.66	5.6 at 1.72	98.4 at 5.12	53.6	43.4	94	4.3

Table C.1e Structural Response to Filtered Ground Motion Records

Ground Motion Record: Coyote Lake Dam, 285° Structural Frequency: 0.1 hz
Duration: 10.24 seconds Damping: 0%

Filter Bandwidth, hz	Maximum Relative Displacement, in, at time, sec	Maximum Relative Velocity, in/sec, at time, sec	Maximum Input Energy, in-lb, at time, sec	Total Hysteretic Energy, in-lb +R	Total Hysteretic Energy, in-lb -R	Number of Velocity Sign Changes	Equivalent Hysteretic Cycles
Full	4.7 at 4.94	-29.5 at 3.62	434.6 at 3.62	0	0	28	0
0.0- 0.98	4.2 at 4.74	8.4 at 2.90	35.2 at 2.90	0	0	9	0
0.0- 1.95	4.6 at 4.97	-25.4 at 3.98	323.4 at 3.98	0	0	16	0
0.0- 5.08	4.7 at 4.93	-30.6 at 3.61	470.0 at 3.61	0	0	25	0
0.0- 7.62	4.7 at 4.94	-29.8 at 3.62	443.4 at 3.62	0	0	25	0
0.0-10.16	4.7 at 4.94	-29.4 at 3.63	434.1 at 3.63	0	0	26	0
0.0-12.50	4.7 at 4.94	-29.4 at 3.62	432.5 at 3.62	0	0	28	0
0.0-15.04	4.7 at 4.94	-29.5 at 3.62	434.4 at 3.62	0	0	28	0
0.0-20.12	4.7 at 4.94	-29.5 at 3.62	436.6 at 3.62	0	0	28	0
0.0-25.00	4.7 at 4.94	-29.5 at 3.62	436.0 at 3.62	0	0	28	0

Table C.1f Structural Response to Filtered Ground Motion Records

Ground Motion Record: Coyote Lake Dam, 285° Structural Frequency: 1.0 hz
Duration: 10.24 seconds Damping: 0%

Filter Bandwidth, hz	Maximum Relative Displacement, in, at time, sec	Maximum Relative Velocity, in/sec, at time, sec	Maximum Input Energy, in-lb, at time, sec	Total Hysteretic Energy, in-lb +R	Total Hysteretic Energy, in-lb -R	Number of Velocity Sign Changes	Equivalent Hysteretic Cycles
Full	-8.5 at 3.72	-32.7 at 3.58	1712.7 at 8.32	618.6	924.2	29	2.6
0.0- 0.98	2.9 at 3.32	15.7 at 6.28	235.9 at 6.54	49.4	59.9	20	3.0
0.0- 1.95	-8.2 at 3.74	-38.7 at 3.92	1683.5 at 8.70	709.9	819.6	25	2.7
0.0- 5.08	-8.4 at 3.72	-34.3 at 3.58	1710.0 at 8.33	626.9	912.7	30	2.6
0.0- 7.62	-8.5 at 3.72	-33.0 at 4.37	1717.0 at 8.34	624.4	921.7	30	2.6
0.0-10.16	-8.5 at 3.72	-32.8 at 3.57	1717.8 at 8.33	625.4	921.8	29	2.6
0.0-12.50	-8.5 at 3.72	-32.8 at 3.58	1718.0 at 8.33	624.3	923.0	31	2.6
0.0-15.04	-8.5 at 3.72	-32.8 at 3.58	1718.0 at 8.33	624.0	923.3	33	2.6
0.0-20.12	-8.5 at 3.72	-32.8 at 3.58	1718.0 at 8.33	624.1	923.2	31	2.6
0.0-25.00	-8.5 at 3.72	-32.8 at 3.58	1718.0 at 8.33	624.1	923.2	31	2.6

Table C.1g Structural Response to Filtered Ground Motion Records

Ground Motion Record: Coyote Lake Dam, 285° Structural Frequency: 5 hz
Duration: 10.24 seconds Damping: 0%

Filter Bandwidth, hz	Maximum Relative Displacement, in, at time, sec	Maximum Relative Velocity, in/sec, at time, sec	Maximum Input Energy, in-lb, at time, sec	Total Hysteretic Energy, in-lb +R	Total Hysteretic Energy, in-lb -R	Number of Velocity Sign Changes	Equivalent Hysteretic Cycles
Full	4.4 at 4.11	26.3 at 3.78	1667.6 at 10.02	1001.4	661.1	91	3.8
0.0- 0.98	0.0 at 3.26	0.2 at 3.54	0.5 at 3.26	0	0	64	0
0.0- 1.96	4.3 at 4.10	22.6 at 3.92	1063.4 at 4.60	2657.4	401.0	89	2.5
0.0- 5.08	4.1 at 4.10	25.2 at 3.81	1595.5 at 9.89	936.6	653.8	86	4.0
0.0- 7.62	4.4 at 4.11	26.4 at 3.78	1660.2 at 10.01	992.8	662.4	88	3.9
0.0-10.16	4.4 at 4.11	26.2 at 3.78	1667.8 at 10.01	1000.5	662.3	91	3.9
0.0-12.50	4.4 at 4.11	26.1 at 3.78	1671.0 at 10.01	1001.0	665.0	91	3.9
0.0-15.04	4.4 at 4.11	26.2 at 3.78	1671.8 at 10.01	1001.2	665.6	91	3.9
0.0-20.12	4.4 at 4.11	26.4 at 3.78	1673.9 at 10.01	1003.6	665.2	91	3.9
0.0-25.00	4.4 at 4.11	26.4 at 3.78	1674.1 at 10.01	1003.6	665.4	91	3.9

Table C.1h Structural Response to Filtered Ground Motion Records

Ground Motion Record: Coyote Lake Dam, 285° Structural Frequency: 10 hz
Duration: 10.24 seconds Damping: 0%

Filter Bandwidth, hz	Maximum Relative Displacement, in, at time, sec	Maximum Relative Velocity, in/sec, at time, sec	Maximum Input Energy, in-lb, at time, sec	Total Hysteretic Energy, in-lb +R	Total Hysteretic Energy, in-lb -R	Number of Velocity Sign Changes	Equivalent Hysteretic Cycles
Full	6.2 at 4.77	26.2 at 3.78	1262.5 at 5.87	933.1	328.1	172	2.0
0.0- 0.98	0.0 at 3.25	0.0 at 3.48	0.1 at 3.25	0	0	167	0
0.0- 1.95	3.3 at 4.08	19.4 at 3.92	831.3 at 4.55	506.4	323.7	180	2.5
0.0- 5.08	5.3 at 4.10	24.5 at 3.81	1114.6 at 5.20	812.4	301.0	135	2.1
0.0- 7.62	6.3 at 4.77	26.4 at 3.78	1198.8 at 5.40	907.2	290.3	147	1.9
0.0-10.16	6.1 at 4.77	25.9 at 3.78	1245.1 at 10.08	918.4	325.5	170	2.0
0.0-12.50	6.1 at 4.77	25.8 at 3.78	1254.2 at 5.87	924.2	328.7	170	2.0
0.0-15.04	6.2 at 4.77	26.0 at 3.78	1258.2 at 5.87	926.8	330.2	172	2.0
0.0-20.12	6.2 at 4.77	26.1 at 3.78	1256.1 at 5.87	928.5	326.3	172	2.0
0.0-25.00	6.2 at 4.77	26.1 at 3.78	1254.3 at 5.87	927.2	325.9	174	2.0

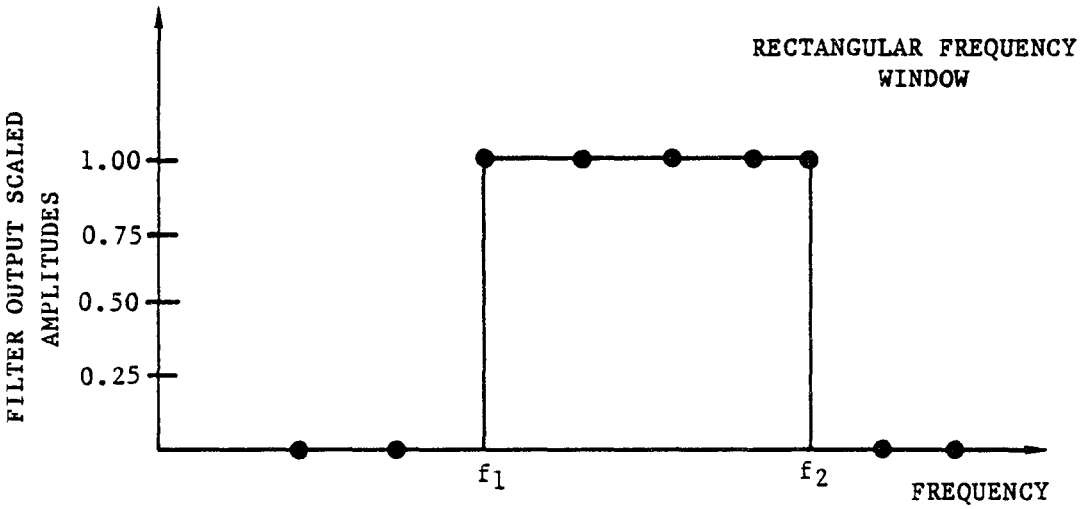

RECTANGULAR FREQUENCY WINDOW
AMPLITUDES

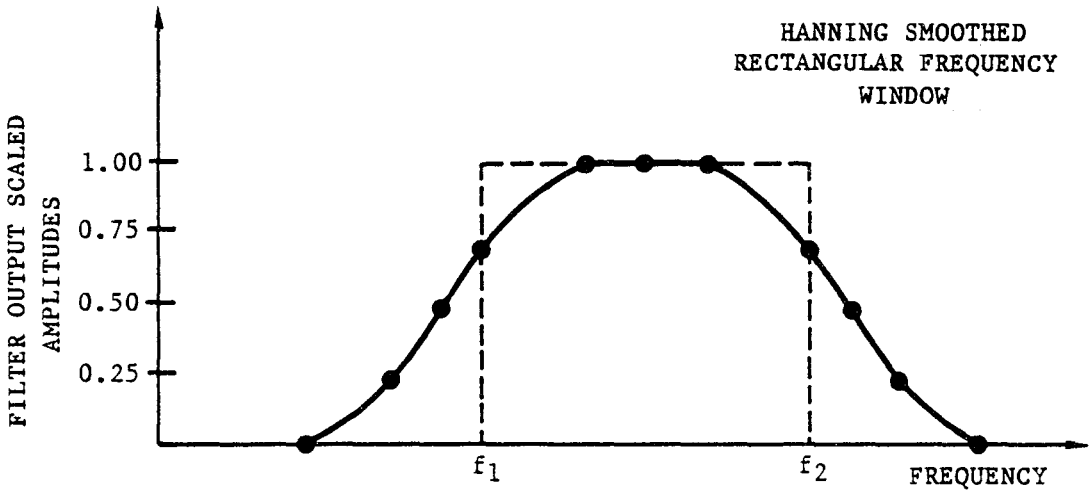

HANNING FREQUENCY WINDOW
AMPLITUDES

HANNING WINDOW COEFFICIENTS:

$$f_1 = (0.25\ f_{i-1}) + (0.50\ f_i) + (0.25\ f_{i+1})$$

Figure C.1 Rectangular Frequency Window as Smoothed by Hanning Window Function

APPENDIX D

DEVELOPMENT OF STRAIN-DISPLACEMENT AND STRAIN-DUCTILITY RELATIONSHIPS

D.1 Introduction

The accumulation of damage through cyclic response of steel members has been described by Morrow (44) and others in terms of strains. For most engineering purposes, localized strains as employed in fatigue studies for example are not a convenient parameter to use in building design. Rather, displacements or ductilities are a preferred measure of the response to loading. The development in Section D.2 provided the basis for the interpretation of experimental data in Chapter 4. The development of Section D.3 of this appendix was to demonstrate the conceptual relationship between strains as used in the fatigue hypothesis and displacements as used in a similar hypothesis in building design.

D.2 Development of Strain-Displacement Relations

In studying the interrelationship between strain and displacement, it is convenient to derive the equations to relate a particular end displacement to the strain in the member using plastic hinge theory. The most basic member for demonstration purposes is the cantilever beam which also is a widely used test member in the laboratory. The relationship are valid for other end conditions as well.

A cantilever with a single end load, P, is shown in Fig. D.1. When the load P is increased sufficiently, the section reaches yielding at the extreme fibers of the beam. If the load is increased until the

section is fully yielded, a plastic hinge forms. Because the moment diagram is linear, the moment at the position of yielding of extreme fibers can be readily found as

$$M_y = P(L - a), \tag{D.1}$$

where L is the span length and a is the length of the plastic hinge. Similarly, the moment at the support can be found as

$$M_Y = PL. \tag{D.2}$$

The moment required to fully yield a cross section is related through the moment to cause yielding of the extreme fibers of the beam through the shape factor, f, or

$$M_Y = fM_y , \tag{D.3}$$

where the symbol Y denotes a fully yielded cross section and y denotes yielding of the extreme fibers of the beam.

Through use of Eqs. (D.1), (D.2) and (D.3), we can obtain an expression for P, where P is the same load in all cases, as

$$P = \frac{fM_y}{L} = \frac{M_Y}{L} , \tag{D.4}$$

but $M_Y = fM_y$

$$\frac{M_Y}{L-a} = \frac{fM_y}{L} ,$$

which leads to the expression

$$L = f(L - a),$$

and finally

$$a = \frac{(f-1)L}{f} \quad . \tag{D.5}$$

This relationship provides the length of the plastic hinge in terms of the shape factor for the section. For most I sections, the value of the shape factor is approximately 1.10 to 1.15; for rectangular sections, it has a value of 1.5.

For analysis purposes, the hinge can be considered to be concentrated approximately at a/2 from the fixed end. The total deflection of the beam can be considered to be comprised of an elastic portion corresponding to full yield, plus a plastic deflection caused by rotation of the plastic hinge as described by Popov and Bertero (57). This concept is shown in Fig. D.1 as well. The total deflection, Δ_T, is composed of the plastic deflection, Δ_P, plus the full yield deflection, Δ_Y, or

$$\Delta_T = \Delta_Y + \Delta_P \quad . \tag{D.6}$$

For the cantilever, the deflection for any load P is

$$\Delta = \frac{PL^3}{3EI} \quad . \tag{D.7}$$

This equation can be related to the moment by

$$M = PL = \frac{\sigma I}{c} \quad , \tag{D.8}$$

where σ is the maximum bending stress, I is the moment of inertia and c is one-half of the height of the cross section.

At first yielding of the cross section at the extreme fibers, the moment is

$$M_y = P_y L = \frac{\sigma_y I}{c} \quad . \tag{D.9}$$

At full yielding of the cross section, the moment is

$$M_Y = fM_Y = P_Y L = \frac{f\sigma_y I}{c} \quad . \tag{D.10}$$

This value of moment can be substituted into Eq. (D.7) to obtain the deflection corresponding to a fully yielded cross section.

$$\Delta_Y = \frac{fP_y L^3}{3EI} = \frac{fM_y L^2}{3EI} = \frac{f\sigma_y L^2}{3Ec} \quad . \tag{D.11}$$

The deflection, Δ_P, caused by the plastic hinge rotation, Θ, is, in general, from structural theory

$$\Delta = \Theta L.$$

It was assumed that the plastic hinge can be modeled as acting over a distance as determined earlier. However, for these calculations, the hinge action is assumed to be concentrated at a/2, so the plastic deflection is

$$\Delta_P = \Theta(L - \tfrac{a}{2}), \tag{D.12}$$

where Θ is the plastic hinge rotation and a is the plastic hinge length from Eq. (D.5). The total deflection, Δ_T, is then

$$\Delta_T = \Delta_Y + \Delta_P = \Delta_Y + \Theta(L - \tfrac{a}{2}) \quad . \tag{D.13}$$

This equation can be solved for the rotation, Θ, or

$$\Theta = \frac{\Delta_T - \Delta_Y}{L - a/2} \tag{D.14}$$

This value of plastic hinge rotation can be related to the corresponding plastic strain through examination of the strain distribution. Theoretically, if the plastic hinge occurs at a point, the corresponding strains would be infinite. However, the hinge has an actual length, a, over which the hinge acts. An average curvature, ϕ, can be defined based on the hinge rotation, Θ, and the plastic hinge length. Hodge (22) recommends that one-half of the hinge length be used in this calculation or a/2, so the curvature can be defined as

$$\phi = \frac{\Theta}{a/2} \quad . \tag{D.15}$$

From the linear strain distribution, the curvature is the extreme fiber strain divided by one-half of the section height or

$$\phi = \frac{\epsilon}{c} \tag{D.16}$$

By equating these last two expressions and solving for strain, the following expression is obtained

$$\epsilon_p = \frac{\Theta(2c)}{a} \tag{D.17}$$

Therefore, through the use of Eqs. (D.5), (D.14), and (D.17), the displacement of a section can be related to the corresponding plastic strain.

D.3 Development of Strain-Ductility Relationships

The low-cycle fatigue damage relationship proposed by Morrow (44) was defined as

$$\frac{\Delta\epsilon^*}{2} = \epsilon_f'(2N_f)^{-0.6} \quad , \tag{D.18}$$

where $\Delta\epsilon^*/2$ is the amplitude of each strain cycle, ϵ_f' is the fatigue ductility coefficient corresponding to one reversal and $2N_f$ is the number of reversals to failure.

In terms of notation from this study, this equation can be rewritten as

$$\frac{\Delta\epsilon^*}{2} = \frac{\Delta\epsilon_p}{2}(2N_f)^{-0.6} \quad , \tag{D.19}$$

where $\Delta\epsilon^*/2$ is the hysteretic plastic strain amplitude, $\Delta\epsilon_p/2$ is the monotonic plastic strain causing failure in one reversal, and $2N_f$ is the number of reversals as before.

From the preceding development, the plastic strain terms can be converted to displacement terms by noting that

$$\epsilon = \frac{\Theta(2c)}{a} \quad ,$$

and

$$\Theta = \frac{\Delta_T - \Delta_Y}{L - a/2} \quad , \tag{D.20}$$

or

$$\epsilon = \frac{\Delta_T - \Delta_Y}{L - a/2}\left(\frac{2c}{a}\right) \quad .$$

But the term $\Delta_T - \Delta_Y$ is the plastic deformation Δ_p, or

$$\epsilon = \frac{2c}{a(L - a/2)}\Delta_p \quad . \tag{D.21}$$

If this equation is substituted into Eq. (D.19), the equation becomes

$$\frac{\Delta^*}{2}\ \frac{2c}{a(L - a/2)} = \frac{\Delta_p}{2}\ \frac{2c}{a(L - a/2)}\ (2N_f)^{-0.6}. \qquad (D.22)$$

If both sides are divided by the yield displacement at full yield, Δ_Y, then one obtains

$$\frac{\Delta^*}{2\Delta_Y}\ \frac{2c}{a(L - a/2)} = \frac{1}{2}\ \frac{\Delta_P}{\Delta_Y}\ \frac{2c}{a(L - a/2)}\ (2N_f)^{-0.6}. \qquad (D.23)$$

Common terms can be canceled out and the generic definition of ductility

$$\mu = \frac{\Delta_m}{\Delta_Y} \qquad (D.24)$$

can be substituted. This operation results in the final expression,

$$\mu^* = \mu_p(2N_f)^{-0.6}, \qquad (D.25)$$

where μ^* is the hysteretic plastic ductility, μ_p is the monotonic plastic ductility, and $2N_f$ is the number of reversals, as before.

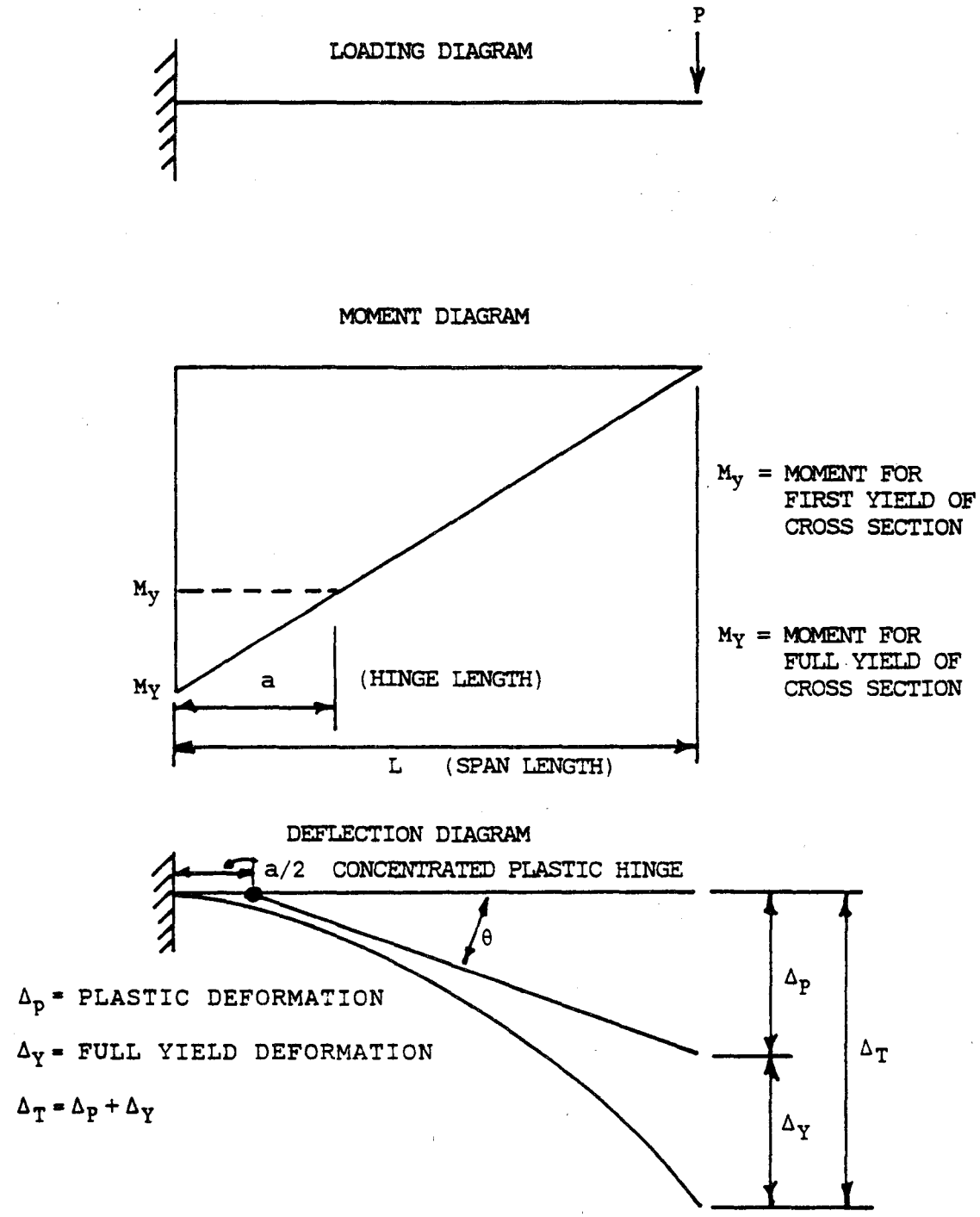

Figure D.1 Plastic Hinge Relationships

LIST OF REFERENCES

1. American Society of Civil Engineers, Plastic Design in Steel, A Guide and Commentary, ASCE Manual No. 41, Second Edition, New York, 1971.

2. Applied Technology Council, An Investigation of the Correlation Between Earthquake Ground Motion and Building Performance, Applied Technology Council, Palo Alto, California, November, 1982.

3. Applied Technology Council, Tentative Provisions for the Development of Seismic Regulations for Buildings, Publication ATC3-06, National Bureau of Standards, Special Publications 510, U.S. Government Printing Office, Washington, D.C., 1978.

4. Arias, A., "A Measure of Earthquake Intensity," Seismic Design for Nuclear Power Plants, R. Hanson, Editor, The MIT Press, pp. 438-483, 1970.

5. Bakun, W. H., M. M. Clark, R. S. Cockerham, W. L. Ellsworth, A. G. Lindh, W. H. Prescott, A. F. Shakal, and P. Spudich, "The 1984 Morgan Hill, California, Earthquake," Science, Vol. 225, No. 4659, pp. 288-291, July 20, 1984.

6. Banon, H. and D. Veneziano, "Seismic Safety of Reinforced Concrete Members and Structures," Earthquake Engineering and Structural Dynamics, vol. 10, 1982, pp. 179-193.

7. Bathe, K. J. and E. L. Wilson, Numerical Methods in Finite Element Analysis, Prentice-Hall, Inc., Englewood Cliffs, New Jersey, 1976.

8. Beedle, L. S., Plastic Analysis of Steel Frames, Wiley, New York, 1958.

9. Benham, P. P. and H. Ford, "Low Endurance Fatigue of a Mild steel and an Aluminum Alloy," Journal of Mechanical Engineering Science, Institution of Mechanical Engineers, London, vol. 3, No. 2, pp. 119-132, 1961.

10. Berg, G. V. and S. S. Thomsaides, "Energy Consumption by Structures in Strong-Motion Earthquakes," Proceedings of the Second World Conference on Earthquake Engineering, pp. 681-697, 1960.

11. Bertero, V. V. and E. P. Popov, "Effect of Large Alternating Strains of Steel Beams," Journal of the Structural Division, ASCE, Vol. 91, No. ST1, pp. 1-12, February, 1965.

12. Bertero, V. V., E. P. Popov, and H. Krawinkler, "Beam-Column Subassemblage Under Repeated Loading," Journal of the Structural Division, ASCE, Vol. 98, No. ST5, May, 1972, pp. 1137-1159.

13. Blume, J. A., "Structural Dynamics in Earthquake-Resistant Design," Transactions, ASCE, Vol. 125, pp. 1088-1139, 1960.

14. Building Seismic Safety Council and Federal Emergency Management Agency, "NEHRP Recommended Provisions for the Development of Seismic Provisions for New Buildings," Earthquake Hazards Reduction Services Report 17, 18, and 19, Washington, DC, 1985.

15. California Division of Mines and Geology, Department of Conservation, Private Communication Accompanying Tape of Morgan Hill Earthquake Data, July 5, 1984.

16. Coffin, L. F., Jr. and J. F. Tavernelli, "The Cyclic Straining and Fatigue of Metals," Transactions of the Metallurgical Society of AIME, AIME, Vol. 215, pp. 794-806, October, 1959.

17. Dowling, N. E., "Fatigue Failure Predictions for Complicated Stress-Strain Histories," T&AM Report No. 337, Dept. of Theoretical and Applied Mechanics, University of Illinois at Urbana-Champaign, January, 1971.

18. Fischer, E. G. and F. H. Wolff, "Comparison of Fatigue Effects in Simulated and Actual Earthquakes," Experimental Mechanics, Vol. XXX, No. 2, December, 1973, pp. 531-538.

19. Goel, S. C. and G. V. Berg, "Inelastic Earthquake Response of Tall Steel Frames," Journal of the Structural Division, ASCE, Vol. 94, No. ST8, August, 1968, pp. 1907-1934.

20. Hamming, R. W., Digital Filters, Second Edition, Prentice-Hall, Englewood Cliffs, N. J., 1977.

21. Hanson, R. D., "Comparison of Static and Dynamic Hysteresis Curves," Journal of the Engineering Mechanics Division., ASCE, Vol. 92, No. EM5, October, 1966, pp. 87-113.

22. Hodge, P. G., Jr. Plastic Analysis of Structures, Krieger, Malabar, Florida, 1981.

23. Housner, G. W., "Behavior of Structures During Earthquakes," Journal of Engineering Mechanics Division, ASCE, Vol. 85, No. EM4, pp. 109-129, October, 1959.

24. Housner, G. W., "Limit Design of Structures to Resist Earthquakes," Proceedings of First World Conference on Earthquake Engineering, EERI, pp. 5-1 to 5-11, 1956.

25. Housner, G. W., "The Plastic Failure of Frames During Earthquakes," Proceedings of Second World Conference on Earthquake Engineering, Science Council of Japan, Tokyo, pp. 997-1012, 1960.

26. Housner, G. W. and P. C. Jennings, Earthquake Design Criteria, EERI Monograph Series, Berkeley, California, 1982.

27. Hudson, D. E., Reading and Interpreting Strong Motion Accelerograms, EERI Monograph Series, Berkeley, California, 1979.

28. Hudson, D. E., M. D. Trifunac, and A. G. Brady, "Analysis of Strong-Motion Accelerograms," Vol. I, Parts A-Y, Vol. II, Parts A-Y, Vol. III, Parts A-Y, Vol. IV, Parts A-Y, Index Vol., EERL Report 76-02, Earthquake Engineering Research Laboratory, California Institute of Technology, Pasadena, California.

29. Iemura, H. and P. C. Jennings, "Hysteretic Response of a Nine-Story Reinforced Concrete Building," Earthquake Engineering and Structural Dynamics, Vol. 3, No. 2, pp. 183-201, October-December, 1974.

30. Jacobson, L. S. and R. S. Ayre, Engineering Vibrations, McGraw-Hill, New York, 1958.

31. Jennings, P. C. "Earthquake Response of a Yielding Structure," Journal of the Engineering Mechanics Division, ASCE, Vol. 91, No. EM 4, August, 1965, pp. 41-68.

32. Jennings, P. C. and R. A. Guzman, "Seismic Design Criteria for Nuclear Power Plants," Proceedings of U.S. National Conference on Earthquake Engineering, EERI, 1975, p. 479, 1975.

33. Juvinall, R. C., Engineering Considerations of Stress, Strain and Strength, McGraw-Hill, New York, 1967, pp. 221-222.

34. Kasiraj, I. and J. T. P. Yao, "Fatigue Damage in Seismic Structures," Journal of the Structural Division, ASCE, Vol. 95, No. ST8, August 1969, pp. 1673-1692.

35. Kennedy, R. P., "Peak Acceleration as a Measure of Damage," Proceedings of the Sixth Structural Mechanics in Reactor Technology Conference, 1981.

36. Kennedy, R. P., S. A, Short, K. L. Mezz, F. J. Tokarz/SMAI, I. M. Idriss, M. S. Power, and K. Sadigh/WCC, "Engineering Characterization of Ground Motion, Task I: Effects of Characteristics of Free-Field Motion on Structural Response," U.S. Nuclear Regulatory Commission, NUREG/CR-3805, May, 1984.

37. Krawinkler, H. and M. Zohrei, "Cumulative Damage in Steel Structures Subjected to Earthquake Ground Motions," Computers and Structures, Vol. 16, No. 1-4, pp. 531-541, 1983.

38. Krawinkler, H., Mahmud Zohrei, Bahman Lashkari-Irvani, Nathional G. Cofie, and Hasan Hadidi-Tamjed, "Recommendations for Experimental Studies on the Seismic Behavior of Steel Components and Materials," The John A. Blume Earthquake Engineering Center, Report No. 61, Dept. of Civil Engineering, Stanford University, Stanford, September, 1983.

39. Landgraf, R. W., "Cumulative Fatigue Damage under Complex Strain Histories," Cyclic Stress-Strain Behavior, ASTM STP 519, 1973, pp. 213-228.

40. Lashkari-Irvani, B., "Cumulative Damage Parameters for Bilinear Systems Subjected to Severe Earthquakes," Proceedings of ATC Ground Motion Conference, March 27, 1984.

41. Mahin, S. A. and Bertero, V. V., "An Evaluation of Inelastic Seismic Design Spectra," Journal of the Structural Division, ASCE, Vol. 107, No. ST9, Sept., 1981, pp. 1777-1795.

42. Manson, S. S., "Fatigue: A Complex Subject - Some Simple Approximations," Experimental Mechanics, Vol. 5, No. 7, July, 1965, pp. 193-226.

43. Morrison, D. G. and M. A. Sozen, "Response of Reinforced Concrete Plate-Column Connections to Dynamic and Static Horizontal Loads," Structural Research Series No. 490, Civil Engineering Studies, University of Illinois at Urbana-Champaign, Illinois, May, 1982.

44. Morrow, J. D., "Cyclic Plastic Strain Energy and Fatigue of Metals," Internal Friction Damping and Cyclic Plasticity, ASTM STP 378, 1965, pp. 45-84.

45. Nau, J. M. and W. J. Hall, "An Evaluation of Scaling Methods for Earthquake Response Spectra," Structural Research Series No. 499, Civil Engineering Studies, University of Illinois at Urbana-Champaign, Illinois, May, 1982.

46. Newmark, N. M., "A Method of Computation for Structural Dynamics," Journal of the Engineering Mechanics Division, ASCE, Vol. 85, No. EM3, July, 1959.

47. Newmark, N. M., "An Engineering Approach to Blast Resistant Design," Transactions, ASCE, Vol. 121, 1956, pp. 45-64.

48. Newmark, N. M., J. A. Blume, and K. K. Kapur, "Seismic Design Spectra for Nuclear Power Plants," Journal of the Power Division, ASCE, Vol. 99, No. PO2, pp. 287-303, November, 1973.

49. Newmark, N. M. and W. J. Hall, "Development of Criteria for Seismic Review of Selected Nuclear Power Plants," U.S. Nuclear Regulatory Commission, NUREG CR0098, May, 1978.

50. Newmark, N. M. and W. J. Hall, Earthquake Spectra and Design, EERI Monograph Series, Berkeley, California, 1982.

51. Newmark, N. M. and E. Rosenblueth, Fundamentals of Earthquake Engineering, Prentice-Hall, Inc., Englewood Cliffs, New Jersey, 1971.

52. Nigam, N. C. and P. C. Jennings, "Digital Calculation of Response Spectra from Strong-Motion Earthquake Records," Earthquake Engineering Research Laboratory Report, California Institute of Technology, Pasadena, Calif., June, 1968.

53. Oppenheim, A. V. and R. W. Schafer, Digital Signal Processing, Prentice-Hall, Inc., Englewood Cliffs, New Jersey, 1975.

54. Page, R. A., J. A. Blume, and W. B. Joyner, "Earthquake Shaking and Damage to Buildings," Science, Vol. 189, No. 4203, pp. 601-608, August 22, 1975.

55. Perez, V. and A. G. Brady, "Degradation of Building Strength Due to Cyclic Loading," Proceedings of Applied Technology Council Conference on Earthquake Ground Motion, March 27, 1984.

56. Popov, E. P., N. R. Amin, J. J. C. Louie, and R. M. Stephen, "Cyclic Behavior of Large Beam-Column Assemblies," Earthquake Spectra, EERI, Vol. 1, No. 2, February, 1985, pp. 203-238.

57. Popov, E. P. and V. V. Bertero, "Cyclic Loading of Steel Beams and Connections," Journal of the Structural Division, ASCE, Vol. 99, No. ST6, June, 1973, pp. 1189-1204.

58. Popov, E. P. and V. V. Bertero, "Seismic Analysis of Some Steel Building Frames," Journal of the Engineering Mechanics Division, ASCE, Vol. 106, EMI, pp. 75-92, February, 1980.

59. Popov, E. P. and R. B. Pickney, "Behavior of Steel Building Connections Subjected to Repeated Inelastic Strain Reversal," Earthquake Engineering Research Center Reports No. 67-30 and 67-31 (Experimental Data), University of California, Berkeley, December, 1967.

60. Popov, E. P. and R. B. Pinkney, "Cyclic Yield Reversals in Steel Building Connections," Journal of the Structural Division, ASCE, Vol. 95, No. ST3, March, 1969, pp. 327-353.

61. Popov, E. P. and R. M. Stephen, "Cyclic Loading of Full-Size Steel Connections," Earthquake Engineering Research Center, Report No. EERC 70-3, University of California, Berkeley, July, 1970.

62. Richart, F. E., Jr. and N. M. Newmark, "An Hypothesis for the Determination of Cumulative Damage in Fatigue," Proceedings of Fifty-First Annual Meeting of ASTM, ASTM, 1948.

63. Riddell, R. and N. M. Newmark, "Statistical Analysis of the Response of Nonlinear Systems Subjected to Earthquakes," Civil Engineering Studies, Structural Research Series No. 468, University of Illinois at Urbana-Champaign, Illinois, August, 1979.

64. Sawyer, H. A., Jr., "An Elastic Criterion for Plastic Design," Journal of the Structural Division, ASCE, Vol. 84, No. ST2, pp. 1566-1 to 1566-17, March, 1958.

65. Shibata, A. and M. A. Sozen, "The Substitute Structure Method for Earthquake Resistant Design of Reinforced Concrete Frames," Civil Engineering Studies, Structural Research Series No. 412, University of Illinois at Urbana-Champaign, Illinois, October, 1974.

66. Suidan, M. T. and R. A. Eubanks, "Cumulative Fatigue Damage in Seismic Structures," Journal of the Structural Division, ASCE, Vol. 99, No. ST5, May, 1969, pp. 327-353.

67. Tang, J. P. and J. T. P. Yao, "Expected Fatigue Damage of Seismic Structures," Journal of the Engineering Mechanics Division, ASCE, Vol. 98, No. EM3, June, 1972, pp. 695-708.

68. Uniform Building Code, Part V, Chapter 23, "General Design Requirements," pp. 120-147, 1985.

69. Veletsos, A. S. and N. M. Newmark, "Effect of Inelastic Behavior on the Response of Simple Systems to Earthquake Motions," Proceedings of the Second World Conference on Earthquake Engineering, Tokyo, 1960, pp. 895-912.

70. Veletsos, A. S. and N. M. Newmark, "Response Spectra of Single Degree of Freedom Elastic and Inelastic Systems," from Design Procedures for Shock Isolation Systems of Underground Protective Structures, Vol. III, Technical Documentary Report, No. RTD TDR-63-3096, Urbana, Illinois, 1963.

71. Yao, J. T. P. and W. H. Munse, "Low-Cycle Axial Fatigue Behavior of Mild Steel," ASTM Special Technical Publication No. 338, 1963, pp. 5-24.

72. Zahrah, T. F. and W. J. Hall, "Seismic Energy Absorption in Simple Structures," Civil Engineering Studies, Structural Research Series No. 501, University of Illinois at Urbana-Champaign, Illinois, July, 1982.